



COMPRESSIVE BEHAVIOR OF HOLLOW CONCRETE COLUMNS REINFORCED WITH GFRP BARS

A Thesis submitted by

Omar Saleh Awad Alajarmeh

MSc (Civil/Structural), BSc (Civil)

For the award of

Doctor of Philosophy

2020

Abstract

Hollow concrete columns (HCCs) reinforced with steel bars have been employed extensively for bridge piers, ground piles, and utility poles because they offer higher structural efficiency compared to solid concrete columns with the same concrete area. Many experimental studies have been conducted to investigate the behavior of HCCs under different loading conditions and have found that the structural performance of HCCs is critically affected by the inner-to-outer diameter, reinforcement ratio, volumetric ratio, and concrete compressive strength. The improper design of the HCCs led to brittle failure behavior due to either buckling of the longitudinal bars or concrete wall crushing. Moreover, the corrosion of steel bars in HCCs is a critical issue due to their inner and outer exposed surfaces. Therefore, this research systematically investigated the fundamental behavior of HCCs reinforced with GFRP bars in compression to develop new, durable and structurally reliable construction systems.

Firstly, HCCs with different inner-to-outer diameter (i/o) ratios was investigated by testing four concrete columns 250 mm in external diameter and reinforced longitudinally with six 15.9 mm diameter GFRP bars with different inner diameters (0, 40, 65, and 90 mm). One HCC reinforced with steel bars was also prepared and tested as a control sample. Based on the experimental results, increasing the i/o ratio up to 0.36 changed the failure behavior from brittle to ductile. GFRP-reinforced HCCs exhibited higher deformation capacity and confinement efficiency compared to the GFRP-reinforced SCC and steel-reinforced HCC. The optimal (i/o) ratio was found at 0.36 as it resulted in the highest confined strength and ductility for GFRP-reinforced HCC. Similarly, reinforcing with longitudinal GFRP bars enhanced the overall behavior of HCCs.

The effect of varying the reinforcement ratio was investigated as the second study. To study this parameter, six HCCs reinforced longitudinally with GFRP bars with different reinforcement ratios (1.78%, 1.86%, 2.67%, 2.79%, 3.72%, and 4.00%) were prepared and tested. These reinforcement ratios were achieved by changing the bar diameter (12.7 mm, 15.9 mm, and 19.1 mm) and number of bars (4, 6, 8, and 9 bars). The test results show that the increase in the bar diameter and number enhanced the strength, ductility and confinement efficiency of HCCs. For columns with equal reinforcement ratios, using a higher number and smaller diameter of GFRP bars yielded 12% higher confinement efficiency than in the columns with a lesser number

and larger diameter of GFRP bars. The capacity of the GFRP-reinforced HCC can be reliably predicted by considering the contribution of the concrete and up to $3000 \mu\epsilon$ in the longitudinal reinforcement. The crushing strain of the GFRP bars embedded in the HCCs was 52.1% of the ultimate tensile strain, and was affected by the confinement provided by the lateral reinforcements and the compressive strength of concrete.

The effect of spiral spacing and concrete compressive strength was investigated as the third study. Seven large-scale HCCs with (*i/o*) ratio of 0.36, and reinforced with six longitudinal GFRP bars were prepared and tested. Out of these seven columns, three had spiral spacing of 50 mm, 100 mm, and 150 mm, and one had no spirals to investigate the effect of this design parameter. The f'_c of the other three columns were varied from 21 to 44 MPa to investigate the effect of the concrete compressive strength. Test results show that reducing the spiral spacing resulted in increasing the design load capacity, ductility, and confined strength of the HCCs due to the high lateral confinement. Increasing f'_c , on the other hand, increased the axial load capacity and reduced the ductility and confinement efficiency due to the brittle behavior of the high concrete compressive strength. The analytical model was then developed considering the contribution of the GFRP bars and the confined concrete core, which accurately predicted the post-loading behavior of the HCCs.

The experimental results from the three experimental studies demonstrated that the (*i/o*) ratio, ρ , ρ_v , and f'_c affect the overall behavior of GFRP-reinforced HCCs. Therefore, a new design-oriented model considering the effects of these design parameters was developed in the fourth study to accurately and reliably describe the behavior of the GFRP-reinforced HCCs. The new design-oriented model was based on the plasticity theory of concrete and considered the critical design parameters to precisely model the compressive load–strain behavior of GFRP-reinforced HCCs under monotonic and concentric loading. The results demonstrated that the proposed design-oriented model was accurate and yielding a very good representation of the axial compressive load behavior of GFRP-reinforced hollow concrete columns.

From the results of this research, a detailed understanding on how the critical design parameters affect the structural performance of GFRP-reinforced HCCs was gained. Moreover, the results from this research will provide useful information in revealing the many benefits of this new structurally efficient and non-corrosive construction system, which support the work of the technical committees engaged in the development of design provisions for GFRP-reinforced concrete columns.

Certification of Thesis

This thesis is entirely the work of *Omar Saleh Awad Alajarmeh* except where otherwise acknowledged. The work is original and has not previously been submitted for any other award, except where acknowledged.

Student and supervisors' signatures of endorsement are held at USQ.

Omar Saleh Awad Alajarmeh

04 February 2020

PhD Candidate

Date

Endorsement

Professor Allan Manalo

04 February 2020

Principal Supervisor

Date

Professor Karu Karunasena

04 February 2020

Associate Supervisor

Date

Statements of Contributions

The articles produced from this study were a joint contribution of the authors. The details of the scientific contribution of each author are provided below:

Manuscript 1: Omar AlAjarmeh, Allan Manalo, Brahim Benmokrane, Warna Karunasena, Wahid Ferdous and Priyan Mendis, (2019) “Hollow concrete columns: review of structural behavior and new reinforcing design using GFRP reinforcements” Engineering Structures Journal, vol. 203, 109829. (Impact factor: 3.084 and SNIP: 2.089).

DOI: <https://doi.org/10.1016/j.engstruct.2019.109829>

The overall contribution of Omar AlAjarmeh was 65% related to the data collection, critical review of related literature, analysis and interpretation of data, drafting and revising the final submission. Allan Manalo, Brahim Benmokrane, Warna Karunasena, Wahid Ferdous and Priyan Mendis contributed to the structuring the manuscript, statistical analysis, analysis and interpretation of data, editing and providing important technical inputs.

Manuscript 2: Omar AlAjarmeh, Allan Manalo, Brahim Benmokrane, Warna Karunasena, Priyan Mendis, and Kate Nguyen, (2019) “Compressive behavior of axially loaded circular hollow concrete columns reinforced with GFRP bars and spirals” Construction and Building Materials Journal, vol. 194, pp. 12-23. (Impact factor: 4.046 and SNIP: 2.369)

DOI: <https://doi.org/10.1016/j.conbuildmat.2018.11.016>

The overall contribution of Omar AlAjarmeh was 60% to the concept development, design of experiments, experimental works, analysis and interpretation of data, drafting and revising the final submission. Allan Manalo, Brahim Benmokrane, Warna Karunasena, Priyan Mendis, and Kate Nguyen contributed to the concept development, design of experiments, analysis and interpretation of data, editing and providing important technical inputs.

Manuscript 3: Omar AlAjarmeh, Allan Manalo, Brahim Benmokrane, Warna Karunasena, and Priyan Mendis, (2019) “Axial performance of hollow concrete columns reinforced with GFRP composite bars with different reinforcement ratios”

Composite Structures Journal, vol. 213, pp. 153-164. (Impact factor: 4.829 and SNIP: 2.035)

DOI: <https://doi.org/10.1016/j.compstruct.2019.01.096>

The overall contribution of Omar Alajarmeh was 70% to the concept development, design of experiments, experimental works, analysis and interpretation of data, drafting and revising the final submission. Allan Manalo, Brahim Benmokrane, Warna Karunasena, and Priyan Mendis contributed to the concept development, design of experiments, analysis and interpretation of data, editing and providing important technical inputs by 15%, 5%, 5% and 5%, respectively.

Manuscript 4: Omar AlAjarmeh, Allan Manalo, Brahim Benmokrane, Warna Karunasena, and Priyan Mendis, (2019) “Effect of spiral spacing and concrete strength on behavior of GFRP-reinforced hollow concrete columns” Composite for Constructions Journal, vol. 24, issue 1. (Impact Factor: 2.592 and SNIP: 1.811)

DOI: [10.1061/\(ASCE\)CC.1943-5614.0000987](https://doi.org/10.1061/(ASCE)CC.1943-5614.0000987)

The overall contribution of Omar Alajarmeh was 65% to the concept development, design of experiments, experimental works, analysis and interpretation of data, drafting and revising the final submission. Allan Manalo, Brahim Benmokrane, Warna Karunasena, and Priyan Mendis contributed to the concept development, design of experiments, analysis and interpretation of data, editing and providing important technical inputs.

Manuscript 5: Omar AlAjarmeh, Allan Manalo, Brahim Benmokrane, Warna Karunasena, Wahid Ferdous and Priyan Mendis, (2019) “A new design-oriented model of GFRP reinforced hollow concrete columns” ACI Structural Journal, vol 117, No. 2. (Impact factor: 1.197 and SNIP: 1.217)

DOI: [10.14359/51720204](https://doi.org/10.14359/51720204)

The overall contribution of Omar Alajarmeh was 65% to the model development, experimental works, analysis and interpretation of data, drafting and revising the final submission. Allan Manalo, Brahim Benmokrane, Warna Karunasena, Wahid Ferdous and Priyan Mendis contributed to the model development, analysis and interpretation of data, editing and providing important technical inputs.

Acknowledgements

First and foremost, I would like to thank the **almighty Allah**, who guided me and gave me the strength to make such work. Without his guidance I would have never been able to know the wonderful people whom I met and worked with during my PhD journey. Praise to **Allah**, everything went fairly well.

I have much appreciation and gratitude to all the people whom without, this thesis might not have been possible in the current form:

Associate professor **Allan Manalo**, my principle supervisor. I do really feel that I was blessed to meet him and work under his supervision which enlightened within me the first glance of research. It is impossible to find words expressing my full gratefulness to him. His unique piece of mind and immense knowledge were my source to build my research character and to think constructively. His incessant motivation, cooperative behavior, and positive attitude added very worthy values to my life.

Professor **Karu Karunasena**, my associate supervisor. Special thanks and appreciation for his encouragement, guidance, and motivation, which made me stronger and optimistic.

Professor **Brahim Benmokrane**. My words cannot suffice to show my thanks to his insightful comments, suggestions, and constructive ideas which were essential in improving the quality of this research.

Professor **Priyan Mendis**, and Dr **Kate Nguyen**. Grateful thanks for your support, guidance, and various pieces of advice that helped me to complete my work.

Dr **Wahid Ferdous**. Sincere thanks to his friendship, support, ideas, and motivation during my PhD.

Mr. **Darren Lutze** and **V-Rod® Australia**. Thank you for the materials support.

My **colleagues** at USQ, especially in the Centre of Future Materials, and the **technical staff**. Many thanks to their friendship and technical supports.

A special thanks goes to my beloved wife **Aseel** and my adorable son **Saif-aldeen** for their love, encourage, patience, and sacrifice. My **parents** and my **brothers** and **sister** who live far away from here, endless thanks for their love, patient and believing in me.

I highly appreciate the financial support of Tafila Technical University and the University of Southern Queensland who helped me to complete my PhD.

To those whom I failed to mention but have a part of this journey, **thank you All**.

Table of Contents

Abstract	ii
Certification of Thesis	v
Statements of Contributions	vi
Acknowledgements	ix
Table of Contents	x
Chapter 1: Introduction	1
<i>Background and motivation</i>	3
<i>Objectives</i>	4
<i>Thesis organization</i>	5
<i>Summary</i>	8
<i>References</i>	8
Chapter 2: Hollow concrete columns: Review of structural behavior and new reinforcing design using GFRP reinforcements	11
Chapter 3: Compressive behavior of axially loaded circular hollow concrete columns reinforced with GFRP bars and spirals	28
Chapter 4: Axial performance of hollow concrete columns reinforced with GFRP composite bars with different reinforcement ratios	41
Chapter 5: Effect of spiral spacing and concrete strength on behavior of GFRP-reinforced hollow concrete columns	54
Chapter 6: A new design-oriented model for GFRP reinforced hollow concrete columns	69
Chapter 7: Conclusions	86
<i>State-of-the-art review on the behavior of HCCs</i>	86
<i>Effect of (i/o) ratio on the behavior of GFRP-reinforced HCCs</i>	87
<i>Effect of the reinforcement ratio (ρ) on the behavior of GFRP-reinforced HCCs</i>	88
<i>Effect of volumetric ratio (ρ_v) on the behavior of GFRP-reinforced HCCs</i>	90
<i>Effect of concrete compressive strength (f'_c) on the behavior of GFRP-reinforced HCCs</i>	90
<i>Modelling the compressive behavior of the GFRP-reinforced HCCs</i>	91
<i>Contribution of the study</i>	92
<i>New opportunities and future research</i>	92

Appendix A: Mechanical and physical properties of the GFRP reinforcements	95
Appendix B: Conference papers	96

Chapter 1

Introduction

Background and motivation

Reinforced concrete columns are essential structural elements providing stability to the concrete structures and transferring the applied loads to the foundation. These structural elements need to have high strength and sufficient stiffness. Hollow concrete columns (HCCs) therefore has emerged to increase the structural efficiency of reinforced concrete columns due to their higher strength- and stiffness-to-weight ratios than the solid concrete columns (SCCs) of the same cross-section area (Mander 1983; Zahn 1986; Whittaker 1987). The reduction in material usage in HCCs resulted in a low self-weight and reduction in the size of the supporting structures. Current design of HCCs are reinforced with steel bars. Many studies extensively investigated the behavior of the steel-reinforced HCCs under different loading conditions (Mander 1983; Zahn 1986; Whittaker 1987; Osada et al. 1999; Hoshikuma and Priestley 2000; Ranzo and Priestley 2001; Yeh et al. 2001; Yeh et al. 2002; Mo et al. 2003; Pinto et al. 2003; Pavese et al. 2004; Lignola et al. 2007; Kusumawardaningsih and Hadi 2010; Lee et al. 2015; Liang et al. 2015). Steel-reinforced HCCs are significantly affected by several design parameters including axial load ratio ($\frac{P_o}{f'_c A_c}$) (the ratio between applied and ultimate axial load capacities) (Mander 1983; Zahn 1986), inner-to-outer diameter (i/o) ratio (Whittaker 1987; Lee et al. 2015), reinforcement ratio (ρ) (Hoshikuma and Priestley 2000; Ranzo and Priestley 2001), volumetric ratio (ρ_v) (Yeh et al. 2001; Yeh et al. 2002), concrete compressive strength (f'_c) (Osada et al. 1999; Mo et al. 2003), aspect ratio (AR) (Pinto et al. 2003; Pavese et al. 2004), and geometry (G) (Kusumawardaningsih and Hadi 2010; Liang et al. 2015). These design parameters were observed to be more critical in HCCs than the SCCs due to the unconfined concrete in the core often resulting to a brittle failure behavior as shown in Figure 1.1.

Steel-reinforced HCCs exhibit low deformation capacity (Pavese et al. 2004) and sudden reduction in strength (Kusumawardaningsih and Hadi 2010). This behavior is normally caused by either buckling of the reinforcement due to insufficient reinforcement details or crushing of the concrete wall caused by low concrete strength.

Moreover, steel bars provide no additional resistance after yielding which lead to overstressing and crushing of the unconfined concrete wall. Whittaker (1987) therefore suggested that well-designed steel-reinforced HCCs should have proper reinforcement detailing and made them continuously intact with the concrete wall and well-confined by the transverse steel reinforcements. These design parameters, therefore, should be carefully considered for the HCCs to ensure the functionality and sustainability, and to change the failure behavior from brittle to ductile.

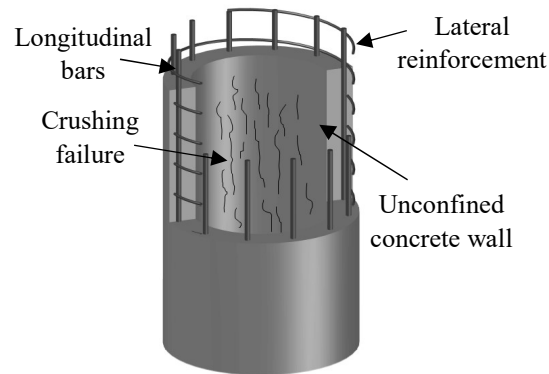


Figure 1.1. Concrete core crushing of the HCC

Corrosion of steel reinforcement (see Figure 1.2) is becoming crucial for HCCs considering the outer and inner surfaces of the column. Steel corrosion can significantly reduce the strength of the columns and eliminate the confinement of the lateral reinforcements leading to a brittle failure (Li et al. 2009; Pantelides et al. 2013). In fact, many steel-reinforced concrete bridge piers are now being repaired or retrofitted due to the significant steel corrosion problem to prolong their service lives (Aboutaha 2004). Maintaining these deteriorating structures are very expensive considering material and labour expenses in addition to the shutdown processes. Similar problems are now being experienced by hollow steel structures (Elchalakani 2016). Various techniques have been implemented to minimise deterioration of steel reinforcement such as the use of galvanising steel, epoxy coating, and applying cathodic protection, but they could not entirely eliminate steel corrosion and added high costs (Nkurunziza et al. 2005). Therefore, there is a need to explore the use of non-corrosive reinforcements such as glass fibre reinforced polymer (GFRP) bars in HCCs in order to mitigate the corrosion issues related to steel and to develop a more reliable and durable concrete structure.



Figure 1.2. Steel corrosion in bridge piers (Aboutaha 2004)

Glass fibre reinforced polymer (GFRP) composite bars have been successfully implemented as internal reinforcement to concrete structures due to their many superior mechanical and environmental resisting properties (Manalo et al. 2014). GFRP bars were successfully used as reinforcement in concrete beams (Maranan et al. 2019), slabs (Abdul-Salam et al. 2016), and walls (Mohamed et al. 2014) due to their high strength and almost similar modulus of elasticity to concrete. The GFRP reinforcements are also found effective in concrete columns as an alternative to steel reinforcements (Tobbi et al. 2014; Hadi et al. 2016), where the GFRP-reinforced SCCs showed higher strength and displacement capacity than the steel-reinforced SCCs. This behavior is due to the high strength and linear elastic behavior of GFRP longitudinal and transverse reinforcements, where they keep resisting the axial and lateral loads, respectively, until failure without any reduction in their stiffness. This behavior can be potentially a solution to overcome the brittle behavior of the steel-reinforced HCCs.

This thesis systematically investigated the effect of the critical design parameters influencing the structural behavior of GFRP-reinforced HCCs experimentally and analytically under concentric compression load. It focused on investigating the effect of (i/o) ratio, reinforcement ratio (ρ), volumetric ratio (ρ_v), and concrete compressive strength (f'_c) as they are identified the most critical parameters affecting the behavior of HCC under concentric compression load. Finally, an analytical and empirical approach was developed to accurately describe the compressive behavior of the GFRP-reinforced HCCs considering the effect of the investigated parameters. The development of new equations was motivated by the existing models were found not applicable for GFRP-reinforced HCCs. The experimental data and understanding gained from this study demonstrated the effective

use of GFRP bars as internal reinforcements for the reliable, safe and durable HCCs. The developed analytical model provided a useful design tools for asset owners and engineers to safely and effectively design GFRP-reinforced HCCs to comply the design requierments.

Objectives

The main objective of this research is to investigate the compressive behavior of hollow concrete columns reinforced with GFRP bars under concentric compression load and to identify how the critical design parameters affect their behaviour. It also aims to develop a new construction system that is durable and with reliable structural performance. To address these objectives, the specific objectives of the study were identified as follows:

1. To investigate the effect of removing the concrete core from the solid concrete column and changing the inner-to-outer diameter ratio on the overall behavior of hollow concrete columns reinforced with GFRP bars.
2. To evaluate the effect of reinforcement ratio by varying the number and diameter of the longitudinal GFRP bars on the compressive behavior of hollow concrete columns.
3. To examine in detail the behavior of GFRP-reinforced HCCs with different spacing of spiral reinforcements and with different levels of concrete compressive strength.
4. To develop theoretical and empirical model that will accurately describe the concentric compressive behavior of hollow concrete columns reinforced longitudinally and transversely with GFRP bars.

Study limitations

This thesis studied the concentric behavior of HCCs reinforced with longitudinal and spiral GFRP bars. The reinforcements used in this study are high modulus sand-coated GFRP reinforcements made by pultrusion process as these bars are now extensively used as internal reinforcements in many concrete structures. The GFRP bars were manufactured and supplied by Pultrall Canada and came from the same production lot of the bars investigated by Benmokrane et al. (2017). The mechanical properties of these bars are reported in Table A.1 in Appendix A. All columns were manufactured

using normal strength concrete strength containing Ordinary Portland Cement, fine and coarse aggregates, and supplied by a pre-mix concrete company in Toowoomba.

The outer diameter of the cross-section of the concrete columns was limited to 250 mm based on the maximum load capacity of the testing equipment. Nevertheless, this size was able to provide sufficient data to evaluate the effect of different design parameters on the axial compressive behavior of HCCs. To support the experimental results and to have a better understanding of the different material components during the entire loading, several strain gauges were attached to the reinforcements (bars and spirals) and the concrete. The concrete columns in this study have a reinforcement ratio between 1% and 4% in accordance to AS 3600 to avoid the congestion of the reinforcements. The lateral reinforcements were limited to be GFRP spirals with a 10 mm in diameter and spaced at a minimum of 50 mm centre-to-centre to avoid any segregation in concrete.

Thesis organisation

The research work is presented by thesis by publication. It consists of an Introduction in Chapter 1 providing the research background and motivation, objectives, and limitations of this research. An extensive review of literature is presented in Chapter 2 highlighting the state-of-the-art in the field, identifying the challenges and opportunities as well as the gaps in research, which helped in formulating the objectives and the methodology as well as justifying the novelty of the work. Three experimental studies were then carefully planned and implemented, with the significant results and findings presented in Chapters 3 to 5. Chapter 6 presents the development of the empirical model to describe the overall behavior of GFRP-reinforced hollow columns considering the investigated design parameters. Finally, the Conclusion in Chapter 7 highlights the main findings of the work and significant contributions of this study. New opportunities and future researches were also suggested as recommendations. The below chart in Figure 1.3 shows the general structure of this thesis.

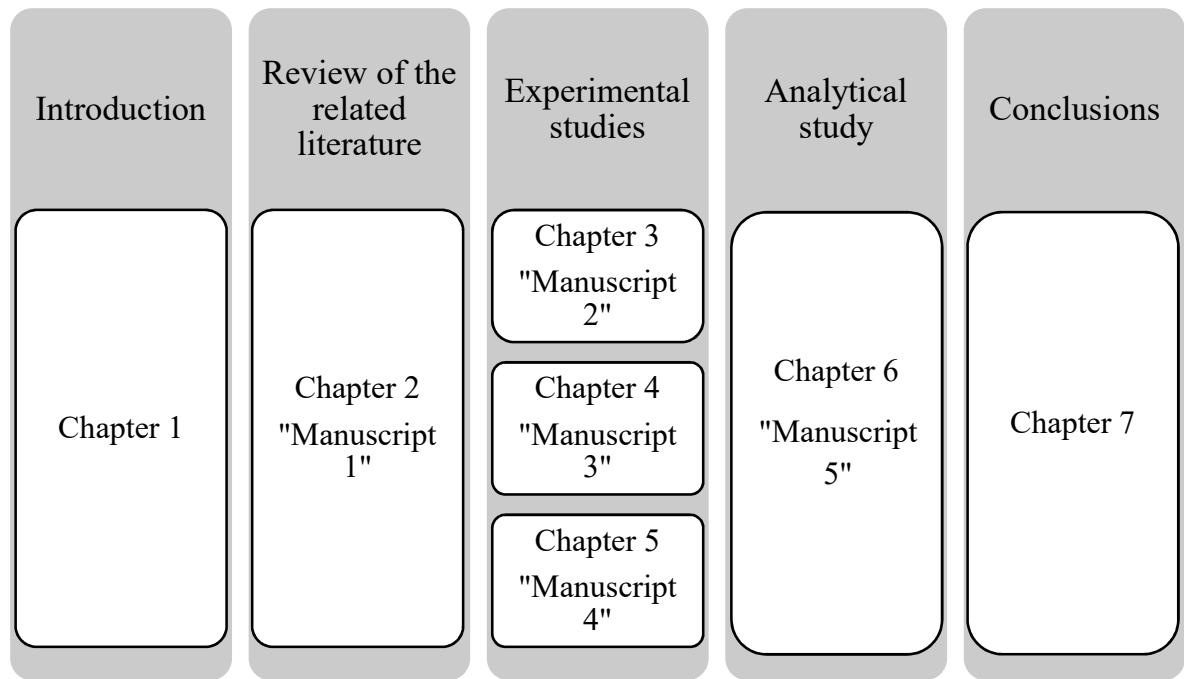


Figure 1.3. Thesis flow chart

From the outcome of this work, five journal papers were published or are currently under review in Q1 international journals. Moreover, the significant findings and outcome of this research were also presented in related national and international conferences as listed in Appendix A. An overview of the journal papers from this work is as follows:

Manuscript 1: Omar AlAjarmeh, Allan Manalo, Brahim Benmokrane, Warnas Karunasena, Wahid Ferdous and Priyan Mendis, (2019) “Hollow concrete columns: review of structural behavior and new reinforcing design using GFRP reinforcements” Engineering Structures Journal, vol. 203, 109829. (Impact factor: 3.084 and SNIP: 2.089).

DOI: <https://doi.org/10.1016/j.engstruct.2019.109829>

The extensive review of the related literature presented in this manuscript described in detail the general behavior of the HCCs and the difference in their structural behavior to SCCs. The most investigated design parameters and their effect on the behavior of HCCs as reported by different researchers were analysed. Afterwards, the structural and durability challenges on the design of HCCs were identified. Based on the current limitations, glass fibre reinforced polymer (GFRP) reinforcements were suggested to

overcome the limited ductility and corrosion of reinforcement in steel-reinforced HCCs.

Manuscript 2: Omar AlAjarmeh, Allan Manalo, Brahim Benmokrane, Warna Karunasena, Priyan Mendis, and Kate Nguyen, (2019) “Compressive behavior of axially loaded circular hollow concrete columns reinforced with GFRP bars and spirals” Construction and Building Materials Journal, vol. 194, pp. 12-23. (Impact factor: 4.046 and SNIP: 2.369)

DOI: <https://doi.org/10.1016/j.conbuildmat.2018.11.016>

This manuscript addressed the first objective of this research where the effect of the (i/o) ratio on the compressive behavior of GFRP-reinforced HCCs was evaluated. A comparative study between solid and hollow concrete columns was conducted to determine the effect of removing the inner concrete core from the SCC. Besides, the effect of increasing (i/o) ratio was also identified. Lastly, the use of steel and GFRP bars as longitudinal reinforcements in HCCs was compared and analysed. The results from the experimental work were presented and compared in term of failure mode, load and deformation behaviour, ductility, and strength and confinement efficiency. Moreover, analytical equations were introduced describing the load-deformation behavior of GFRP-reinforced HCCs. From this study, it was concluded that using GFRP reinforcements improved the overall behavior of HCCs compared to that of steel-reinforced HCCs. The results from this study also demonstrates the effectiveness of GFRP bars as internal reinforcements in HCCs, which has driven the need to investigate the effect of other critical design parameters identified in the literature.

Manuscript 3: Omar AlAjarmeh, Allan Manalo, Brahim Benmokrane, Warna Karunasena, and Priyan Mendis, (2019) “Axial performance of hollow concrete columns reinforced with GFRP composite bars with different reinforcement ratios” Composite Structures Journal, vol. 213, pp. 153-164. (Impact factor: 4.829 and SNIP: 2.035)

DOI: <https://doi.org/10.1016/j.compstruct.2019.01.096>

The third manuscript presents the effect of reinforcement ratio (ρ) on the behavior of HCCs under concentric compressive load. To achieve HCCs with different ρ , the

number and diameter of the longitudinal GFRP bars were varied. Test results from this study were analysed and compared based on the failure mode, load-deformation capacity, strain behavior of the GFRP reinforcements, ductility, and axial strength and confinement efficiency. A new analytical model for the compressive strength of the GFRP bars was also developed. The significant outcome and findings from the second and third manuscripts concluded the effective use of longitudinal GFRP bars as internal reinforcements for HCCs. This reinforcement enhanced the overall behavior and overcame the brittle failure behavior exhibits by the steel-reinforced HCCs.

Manuscript 4: Omar AlAjarmeh, Allan Manalo, Brahim Benmokrane, Warn Karunasena, and Priyan Mendis, (2019) “Effect of spiral spacing and concrete strength on behavior of GFRP-reinforced hollow concrete columns” Composite for Constructions Journal, vol. 24, issue 1. (Impact Factor: 2.592 and SNIP: 1.811)
DOI: [10.1061/\(ASCE\)CC.1943-5614.0000987](https://doi.org/10.1061/(ASCE)CC.1943-5614.0000987)

The fourth manuscript presents the investigation on the effect of different spacing between the lateral spirals and the effect of four levels of concrete compressive strength on the behavior of GFRP-reinforced HCCs. This study was divided into two parts; (1) the effect of the volumetric ratio, and (2) the effect of concrete compressive strength. For the first part, the influence of lateral reinforcement and the different spacing between GFRP spirals was determined. For the second part, the use of four concrete compressive strength (21.1 MPa, 26.8 MPa, 36.8 MPa, and 44.0 MPa) was assessed. The main experimental variables in these studies were the failure mode, load-deformation behaviour, load-strain behavior of the reinforcements, and the volumetric strain behaviour. From the results of the experimental work, a new model was developed to reliably describe the critical behavior and design strength of the GFRP-reinforced HCCs.

Manuscript 5: Omar AlAjarmeh, Allan Manalo, Brahim Benmokrane, Warn Karunasena, Wahid Ferdous and Priyan Mendis, (2020) “A new design-oriented model of GFRP reinforced hollow concrete columns” ACI Structural Journal, vol 117, No. 2. (Impact factor: 1.197 and SNIP: 1.217)
DOI: [10.14359/51720204](https://doi.org/10.14359/51720204)

The fifth manuscript presents the development of the empirical and analytical models accounting for the effect of the investigated design parameters in the second to fourth manuscripts on the concentric compressive behavior of the GFRP-reinforced HCCs. In this manuscript, a new design-oriented model was generated based on the constitutive material model for GFRP bars and concrete accurately and reliably describe the load-strain behavior of the GFRP-reinforced HCCs. This new model can safely and precisely predict the behavior of GFRP-reinforced HCCs with different (i/o) ratio, ρ , ρ_v , and f'_c under concentric compressive load.

Summary

Hollow concrete columns (HCCs) have higher strength- and stiffness-to-weight ratios than the solid concrete columns (SCCs) of the same cross-section area. However, the behavior of steel-reinforced HCCs are affected by many critical design parameters and their failure behavior is governed by either the brittle crushing failure of the inner concrete wall or yielding of the longitudinal steel bars. Corrosion of steel reinforcements is also a major issue in steel-reinforced HCCs. Glass fibre reinforced polymer (GFRP) reinforcements can provide a non-corrosive reinforcement to HCCs and can potentially eliminate the brittle behavior of the steel-reinforced HCCs due to their high strength and linear elastic behavior up to failure. Understanding the behavior of this new construction system is the main motivation of this research.

References

- Abdul-Salam, B., Farghaly, A. S., and Benmokrane, B. (2016). "Mechanisms of shear resistance of one-way concrete slabs reinforced with FRP bars." *Construction and Building Materials*, 127, 959-970.
- Aboutaha, R. (2004). "Guide for maintenance, and rehabilitation of concrete bridge components with FRP composites-research into practice." *TIRC & NYSDOT, NY, USA*.
- Benmokrane, B., Manalo, A., Bouhet, J.-C., Mohamed, K., and Robert, M. (2017). "Effects of Diameter on the Durability of Glass Fiber-Reinforced Polymer Bars Conditioned in Alkaline Solution." *Journal of Composites for Construction*, 21(5), 04017040.
- Elchalakani, M. (2016). "Rehabilitation of corroded steel CHS under combined bending and bearing using CFRP." *Journal of Constructional Steel Research*, 125, 26-42.
- Hadi, M. N., Karim, H., and Sheikh, M. N. (2016). "Experimental investigations on circular concrete columns reinforced with GFRP bars and helices under different loading conditions." *Journal of Composites for Construction*, 20(4).
- Hoshikuma, J., and Priestley, M. (2000). "Flexural behavior of circular hollow columns with a single layer of reinforcement under seismic loading." *SSRP*, 13.
- Kusumawardaningsih, Y., and Hadi, M. N. (2010). "Comparative behaviour of hollow columns confined with FRP composites." *Composite Structures*, 93(1), 198-205.
- Lee, J.-H., Choi, J.-H., Hwang, D.-K., and Kwahk, I.-J. (2015). "Seismic performance of circular hollow RC bridge columns." *KSCE Journal of Civil Engineering*, 19(5), 1456-1467.
- Li, J., Gong, J., and Wang, L. (2009). "Seismic behavior of corrosion-damaged reinforced concrete columns strengthened using combined carbon fiber-reinforced polymer and steel jacket." *Construction and Building Materials*, 23(7), 2653-2663.

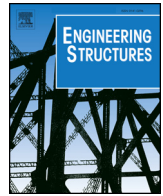
- Liang, X., Beck, R., and Sritharan, S. (2015). "Understanding the Confined Concrete Behavior on the Response of Hollow Bridge Columns."
- Lignola, G. P., Prota, A., Manfredi, G., and Cosenza, E. (2007). "Experimental performance of RC hollow columns confined with CFRP." *Journal of Composites for Construction*, 11(1), 42-49.
- Manalo, A., Benmokrane, B., Park, K.-T., and Lutze, D. (2014). "Recent developments on FRP bars as internal reinforcement in concrete structures." *Concrete in Australia*, 40(2), 46-56.
- Mander, J. B. (1983). "Seismic design of bridge piers."
- Maranan, G., Manalo, A., Benmokrane, B., Karunasena, W., Mendis, P., and Nguyen, T. (2019). "Flexural behavior of geopolymer-concrete beams longitudinally reinforced with GFRP and steel hybrid reinforcements." *Engineering Structures*, 182, 141-152.
- Mo, Y., Wong, D., and Maekawa, K. (2003). "Seismic performance of hollow bridge columns." *Structural Journal*, 100(3), 337-348.
- Mohamed, N., Farghaly, A. S., Benmokrane, B., and Neale, K. W. (2014). "Experimental investigation of concrete shear walls reinforced with glass fiber-reinforced bars under lateral cyclic loading." *Journal of Composites for Construction*, 18(3), A4014001.
- Nkurunziza, G., Debaiky, A., Cousin, P., and Benmokrane, B. (2005). "Durability of GFRP bars: a critical review of the literature." *Progress in structural engineering and materials*, 7(4), 194-209.
- Osada, K., Yamaguchi, T., and Ikeda, S. (1999). "Seismic performance and the strengthening of hollow circular RC piers having reinforced cut-off planes and variable wall thickness." *Concrete Res. and Tech*, 101, 13-24.
- Pantelides, C. P., Gibbons, M. E., and Reaveley, L. D. (2013). "Axial load behavior of concrete columns confined with GFRP spirals." *Journal of Composites for Construction*, 17(3), 305-313.
- Pavese, A., Bolognini, D., and Peloso, S. (2004). "FRP seismic retrofit of RC square hollow section bridge piers." *Journal of earthquake engineering*, 8(spec01), 225-250.
- Pinto, A., Molina, J., and Tsionis, G. (2003). "Cyclic tests on large-scale models of existing bridge piers with rectangular hollow cross-section." *Earthquake engineering & structural dynamics*, 32(13), 1995-2012.
- Ranzo, G., and Priestley, M. N. (2001). *Seismic performance of circular hollow columns subjected to high shear*, Structural Systems Research Project, University of California, San Diego.
- Tobbi, H., Farghaly, A. S., and Benmokrane, B. (2014). "Behavior of concentrically loaded fiber-reinforced polymer reinforced concrete columns with varying reinforcement types and ratios." *ACI Structural Journal*, 111(2), 375.
- Whittaker, D. (1987). "Seismic performance of offshore concrete gravity platforms."
- Yeh, Y.-K., Mo, Y., and Yang, C. (2001). "Seismic performance of hollow circular bridge piers." *Structural Journal*, 98(6), 862-871.
- Yeh, Y.-K., Mo, Y. L., and Yang, C. (2002). "Seismic performance of rectangular hollow bridge columns." *Journal of Structural Engineering*, 128(1), 60-68.
- Zahn, F. (1986). "Design of reinforced concrete bridge columns for strength and ductility."

Chapter 2

Hollow concrete columns: Review of structural behavior and new reinforcing design using GFRP reinforcements

The state-of-the-art review of the literature identifies the overall behavior of hollow concrete columns (HCCs) with steel reinforcements and their behavioural differences with solid concrete columns. This article also analyses the behavior of steel-reinforced HCCs under different loading conditions and critically reviews the different design parameters and their effect on the overall behavior of the HCCs. From this review, it was identified that steel-reinforced HCCs normally fail in a brittle manner due to either crushing the inner concrete core or yielding and buckling of the longitudinal steel bars. Moreover, corrosion of the steel bars is a significant issue in HCCs due to the presence of the inner and outer surfaces, which can reduce the performance of HCCs and damage the whole structure.

Glass fibre reinforced polymer (GFRP) composite bars were identified as an effective alternative to steel bars due to their non-corrosive and high tensile strength. This type of reinforcements has successfully implemented in different concrete structural elements including beams, slabs, walls, and joints. The effective use of GFRP bars in solid concrete columns (SCCs) has been also successfully demonstrated by other researchers. The high strength and strain, and the linear elastic behavior up to the failure of GFRP bars combine with the non-linear behavior of concrete in compression to show the potential of using GFRP reinforcements in HCCs to overcome the performance and durability issues related to using the steel bars as longitudinal reinforcement in HCCs. The effect of the critical design parameters on the compressive behavior of HCCs identified in state-of-the art review was systematically investigated and analysed, where the significant results are presented in Chapters 3 to 5.



Hollow concrete columns: Review of structural behavior and new designs using GFRP reinforcement

O.S. AlAjarmeh^{a,*}, A.C. Manalo^a, B. Benmokrane^b, K. Karunasena^a, W. Ferdous^a, P. Mendis^c

^a University of Southern Queensland, Centre for Future Materials (CFM), School of Civil Engineering and Surveying, Toowoomba 4350, Australia

^b University of Sherbrooke, Department of Civil Engineering, Sherbrooke, Quebec, Canada

^c The University of Melbourne, Department of Infrastructure Engineering, Victoria 3010, Australia

ARTICLE INFO

Keywords:

Hollow concrete column
Axial-load ratio
Inner-to-outer diameter ratio
Steel
GFRP
Ductility
Confined strength

ABSTRACT

Hollow concrete columns (HCCs) reinforced with steel bars have been employed extensively for bridge piers, ground piles, and utility poles because they use fewer materials and offer higher structural efficiency compared to solid concrete columns with the same concrete area. Many experimental studies have been conducted to investigate the behavior of HCCs under different loading conditions and found that the structural performance of HCCs is critically affected by many design parameters. If not designed properly, HCCs exhibit brittle failure behavior, due to longitudinal bars buckling or the concrete wall failing in shear. In addition, the corrosion of steel bars has become an issue in reinforced-concrete structures. Therefore, this paper critically reviews the different design parameters that affect the performance of HCCs and identifies new opportunities for the safe design and effective use of this construction system. Moreover, the use of GFRP bars as reinforcement in hollow concrete columns is explored with the aim of developing a non-corroding and structurally reliable construction system.

1. Introduction

Steel-reinforced hollow concrete columns (HCCs) have been used for bridge piers, piles, and utility poles due to their enhanced structural efficiency and their higher strength- and stiffness-to-mass ratios than solid concrete columns (SCCs) with the same cross-section area [1,2]. Creating a hollow section reduces the amount of materials used in the columns and minimizes the self-weight, thereby leading to an efficient construction system. The structural behavior of HCCs with steel reinforcement under different loading conditions has been extensively investigated [1–15]. This type of column is profoundly affected by several design parameters, including the axial-load ratio ($\frac{R_b}{f_c A_c}$) (the ratio between the applied and ultimate axial-load capacities) [3,4], inner-to-outer diameter (i/o) ratio [5,6], reinforcement ratio (ρ) [7,8], volumetric ratio (ρ_v) [9,10], concrete compressive strength (f_c') [11,12], aspect ratio (AR) [13,14], and geometry (G) [2,15]. These parameters were found more critical in HCCs than the SCCs, owing to the lack of concrete confinement in HCCs compared to SCCs, which leads to crushing of the inner concrete wall and brittle failure.

HCCs have low deformation capacity [14] and experience a sudden

reduction in strength [2] resulting in brittle failure behavior. This behavior is normally caused by defective design resulting in the buckling of the reinforcement due to insufficient reinforcement details or crushing of the inner unconfined concrete wall as a result of inadequate concrete strength. The brittle failure of HCCs is also caused by the yielding of longitudinal bars. At this point, the reinforcement can no longer resist, leading to overstressing and crushing of the unconfined concrete wall. Whittaker [5] reported that HCCs with steel reinforcement can be detailed appropriately if the longitudinal bars are held by the concrete wall and confined by lateral reinforcement until failure. Therefore, the design parameters should be carefully considered to ensure HCCs are functional and sustainable, and fail in a ductile manner. The corrosion of steel reinforcement is also becoming a significant challenge with steel-reinforced SCCs and HCCs. The problem is more critical with HCCs than SCCs because their outer and inner surfaces expose more concrete surface area. Therefore, there is a need to explore non-corroding reinforcing options that can overcome the limited strain and strength capacities of HCCs.

Glass fiber-reinforced polymer (GFRP) composite bars have been successfully used as internal reinforcement in concrete structures given

* Corresponding author.

E-mail addresses: omar.alajarmeh@usq.edu.au (O.S. AlAjarmeh), Allan.Manalo@usq.edu.au (A.C. Manalo), Brahim.Benmokrane@USherbrooke.ca (B. Benmokrane), Karu.Karunasena@usq.edu.au (K. Karunasena), Wahid.Ferdous@usq.edu.au (W. Ferdous), Pamendis@unimelb.edu.au (P. Mendis).

<https://doi.org/10.1016/j.engstruct.2019.109829>

Received 10 August 2019; Received in revised form 16 October 2019; Accepted 18 October 2019

0141-0296/ © 2019 Elsevier Ltd. All rights reserved.

their many superior mechanical and environmental-resistance properties [16]. Examples are as reinforcement in concrete beams [17,18], slabs [19,20], and walls [21,22], because their high strength and modulus of elasticity is almost similar to that of concrete. Recently, GFRP bars have also been used as reinforcement in concrete columns [23–36]. Accordingly, concrete columns with longitudinal and transverse GFRP reinforcement under axial loads have been shown to have better performance and more stable behavior than their steel-reinforced counterparts after the concrete's peak strength has been reached. This can be attributed to the high strength and linear elastic behavior of GFRP longitudinal and transverse reinforcement, which continue to resist axial and lateral loads, respectively, until failure without any reduction in their stiffness. Very recently, a study [37] investigated comprehensively the behavior of the GFRP bars under compression, where it predicted the mode of failure and the maximum compressive strength of these bars based on the diameter and the length counting for the low modulus of elasticity of such bars. Because of this behavior, GFRP bars have the potential to overcome the brittle behavior of steel-reinforced HCCs.

This study reviews the state-of-the-art in HCCs to identify the effect of the main design parameters influencing the structural behavior of HCCs and determines the general structural issues associated with steel-reinforced HCCs. Moreover, this review study addresses the challenges affecting the durability and sustainability of the existing steel-reinforced concrete columns. In addition, the fundamental behavior of concrete columns internally reinforced with glass fiber-reinforced polymer (GFRP) bars is analyzed to explore the potential of using these materials to overcome the structural and environmental issues of steel-reinforced HCCs.

2. HCC behavior and design parameters

2.1. Comparison of steel-reinforced solid and hollow concrete columns

HCC behavior is affected by a number of design parameters. The displacement capacity and the strength after steel yielding in HCCs are generally low due to the unconfined concrete core. This can be explained by the differences in stress distribution in SCCs and HCCs. The SCC cross section subjected to axial stress (σ_{axial}) tends to expand laterally from the center to release the stored energy. The confining stress induced by the lateral reinforcement, however, acts to prevent the SCCs from failure, initiating in-plane stress in the circumferential (σ_{circ}) and radial (σ_{rad}) directions, as shown in Fig. 1a. In this case, the section is subjected to three types of stress (triaxial stress state). Since HCCs have no inner concrete core, lateral expansion caused by axial stress (σ_{axial}) can result in nonuniform lateral confining stress as there will be no σ_{rad} resisting the σ_{circ} in the concrete wall (Fig. 1b). In that case, the section is subjected to biaxial stress. These internal stresses act in the cross section to provide resistance to the applied loads. The effect of triaxial and biaxial stresses becomes critical if the outer surface of the concrete section is confined to prevent lateral expansion. Otherwise, concrete crushing will occur because of the brittleness of the concrete. Based on the definition of both stress formations, triaxial stress can lead to higher confined strength values than biaxial stress due to the former's higher lateral confinement. Past research [38] found that both solid and hollow confined concrete columns showed almost the same axial strain at failure, but the SCCs had lateral expansion 4 times greater than the HCCs (Fig. 2a). It should be mentioned that this ratio is limited to this experimental study but the behavior behind that is due to the discontinuity in the radial stress inside the concrete core of the HCCs owing to the hollowness. Liang and Sritharan [39] explained that the lateral expansion of concrete increases as the concrete wall thickness increases and converges on that of SCCs (see Fig. 2b). This means that, unless SCCs have high lateral stiffness to confine the concrete, high axial-deformation capacity cannot be achieved and early failure can be expected. On the other hand, the concrete wall of the HCC has to be

thick enough (at least 10% of the outer diameter) to prevent the concrete from failing in shear [8,40].

2.2. Experimental investigations on steel-reinforced HCCs

A comprehensive review of the experimental works on HCCs was conducted and is summarized in Table 1. The review was limited to HCCs with steel reinforcement or plain concrete without inner confinement of the concrete core. Table 1 presents the studies by publication year and loading conditions. The detailed design parameters for the experimental samples are then reported such as the axial-load ratio ($\frac{P_o}{f'_c A_c}$) (the ratio between the applied axial load to the maximum axial load capacity), geometry of the cross section (G), height of samples (H), the outer diameter of the circular section (o) or the outer dimensions of the square and rectangular sections (OD), the inner diameter of the circular section (i) or the outer dimensions of the square and rectangular sections (ID), the inner-to-outer diameter (i/o) ratio, reinforcement ratio (ρ), number of longitudinal reinforcement bars (N_L), presence of cross ties (CT), volumetric ratio (ρ_v), concrete compressive strength (f'_c), circular column (C), square column (S), rectangular column (R), yes (Y), no (N), both (B), and the design parameters of the experimental study.

A statistical study was conducted on the information presented in Table 1 to illustrate the cumulative percentage of the experimental studies on HCCs published from 1983 to 2018 (Fig. 3). Fig. 3 shows that research focusing on HCCs has significantly increased in the last two decades, underscoring the structural importance and effectiveness of such systems for structural columns. These experimental studies can be divided into four regions. Period A (1983–1997) consists of the first attempts at investigating HCCs by identifying their behavior and capacity according to some design parameters such as axial-load ratio ($\frac{P_o}{f'_c A_c}$), i/o ratio, and volumetric ratio (ρ_v). Period B (1998–2005) witnessed a significant increase in the number of experimental studies exploring the effect of other design parameters—such as reinforcement ratio (ρ), geometry (G), and aspect ratio (AR)—to gain a greater understanding of HCC behavior. Experimental studies in Period C (2006–2011) included the incorporation of new techniques to improve HCC behavior, such as wrapping the column with carbon-fiber sheets. Significant field testing began after 2012 (Period D), exploring with new approaches and techniques such as changing the lateral-reinforcement configuration and increasing the reinforcement ratio by providing double layers of longitudinal reinforcement. Inserting double skin (outer and inner) tubes and externally wrapping with composite materials were also attempted. For a review and discussion of these techniques, see Al-Saadi et al. [67] and Han et al. [68].

As presented in Fig. 4, most of the studies (63%) adopted the hysteretic type of loading to investigate HCC behavior. This type of loading has been primarily adopted for HCCs because axial and lateral cyclic loads are the loading requirements for designing bridge piers. The second-most frequent loading type investigated (24%) focused on HCC axial behavior. This is because as it was found that the axial-load ratio applied during hysteretic load tests significantly affected HCC overall behavior. Cyclic and monotonic lateral loading, bending, and shear accounted for 7%, 3%, and 3%, respectively, of the total experimental studies. They were investigated as they are the loading conditions that HCCs are subjected to when used as slender columns and electric poles.

Geometry is another important factor in HCC design as it affects the stress distribution within the column cross section. Square and rectangular sections create a nonuniform stress state, leading to localized stress concentration, whereas circular sections provide uniform stress within the column [3]. Correspondingly, most of the HCCs investigated had circular cross sections (45% of the total cross sections tested), as shown in Fig. 4b. To evaluate the effectiveness of HCCs in concrete bridge piers, Mander [3], Yeh et al. [9], and Mo et al. [12,42] investigated square HCCs. For the same reason, Pinto et al. [13], Delgado

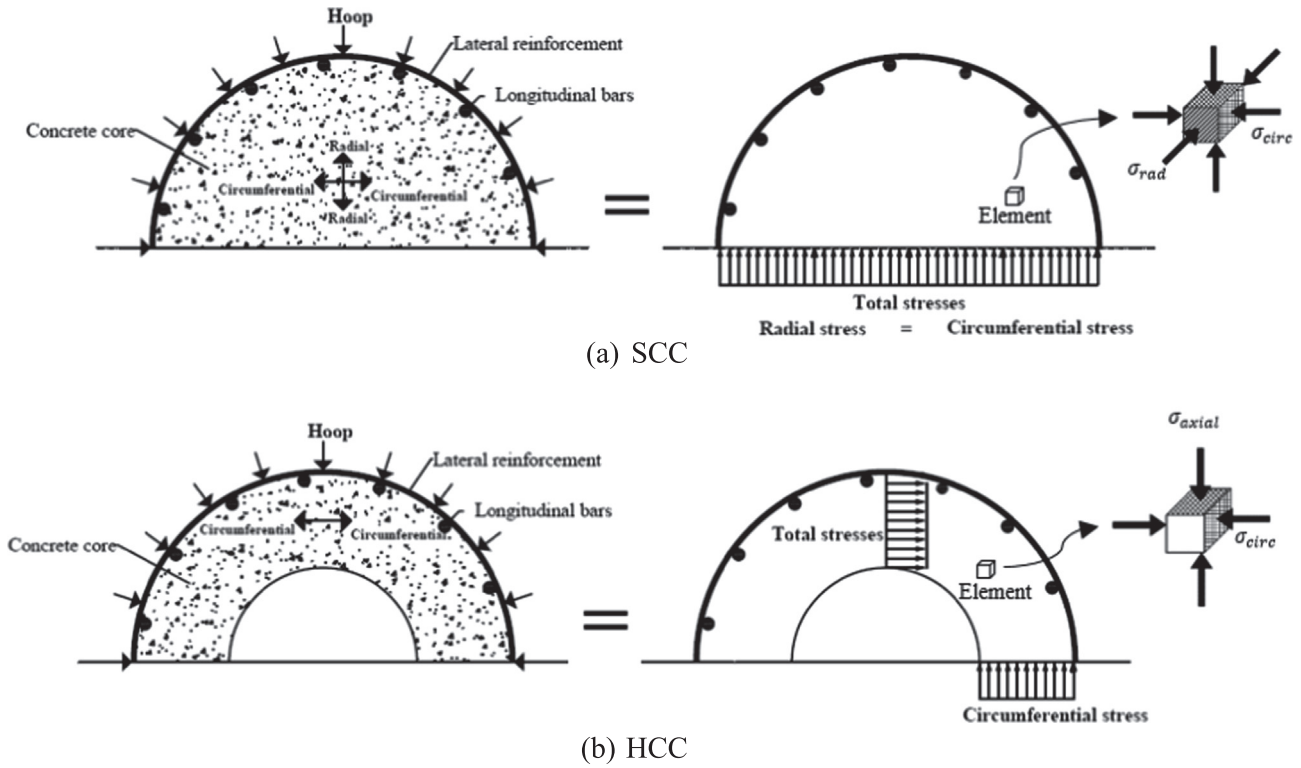


Fig. 1. Stress formation within the concrete core of SCC and HCC.

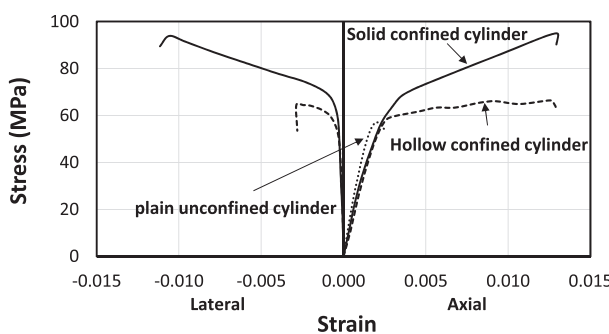
et al. [47], and Kim et al. [51] investigated rectangular HCCs to increase HCC rigidity in the main loading direction. Out of the published studies on HCCs, 29.0% involved square sections, compared to 26.0% with rectangular cross sections.

Critical design parameters affecting overall HCC behavior were also analyzed (see Fig. 5). As most HCCs were tested under hysteretic loads, the axial-load ratio ($\frac{P_0}{f_c A_c}$) would be expected to be the parameter most studied, as this represents the applied load under combined axial and lateral cyclic loading. Studies involving this parameter comprised 21.6% of the total number of studies. It should be mentioned that the axial load in some studies that adopted hysteretic loading [41,66] was achieved by adding prestressed reinforcement instead of an externally applied axial load. The second-most investigated parameter was volumetric ratio (ρ_v) (20.3% of the total number of studies). This design parameter was investigated either by increasing the diameter of the steel ligatures or decreasing the spacing between them. Some studies manipulated the arrangements of the lateral reinforcement [12,53] by tying together two layers of longitudinal reinforcement

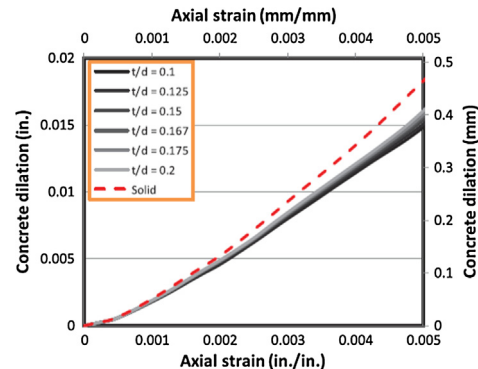
[9,10,12,42,51,53]. A number of experimental studies were implemented to increase HCC stiffness and compensate for the absence of an inner concrete core by increasing the reinforcement ratio (ρ). Increasing ρ can be achieved by either increasing the diameter or the number of longitudinal bars. Studies on this parameter comprise 13.3% of the total studies reported in Table 1. Studies have shown that HCCs have to have adequately thick wall to prevent premature shear failure and minimize compression failure in the concrete core. Therefore, the effect of the i/o ratio was studied in 12.0% of the total reported studies. Other design parameters investigated were f'_c , aspect ratio, and geometry, comprising 12.0%, 10.7%, and 10.7%, respectively, of the total reported studies.

2.3. Influence of the critical design parameters on HCCs

The critical design parameters based on the priority in Fig. 5 (ρ_v , ρ , i/o , and f'_c) were analyzed in detail to evaluate their effects on HCC behavior. The ($\frac{P_0}{f_c A_c}$) ratio was taken as equal to 1.0 (full axial load) to



(a) Stress-strain behavior [38]



(b) Lateral concrete dilation [39]

Fig. 2. Behavioral comparison of HCCs and SCCs.

Table 1
Review of past experimental studies conducted on HCCs.

Study number	Author	Year	Loading Type	$\frac{f_{b,c}}{f_{c,A_c}}$	G	H (mm)	(o) or OD (mm)	(i) or ID (mm)	i/oratio (%)	ρ (%)	N _L	CT	ρ_v (%)	f_c (MPa)	Design Parameter
1	Mander [3]	1983	Hysteretic	0.1 0.3 0.6	S	3200	750 × 750	510 × 510	0.68	1.55	2	Y	1.72, 1.29, 0.86	30.0	$\frac{f_{b,c}}{f_{c,A_c}}, \rho_v$
2	Zhan [4]	1986	Hysteretic	0.05–0.28	C	1600	400	212 250 290	0.53 0.63 0.73	2.56	1	–	1.13–1.36	29.6	$\frac{f_{b,c}}{f_{c,A_c}}, \rho_v, i/o$ ratio
3	Whittaker [5]	1987	Hysteretic	0.125 0.3	C	3150	800	600 700	0.75 0.88	2.29 2.88	2	Y	1.38– 2.37	35.0	$\frac{f_{b,c}}{f_{c,A_c}}, \rho_v, \rho, i/o$ ratio
4	Kishida et al. [41]	1998	Hysteretic	–	C	900	300	180 225	0.60 0.75	1.41 1.66	1	–	–	93.5	$\frac{f_{b,c}}{f_{c,A_c}}, \rho_v, \rho, i/o$ ratio
5	Osada et al. [111]	1999	Hysteretic	0.040	C	1800	350	150	0.43	3.4	1	–	0.14	23.5	$f_c, wrapping$
6	Hoshikuma and Priestely [7]	2000	Hysteretic	0.13	C	3480	1524	1244	0.82	1.45	1	–	0.71	45.0	ρ
7	Ranzo and Priestely [8]	2001	Hysteretic	0.05 0.15	C	3880	1560 1524	152 139	0.81 0.82	3.18 2.25	1	–	0.35	35.0	$\frac{f_{b,c}}{f_{c,A_c}}, \rho$
8	Fam and Rizkalla [38]	2001	Axial	Full	C	336	219	95 133	0.49 0.68	N/A	1	–	8.96 6.40	58.0	i/oratio, wrapping
9	Yeh et al. [9]	2001	Hysteretic	0.10	C	5500	1500	900	0.60	2.15	2	Y	0.28–0.625 0.185	32.1	ρ_v
10	Yeh et al. [10]	2002	Hysteretic	0.082–0.176	S	6500 4500	1500 × 1500	900 × 900	0.60	1.7	2	Y	0.01–0.032	32.3	$\frac{f_{b,c}}{f_{c,A_c}}, \rho_v$
11	Mo and Nien [42]	2002	Hysteretic	0.054–0.132	S	1800	500 × 500 500 × 500	260 × 260 260 × 260	0.52 0.52	1.9 2.07	2	Y	0.44–1.36	58.7	$\frac{f_{b,c}}{f_{c,A_c}}, \rho_v, AR$
12	Mo et al. [12]	2003	Hysteretic	0.06 0.19	S	2000	500 × 500	300 × 300	0.60	1.13	2	Y	0.49–0.98	24.6–49.9	$\frac{f_{b,c}}{f_{c,A_c}}, \rho_v, f_c$
13	Pinto et al. [13]	2003	Hysteretic	0.09	R	5750 13,250	2740 × 1020	2320 × 680	0.72	0.4	2	N	0.09	38.9	AR
14	Pavese et al. [14]	2004	Hysteretic	0.06 0.19	S	900 1350	450 × 450	300 × 300	0.67	1.07 1.76	2	Y	0.13 0.25	51.6 33.0	$\frac{f_{b,c}}{f_{c,A_c}}, AR, wrapping$
15	Calvi et al. [43]	2005	Hysteretic	0.06–0.21	S	900 1350	450 × 450	300 × 300	0.67	1.07	2	N	0.13 0.25	32.5	$\frac{f_{b,c}}{f_{c,A_c}}, AR$
16	Modarelli et al. [44] and Micelli and Modarelli [45]	2005, 2013	Axial	1.0	C	300 500	150 250	50 150	0.33 0.60	–	–	–	–	28.0 38.0	$f_c, G, wrapping$
17	Yeh and Mo [46]	2005	Hysteretic	0.08–0.19	C	3500	1500 1500 × 1500	900 900 × 900	0.60 0.60	1.69 2.15	2	Y	0.64 0.71	18.0 31.0	$\frac{f_{b,c}}{f_{c,A_c}}, f_c, wrapping$
18	Lignola et al. [1]	2007	Axial	1.0	S	3020	360 × 360	240 × 240	0.67	1.75	1	–	0.26	32.0	Wrapping
19	Delgado et al. [47]	2008	Hysteretic	0.063 0.070	S	1600	450 × 450	300 × 300	0.67	1.79	1	–	0.075	35.0	G, wrapping
20	Turno et al. [48]	2009	Shear	0	C	3000	900 × 450 600	750 × 300 400	0.75 0.67	2.4	1	–	0.15	24.7	f_c
21	Kusumawardaningsih and Hadi [2]	2010	Axial	1.0	C	925	205 182 × 182	69 61 × 61	0.34 0.33	2.32	1	–	2.95	72.0	G, wrapping
22	Lignola et al. [49]	2011	Axial	1.0	R	3050	737 × 508	509 × 280	0.62	1.77	1	–	0.29	44.7	Wrapping
23	Yazici [50]	2012	Axial	1.0	C	500 885	150	56	0.37	3.5	1	–	2.41	76.5	AR, wrapping

(continued on next page)

Table 1 (continued)

Study number	Author	Year	Loading Type	$\frac{f_b}{f_c A_c}$	G	H (mm)	(o) or OD (mm)	(i) or ID (mm)	l/o ratio	ρ (%)	N _L	CT	ρ_p (%)	f_c (MPa)	Design Parameter
24	Kim et al. [51]	2012	Monotonic lateral and pure cyclic	0	R	900–1800	900 × 600	540 × 400 640 × 340 740 × 440 750	0.63 0.63 0.78 0.50	1.8 2.7 0.83–2.00	1	–	0	24.6	ρ , l/o ratio, AR
25	Cheon et al. [52]	2012	Hysteretic	0.065–0.15	C	3500	1000	500 750	0.75 0.50	0.83–2.00	1	–	0.60 1.20	32.5	$\frac{f_b}{f_c A_c}$, ρ_v , ρ , l/o ratio
26	Kim et al. [53]	2013	Axial	1.0	C	1000	1990	1590	0.80	1.2	2	Y	0.36	27.0	ρ_v , G
27	Han et al. [54]	2013	Hysteretic	0.1	R	600	540 × 150*	–	–	1.8	2	Y	0.84	21.0	ρ_v , G
28	Zhang et al. [55]	2013	Hysteretic	0.2	R	1400	550 × 360	260 × 120	0.42	1.4	2	Y	2.50	42.6	$\frac{f_b}{f_c A_c}$, ρ_v , ρ
29	Shin et al. [56]	2013	Monotonic lateral and pure cyclic	0.1	R	1240	500 × 360	300 × 160	0.52	2.1 1.40	1	–	0.72	38.7 43.8	f_c
30	Hadi and Le [57]	2014	Axial	1.0	S	800	200 × 200	80 × 80	0.40	1.35	1	–	0.94	40.0	Wrapping
31	Han et al. [58]	2014	Hysteretic	0.2	R	1400	2800	330 × 130	0.47	1.05	2	Y	0.49	30.4	AR, wrapping
32	Volgyi et al. [59]	2014	Shear and flexure	0	C	3000	300	55	0.18	1.92–2.56	1	–	0.21–0.46	60.0	ρ , l/o ratio, ρ_v , f_c
33	Kim et al. [60]	2014	Hysteretic	0.1	C	4900	1400	1000	0.71	1.30–1.53	2	Y	0.09–1.0	75.0 22.0	ρ_v , ρ , G
34	Liang et al. [15]	2015	Hysteretic	0.03–0.20	S	1200	1000 × 1000	500 × 500	0.50	1.56	1	–	1.80	46.8	$\frac{f_b}{f_c A_c}$, l/o ratio, G
35	Lee et al. [6]	2015	Hysteretic	0.065–0.15	C	4000	1000	500 750 980	0.80 0.5 0.75	0.83–2.00	1	–	0.69 1.38	32.5	$\frac{f_b}{f_c A_c}$, ρ_v , ρ , l/o ratio
36	Prado et al. [61]	2016	Hysteretic	0.08 0.125	R	5400	1400	150	0.7	1.0	2	B	0.19–0.38	27.5	ρ_v
37	Cassese et al. [62]	2017	Hysteretic	0.06	R	4500	1200 × 800	400 × 200	0.68	2.79	2	Y	0.01–0.02	26.9	AR
38	Jameel et al. [63]	2017	Axial	0.05	R	900	600 × 400	35 × 35	0.58	0.88	1	–	0.12	17.0	G
39	Hadi et al. [64]	2017	Axial	1.0	C	300	106 × 106	50 × 50	0.33	–	–	–	–	45.0	G
40	Cassese et al. [65]	2018	Hysteretic	1.0	C	800	212	350	0.27	1.28	1	–	2.00	47.0	G
41	Irawan et al. [66]	2018	Hysteretic	0.05	S	800	150 × 150	200	0.33	2.26	1	–	0.06	15.6	AR
				0.08 0.16	C	1100 1650	400	200	0.64	0.85	1	–	0.16	54.4 67.5	$\frac{f_b}{f_c A_c}$, f_c

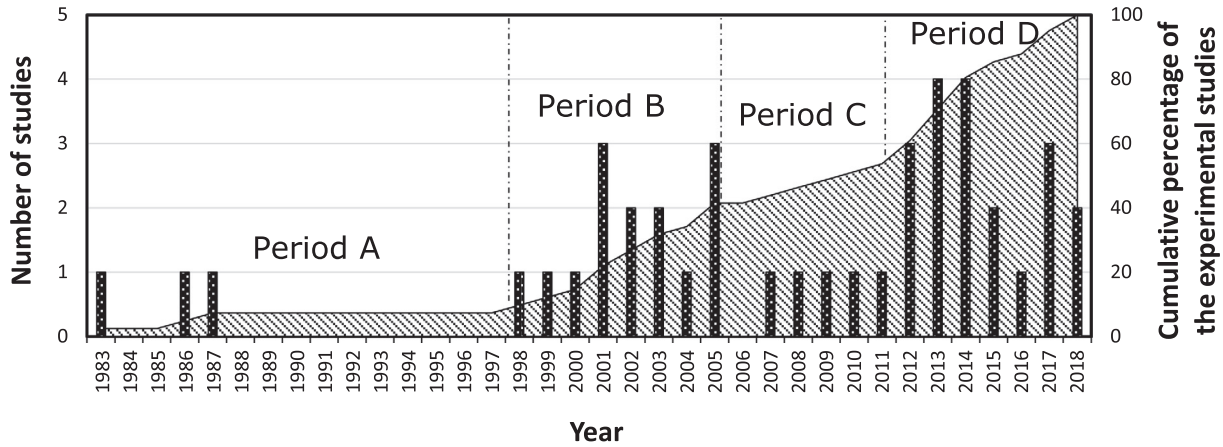


Fig. 3. Cumulative percentages of the experimental studies on HCCs from 1983 to 2018.

eliminate the contribution of the lateral load and the effect of this loading on the behavior of the HCC system. It should be noted that the HCC samples tested under the hysteretic-loading condition were adopted only at maximum lateral displacement as this results in the ultimate compressive stress in the inner concrete wall.

2.3.1. Inner-to-outer diameter (*i/o*) ratio

Increasing the *i/o* ratio reduces the amount of material used and increases the effect of biaxial stress in the cross section of HCCs. The increase in *i/o* ratio decreases the thickness of the inner concrete core, which leads to brittle failure, driven mostly by the shear of the concrete after it reaches its ultimate compressive strength capacity. Referring to Table 1, nine studies considered the *i/o* ratio as a design parameter: five subjected their samples to hysteretic loading; one to cyclic and monotonic lateral load; one to concentric compression; and one to shear loading.

Table 2 gives the influence of the *i/o* ratio under hysteretic load on the ductility, load capacity, and failure mode. The ductility (Δ_u/Δ_y) ratio in the table is the ratio of the ultimate displacement (Δ_u) corresponding to 80% of the maximum load after peak strength to the displacement corresponding to the yielding of the steel bars (Δ_y); the mode of failure is categorized as flexural (F), concrete-core crushing (C), shear (S), or a combination. Accordingly, the higher *i/o* ratio resulted in failure that was less ductile and in lower lateral load capacity than HCCs with low *i/o* ratios. This parameter is, however, also affected by other design parameters such as ($\frac{P_o}{f_c A_c}$) ratio, ρ_v , ρ , and f'_c . These findings can be seen in the change in failure mode when the higher *i/o* ratio (thickness reduction of the inner concrete core) led to concrete-core

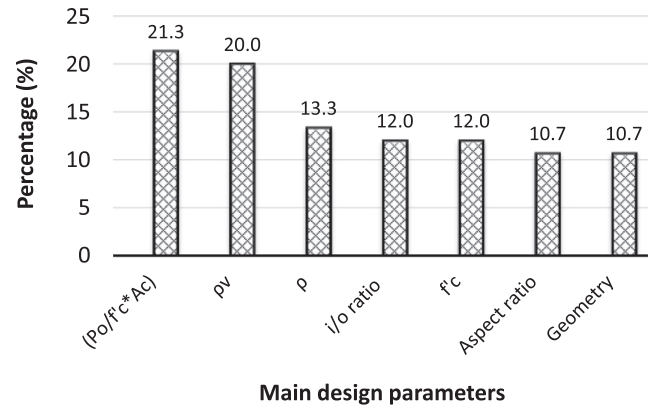


Fig. 5. Critical design parameters for HCCs.

crushing or shear failure (see Table 2). There is an inverse relationship between the thickness of the concrete wall and the concrete core achieving its ultimate compressive strength. Therefore, it can be concluded from Table 2 that failure was governed by flexure in the HCCs with adequately thick concrete cores (*i/o* ratios of up to 0.6). At higher *i/o* ratios (0.6 to 0.8), the mode of failure shifted from flexural to concrete-wall crushing due to the lower capacity of the thin core to resist the applied load. Shear failure will always occur in HCCs with *i/o* ratios of more than 0.8 when high amounts of lateral reinforcement (ρ_v) is provided. Conversely, the failure would occur as concrete-core crushing. Furthermore, Zahn [4] reported the mechanism of the HCCs under eccentric and flexural loads by that the increase in the concrete

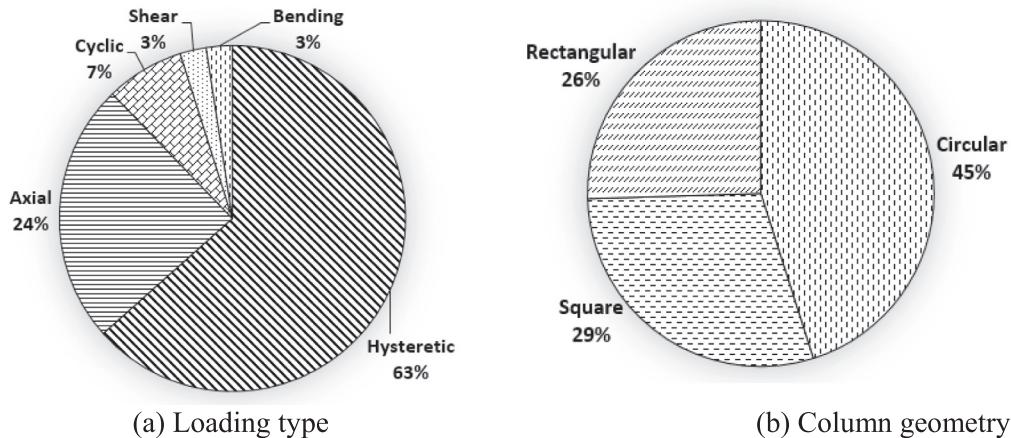


Fig. 4. Distribution of studies on HCCs based on loading conditions and geometric configurations.

Table 2
Effect of i/o ratio on ductility and load capacity.

Study Number	Authors	i/o ratio	Δ_u/Δ_y	Load Capacity (kN)	Mode of Failure
2	Zahn [4]	0.53	12.4	225	F
		0.63	5.2	221	F-C
		0.73	4.6	211	F-C
3	Whittaker [5]	0.75	12.0	440	F-C
		0.88	2.5	260	C
4	Kishida et al. [11]	0.60	5.5	370	F
		0.75	3.4	325	C
24	Kim et al. [51]	0.63	1.9	522	F-S
		0.78	1.6	337	S
25	Cheon et al. [52]	0.50	7.4	642	F
		0.75	3.7	596	F-C
34 & 35	Liang et al. [15] and Lee et al. [6]	0.67	5.2	70	F
		0.83	1.9	38	S

wall thickness in HCC resulting in a closer neutral axis to the inner unconfined concrete wall which leads to reduce the longitudinal strain at that part of concrete and shows flexural failure behavior compared to the thinner walled HCC that showed concrete crushing.

Micelli and Modarelli [45] tested hollow plain-concrete columns with i/o ratios of 0.33 and 0.60 under pure concentric load, as detailed in Table 1. They found an insignificant reduction (within the standard deviation of f'_c) in the axial strength for columns with an i/o ratio of 0.33 compared to the solid columns. A 60% reduction in axial strength was, however, observed in the columns with an i/o ratio of 0.60 due to the shear effect, which led to the premature failure of the thinner concrete wall. In the same experiment, hollow plain-concrete columns with i/o ratios of 0.33 and 0.60 confined externally with fully wrapped CFRP sheets were tested. The stress-strain relationship (see Fig. 6a) shows that the increase in i/o ratio from 0.33 to 0.60 increased the strength and strain by 51% and 13%, respectively. Fam and Rizkalla [38] used the same test setup by fully wrapping two hollow plain-concrete columns with i/o ratios of 0.49 and 0.68 with CFRP sheets. The stress-deformation behavior in Fig. 6b shows that 10% and 18% enhancement in the strength and deformation, respectively, were achieved by reducing the i/o ratio from 0.68 to 0.49.

2.3.2. Reinforcement ratio and longitudinal-bar arrangement

Table 1 provides data from 10 studies that evaluated the effect of reinforcement ratio (ρ) on HCC behavior: eight used hysteretic loading; one monotonic lateral loading; and another bending. The main aim of increasing ρ was to increase the strength and compensate for the reduction in stiffness of HCCs due to the lack of concrete core. The

increase in ρ was achieved by increasing the diameter [7,8,54] or the number [6,13] of the longitudinal bars. Table 3 summarizes the effect of increasing ρ on the load capacity and ductility of the HCCs. Note that the load capacity was normalized in Table 3 by dividing the higher on the lower load capacity of the columns tested by each researcher. The test results in Fig. 7a show that the higher ρ increased the load capacity of the HCCs. Fig. 7b also shows a reduction in ductility as a result of increasing ρ due to the severe compression crushing in the inner concrete wall. It should be mentioned that increasing ρ by increasing the number of bars yielded less reduction in ductility than increasing the bar diameter, owing to the increased lateral confinement as more bars were covering the unconfined concrete-core area. Han et al. [54] and Lee et al. [6] also observed this behavior. When the longitudinal bars yielded, the high axial load resisted by the steel reinforcement was directly transferred to the concrete wall, overstressing and crushing the concrete. This mechanism is due to the fact that steel reinforcement significantly losing its stiffness after reaching its yield strain while the concrete is still resisting due to the higher ultimate compressive strain until reaching its peak strength where it starts to fail by crushing.

Several authors [6,9,12,60] changed the arrangement of the longitudinal reinforcement to overcome the brittle failure behavior of HCCs. They reinforced HCCs with two layers of steel bars: one near the outer face and one near the inner face. This approach significantly enhanced the strength and ductility of the HCCs due to the higher confinement efficiency compared to columns with a single layer of longitudinal steel bars, especially when cross ties (CTs) between the two reinforcing layers were provided [6,53]. This kind of design, however, requires more reinforcing materials and increases construction costs.

2.3.3. Volumetric ratio (ρ_v) and spacing between lateral reinforcement

The parameter of volumetric ratio and spacing between lateral reinforcement was the second-most frequently investigated parameter for HCCs (a total of 15 studies). The purpose was to address the limited ductility exhibited by HCCs with low lateral confinement. Thirteen of the 15 studies tested HCCs under hysteretic loading; one under axial loading; and one under flexural loading. It is worthy to mention that the mechanism of providing high volumetric ratio increases the resistance of the lateral reinforcement by confining the concrete core to delay the failure and/or increase the axial strength capacity in advance of the characterized strength. Mander [3] varied the ρ_v , finding that the HCCs behaved in a ductile manner similar to that of solid columns at high ρ_v levels. He also suggested that the increase in ρ_v can be achieved by reducing the spacing between lateral reinforcement or increasing its diameter. Lignola et al. [49] reported that the wide spacing between ligatures resulted in premature HCC failure due to compression crushing of the concrete wall and buckling in the longitudinal

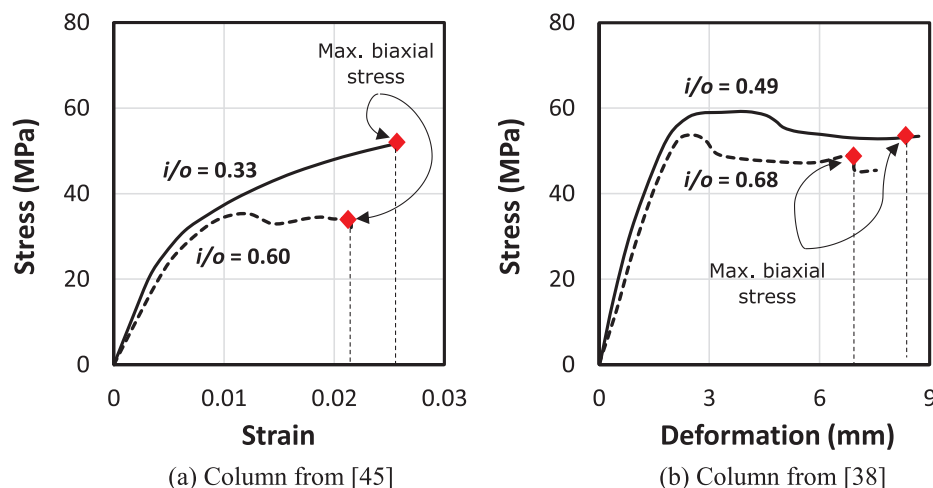


Fig. 6. Stress-strain and deformation of fully wrapped HCCs with different i/o ratios.

Table 3
Effect of ρ on ductility and load capacity.

Study Number	Authors	ρ (%)	Δ_u/Δ_y	Load Capacity (kN)	Normalized Load Capacity
6	Hoshikuma and Priestley [7]	1.45	3.18	4.83	2.34
7	Ranzo and Priestley [8]	1.34	2.25	7.85	4.17
14	Pavese et al. [14]	1.07	1.76	7.17	3.25
27	Han et al. [54]	1.40	2.10	5.40	5.20
35	Lee et al. [6]	1.17	2.00	4.60	3.70

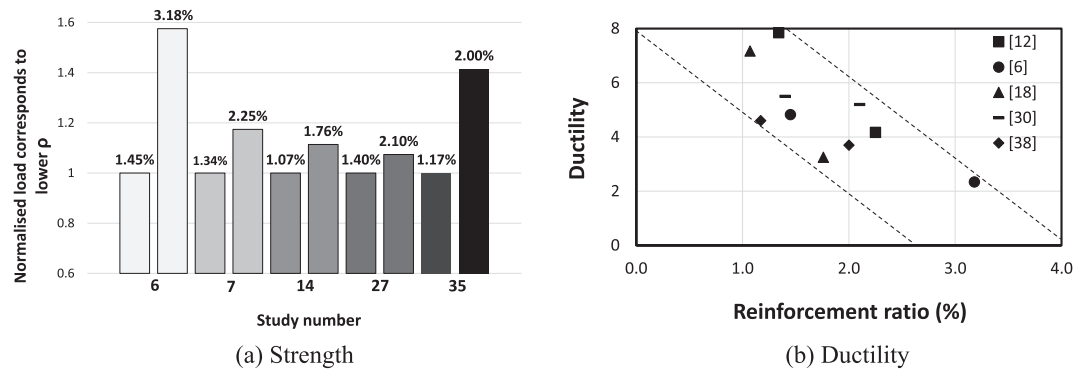


Fig. 7. Effect of ρ on HCC strength and ductility.

Table 4
Effect of ρ_v on ductility and load capacity.

Study Number	Authors	ρ_v (%)	Δ_u/Δ_y	Load Capacity (kN)	Normalized Load Capacity
1	Mander [3]	2.08	3.12	5.92	8.15
3	Whittaker [5]	1.97	2.37	4.07	5.04
9	Yeh et al. [9]	2.80	6.30	2.80	9.00
10	Yeh et al. [10]	1.50	3.20	3.45	5.54
11	Mo and Nien [42]	0.76	1.36	3.90	4.30
25	Cheon et al. [52]	0.60	1.20	6.00	7.40
27	Han et al. [54]	2.50	3.50	3.70	5.20
33	Kim et al. [60]	0.86	1.94	6.10	6.30

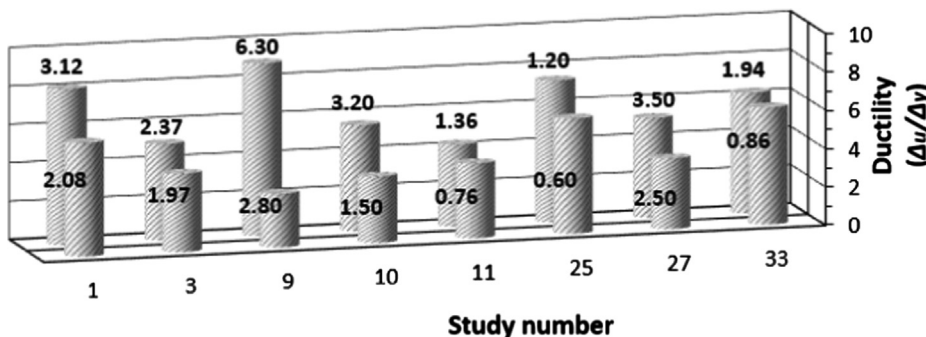


Fig. 8. Effect of increasing ρ_v on HCC ductility.

reinforcement. Table 4 summarizes the test results from the literature showing the effect of ρ_v on ductility and load-carrying capacity of the HCCs. As shown in Fig. 8, the increase in ρ_v generally increased the ductility. The increase in ρ_v by increasing the spacing of the lateral reinforcement [3,9,10] was found to yield higher ductility than did increasing the diameter of the lateral reinforcement [42,60]. This is because reducing the spacing of the lateral reinforcement confined the concrete while increasing the crushing strength of the concrete core and the buckling strength of the longitudinal bars. On the other hand, increasing ρ_v slightly affected the load-carrying capacity. Increasing the lateral confinement yielded no more than an 11% increase in column capacity, except in one study [54] in which the columns were subjected to bilateral instead of unilateral cyclic load.

Some studies compared the behavior of the HCCs with and without external CFRP wrapping [2,14,47,49,50,57,58,64] (denoted in Table 1 as wrapping). Kusumawardaningsih and Hadi [2] fully wrapped the outer surface of steel-reinforced HCCs with CFRP sheets. They found that the fully wrapped columns exhibited deformation capacity and strength more than 100% and 50% higher, respectively, than the unwrapped columns (Fig. 9a). Yazici [50] observed the same enhancement, as shown in Fig. 9b, when the deformation was six times higher and the strength enhanced by more than 80% after wrapping steel-reinforced HCCs with CFRP sheets. This significant enhancement in strength and ductility might be due HCCs having lower lateral expansion than SCCs. This would allow them to resist higher stresses and exhibit more deformation before failure. Fam and Rizkalla [38] also

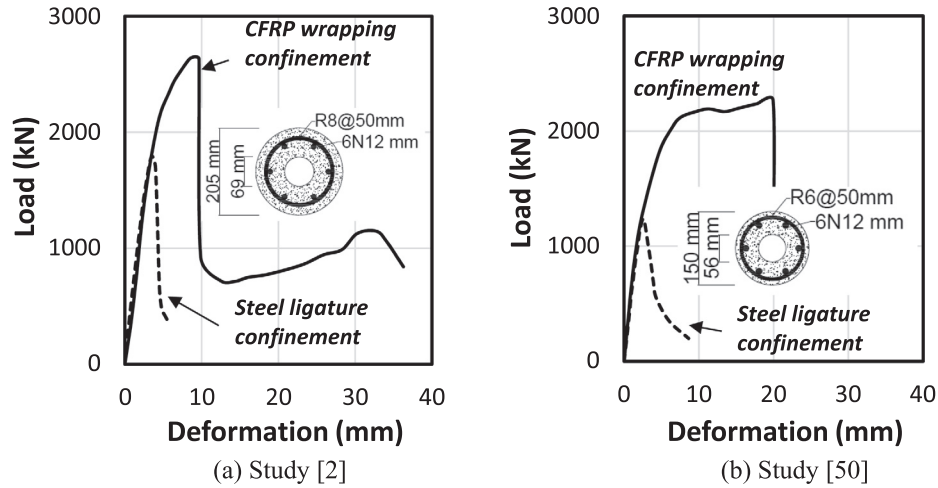


Fig. 9. Effect of providing full confinement to HCCs with CFRP-sheet wrapping [2,50].

observed that the inner face of the hollow concrete underwent tension until reaching the elastic peak strength due to the concrete wall's lateral expansion. Afterwards, inward expansion of the HCC inner face was observed when the stress in the concrete shifted from tension to compression. This means that the section increased in area, which resulted in increased deformations and load capacity.

2.3.4. Concrete compressive strength

Concrete compressive strength (f'_c) plays a major role in the overall behavior of HCCs. Increasing f'_c increases the brittle behavior of the concrete due to the reduction in the Poisson's ratio effect [12,69,70]. This design parameter has been examined nine times, as listed in Table 1. Of these studies, five using different f'_c in HCCs were conducted under hysteretic loading: two under bending and shear loading; one under monotonic lateral loading; and one under concentric compression loading. Mo et al. [12] tested square HCCs under hysteretic loading with different f'_c and observed that the column with a higher f'_c experienced more ductile failure behavior and energy dissipation than the column with a lower f'_c , as shown in Fig. 10a. The more ductile behavior of HCCs with higher f'_c is due to column failure caused by the rupturing of the steel bars with the concrete still intact during cyclic loading. Columns with lower f'_c could not adequately distribute the shear stress caused by the combined axial and lateral loading. This caused in an abrupt drop in strength and produced very large inclined shear cracks, leading to buckling of the longitudinal bars. These findings are supported by Osada et al. [11], who noted higher ductility and lateral-load

resistance in HCCs with higher f'_c . In contrast, the testing of well-confined HCCs made with plain concrete at different f'_c subjected to pure concentric load [45] showed that the columns with higher f'_c (38 MPa) had 44% less deformation and 27% lower confinement effectiveness (σ_{max}/f'_c) than the columns with lower f'_c (28 MPa), as shown in Fig. 10b. The σ_{max} is the maximum confined stress in the cross-section area at the plastic stage (denoted by the solid circles in Fig. 10b). This behavior was due to the higher Poisson's ratio of concrete with a lower f'_c , which led to a better distribution of lateral stresses and higher axial deformation [69]. Another method of increasing f'_c is to increase the concrete's tensile-strength capacity, as did Zhang et al. [55] and Shin et al. [56], by adding steel fibers to the concrete. They found that using steel fibers significantly increased the strength, ductility, and energy dissipation of the HCCs, allowing the columns to exhibit higher cyclic capacity and lower strength loss by limiting the growth of shear cracks and facilitating flexural failure compared to the columns without steel fibers.

2.4. Slenderness and geometry

Fig. 5 shows that aspect ratio (AR) and geometry (G) were the least investigated design parameters for HCCs with a total of eight studies for each parameter. Aspect ratio (AR) is the ratio between the distance from the location of the load to the column base and the dimension of the column in the direction of loading. Table 5 summarizes the studies that considered AR as a design parameter. The results indicate that an

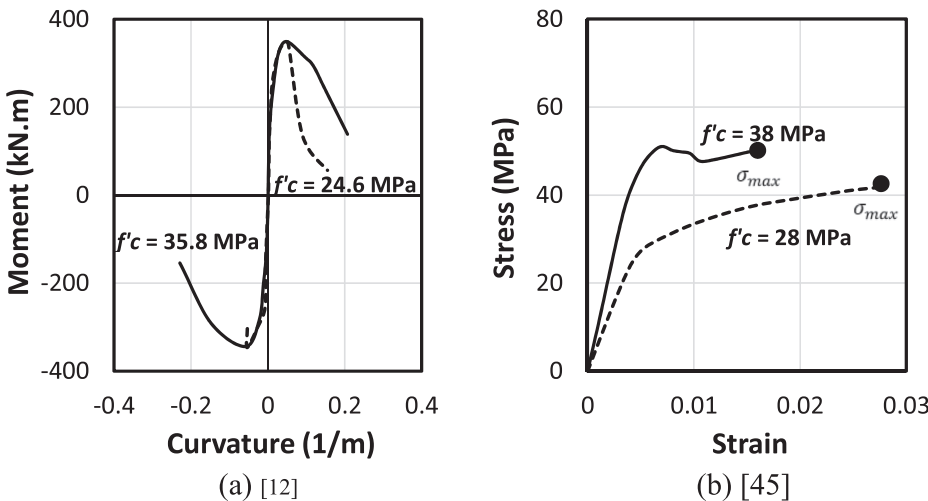


Fig. 10. Effect of f'_c on the (a) hysteretic and (b) axial behaviors of HCCs.

Table 5
Effect of AR on ductility, moment capacity, and failure mode.

Study Number	Authors	Load Arm (m)		AR	Δ_u/Δ_y		Load Capacity (kN)		Moment (kN-m)	
11	Mo and Nien [42]	1.50	1.80	3.00	3.60	4.40	364	332	546	598
13	Pinto et al. [13]	5.75	13.25	2.10	4.84	10.30	1300	800	7475	10,600
14–15	Pavese et al. [14] & Calvi et al. [43]	0.90	1.35	2.00	3.00	6.30	217	217	195	293
24	Kim et al. [51]	0.90	1.80	1.00	2.00	–	525	259	473	466
31	Han et al. [58]	1.40	2.80	2.55	5.09	8.60	163	77	228	216
37	Cassese et al. [62]	0.90	1.50	1.50	2.50	1.35	278	168	250	252
40	Cassese et al. [65]	1.10	1.65	2.00	3.00	5.70	167	108	184	178

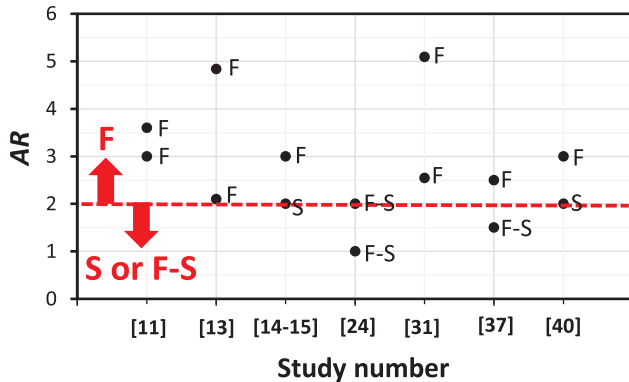


Fig. 11. Effect of the aspect ratio on the failure mode of HCCs.

increase in AR shifted the failure mode from shear (in the concrete) to flexure (in the reinforcement). This is due to better energy dissipation with a more progressive failure compared to the sudden failure observed in columns with low AR. The lateral-force capacity of the shorter columns was higher than the slender ones, although the amount of resisted bending moments were almost same or slightly more for the slender columns by considering the different lever arms. Moreover, flexural failure can be expected for columns subjected to hysteretic or cyclic loads at AR greater than 2 (Fig. 11).

The effect of geometry on HCC behavior has been studied by eight researchers, as listed in Table 1. Their studies all indicated that the circular columns had more uniform internal stress distribution than the square or rectangular columns due to the better confinement of the concrete core, which led to higher strength (Fig. 12a). This behavior is due to the stress concentration at the corners of square and rectangular columns, causing uneven confined stress within the concrete wall. Some attempts to round the corners of square concrete columns were implemented to reduce the stress concentration [63,64] and to enhance

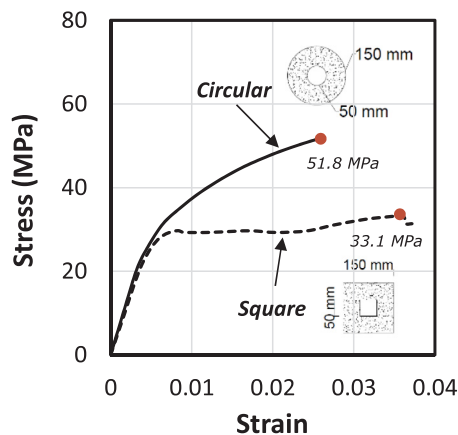
the behavior and confined strength of these columns (Fig. 12b).

2.5. Challenges in the design of steel-reinforced HCCs

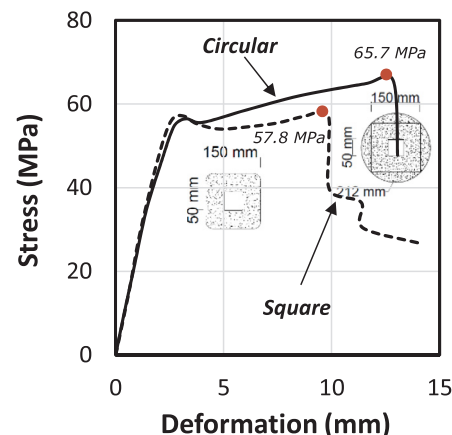
The preceding sections highlight that, overall, steel-reinforced HCCs behave significantly differently than SCCs due to the absence of the concrete core, which changes the inner stress formation from triaxial in SCCs to biaxial in HCCs. Moreover, the capacity of HCCs can be comparable to or even exceed that of SCCs when appropriate levels of design parameters ((i/o) ratio, ρ , ρ_v , f'_c , AR, G) are achieved. The limited ductility due to the compression failure of the inner concrete core is a significant concern in designing HCCs using steel bars. Similarly, steel corrosion has become a problem in concrete structures built in aggressive and marine environments, affecting their structural performance and shortening their service lives. These challenges are discussed in detail in the next section as is addressing them.

2.5.1. Brittle failure behavior of steel-reinforced HCCs

HCCs have higher stiffness and flexural strength than SCCs with the same amount of concrete [5,6]. Inadequate reinforcement details and low concrete strength [18] can, however, lead to the brittle failure of HCCs due to the reinforcement buckling or the concrete wall experiencing shear or crushing failure. The latter case is caused mostly by HCCs having thin concrete walls (high i/o ratio). A number of studies [4,8] have suggested limiting the i/o ratio to 0.8 to ensure that HCCs have sufficient shear capacity. The brittle collapse of HCCs is due to buckling or yielding of the longitudinal bars when no additional resistance can be obtained due to the permanent deformation of the steel bars. In a well-detailed steel-reinforced HCC, the longitudinal bars are held together by the concrete wall and sufficiently confined by the lateral reinforcement until failure. Otherwise, insufficient lateral details result in premature elastic buckling of the longitudinal bars and a sudden loss in load-carrying capacity [71]. Because of this, plain-concrete HCCs encased within outer and inner steel or FRP tubes are



(a) Micelli and Modarelli [45]



(b) Hadi et al. [64]

Fig. 12. Effect of geometry on HCC behavior.

currently being used to increase the strength performance of HCCs and to overcome the brittle behavior related to the thin concrete wall [67]. These approaches, however, are difficult to implement and not cost-effective.

2.5.2. Steel-reinforcement corrosion in HCCs

The corrosion of steel reinforcement is becoming a crucial concern with HCCs due to their exposed inner and outer surfaces. Steel corrosion can dramatically reduce column strength and eliminate the confinement of the lateral reinforcement, leading to brittle failure [72,73]. In fact, in efforts to extend their service lives, many steel-reinforced bridge piers are now being repaired or retrofitted because of significant steel corrosion problems [44,49,57,71,74,75]. Maintaining these deteriorating structures is very expensive. Similar problems are now being experienced with hollow steel structures [76,77]. Various techniques have been implemented to minimize deterioration of steel reinforcement such as the use of galvanizing, epoxy coating, and cathodic protection. Such alternatives are expensive and do not entirely eliminate steel corrosion [78]. There is a need therefore to explore the use of noncorroding reinforcement such as glass fiber-reinforced polymer (GFRP) bars in HCCs in order to mitigate the corrosion issues related to steel and to develop a more reliable and durable concrete structures.

3. Concrete columns reinforced with GFRP bars

The use of glass fiber-reinforced polymer (GFRP) composite bars as internal reinforcement in concrete structures has increased in the last 30 years due to their many superior mechanical and environmental-resistance properties [16]. This type of reinforcement has been successfully implemented in concrete beams [17,18], slabs [19,20], and walls [21,22]. The use of GFRP reinforcement for concrete columns has now become popular and effective [23–36]. The results of these studies demonstrated that, under axial loads, the concrete columns with GFRP longitudinal and transverse reinforcement had better and more stable behavior after the peak strength of the concrete or in the post-elastic stage than the steel-reinforced columns. Some studies [79–81] also recommend the use of GFRP reinforcement in concrete columns subject to lateral and cyclic loads due to the high confinement efficiency provided by GFRP stirrups. Similar confinement efficiency and performance was found for GFRP-reinforced shear walls [22], demonstrating the high potential of using GFRP bars and stirrups for HCCs to overcome steel corrosion and obtain more reliable performance than steel-reinforced columns. Supporting these findings, a recent study [37] progressively investigated the behavior of the GFRP bars in compression where the test results showed significant axial resistance of these bars under compression. However, this axial resistance depends on the GFRP bar diameter and the length of the bar. Furthermore, this study provided a model to predict the maximum compressive strength of the GFRP bars accounting for different diameters and lengths, besides predicting their mode of failure.

3.1. Comparison between steel- and GFRP-reinforced SCCs: Overall behavior

Steel and GFRP bars have different material properties: the former has higher stiffness and elastic-plastic behavior before yielding, while the latter has higher strength and linear elastic behavior up to failure. Fig. 13 illustrates the typical load–strain behavior of a steel-reinforced SCC (Fig. 13a) and a GFRP-reinforced SCC (Fig. 13b). These examples are based on columns with the same dimensions (230 mm outer diameter), concrete compressive strength (32 MPa), and reinforcing details (6 12.7 mm longitudinal bars and 140 mm clear spacing between 10 mm lateral ligatures). The steel-reinforced column is modelled using the confinement model developed by Mander et al. [82], while the GFRP-reinforced column is modelled using the confinement model proposed by Karim et al. [36]. Both models express the compressive

behavior of the confined SCCs with steel and GFRP reinforcement, respectively, and account for the lateral stress confinement provided by discrete lateral reinforcement. Both methods are based on the superposition of the constitutive material behavior such as the unconfined outer concrete cover, the inner confined concrete core, and the reinforcing material: either steel bars ($E = 200$ GPa and $f_y = 400$ MPa) or GFRP bars ($E = 60$ GPa and $f_y = 1250$ MPa).

Based on Fig. 13, the behavior of the unconfined outer concrete cover is similar for both columns and also from the columns modelled by Samani et al. [70], although the behavior of reinforcement and confined concrete differ. First, steel reinforcement has higher load contribution than GFRP bars due to its higher modulus of elasticity before yielding, denoted by the solid circle in Fig. 13a. It should be noted that axial load contribution of the steel bars to the GFRP bars with the same cross-section is more than 3 ($= 200$ GPa/60 GPa) times at the peak load. Afterwards, the significant reduction in the stiffness of the longitudinal steel bars is caused by yielding, while the GFRP bars continuously withstand the axial loads with the same stiffness until failure. On the other hand, the confined concrete behavior in both columns shows a reduction after the peak strength due to the gradual spalling/crushing of the concrete core. The steel-reinforced SCCs have lower level of confinement due to the yielding of the lateral reinforcement, as denoted by the solid diamond shape in Fig. 13a, compared to that of GFRP-reinforced SCCs. Overall, steel-reinforced SCC exhibits a higher strength capacity than the GFRP-reinforced SCC at the first peak (solid triangle). However, a stable load behavior after the first peak and further increase in the strength can be observed for GFRP-reinforced SCCs due to the linear elastic and high strength of GFRP bars.

3.2. Comparison of experimental results: Axial-compressive loading behavior

A comprehensive evaluation of the concentric axial behavior of SCCs with steel and GFRP reinforcement published in the literature was conducted. It focused on the first peak strength (σ_1) (the first peak strength after the elastic state), the confined strength (σ_2) (the strength induced by the concrete core due to lateral confinement), and the axial-displacement capacity. A total of 10 experimental studies were reviewed representing 20 columns and their results are summarized in Table 6. Fig. 14 shows the comparison between the investigated parameters for both reinforcing systems. In Fig. 14a, all of the studies showed that the σ_1 of the steel-reinforced SCCs was higher than that of the GFRP-reinforced SCCs. This is due to the higher modulus of the longitudinal steel bars, contributing almost 10% to 28%, while the lower modulus of the GFRP bars contributed only 3% to 14% (Table 6). In contrast, Fig. 14b shows that the GFRP-reinforced SCCs had higher confined strength (σ_2/f'_c) than the steel-reinforced columns. This finding can be explained by the higher strength and linear elastic behavior of the GFRP bars up to failure, unlike steel reinforcement, which cannot resist additional load after yielding. The load contribution of the GFRP bars at failure was therefore 50% higher than that of the steel bars [29]. Moreover, the lateral GFRP reinforcement provided higher confining stress than the steel bars. The confinement provided by the linear elastic GFRP ligatures increased with the load, while the confinement provided by the steel ligatures was the same after yielding. On the other hand, the experimental results in Fig. 14c show that the GFRP-reinforced SCCs exhibited more deformation before failing than their steel-reinforced counterparts. This can also be attributed to the linear elastic behavior of GFRP reinforcement: the crushing strain of GFRP bars is four to five times higher than the yield strain of steel bars [27].

3.3. Comparison of experimental results: Hysteretic loading behavior

HCC behavior has been investigated primarily under hysteretic loading, as shown in Fig. 4a. Table 7 summarizes the test results in the literature on GFRP reinforcement in SCCs and concrete walls, as well as

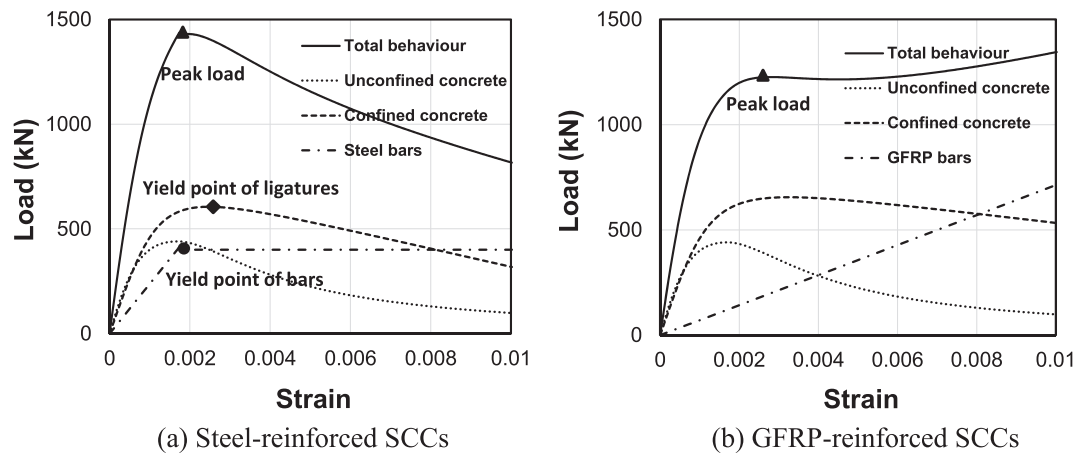


Fig. 13. Effect of reinforcing material on the behavior of SCCs.

comparisons with their steel-reinforced counterparts. For the columns tested under axial lateral loads, the most investigated behaviors were ductility (μ_{Δ}) and lateral-load capacity. For direct comparison, the bending moment (M) was calculated by multiplying the lateral load by the column height. The confined strength ($\sigma_c = Mc/I_{cr}$) was then derived and normalized based on the concrete compressive strength (f'_c). In the calculation of σ_c , c is the mid-height of the section (mm) in the direction of loading and I_{cr} is the moment of inertia of the cracked section approximated as $0.35I_g$ (I_g is the gross moment of inertia of the section) [88]. It should be mentioned that c is assumed to be the mid-height of the section even with the cracked section just to easily comparing between the columns with the two reinforcing systems where this value applied equally for both as this value is hard to be exactly calculated. The test results in Fig. 15a show that using GFRP reinforcement enhanced the lateral-load capacity and confined strength by up to 22%. The columns with steel bars, however, evidenced more energy dissipation [89,90]. The behavioral difference between these reinforcing materials is the main reason behind these findings: the steel-reinforced columns exhibited strength degradation after the yielding of the steel and failed due to buckling of longitudinal steel bars. On the other hand, the GFRP-reinforced columns experienced no strength degradation due to their linear elastic behavior up to failure. Concrete crushing at advanced loading levels, however, caused splitting in the longitudinal GFRP bars. Fig. 15b shows higher ductility in the GFRP-reinforced SCCs and concrete walls compared to the steel-reinforced ones. This behavior can be attributed to the GFRP bars having higher strain at failure than the steel bars. Moreover, the ductility is controlled primarily by the reinforcement ratio and the spacing between the lateral reinforcement: a decrease in reinforcement or increase in spacing can cause splitting failure in longitudinal GFRP bars [81,91].

3.4. Benefits of using GFRP bars in SCCs

The reviewed experimental studies showed the benefits and effectiveness of using GFRP bars as internal reinforcement in SCCs subject to axial and cyclic loading. Furthermore, GFRP bars were found to be suitable for SCCs in mitigating strength degradation after concrete cover spalling due to their high strength and linear elastic behavior up to failure. Moreover, the linear elastic nature of GFRP reinforcement, combined with the nonlinear behavior of concrete in compression and their relatively close moduli of elasticity, can provide a reinforced-concrete column with better overall performance and higher deformation capacity with a more progressive failure behavior than steel-reinforced SCCs. These positive attributes would be beneficial in addressing the limited performance of steel-reinforced HCCs. Therefore, the potential of GFRP bars and spirals as reinforcing materials for hollow concrete columns should be explored and their axial behavior should be investigated as a first step in understanding the structural performance of this construction system.

4. GFRP bars as reinforcement for HCCs

4.1. Results of recent investigations

Most research and developments on concrete structures reinforced with GFRP bars have focused solely on SCCs. The authors, however, recently undertook pioneering experimental and analytical work on GFRP-reinforced HCCs. Experimental investigations on the concentric compressive behavior of GFRP-reinforced HCCs considering different design parameters such as the inner-to-outer diameter ratio (i/o) ratio [34], reinforcement ratio (ρ) [33], volumetric ratio (ρ_v), and concrete

Table 6
Experimental studies compared the axial behavior between steel and GFRP-reinforced SCCs.

Authors	f'_c (MPa)	Load Contribution at σ_1 (%)		Maximum Axial-Load Ratio (σ_1/f'_c)		Confinement Efficiency (σ_2/f'_c)		Displacement Capacity	
		Steel	GFRP	Steel	GFRP	Steel	GFRP	Steel	GFRP
De Luca et al. [32]	34.5	11.6	4.2	0.90	0.88	—	—	1.36	1.97
Tobbi et al. [24]	32.6	12.0	10.0	1.05	0.99	1.26	1.36	—	—
Afifi et al. [23]	42.9	15.0	9.0	1.05	0.98	1.69	1.74	1.90	2.00
Pantelides et al. [73]	36.0	11.1	3.2	1.22	1.08	1.35	1.36	2.70	3.60
Mohammad et al. [83]	42.9	15.0	8.0	1.04	0.96	1.69	1.74	1.90	2.00
Hadi et al. [29]	37.0	26.6	13.4	1.25	1.00	1.37	1.50	8.70	9.00
Hales et al. [84]	90.0	—	—	1.09	1.02	—	—	—	—
Elchalakani and Ma [85]	32.8	15.8	3.2	1.13	1.06	2.60	2.46	1.10	1.50
Hasan et al. [86]	85.0	10.1	6.7	0.93	0.92	1.13	1.13	3.30	2.60
Al-Shareedah [87]	30.0	27.8	11.8	0.96	0.96	1.27	1.55	2.00	2.27

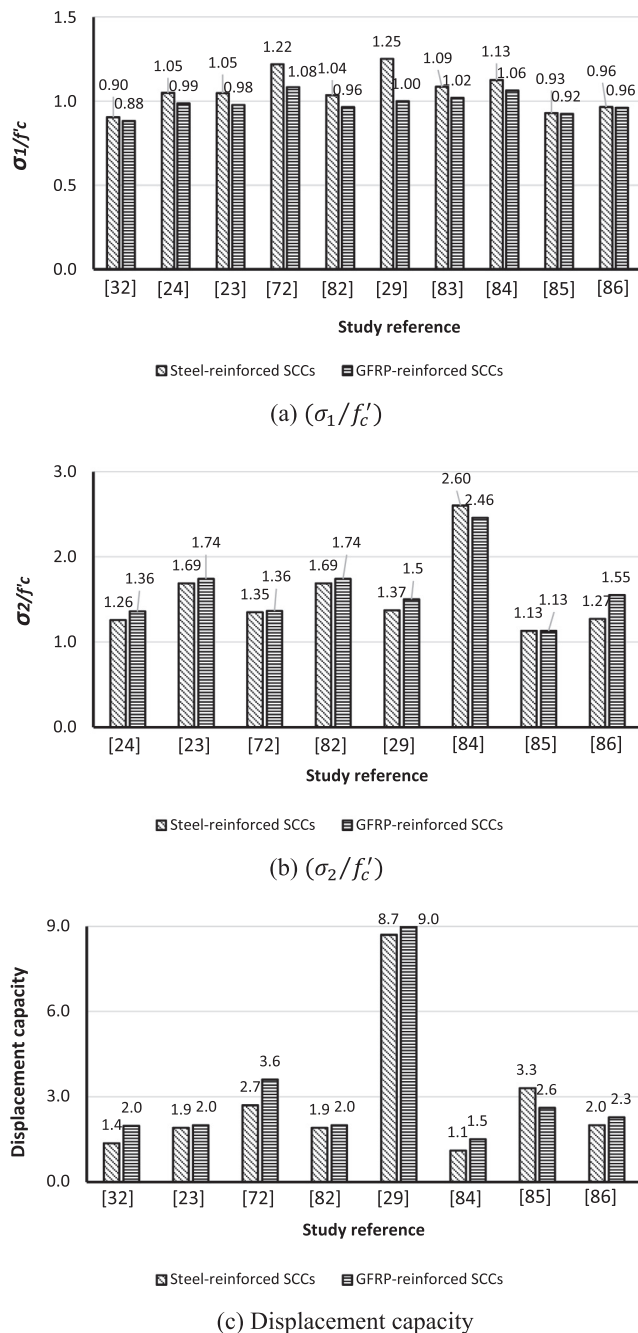


Fig. 14. Effect of reinforcing material on the axial behavior of SCCs.

Table 7

Experimental studies comparing the hysteretic behavior between steel- and GFRP-reinforced SCCs.

Authors	Sample Name		μ_Δ		σ_c/f'_c	
	Steel	GFRP	Steel	GFRP	Steel	GFRP
Nayera et al. [22]	ST15	G15	2.6	3.1	1.59	1.96
Tavassoli et al. [89,90]	P28-LS-12-50-7	P28-B-12-50	4.7	9.2	2.06	2.16
	P40-LS-12-160-6	P42-C12-160	3.1	3.7	0.93	1.05
Ali and El-salakawy [81]	S-1.3-10-75	G-1.3-10-75	8.5	12.5	1.54	1.83
Elshamandy et al. [91]	ST12N10-C4-100	G12N13-C4-100	7.7	10.4	2.35	2.36
	ST8N10-C1-100	G8N13-C1-100	6.6	5.5	1.98	2.22
Arafa et al. [92]	SX4	GX4	2.0	3.0	1.16	1.74
Deng et al. [93]	6SG-120	2GG-120	4.78	1.57	1.88	1.77
	11SG-120	9GG-120	4.68	1.58	1.31	1.36

compressive strength (f'_c) (the work is under review) were implemented. These studies found that increasing the i/o ratio in GFRP-reinforced HCCs resulted in more stable load-deformation behavior than in GFRP-reinforced SCCs and steel-reinforced HCCs by increasing the displacement capacity and confined strength (see Fig. 16a). This behavior contradicts that reported by Fam and Rizkalla [38] and Micelli and Modarelli [45], namely that increasing the (i/o) ratio decreased the strength in plain-concrete HCCs due to increase the shear effect on the thinner unreinforced concrete wall. GFRP bars as internal reinforcement in HCCs improves their performance due to GFRP's elastic linear behavior. This provides for maintaining the strength in concrete columns with higher (i/o) ratios and overcomes the brittle failure caused by crushing of the inner concrete wall. In the same study, AlAjarmeh et al. [34] evaluated the effect of using longitudinal steel and GFRP bars in HCCs. The results show that the steel-reinforced HCCs behaved the same behavior as the columns tested by Kusumawardaningsih and Hadi [2], and Yazici [50], who observed a reduction in compressive strength after the peak. In contrast, the GFRP-reinforced HCCs exhibited a strength increase after the first peak without any degradation and significantly high deformation before failure.

The increase in ρ achieved by increasing the number of longitudinal bars led to a significant increase in the confined strength but had no effect on the displacement capacity, as the longitudinal GFRP bars had a crushing strain almost same as that of the concrete [33] (see Fig. 16b). These findings are consistent with the observations of Afifi et al. [23] and Tobbi et al. [26] for GFRP-reinforced SCCs. On the other hand, closely spaced lateral reinforcement delayed failure and increased both displacement capacity and confined strength (Fig. 16c). This is due to the GFRP lateral reinforcement increasing the concrete confinement. GFRP spirals with a small spacing also provided higher strength and displacement than the steel-reinforced HCCs wrapped with CFRP sheets—based on Kusumawardaningsih and Hadi [2] and Yazici [50]—and higher than the GFRP-reinforced SCCs with close lateral reinforcement—based on Afifi et al. [23] and Maranan et al. [27]. In contrast, the GFRP-reinforced HCCs experienced reduced displacement capacity and an insignificant decrease in confined strength (see Fig. 16d), when the concrete compressive strength (f'_c) was high. This is due to the increased brittleness of high compressive strength concrete. This finding is consistent with [45], as shown in Fig. 10b, where the increase in f'_c decreased the displacement capacity of the HCCs. Moreover, using GFRP bars and concrete with high f'_c in HCCs (Fig. 16d) can maintain the confined strength, whereas a reduction was observed in the HCCs with higher concrete strength (see Fig. 10b).

4.2. New opportunities and future research on GFRP-reinforced HCCs

The effects of different design parameters have been well investigated and studied for HCCs with steel reinforcement. Some techniques have also been suggested to improve the performance and enhance the ductility of HCCs, including the use of multilayers of

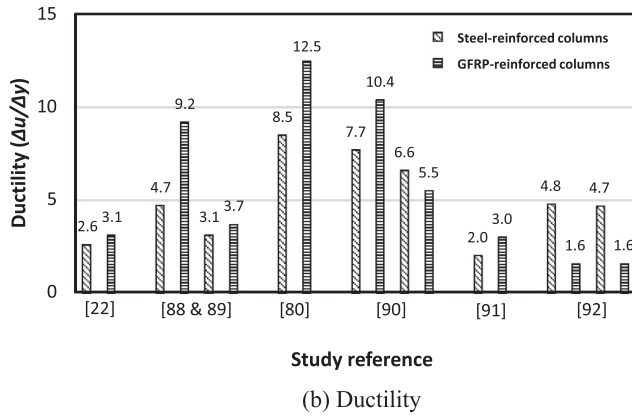
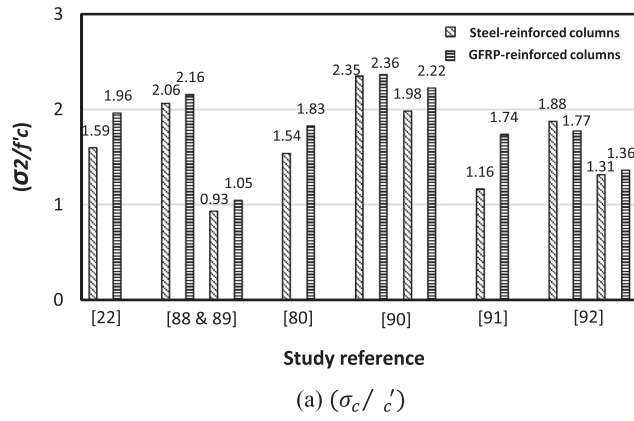


Fig. 15. Effect of reinforcing material on the hysteretic behavior of SCCs.

longitudinal reinforcement, changing the lateral-reinforcement configuration, and wrapping the outer face of the HCCs with FRP sheets. While such techniques have significantly improved the behavior of HCCs, the corrosion of steel bars remains a significant issue in steel-

reinforced HCCs.

The effectiveness of GFRP reinforcement in SCCs, as shown by the results on the recent work on the GFRP-reinforced HCCs (Fig. 16), demonstrates the high potential for extensively investigating the behavior of this new construction system to develop noncorroding, structurally reliable civil-engineering structures.

The use of GFRP bars is anticipated to increase the ductility and strength of HCCs to take advantage of their high strength and strain capacities. These qualities allow GFRP reinforcement to contribute continuously in carrying the applied load with concrete until failure, resulting in a better stress distribution inside HCCs and leading to significantly enhanced overall performance. Moreover, this system may provide a better solution than wrapping the outer surface of steel-reinforced HCCs with FRP or using the double-skin tube system, because it will totally eliminate the corrosion issue and be a more effective construction method.

5. Conclusions

This state-of-the-art review on hollow concrete columns identified the critical design parameters and their structural performance under different loading conditions. The challenges and opportunities in using GFRP reinforcement in this type of construction system were also critically analyzed. Based on this extensive review and analysis, the following conclusions can be drawn:

1. The use of hollow concrete columns is drawing growing interest, as shown by the greater number of relevant studies in the last 10 years. From 1993 to 2018, there were 41 reported studies on HCCs investigating the behavior of this construction system under different loading conditions and with different design parameters.
2. The behavior of HCCs has been widely investigated under hysteretic and axial loading conditions, representing 87% of the total number of studies, as these loading conditions are required in designing bridge piers. Moreover, the ratio of the inner-to-outer diameter, reinforcement ratio, volumetric ratio, and concrete compressive strength have been identified as the most critical and well-

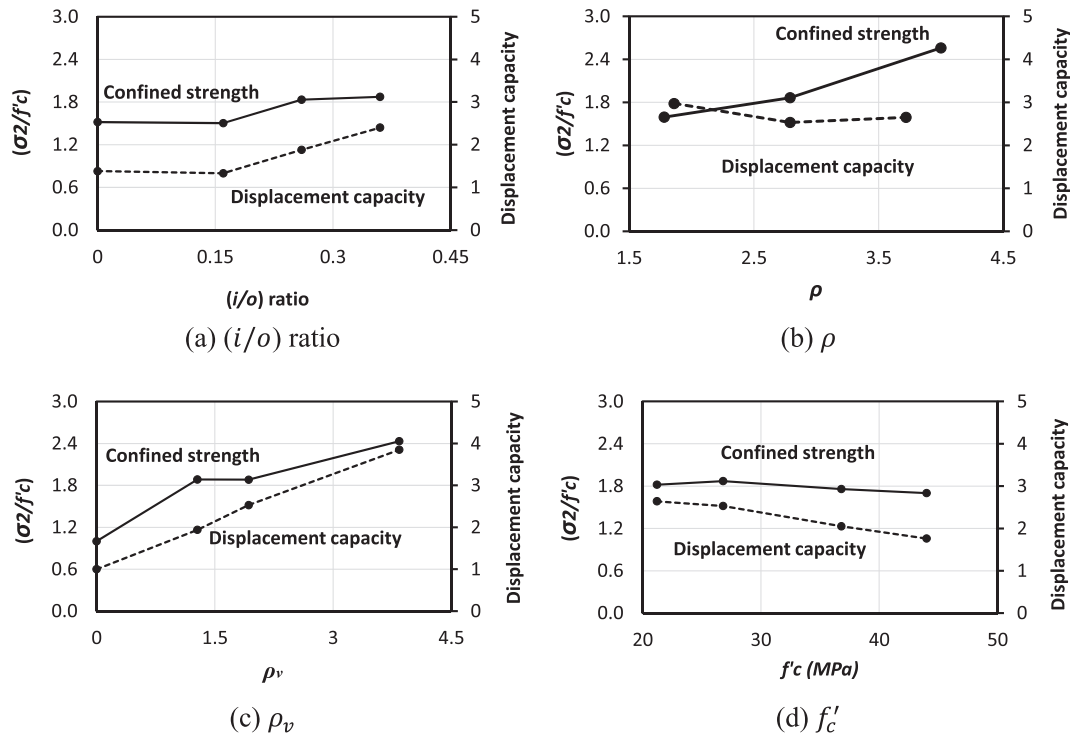


Fig. 16. Effect of the design parameters on the behavior of GFRP-reinforced HCCs.

investigated design parameters primarily affecting the structural performance of steel-reinforced hollow concrete columns.

3. The overall behavior of steel-reinforced HCCs is significantly different than that of SCCs due to the absence of the concrete core, which changes the inner stress formation from triaxial in the latter to biaxial in the former. This change reduces the lateral expansion of the cross section in the former, leading to more axial stability to achieve greater axial deformation. Therefore, the capacity of HCCs is comparable to or even higher than their solid counterparts when the appropriate levels of design parameters are used.
4. Steel-reinforced hollow concrete columns typically failed in a brittle manner due to either crushing of inner concrete core or buckling/yielding of the longitudinal bars. Steel-reinforced HCCs can be effectively designed by providing adequate inner-wall thickness (less than 0.8) or sufficient spacing between lateral reinforcement.
5. Glass fiber-reinforced (GFRP) bars can be the solution to overcome the brittle behavior of steel-reinforced HCCs. The linear elastic nature of GFRP bars, combined with the nonlinear behavior of concrete in compression and their relatively close moduli of elasticity, can provide HCCs with a higher deformation capacity and a more progressive failure behavior than steel-reinforced HCCs. In addition to using GFRP bars, creating a hollow section inside the concrete column leads to higher deformation capacity than in SCCs due to the lower lateral expansion and, therefore, GFRP-reinforced HCCs would be a good solution to overcome the brittle behavior of such columns.
6. Preliminary investigations indicate that GFRP-reinforced hollow concrete columns will benefit from the high strength and strain capacities of GFRP bars. This new construction system has exhibited higher strength and ductility than steel-reinforced columns due to the better stress distribution within the hollow concrete wall, leading to a significant enhancement in overall performance.

The outcomes of this review also point to opportunities and new research areas that can be explored to further understand how the critical design parameters affect the structural performance of GFRP-reinforced hollow concrete columns. Moreover, the behavior of GFRP-reinforced hollow concrete columns under the different loading conditions in which this construction system is heavily used should be investigated. The results of these investigations will be useful in revealing the many benefits of this new construction system and to provide useful information to support the work of the technical committees engaged in the development of standards and design provisions for GFRP-reinforced concrete columns.

Declaration of Competing Interest

No conflict of interest

Acknowledgements

The first author gratefully acknowledges Tafila Technical University, the University of Southern Queensland, and the Natural Science and Research Council of Canada (NSERC) for their financial support. The assistance from the Centre of Future Materials (CFM) is also acknowledged.

References

- [1] Lignola GP, et al. Experimental performance of RC hollow columns confined with CFRP. *J Compos Constr* 2007;11(1):42–9.
- [2] Kusumawardaningsih Y, Hadi MN. Comparative behaviour of hollow columns confined with FRP composites. *Compos Struct* 2010;93(1):198–205.
- [3] Mander JB. Seismic design of bridge piers; 1983.
- [4] Zahn F. Design of reinforced concrete bridge columns for strength and ductility; 1986.
- [5] Whittaker D. Seismic performance of offshore concrete gravity platforms; 1987.
- [6] Lee J-H, Choi J-H, Hwang D-K, Kwahk I-J. Seismic performance of circular hollow RC bridge columns. *KSCSE J Civ Eng* 2015;19(5):1456–67.
- [7] Hoshikuma J, Priestley M. Flexural behavior of circular hollow columns with a single layer of reinforcement under seismic loading. *SSRP* 2000:13.
- [8] Ranzo G, Priestley MN. Seismic performance of circular hollow columns subjected to high shear. 2001: Structural Systems Research Project, University of California, San Diego.
- [9] Yeh Y-K, Mo Y, Yang C. Seismic performance of hollow circular bridge piers. *Struct J* 2001;98(6):862–71.
- [10] Yeh Y-K, Mo YL, Yang C. Seismic performance of rectangular hollow bridge columns. *J Struct Eng* 2002;128(1):60–8.
- [11] Osada K, Yamaguchi T, Ikeda S. Seismic performance and the strengthening of hollow circular RC piers having reinforced cut-off planes and variable wall thickness. *Concrete Res. and Tech* 1999;101:13–24.
- [12] Mo Y, Wong D, Maekawa K. Seismic performance of hollow bridge columns. *Struct J* 2003;100(3):337–48.
- [13] Pinto A, Molina J, Tsionis G. Cyclic tests on large-scale models of existing bridge piers with rectangular hollow cross-section. *Earthquake Eng Struct Dyn* 2003;32(13):1995–2012.
- [14] Pavese A, Bolognini D, Peloso S. FRP seismic retrofit of RC square hollow section bridge piers. *J Earthquake Eng* 2004;8(spec01):225–50.
- [15] Liang X, Beck R, Sritharan S. Understanding the confined concrete behavior on the response of hollow bridge columns. In: Department of Civil, Construction and Environmental Engineering. Iowa State University: California Department of Transportation; 2015.
- [16] Manalo A, Benmokrane B, Park K-T, Lutz D. Recent developments on FRP bars as internal reinforcement in concrete structures. *Concrete Australia* 2014;40(2):46–56.
- [17] El-Nemr A, Ahmed EA, Benmokrane B. Flexural behavior and serviceability of normal-and high-strength concrete beams reinforced with glass fiber-reinforced polymer bars. *ACI Struct J* 2013;110(6).
- [18] Maranan G, Manalo A, Benmokrane B, Karunasena K, Mendis P. Evaluation of the flexural strength and serviceability of geopolymer concrete beams reinforced with glass-fibre-reinforced polymer (GFRP) bars. *Eng Struct* 2015;101:529–41.
- [19] Michalak CR, Rizkalla S, Tadros G, Benmokrane B. Flexural behavior of one-way concrete slabs reinforced by fiber reinforced plastic reinforcements. *ACI Struct J* 1998;95:353–65.
- [20] El-Sayed A, El-Salakawy E, Benmokrane B. Shear strength of one-way concrete slabs reinforced with fiber-reinforced polymer composite bars. *J Compos Constr* 2005;9(2):147–57.
- [21] Hassanein A, Mohamed N, Farghaly A, Benmokrane B. STR 830: enhancing the deformation capacity of concrete shear walls reinforced with GFRP bars; 2016.
- [22] Mohamed N, Farghaly A, Benmokrane B, Neale K. Experimental investigation of concrete shear walls reinforced with glass fiber-reinforced bars under lateral cyclic loading. *J Compos Constr* 2014;18(3):A4014001.
- [23] Afifi MZ, Mohamed HM, Benmokrane B. Axial capacity of circular concrete columns reinforced with GFRP bars and spirals. *J Compos Constr* 2013;18(1).
- [24] Tobbi H, Farghaly AS, Benmokrane B. Concrete columns reinforced longitudinally and transversally with glass fiber-reinforced polymer bars. *ACI Struct J* 2012;109(4):551.
- [25] Alsayed S, Salloum Y, Almusallam T, Amjad M. Concrete columns reinforced by glass fiber reinforced polymer rods. *Spec Publ* 1999;188:103–12.
- [26] Tobbi H, Farghaly AS, Benmokrane B. Behavior of concentrically loaded fiber-reinforced polymer reinforced concrete columns with varying reinforcement types and ratios. *ACI Struct J* 2014;111(2):375.
- [27] Maranan G, Manalo A, Benmokrane B, Karunasena K, Mendis P. Behavior of concentrically loaded geopolymer-concrete circular columns reinforced longitudinally and transversely with GFRP bars. *Eng Struct* 2016;117:422–36.
- [28] Zadeh HJ, Nanni A. Design of RC columns using glass FRP reinforcement. *J Compos Constr* 2012;17(3):294–304.
- [29] Hadi MN, Karim H, Sheikh MN. Experimental investigations on circular concrete columns reinforced with GFRP bars and helices under different loading conditions. *J Compos Constr* 2016;20(4).
- [30] Hadi MN, Hasan HA, Sheikh MN. Experimental investigation of circular high-strength concrete columns reinforced with glass fiber-reinforced polymer bars and helices under different loading conditions. *J Compos Constr* 2017;04017005.
- [31] Hadhood A, Mohamed HM, Benmokrane B. Experimental study of circular high-strength concrete columns reinforced with GFRP bars and spirals under concentric and eccentric loading. *J Compos Constr* 2016;04016078.
- [32] De Luca A, Matta F, Nanni A. Behavior of full-scale glass fiber-reinforced polymer reinforced concrete columns under axial load. *ACI Struct J* 2010;107(5):589.
- [33] AlAjarmeh OS, Manalo AC, Benmokrane B, Karunasena K, Mendis P. Axial performance of hollow concrete columns reinforced with GFRP composite bars with different reinforcement ratios. *Compos Struct* 2019;213(1):12.
- [34] AlAjarmeh OS, Manalo AC, Benmokrane B, Karunasena K, Mendis P, Nguyen K. Compressive behavior of axially loaded circular hollow concrete columns reinforced with GFRP bars and spirals. *Constr Build Mater* 2019;194:12–23.
- [35] Hadhood A, Mohamed H, Garib F, Benmokrane B. Efficiency of glass-fiber reinforced-polymer (GFRP) discrete hoops and bars in concrete columns under combined axial and flexural loads. *Compos B Eng* 2017;114:223–36.
- [36] Karim H, Sheikh MN, Hadi MN. Axial load-axial deformation behaviour of circular concrete columns reinforced with GFRP bars and helices. *Constr Build Mater* 2016;112:1147–57.
- [37] AlAjarmeh OS, Manalo AC, Benmokrane B, Vijay PV, Ferdous W, Mendis P. Novel testing and characterization of GFRP bars in compression. *Constr Build Mater* 2019;225:1112–26.
- [38] Fam A, Rizkalla SH. Behavior of axially loaded concrete-filled circular FRP tubes.

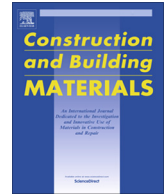
- ACI Struct J 2001;98(3):280–9.
- [39] Liang X, Sritharan S. Effects of confinement in circular hollow concrete columns. *J Struct Eng* 2018;144(9):04018159.
- [40] Zahn F, Park R, Priestley M. Flexural strength and ductility of circular hollow reinforced concrete columns without confinement on inside face. *Struct J* 1990;87(2):156–66.
- [41] Kishida S, Horii M, Kuwabara F, Hayashi S. Experimental study on shear strength of the PHC pile with large diameter. *J Struct Const Eng* 1998;8(519):123–30.
- [42] Mo Y, Nien I. Seismic performance of hollow high-strength concrete bridge columns. *J Bridge Eng* 2002;7(6):338–49.
- [43] Calvi GM, Pavese A, Rasulo A, Bolognini D. Experimental and numerical studies on the seismic response of RC hollow bridge piers. *Bull Earthq Eng* 2005;3(3):267–97.
- [44] Modarelli R, Micelli F, Manni O. FRP-confinement of hollow concrete cylinders and prisms. In: *Proceedings of the 7th international symposium on FRP reinforcement for reinforced concrete structures*, Kansas City, Missouri; 2005. Citeseer.
- [45] Micelli F, Modarelli R. Experimental and analytical study on properties affecting the behaviour of FRP-confined concrete. *Compos B Eng* 2013;45(1):1420–31.
- [46] Yeh Y-K, Mo Y. Shear retrofit of hollow bridge piers with carbon fiber-reinforced polymer sheets. *J Compos Constr* 2005;9(4):327–36.
- [47] Delgado P. *Avaliação da Segurança Estrutural em Pontes*. PhD thesis, FEUP, Porto; 2008 [in Portuguese].
- [48] Turmo J, Ramos G, Aparicio A. Shear truss analogy for concrete members of solid and hollow circular cross section. *Eng Struct* 2009;31(2):455–65.
- [49] Lignola GP, Nardone F, Porta A, Luca A. Analysis of RC Hollow Columns Strengthened with GFRP. *J Compos Constr* 2011;15(4):545–56.
- [50] Yazici V. Strengthening hollow reinforced concrete columns with fibre reinforced polymers. University of Wollongong; 2012.
- [51] Kim I.-H., C.-H. Sun, and M. Shin. Concrete contribution to initial shear strength of RC hollow bridge columns; 2012.
- [52] Cheon J-H, Kim T-H, Lee B-J, Lee J-H, Shin H-M. Inelastic behaviour and ductility capacity of circular hollow reinforced concrete bridge piers under earthquake. *Mag Concr Res* 2012;64(10):919–30.
- [53] Kim T-H, Lee H-J, Choi J-H, Shin H-M. Performance assessment of hollow RC bridge column sections with reinforcement details for material quantity reduction. *Mag Concr Res* 2013;65(21):1277–92.
- [54] Han Q, Du X, Zhou Y, Lee G. Experimental study of hollow rectangular bridge column performance under vertical and cyclically bilateral loads. *Earthquake Eng Vib* 2013;12(3):433–45.
- [55] Zhang Y-Y, Harries KA, Yuan W-C. Experimental and numerical investigation of the seismic performance of hollow rectangular bridge piers constructed with and without steel fiber reinforced concrete. *Eng Struct* 2013;48:255–65.
- [56] Shin M, Choi Y-Y, Kim I-H, Lee K. Effectiveness of low-cost fiber-reinforced cement composites in hollow columns under cyclic loading. *Constr Build Mater* 2013;47:623–35.
- [57] Hadi M, Le T. Behaviour of hollow core square reinforced concrete columns wrapped with CFRP with different fibre orientations. *Constr Build Mater* 2014;50:62–73.
- [58] Han Q, Wen J, Du X, Jia J. Experimental and numerical studies on seismic behavior of hollow bridge columns retrofitted with carbon fiber reinforced polymer. *J Reinf Plast Compos* 2014;33(24):2214–27.
- [59] Völgyi I, Windisch A, Farkas G. Resistance of reinforced concrete members with hollow circular cross-sections under combined bending and shear—Part I: Experimental investigation. *Struct Concr* 2014;15(1):13–20.
- [60] Kim T-H, Lee J-H, Shin HM. Performance assessment of hollow RC bridge columns with triangular reinforcement details. *Mag Concr Res* 2014;66(16):809–24.
- [61] Prado NI, Aguilar G, López O, Gómez R, Escobar J. Arrangement of transverse reinforcement in hollow piers subjected to lateral load. *ACI Struct J* 2016;113(4):723.
- [62] Cassese P, Ricci P, Verderame GM. Experimental study on the seismic performance of existing reinforced concrete bridge piers with hollow rectangular section. *Eng Struct* 2017;144:88–106.
- [63] Jameel MT, Sheikh MN, Hadi MN. Behaviour of circularized and FRP wrapped hollow concrete specimens under axial compressive load. *Compos Struct* 2017;171:538–48.
- [64] Hadi MN, Jameel MT, Sheikh MN. Behavior of circularized hollow RC columns under different loading conditions. *J Compos Constr* 2017;21(5):04017025.
- [65] Cassese P, De Risi MT, Verderame GM. Seismic assessment of existing hollow circular reinforced concrete bridge piers. *J Earthquake Eng* 2018;1–36.
- [66] Irawan C, Djameluddin R, Raka G, Faimun, Suprobo P, Gambiro. Confinement behavior of spun pile using low amount of spiral reinforcement—an experimental study. *Int J Adv Sci Eng Inform Technol* 2018;8(2):501–7.
- [67] Al-saadi AU, Aravinthan T, Lokuge W. Structural applications of fibre reinforced polymer (FRP) composite tubes: a review of columns members. *Compos Struct* 2018.
- [68] Han S, Han T, Kang Y, Park J, Lim N. Nonlinear concrete model for an internally confined hollow reinforced concrete column. *Mag Concr Res* 2008;60(6):429–40.
- [69] Simmons J. Poisson's ratio of concrete: a comparison of dynamic and static measurements. *Mag Concr Res* 1955;7(20):61–8.
- [70] Samani AK, Attard MM. A stress-strain model for uniaxial and confined concrete under compression. *Eng Struct* 2012;41:335–49.
- [71] Lignola G, Prota A, Manfredi G, Cosenza E. Analysis of the confinement of RC hollow columns wrapped with FRP. *Mater Charact* 2007;3(S3):300.
- [72] Li J, Gong J, Wang L. Seismic behavior of corrosion-damaged reinforced concrete columns strengthened using combined carbon fiber-reinforced polymer and steel jacket. *Constr Build Mater* 2009;23(7):2653–63.
- [73] Pantelides CP, Gibbons ME, Reaveley LD. Axial load behavior of concrete columns confined with GFRP spirals. *J Compos Constr* 2013;17(3):305–13.
- [74] Yazici V, Hadi MN. Axial load-bending moment diagrams of carbon FRP wrapped hollow core reinforced concrete columns. *J Compos Constr* 2009;13(4):262–8.
- [75] Hadigheh A, Falsafi T, Morshed R, Shaiganfarid R. Experimental study on behaviour of prismatic and cylindrical hollow concrete columns reinforced with FRP materials; 2010.
- [76] Zhao X-L, Zhang L. State-of-the-art review on FRP strengthened steel structures. *Eng Struct* 2007;29(8):1808–23.
- [77] Elchalakani M. Rehabilitation of corroded steel CHS under combined bending and bearing using CFRP. *J Constr Steel Res* 2016;125:26–42.
- [78] Nkurunziza G, Debaiky A, Cousin P, Benmokrane B. Durability of GFRP bars: a critical review of the literature. *Prog Struct Mat Eng* 2005;7(4):194–209.
- [79] Tavassoli A. Behaviour of circular concrete columns internally reinforced with steel and GFRP under combined axial load and bending. In: *Master of applied science in civil engineering*. University of Toronto; 2015.
- [80] Tavassoli A, Sheikh SA. Seismic resistance of circular columns reinforced with steel and GFRP. *J Compos Constr* 2017;21(4):04017002.
- [81] Ali MA, El-Salakawy E. Seismic performance of GFRP-reinforced concrete rectangular columns. *J Compos Constr* 2015;20(3):04015074.
- [82] Mander JB, Priestley MJ, Park R. Theoretical stress-strain model for confined concrete. *J Struct Eng* 1988;114(8):1804–26.
- [83] Mohamed HM, Afifi MZ, Benmokrane B. Performance evaluation of concrete columns reinforced longitudinally with FRP bars and confined with FRP hoops and spirals under axial load. *J Bridge Eng* 2014;19(7):04014020.
- [84] Hales TA, Pantelides CP, Reaveley LD. Experimental evaluation of slender high-strength concrete columns with GFRP and hybrid reinforcement. *J Compos Constr* 2016;20(6):04016050.
- [85] Elchalakani M, Ma G. Tests of glass fibre reinforced polymer rectangular concrete columns subjected to concentric and eccentric axial loading. *Eng Struct* 2017;151:93–104.
- [86] Hasan HA, Sheikh MN, Hadi MN. Performance evaluation of high strength concrete and steel fibre high strength concrete columns reinforced with GFRP bars and helices. *Constr Build Mater* 2017;134:297–310.
- [87] Al-Shareedah Othman S. Performance evaluation of axially loaded circular GFRP-reinforced concrete columns. Civil and architectural engineering department. Oman: Sultan Qaboos University; 2016.
- [88] ACI, (American Concrete Institute), Building code requirements for structural concrete. ACI 318-14M, Farmington Hills, MI; 2014.
- [89] Tavassoli A, Sheikh SA. Seismic resistance of circular columns reinforced with steel and GFRP. *J Compos Constr* 2017;04017002.
- [90] Tavassoli A, Liu J, Sheikh S. Glass fiber-reinforced polymer-reinforced circular columns under simulated seismic loads. *ACI Struct J* 2015;112(1):103.
- [91] Elshamandy MG, Farghaly AS, Benmokrane B. Experimental behavior of glass fiber-reinforced polymer-reinforced concrete columns under lateral cyclic load. *ACI Struct J* 2018;115(2):337–49.
- [92] Arafa A, Farghaly AS, Benmokrane B. Experimental behavior of GFRP-reinforced concrete squat walls subjected to simulated earthquake load. *J Compos Constr* 2018;22(2):04018003.
- [93] Deng Z, Gao L, Wang X. Glass fiber-reinforced polymer-reinforced rectangular concrete columns under simulated seismic loads. *J Braz Soc Mech Sci Eng* 2018;40(2):111.

Chapter 3

Compressive behavior of axially loaded circular hollow concrete columns reinforced with GFRP bars and spirals

The significance of the inner-to-outer diameter (i/o) ratio on the behavior of HCCs was identified in the review paper in Chapter 2. To investigate the effect of this design parameter, large scale concrete columns (250 mm in diameter and 1 m in height) with three different (i/o) ratios were adopted (0, 0.16, 0.26, and 0.36) were cast and tested at the structural laboratory at USQ. All GFRP-reinforced concrete columns were reinforced longitudinally by 6 pcs- 15.9 mm GFRP bars and laterally by 9.5 mm GFRP spirals spaced at 100 mm centre to centre. In addition, 6 pcs- 15.9 mm steel bars were used to reinforce HCC (i/o of 0.36) to compare with the GFRP-reinforced HCC. The results from the experimental work were presented and compared in term of failure mode, load and deformation behaviour, ductility, and strength and confinement efficiency. Moreover, analytical equations were introduced describing the load-deformation behavior of GFRP-reinforced HCCs.

The test results showed that GFRP-reinforced HCCs have more ductile and progressive failure, higher strength, and higher displacement capacity than SCC. The increase in (i/o) ratio resulted in more stable load-deformation behavior and increased in both strength and ductility as a result of the reduction in the lateral expansion of the HCC. Similarly, GFRP-reinforced HCCs exhibited a more ductile behavior than the steel-reinforced HCCs due to the linear elastic behavior of the GFRP reinforcements. A new approach for predicting the failure mode of GFRP-reinforced HCCs considered the confined strength inside the concrete core and the hoop stress of the lateral reinforcements. Based on this study, the optimal (i/o) ratio was 0.36 as it resulted in the most stable behavior and the highest confined strength and ductility for GFRP-reinforced HCC. Similarly, reinforcing with longitudinal GFRP bars significantly enhanced the overall behavior of HCCs. The effect of varying the amount of longitudinal GFRP bars was therefore investigated and the results are presented in the next chapter.



Compressive behavior of axially loaded circular hollow concrete columns reinforced with GFRP bars and spirals

O.S. AlAjarmeh^a, A.C. Manalo^{a,*}, B. Benmokrane^b, W. Karunasena^a, P. Mendis^c, K.T.Q. Nguyen^c

^a University of Southern Queensland, Centre for Future Materials (CFM), School of Civil Engineering and Surveying, Toowoomba 4350, Australia

^b University of Sherbrooke, Department of Civil Engineering, Sherbrooke, Quebec, Canada

^c The University of Melbourne, Department of Infrastructure Engineering, Victoria 3010, Australia

HIGHLIGHTS

- GFRP-reinforced hollow and solid concrete columns under concentric load.
- Effect of inner-to-outer (*i/o*) diameter ratio on hollow concrete columns.
- Axial design load prediction for GFRP-reinforced hollow concrete columns.
- Failure stress index for GFRP-reinforced hollow concrete columns.

ARTICLE INFO

Article history:

Received 20 June 2018

Received in revised form 23 October 2018

Accepted 1 November 2018

Keywords:

Hollow column

Reinforced concrete

GFRP bar

GFRP spiral

Inner-to-outer diameter ratio

Concentric load

ABSTRACT

This study explored the use glass-fiber-reinforced-polymer (GFRP) bars and spirals as reinforcing materials in hollow concrete columns in order to mitigate steel-related corrosion problems and understand the fundamental behavior of such construction system under the applied loads. Four concrete columns 250 mm in external diameter and reinforced longitudinally with six 15.9 mm diameter GFRP bars were cast with different inner diameters (0, 40, 65, and 90 mm) and tested under concentric axial loading. Based on the experimental results, increasing the inner-to-outer diameter ratio up to 0.36 in hollow GFRP reinforced columns changed the failure behavior from brittle to pseudo-ductile. Moreover, the hollow GFRP reinforced columns exhibited higher deformation capacity and higher confinement efficiency compared to the GFRP-reinforced solid columns and steel-reinforced hollow columns. A theoretical model considering the confined-concrete compressive strength and axial strain of 0.0025 in longitudinal GFRP bars can accurately predict the axial-load capacity of hollow concrete columns.

© 2018 Elsevier Ltd. All rights reserved.

1. Introduction

Steel-reinforced hollow concrete columns have been used extensively for bridge piers, piles, and electric poles because of their high capacity for resisting axial forces and bending moments but with the advantages of low self-weight and reduced material usage [1]. Hollow reinforced-concrete (RC) columns have higher structural efficiency due to their high strength-to-mass and stiffness-to-mass ratios than solid columns with the same area. In fact, the void is primarily responsible for the significant differences in behavior compared to solid columns [2]. Accordingly, the structural behavior of hollow steel-reinforced concrete columns—including flexural and shear strength, lateral loading, and seismic capacity—have been investigated by a number of research-

ers [3–11]. They found that the overall behavior of hollow RC columns depends greatly on the ratio of the column's inner-to-outer (*i/o*) diameter ratio, longitudinal-reinforcement ratio, lateral reinforcement details, and axial-load ratio (ratio of the applied load to maximum axial-load capacity). Increasing the *i/o* ratio while keeping the other parameters the same decreased the ductility of the steel-reinforced hollow concrete columns. An abrupt loss of the compressive strength occurred after the peak load was reached. The loss was steeper in the case of higher *i/o* ratios due to the brittle failure behavior [4,10]. In addition, no axial-load response was observed in the post-loading stage for such columns due to the limited axial strain and buckling failure of steel bars. Instead, concrete crushing occurs once the steel bars started to buckle [1,2,12]. The corrosion of steel reinforcement is, however, becoming a concern with hollow RC columns, since they have thinner walls than solid RC structures. It can reduce the axial load capacity of the concrete columns and eliminate the lateral

* Corresponding author.

E-mail address: manalo@usq.edu.au (A.C. Manalo).

confinement by damaging the lateral steel reinforcements [13,14]. In fact, many hollow RC bridge piers are now being repaired or retrofitted so that these structures can continue to perform based on their intended service lives [2,15–19]. Steel-reinforced hollow concrete structures are now experiencing similar problems [20,21]. On the other hand, the various techniques used such as galvanized steel, epoxy coated, and cathodic protection, have not been completely controlled steel reinforcement deterioration [22]. Consequently, the use of non-corroding reinforcement in hollow concrete columns needs investigation to mitigate steel-related corrosion problems and understand the fundamental behavior of such columns under the applied loads.

The use of glass-fiber-reinforced-polymer (GFRP) composite bars as internal reinforcement in concrete structures has increased in the last 20 years due to their many positive characteristics and increased durability performance [23]. This type of reinforcement has been found to be effective in beams, slabs, beam–column joints, and walls due to its high strength and almost similar moduli of elasticity to that of concrete [24–26]. Similarly, the use of GFRP reinforcement in concrete columns has been widely investigated [14,27–36]. These researchers concluded that RC columns reinforced longitudinally and transversely with GFRP bars behaved in a better way than steel-reinforced solid concrete columns, especially, in the post-loading stage. They concluded that using GFRP reinforcement enhanced the post-loading behavior of concrete columns and delayed the failure. This was due to the concrete core having high confined strength because of the higher tensile strength of GFRP reinforcement compared to conventional steel reinforcement. Pantelides et al. observed a 33% higher ductility factor for GFRP-reinforced columns than steel-reinforced ones. Moreover, Ali and El-Salakawy [37], Tavassoli [38], and Tavassoli and Sheikh [39] suggested that GFRP-reinforced columns have 15% higher moment capacity and 200% higher strength at 4% drift ratio than steel-reinforced concrete columns due to the high strength and confinement efficiency provided by GFRP stirrups. Mohamed et al. [40] arrived at similar findings for GFRP-reinforced shear walls. These studies demonstrated the high potential of using GFRP bars and stirrups to construct hollow concrete columns in order to avoid the brittle behavior and the low strength in the post-loading

stage. This behavior was achieved due to the high strength of these reinforcements and the compatibility of their modulus of elasticity to concrete, in addition to their reliable performance and without the problem of steel corrosion.

This study explored the potential GFRP bars and spirals as reinforcing materials for hollow concrete columns reinforced and investigated their axial behavior as a first step in understanding the structural performance of this construction system. It focused on assessing the influence of the inner-to-outer diameter ratio and comparing the behavior of GFRP-reinforced hollow concrete columns to that of steel-reinforced columns. Finally, the applicability of existing design equations for solid concrete columns was assessed for hollow concrete columns reinforced with GFRP bars.

2. Experimental program

2.1. Materials

Grade III #5 GFRP bars [41] with a nominal diameter of 15.9 mm [Fig. 1(a)] were used as longitudinal reinforcement in the circular solid and hollow concrete columns. The transverse reinforcement was Grade III #3 GFRP spirals with a nominal diameter of 9.5 mm [Fig. 1(b)]. The spirals had an inner diameter of 180 mm. Spiral GFRP bars were considered for the transverse reinforcement as Maranan et al. [31] found that they provided higher lateral confinement to the concrete core than conventional circular hoops. The GFRP reinforcement was manufactured by pultruding glass fibers impregnated with modified vinyl-ester resin and had a sand-coated surface. The GFRP bars used in this study came from the same production lot as the bars investigated by Benmokrane et al. [42] and had the physical and mechanical properties reported in Table 1. For comparison, 16.0 mm deformed steel bars with a yield strength of 500 MPa and modulus of elasticity of 200 GPa were used as the longitudinal reinforcement in one of the tested columns.

The column samples were cast with ready-mix concrete. The coarse aggregate had a maximum size of 10 mm and a fresh concrete had a slump of 105 mm when measured according to ASTM/C143 [44]. During concrete casting, six 100 mm diameter and 200 mm high concrete cylinders were prepared based on ASTM/C31 [45] and were tested on the day of column testing following the procedures described in ASTM/C39 [46] and ASTM/C1231 [47]. The average concrete compressive strength at 28 days was around 31.8 MPa, with a standard deviation of 3.54 MPa.

2.2. Specimen details

Five concrete columns 250 mm in diameter and 1 m in height with a height-to-diameter ratio of 4 were cast and tested. Columns with similar height-to-diameter ratios were successfully implemented by Maranan et al. [31] and Karim et al. [36] to



Fig. 1. GFRP reinforcement.

Table 1
Physical and mechanical properties for GFRP bars [42].

Properties	Test Method	Number of Samples	Values	
			No. 5	No. 3
Nominal bar diameter	CSA-S806, Annex A (CSA, 2012)	9	15.9	9.5
Nominal bar area	CSA-S806, Annex A (CSA, 2012)	9	198.5	70.8
Ultimate tensile strength, f_u (MPa)	ASTM D7205/D7205M-06 [43]	6	1237 (33.3)	1315 (31.1)
Modulus of Elasticity, E_{GFRP} (GPa)	ASTM D7205/D7205M-06 [43]	6	60.0 (1.3)	62.5 (0.4)
Ultimate strain, ϵ_u (%)	ASTM D7205/D7205M-06 [43]	6	2.1 (0.1)	2.3 (0.1)

eliminate buckling failure. Four columns were fully reinforced with GFRP bars and spirals, while one column was reinforced longitudinally with steel bars and transversely reinforced with GFRP spirals. All five columns contained six longitudinal reinforcing bars and GFRP spirals spaced at 100 mm on centers along 500 mm length at mid-height, and at 50 mm along 250 mm length at the top and bottom of the columns to avoid premature failure due to stress concentration. Six longitudinal GFRP and steel bars were considered to have the same reinforcement ratio of 2.79%, which complies with the range of 1–4% recommended in AS3600 [48] for steel bars, because there are no standards for GFRP bars. The 100 mm spiral spacing was chosen to ensure the inelastic buckling of the steel bars after yielding and avoid the elastic buckling of the GFRP bars as was successfully demonstrated by Maranan et al. [31]. More importantly, the reinforcement details were made similar for all columns to clearly examine the effect of the inner void size. The inner-to-outer diameter (*i/o*) ratios of the hollow columns were achieved by placing a PVC pipe at the center of the specimens during concrete casting. The PVC pipes had outer diameters of 40 mm, 65 mm, and 90 mm, and a wall thickness of 1 mm. These diameters were based on the commercially available PVC pipes and resulted in *i/o* ratios similar to those investigated by other researchers [1,12,49,50]. A solid concrete column was also prepared and tested as a reference specimen. A concrete column with a maximum diameter of 250 mm was considered due to the limited capacity of the test equipment. A maximum inner core diameter of 90 mm was provided to ensure sufficient concrete cover for the longitudinal reinforcement. Similarly, a hollow column with an inner diameter of 65 mm (*i/o* ratio = 0.26) and reinforced with the same reinforcement details with six 16 mm steel bars was taken as a benchmark for comparison with the GFRP-reinforced columns. Cascardi et al. [51] indicated that the change in the behavior of steel reinforced hollow concrete columns become noticeable after this *i/o* ratio as the columns with smaller voids kept a higher confinement effect than with bigger voids. Moreover, GFRP spirals instead of steel ones were used to reinforce the steel-reinforced hollow column in order to examine the design's impact on strength and ductility since hollow columns fully reinforced with steel have already been investigated [1,12,17]. Likewise, no solid steel-reinforced concrete column has been prepared and tested due to the behavior of this construction system has widely investigated by Pantelides et al. [14]. Fig. 2 shows the cross sections of the tested columns, Table 2 provides the details of the various specimens, and Fig. 3 illustrates the assembled reinforcement cages. Table 2 also gives the reinforcement ratios and volumetric ratios of the columns. In this table, the reinforcement ratio was calculated by dividing the nominal area of the longitudinal reinforcement (1191 mm²) by the gross sectional area of the concrete. On the other hand, the volumetric ratio was calculated by dividing the volume of one spiral round by the concrete core volume within one spiral pitch (100 mm). The diameter of the inner concrete core was measured from the center of the spirals, and the height was the spiral pitch. The specimens were designated as being either solid (S) or hollow (H), followed by the type of longitudinal reinforcement (G for GFRP bars and S for steel bars) and the diameter in mm of the hollow core at the column center. For example, specimen HG65 is a hollow column reinforced with GFRP bars and has an inner core diameter of 65 mm.

2.3. Test setup and instrumentation

The columns were tested under monotonic concentric loading using a 2000 kN hydraulic cylinder with a loading rate of 1.5 mm/min. Prior to testing, a total of six strain gauges were mounted on each column specimen to measure the strain in the

longitudinal reinforcement (2 gauges 3 mm in length), spiral reinforcement (2 gauges 3 mm in length), and outer surface of the concrete (2 gauges 20 mm in length). Fig. 4(a) shows the location of the electrical-resistance strain gauges attached to the reinforcement and concrete surfaces at the mid-height of all columns. Steel clamps measuring 50 mm in width and 10 mm in thickness were used at the top and bottom of the columns; 3 mm thick neoprene cushions were used to prevent premature cracking and ensure that failure occurred in the test region (column mid-height). In addition, 3 mm thick neoprene cushions were placed on the top and bottom of the columns for uniform load distribution, as shown in Fig. 4(b). The applied load was measured with a 2000 kN load cell and the axial deformation was recorded using a string pot. Throughout testing, the load, strain, and axial deformation were recorded with the System 5000 data logger. Failure propagation was also carefully observed during the entire loading regime.

3. Results and discussion

3.1. Failure mode

Fig. 5 shows the tested concrete columns after failure. Failure in all the tested samples initiated with the development of vertical and inclined hairline cracks at column mid-height. With increasing load, more hairline cracks developed, widened, and propagated along column height. This was followed by spalling of the concrete cover, rupturing or buckling of the longitudinal and transverse spiral reinforcement, and crushing of the confined concrete core. The mechanism and extent of rupture of the longitudinal and transverse GFRP reinforcement varied among the tested columns. SG0, HG40, and HG65 exhibited almost the same failure behavior: the lateral spirals fractured first, followed by longitudinal-bar failure, and concrete crushing. Fig. 5(a–c) show the buckled and ruptured longitudinal and spiral GFRP reinforcement in SG0, HG40, and HG65, respectively. Fig. 5(d) shows the rupture of the longitudinal GFRP bars in HG90. Interestingly, while HG90 evidenced no rupture of GFRP spirals, its concrete cover spalled along almost the entire column height. There was also concrete crushing observed at the inner concrete wall, as shown in Fig. 5(c). Fig. 5(e) shows the buckling failure of the longitudinal steel reinforcement in HS65. Like with HG90, the GFRP spirals in HS65 did not rupture, although crushing in the inner concrete wall was observed when the steel bars buckled. Fig. 6 gives a more detailed photo of the failure behavior in the test region. Fig. 6(a) clearly shows the reinforcement failure in SG0 and HG40. Fig. 6(b–d), respectively, depict the reinforcement failure in HG65, HG90, and HS65. Moreover, Table 3 provides a summary of the different reinforcement failure modes. In addition, once failure occurred, inclined shear-

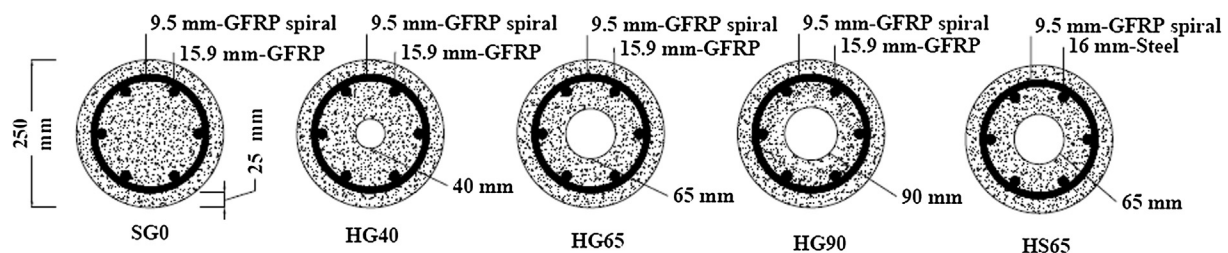


Fig. 2. Concrete-column cross sections.

Table 2
Concrete-column matrices and details.

	Inner Core Diameter (mm)	Inner-to-Outer Diameter Ratio (<i>i/o</i>)	Inner Concrete-Wall Thickness (mm)	Reinforcement Ratio (%)	Volumetric Ratio (%)
SG0	00	0.00	–	2.41	1.49
HG40	40	0.16	70.0	2.47	1.56
HG65	65	0.26	57.5	2.59	1.69
HG90	90	0.36	45.0	2.78	1.92
HS65	65	0.26	57.5	2.59	1.60

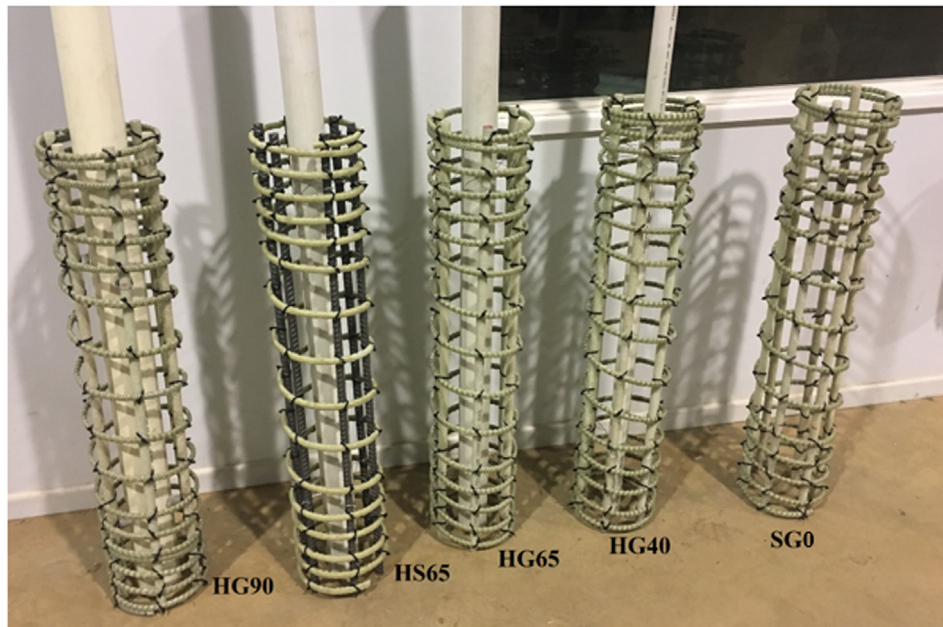
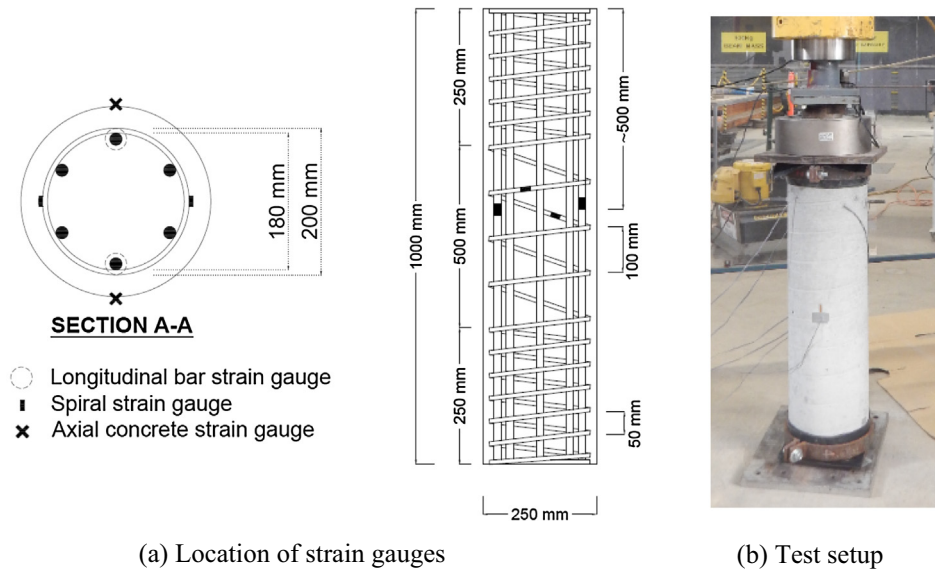


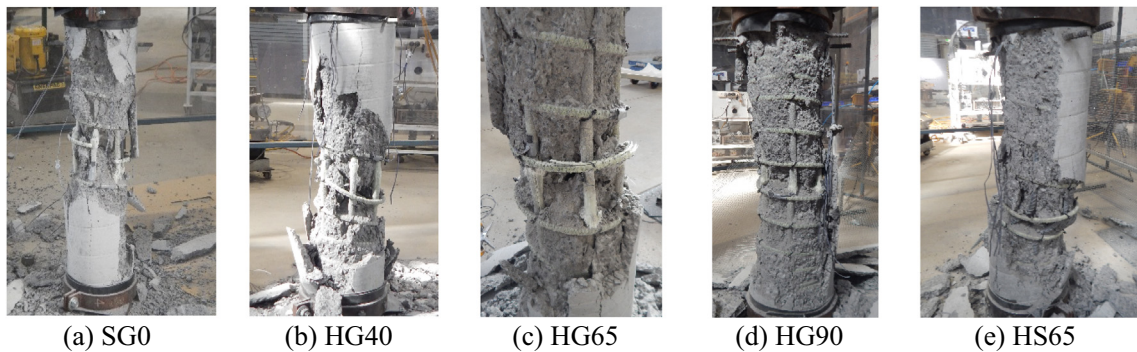
Fig. 3. Assembled GFRP reinforcement for the concrete columns.



(a) Location of strain gauges

(b) Test setup

Fig. 4. Test setup and instrumentation for the hollow concrete columns.



(a) SG0

(b) HG40

(c) HG65

(d) HG90

(e) HS65

Fig. 5. Concrete columns after failure.

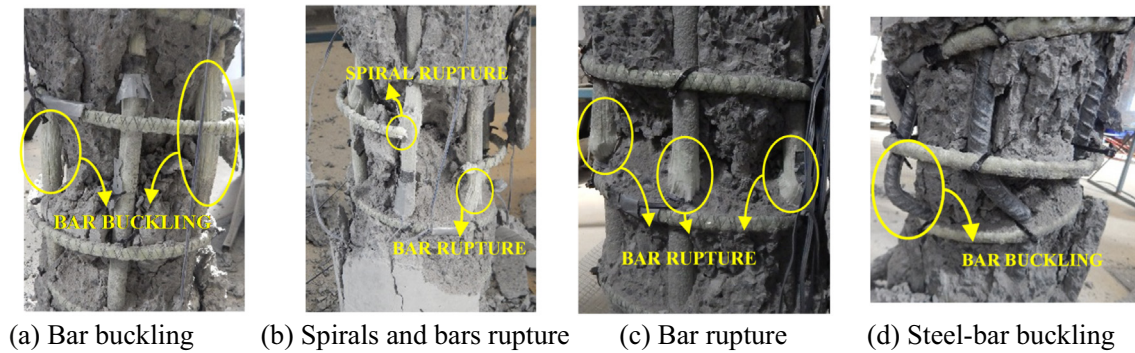


Fig. 6. Different modes of reinforcement failure.

Table 3
Summary of reinforcement failure modes.

Column	Failure of Longitudinal Reinforcement	Failure of Transverse Reinforcement
SG0	Rupture/buckling; GFRP buckling was dominant	Fracture, with a relatively short time between spiral and bar failure
HG40	Rupture/buckling; GFRP buckling was dominant	Fracture, with less time between spiral and bar failure
HG65	Rupture at different GFRP-bar heights	Fracture in spirals concomitant with bar rupture
HG90	Rupture at the same height of the GFRP bars	No failure in GFRP spirals even after bar rupture
HS65	Nonuniform steel-bar buckling	No failure in GFRP spirals even after bar buckling

failure planes were observed in the crushed zone of the failed columns. The inclined failure plane was defined by the failure test zone, as shown in Fig. 5.

3.2. Load and deformation behavior

Fig. 7 shows the actual load and deformation behavior of all the tested columns. Firstly, SG0 exhibited almost linear load–deformation behavior up to an applied load of 1500 kN and axial deformation of 9 mm. Brief nonlinear behavior was then observed until the maximum load of 1588 kN was reached at a deformation of 10.4 mm. This nonlinear load–deformation behavior is due to the development and propagation of cracks in the concrete cover.

The concrete cover then spalled, at which point the load capacity dropped to 1306 kN and the deformation was 12 mm. Afterward, the load increased linearly to 1368 kN and deformation of 14.3 mm. This increase in load can be attributed to the transverse GFRP spirals confining the concrete core. The longitudinal and spiral GFRP reinforcement then ruptured, resulting in final column failure, as shown in Fig. 6.

The load and deformation behavior of HG40, HG65, HG90, and HS65 were similar to that of SG0 up to the maximum applied load. The maximum load achieved for columns HG40, HG65, HG90, and HS65 was 1408 kN, 1559 kN, 1411 kN, and 1408 kN, respectively. After the maximum load was reached, the concrete cover of all columns was spalled, which decreased the load capacity, resulting in load dropping to 1260 kN, 1251 kN, 1267 kN, and 1197 kN for HG40, HG65, HG90, and HS65, respectively. It is interesting to note that the capacity of all the columns was almost the same just after the spalling of the concrete cover, despite the different effective cross-sectional areas. This could be due to the confinement efficiency of the GFRP spirals, as will be discussed in the next section. HG40 and HG90 almost reached load capacity with increasing deformation before final failure. In contrast, the load capacity of HG65 increased to 1458 kN with a deformation of 18.3 mm before the longitudinal and spiral GFRP reinforcement ruptured. Conversely, the load capacity of HS65 continued to decrease up to final failure as demonstrated by the buckling of longitudinal steel bars, as shown in Fig. 6(d). Table 4 shows the test results for the five concrete columns, including peak loads, deformations, and GFRP-bar contribution.

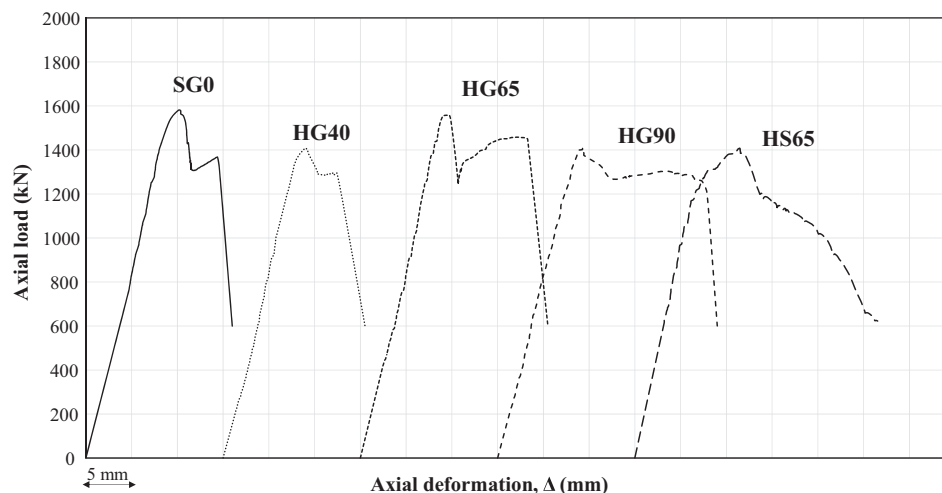


Fig. 7. Axial load and deformation of the tested concrete columns.

Table 4

Summary of the test results.

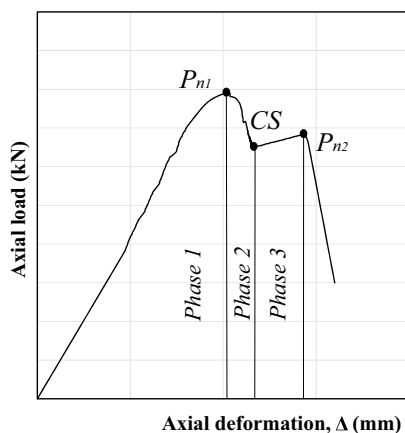
Column	P_{n1} (kN)	P_{n2} (kN)	f'_{cc} (MPa)	f'_{cc}/f'_{co}	Δ_1 (mm)	Δ_2 (mm)	Ductility factor	$\varepsilon_{ur, \text{concrete}}$ ($\mu\varepsilon$)	$\varepsilon_{ur, \text{bar at } P_{n1}}$ ($\mu\varepsilon$)	P_{bar} (kN)	Spiral strain at P_{n1} ($\mu\varepsilon$)	Spiral strain at P_{n2} ($\mu\varepsilon$)
SG0	1588	1368	48.3	1.79	10.4	14.3	1.38	1858	2630	187	1265	–
HG40	1408	1295	47.8	1.77	9.3	12.4	1.33	2285	2520	180	1045	10,989
HG65	1559	1458	58.3	2.16	9.8	18.3	1.88	2242	2710	193	678	12,104
HG90	1411	1304	59.6	2.19	9.3	22.2	2.40	2181	2320	165	643	12,733
HS65	1408	1226	47.8	1.77	11.5	14.0	1.22	1743	2594	603	905	6546

3.3. Ductility

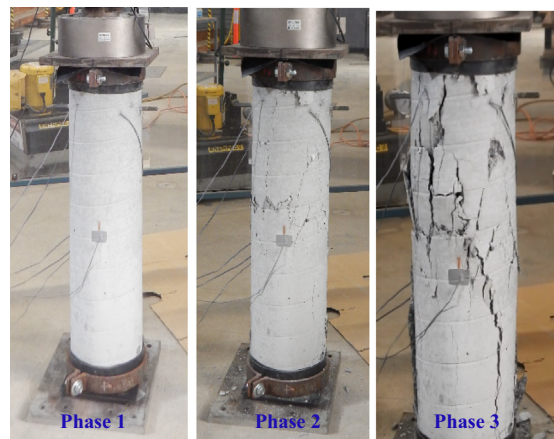
The typical load–deformation behavior of the hollow concrete columns reinforced with GFRP bars and spirals can be divided into three dominant phases, as shown in Fig. 8(a). During the first phase, the columns exhibited a steady state of loading, and the concrete surface was free of cracks identified by a linear-elastic part. Nonlinear behavior was, however, observed due to the propagation of hairline cracks shortly before the peak-load point (P_{n1}) at axial deformation Δ_1 , as shown in phase 1 [Fig. 8(b)]. P_{n1} is the maximum load carried by the gross concrete area and longitudinal reinforcement before total or partial spalling of the outer concrete cover. The second phase was characterized by a significant drop in load due to the cracking of the concrete cover, leading to concrete spalling (CS). At this stage, the effective area of the column was reduced, as shown in phase 2 [Fig. 8(b)]. In phase 3, the concrete cover was partially or completely removed, causing bulging in the lateral reinforcement, as shown in phase 3 [Fig. 8(b)]. Accordingly, depending on the level of lateral confinement provided by the GFRP spirals to the concrete core, the applied load can increase, decrease, or remain the same with the increase in deformation until the second peak load (P_{n2}), which can be taken as the failure load of the confined concrete core at axial deformation Δ_2 .

Ductility is the ability to withstand plastic deformation before failure [19,52]. This behavior was examined to assess the ductility of GFRP-reinforced hollow concrete columns, as shown in Fig. 7, and to compare it to that of steel-reinforced hollow columns, which have been found to exhibit brittle or limited ductile behavior [1]. In this study, the ductility factor (DF) μ_Δ was calculated [Eq. (1)] as the ratio of Δ_2 at 85% of P_{n1} in the post-loading stage or the maximum axial deformation to Δ_1 at P_{n1} , as described in Fig. 9.

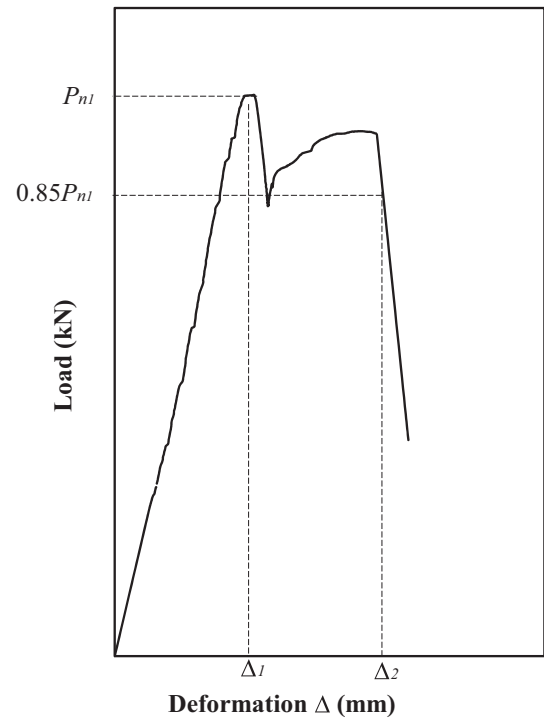
$$\mu_\Delta = \frac{\Delta_2}{\Delta_1} \quad (1)$$



(a) Typical load–deflection curve



(b) Column behavior during loading

Fig. 8. Loading phases in hollow concrete columns.**Fig. 9.** Ductility factor for HG65.

In fact, Δ_2 is considered to be the axial deformation at the failure point for columns that showed stability or increasing in load–deformation behavior at the post-peak stage. Furthermore, it is considered as the axial deformation at the point 85% of P_{n1} for columns that showed descending load–deformation behavior at the

post-peak stage. This approach was implemented by Lignola et al. [53] and Kusumawardaningsih and Hadi [1] to calculate the ductility factor for circular and square hollow and solid concrete columns with and without FRP reinforcement. According to Table 4, HS65 exhibited limited and low ductility. Many researchers have observed this behavior with steel-reinforced hollow concrete columns [4,6,53]. Interestingly, using GFRP reinforcement in hollow concrete columns yielded approximately the same ductility as in hollow concrete columns reinforced with steel bars and wrapped in CFRP material [1,53].

3.4. Strength and confinement efficiency

Table 4 shows the confined strength (f'_{cc}) and confinement efficiency of the tested concrete columns, which is expressed as the strength enhancement of the concrete core after spalling of the concrete cover. These values indicate how effective the spiral reinforcement was in confining the concrete core, as illustrated in Fig. 10. After reaching the peak stress at point P_{n1} , the columns started to lose the concrete cover, and the confinement process was activated by the transverse GFRP spirals until reaching the maximum confined compressive strength (f'_{cc}) at the failure point P_{n2} . Confinement efficiency was then calculated as f'_{cc}/f'_{co} , wherein f'_{cc} is the confined concrete compressive strength (point P_{n2}) and f'_{co} is the unconfined concrete compressive strength (85% of f'_c —the average compressive strength of concrete cylinders tested at 28 days—, when the outer surface was free of cracks). A similar approach was implemented by Tobbi et al. [30], Maranan et al. [31], and Karim et al. [36] wherein they have calculated the f'_{cc} by dividing the peak load (point P_{n2}) by the concrete core area after concrete cover spalling, and f'_{co} was taken as $0.85f'_c$. The concrete core area (A_{core}) was taken from the distance between the centers of GFRP spirals excluding the inner void. Based on the test results, the columns reinforced with GFRP bars had a higher confined concrete compressive strength than the hollow column reinforced

with steel bars. Unlike the GFRP bars, which were able to achieve greater axial strain due to their linear-elastic behavior and higher strength, the steel bars buckled after reaching their yield axial strain. This behavior of the steel-reinforced hollow concrete column is consistent with the findings of Yazici [12], who found that once the steel bars had yielded, it will start to buckle unless there is a high lateral confinement from the spirals. The bars then cannot confine the concrete core and the load capacity of the column will continue to drop, which was also observed in the load-deformation behavior of column HS65.

3.5. Influence of hollowness

The hollow concrete columns reinforced with GFRP bars and spirals (HG90) exhibited some notable behavior compared to the solid column (SG0). As expected, SG0 had the highest failure load owing to it having the largest concrete area. Its failure behavior was brittle due to the lateral and longitudinal reinforcement rupturing. In contrast, HG90 exhibited a pseudo-ductile failure behavior, evidenced as partial crushing of the concrete, followed by bar rupture. The ultimate concrete strain in the solid column reached $1858 \mu\epsilon$, which is 15% less than the concrete strain in HG90, indicating that the concrete cover contributed more to the hollow columns than the solid column before cracking. Furthermore, the longitudinal GFRP bars' contribution in the hollow columns was almost similar to that of the solid column by an average of 12.2% of P_{n1} . The GFRP-bar contribution was calculated by multiplying the average axial strain by the elastic modulus and the total area of the longitudinal GFRP bars, divided by P_{n1} . The measured GFRP-bar contribution was similar to that of Tobbi et al. [30] and Karim et al. [36]. Interestingly, the GFRP bars in the solid and hollow columns showed a compressive-strength capacity at failure of around 50% of their tensile strength, which is consistent with Detiz et al. [54] and Maranan et al. [31]. Compressive strength of the bars was found by multiplying the bars' elastic modulus with the average of the two strain readings on the bars which the difference between strain readings was less than $\pm 4\%$ of the average value. It was also observed that the concrete core was confined more effectively in the hollow columns than the solid one, as represented by their higher deformation capacity and higher confinement efficiency [Table 4]. This table shows that the confinement efficiency of the concrete core in HG90 was 22% higher than that of SG0. Similarly, HG90's ductility was 74% higher than that of SG0 due to higher volumetric and reinforcement ratio, even though, they are reinforced with the same number of bars and spirals. This finding is also refer to the low effect of lateral concrete dilation in HG90 regarding absence of the inner concrete core which affected by the delay in reaching the ultimate lateral plastic concrete expansion resulting in gaining the chance to withstand more axial deformation and axial loads before failure compared with SG0, especially after concrete-cover spalling. It is good to note that lateral strain readings for the elastic and plastic stages were taken from the strain gauges attached on the spirals since it was sufficiently recommended to pick up the lateral strain for the concrete and that is due to the early cracking of the concrete surface at axial strain of $1500 \mu\epsilon$ [55], and this approach was also implemented by [1,56].

3.6. Influence of inner-to-outer (i/o) diameter ratio

Table 4 and Fig. 7 show the behavior and results for the hollow columns with different i/o ratios. As expected, decreasing P_{n1} was observed in the hollow columns with increased i/o ratio due to reduced cross-sectional area, although the failure behavior changed from brittle to ductile with increasing i/o due to the crushing failure of the concrete core with the longitudinal GFRP bars while

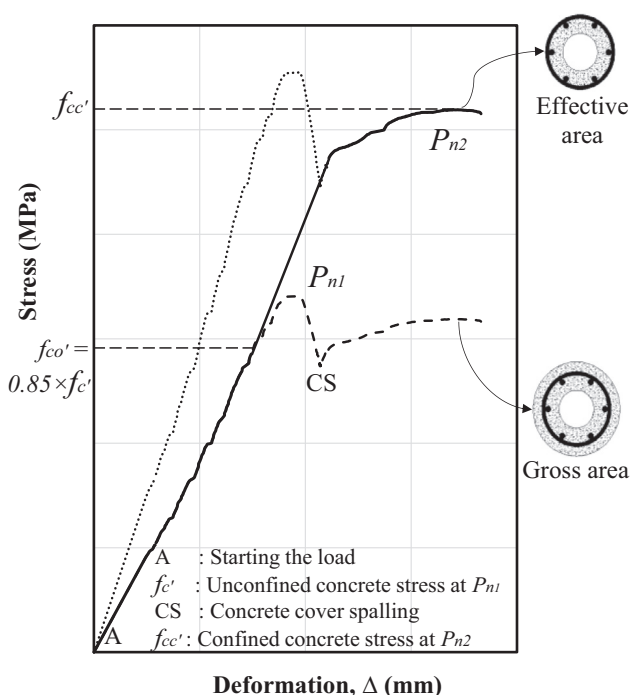


Fig. 10. Confined and unconfined concrete compressive strength for HG65.

the spirals remained intact. Furthermore, increasing the i/o ratio led to an increase in the actual unconfined compressive strength based on gross sectional area. Accordingly, the actual concrete compressive strength of the hollow columns approached the compressive strength obtained from testing standard concrete cylinders. In fact, the columns with i/o ratio of 0.36 and 0.26 achieved almost 94% of f'_c before concrete spalling occurred. This behavior might be related to the lower elastic concrete dilation due to the void existence evidenced by the strain readings related to GFRP spirals at P_{n1} [Table 4]. This finding emphasized the higher stability of the section while increasing the i/o ratio, as reported by Lignola et al. [57].

After P_{n1} , the increase in i/o ratio from 0.16 to 0.36 led to a 24% increase in f'_{cc} . This can be explained by the arch effect suggested by Tobbi et al. [28], in which the thinner reinforced inner concrete wall led to the increase in circumferential stresses exerted by radial stresses provided from the GFRP spirals which the spiral stress can be found by multiplying the measured spiral strain addressed in Table 4 with its modulus of elasticity. In fact, GFRP spirals resisted the deformation of the longitudinal bars and created inward circumferential stress. Accordingly, the concrete-core wall thickness of HG40 and HG65 was adequate to withstand the circumferential stresses resulting in the failure to be initiated in the longitudinal reinforcement and spirals. Conversely, the failure was initiated in the inner concrete wall when the radial stress provided by the GFRP spirals was higher than the circumferential stresses in the concrete core. This point represents the maximum confined stress of the inner concrete wall, which can be evidenced by attaining HG90 the maximum confined strength of 60 MPa [Table 4] followed by gradual degradation in the load-deformation behavior until failure due to concrete core crushing [Fig. 7]. On the other hand, deformation capacity also increased with increasing i/o ratio. This could be explained by the increase in the effective reinforcement ratio when the concrete cover spalled, resulting in increasing the axial stiffness of the GFRP bars compared to the remaining inner concrete, i.e., the reinforcement ratio increased from 2.47% to 3.78%, and from 2.78% to 4.74% for the columns with i/o ratio of 0.16 and 0.36, respectively. Therefore, the column with i/o ratio of 0.36 exhibited 80% higher deformation capacity compared to the column with i/o ratio of 0.16.

Correspondingly, the increase in the effective reinforcement ratio in the post-loading stage led to the GFRP bars providing higher stiffness and, consequently, withstanding higher axial stresses and deformations with increasing i/o ratios. Moreover, the increase in i/o ratio increased the axial deformation capacity for thick-walled sections, as reported by Lignola et al. [57]. This behavior resulted in good distribution of the lateral force pushing the GFRP spirals outward and more stability in the concrete core until failure, which caused more tensile stress to develop along the height of the outer concrete cover with increasing i/o ratio. As a result, the columns lost almost 60%, 70%, 90%, and 100% of concrete cover, as shown in Fig. 11.

3.7. Influence of the type of longitudinal reinforcement

The influence of longitudinal reinforcement type was assessed by comparing the behavior of columns HG65 and HS65. As indicated in Table 3, these columns had the same reinforcement ratio but different reinforcement types: HG65 with GFRP bars and HS65 with steel bars. The results showed that P_{n1} of HG65 was 11% higher than that of HS65 due to early concrete cover cracking in HS65 evidenced by the early starting of the non-linearity in the load-deformation behavior [Fig. 7]. At P_{n1} , when the concrete cover spalled, the longitudinal steel in HS65 reached a compressive strain of 2590 $\mu\epsilon$, while the strain in the longitudinal GFRP bars



Fig. 11. Concrete-cover spalling of tested hollow columns.

in HG65 was 2710 $\mu\epsilon$. However, GFRP bars continued to record axial strains until failure due to the linear-elastic behavior of the GFRP bars and its higher strain capacity compared to the limited strain capacity of the steel bars. Moreover, the fact that the elastic modulus and stiffness of the GFRP reinforcement and concrete were more similar than those of the steel and concrete indicates greater compatibility of GFRP reinforcement with hollow concrete columns.

In post-loading stage, HG65 revealed higher ability to confine the concrete core than HS65 addressed by showing increasing load-deformation response in HG65 compared to a continues degradation in HS65. This finding is due to attain the latter the maximum withstanding axial capacity by reaching the yielding point and then buckling the steel bars, which is evidenced by the difference in the spiral strain readings at failure [Table 4]. Similar finding was found by Kusumawardaningsih and Hadi [1], Yazici [12] and Hadi and Le [2] in steel-reinforced hollow concrete columns. According to Table 4, HG65 attained 22% higher confinement efficiency and 54% higher ductility compared to HS65. Before failure occurred, the longitudinal GFRP bars achieved up to 629 MPa, which is more than 50% of its tensile strength, indicating the effective use of the GFRP bars in hollow columns. Accordingly, the observed behavior and failure mechanism of the hollow concrete columns reinforced with GFRP bars were different from those of the steel-reinforced hollow columns. Several researchers [7,9,16,53] indicated that steel-reinforced hollow concrete columns exhibited brittle failure behavior, either due to premature longitudinal-bar buckling or inner concrete wall crushing, which the latter is consistent with the behavior observed in HS65. On the other hand, HS65 showed brittle failure compared to the solid column reinforced with steel bars and GFRP spirals as also observed by Pantelides et al. [14], owing to the crush in the inner concrete wall following the steel bars buckling.

4. Theoretical assessment of compressive behavior

4.1. Axial design load capacity

The design load capacity of FRP-reinforced concrete columns is provided by the concrete with respect to its gross section area [30] wherein the contribution of the GFRP bars is still ignored by CSA [58] and ACI [59] due to the lack of experimental studies. Various

authors [27,30,31,33] have found that the contribution of the longitudinal GFRP bars is needed to reliably predict the axial design load capacity of concrete columns. However, specifying the exact contribution of the GFRP bars in concrete columns was a controversial issue due to different modes of failure of the GFRP bars in compression. Afifi et al. [27] assumed that the compressive strength of GFRP bars is equal to 35% of the average tensile strength of the GFRP bars as illustrated in Eq. (2). However, this equation overestimated the longitudinal reinforcement contributions due to the higher tensile strength properties of the bars used in this study than that of Afifi et al. [27]. On the other hand, Tobbi et al. [30] suggested the linear-elastic theory for the GFRP bars wherein the compressive strength of GFRP bars can be represented by multiplying the average axial strains at the first peak load, which was 2000 $\mu\epsilon$, by the elastic modulus of GFRP bars [Eq. (3)]. However, the suggested strain level in this model is lower than the actual strain measured in this study, resulting in a lower predicted value than the experimental failure load. The average axial strain at the first peak load of the GFRP bars was (ϵ_{FRP1}) 2500 $\mu\epsilon$ [Eq. (4)], which is consistent with strain level of the unconfined concrete strength for cylinders, as suggested by Samani and Attard [60]. Nevertheless, the concrete area contribution was considered to be equal to 0.85 of the concrete compressive strength similar to solid concrete columns, as recommended in ACI [61]. Further investigations however on the concrete reduction factor may be needed to accurately predict the axial design load capacity of hollow columns reinforced with GFRP bars due to different elastic concrete dilation.

$$P_n = 0.85 \times f'_c \times (A_g - A_{FRP}) + 0.35 \times f_{u,FRP} \times A_{FRP} \quad (2)$$

$$P_n = 0.85 \times f'_c \times (A_g - A_{FRP}) + 0.002 \times E_{FRP} \times A_{FRP} \quad (3)$$

$$P_n = 0.85 \times f'_c \times (A_g - A_{FRP}) + 0.0025 \times E_{FRP} \times A_{FRP} \quad (4)$$

where A_g is gross cross-sectional area of the column; A_{FRP} is cross-sectional area of the FRP longitudinal reinforcement; f'_c is the concrete compressive strength; E_{FRP} is the modulus of elasticity of the FRP longitudinal reinforcement; and $f_{u,FRP}$ is the ultimate tensile strength of the GFRP bar. The ratio of the calculated axial design load capacity (P_n) using Eqs. (2) and (3) to that of the experimentally measured axial-load capacity (P_n) is listed in Table 5, wherein up to 14% difference was observed between the calculated and actual values. This difference is due to the different considerations of the GFRP-bar contribution. As a result, Eq. (4) provided a good agreement between the test results and the predicted axial column capacity [Table 5], except for HG40, for which premature concrete spalling at the bottom of the sample was observed. Further studies, however, are suggested to validate this generalization.

4.2. Confined strength of the hollow concrete column

The lateral confinement provided by the GFRP spirals is significantly activated after the spalling of the concrete cover. This enabled the column to continue carrying the applied axial loads as the spirals prevented the lateral plastic dilation of the remaining

concrete core and avoided the buckling of longitudinal bars, as was also observed by Karim et al. [62]. This lateral confinement resulted in the column exhibiting a second peak load after the concrete-cover spalling. This load was taken as the axial-load capacity of the confined concrete core (effective concrete strength, f_{ce}) and the longitudinal GFRP bars. Although hollow concrete columns are under biaxial stress, the value of f_{ce} still depends on the efficiency of the lateral spirals in preventing the concrete core from failing similar to solid concrete columns. Thus, the f_{ce} was calculated by subtracting the load contribution of the GFRP bars from P_{n2} , then dividing by the effective concrete core area. The effective concrete-core area (A_{cc}) is the area of the concrete core excluding the longitudinal GFRP bars. As a result, the f_{ce} was defined in [Eq. (8)] as a function of the lateral confinement (f_l) and the confinement effectiveness factor (k), which is valid for these results and considered as an initial step to initiate a unified confinement model for hollow concrete columns partially confined with GFRP spirals. Fig. 12 shows the relationship between the effective lateral confinement (kf_l) and (f_{ce}). The k was applied due to the unconfined concrete area between the spirals and generally had a value of less than 1. The lateral confinement stress proposed by Karim et al. [36] for columns reinforced laterally with GFRP spirals was adopted and modified to consider the inner void [Eq. (5)]. On the other hand, the confinement effectiveness factor was adopted by Mander et al. [63] for columns with partial confinement, but it is modified to consider the inner void for hollow columns [Eq. (7)].

$$f_l = \frac{2A_h K_e f_{bent}}{S(D_s - D_i)} \quad (5)$$

$$f_{bent} = \left(0.05 \frac{r}{d_b} + 0.3\right) f_u \leq f_u \quad (6)$$

$$k = \frac{A_{ce}}{A_{cc}} = \frac{\frac{\pi}{4} \left(\left(D_s - \frac{s}{4} \right)^2 - D_i^2 \right)}{\frac{\pi}{4} (D_s^2 - D_i^2) (1 - \rho_e)} \quad (7)$$

$$f_{ce} = 4kf_l + 2.3 \quad (8)$$

In the above equations, A_h is the GFRP spiral cross-sectional area; K_e is the proportion of ultimate strain in GFRP spirals before failure to their ultimate tensile strength, taken as the average of the spiral strains before failure (0.513); f_{bent} is the tensile strength of the bent GFRP bars [Eq. (6)], as recommended by ACI [59]; r is the inner radius of the spiral; d_b is the GFRP spiral diameter; S is the vertical spacing between spirals on centres; D_s is the diameter

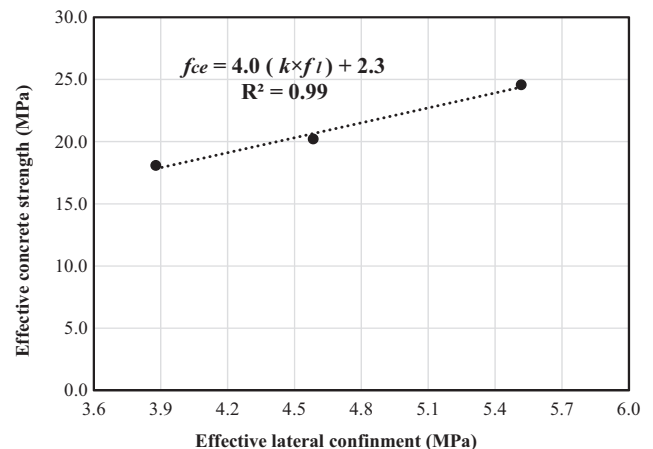


Fig. 12. Effective lateral confinement vs. effective concrete strength.

Table 5

Comparison of failure load between experimental and theoretical results.

	Eq. (2) (P_n/P_{n1})	Eq. (3) (P_n/P_{n1})	Eq. (4) (P_n/P_{n1})
SG0	0.88	0.90	0.93
HG40	0.79	1.00	1.02
HG65	0.91	0.86	0.89
HG90	0.86	0.90	0.92

Table 6

Comparison between theoretical and experimental results for the second peak load and confined strength.

Column	A_{core} (mm ²)	A_{ce} (mm ²)	ρ_e (%)	A_{cc} (mm ²)	k	f_l (MPa)	f_{ce} (MPa)	f'_{cct} (MPa)	P_{nt2} (kN)	f'_{cct}/f'_{cc} (%)	P_{nt2}/P_{n2} (%)
SG0	28,339	–	–	–	–	3.88	–	43.3	1228	89.7	89.7
HG40	27,083	15,249	4.40	25,892	0.789	4.92	17.8	46.8	1268	97.9	97.9
HG65	25,022	13,188	4.76	23,831	0.777	6.06	21.3	51.5	1289	88.4	88.4
HG90	21,980	10,146	5.42	20,789	0.748	7.37	24.1	58.8	1293	98.7	98.7

of spirals on centres; D_i is the diameter of the inner void; A_{ce} is the area of the concrete core, excluding the crushed concrete part due to unconfined concrete between spirals; A_{cc} is the concrete core area, excluding the effective reinforcement ratio of the GFRP bars; s is the clear vertical spacing between spirals; and ρ_e is the effective reinforcement ratio with respect to the concrete core area.

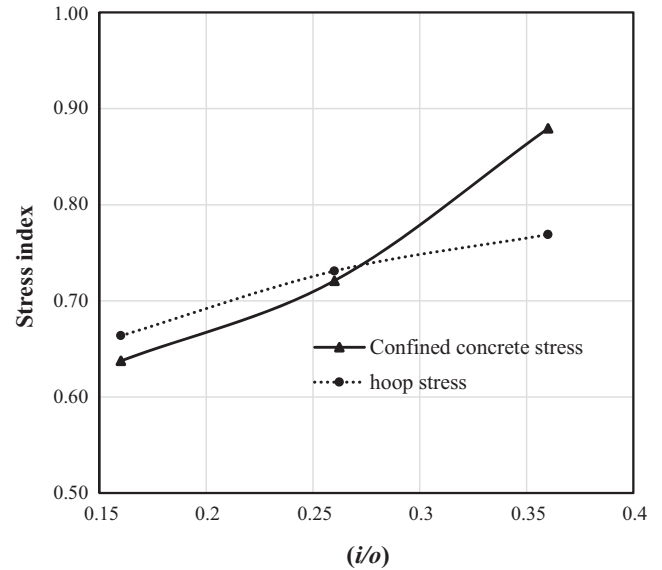
The contribution of the GFRP bars at the second peak was calculated by multiplying the average strain at that load ($\epsilon_{FRP2} = 0.011$), with the elastic modulus and the total area of the GFRP bars. This strain level was 52.4% of the ultimate tensile strain and consistent with the crushing strain of FRP bars (0.0122 ± 0.0012) determined from the compression coupon test by Fillmore and Sadeghian [64]. As a result, Eq. (9) is proposed to predict the axial load capacity at the post-loading stage. In addition, the predicted confined strength f'_{cct} before failure in hollow concrete columns was calculated by dividing the theoretical second peak load (P_{nt2}) by the concrete core area (A_{core}) using Eq. (10). The proposed equations show good agreement with the experimental results, as presented in Table 6. This approach is similar to that of Karim et al. [36] in predicting the confined strength and second axial peak load of the solid concrete column reinforced with GFRP bars.

$$P_{nt2} = f_{ce} A_{cc} + \epsilon_{FRP2} E_{FRP} A_{FRP} \quad (9)$$

$$f'_{cct} = \frac{P_{nt2}}{A_{core}} = \frac{P_{nt2}}{\frac{\pi}{4} (D_s^2 - D_i^2)} \quad (10)$$

4.3. Failure mode prediction

A stress index was obtained for the concrete alone without the bar contribution and the lateral GFRP spirals to predict the final failure mode of hollow concrete columns reinforced with GFRP bars. Stress index of concrete is considered as the value of f_l divided by f'_{co} wherein the stress index of the lateral GFRP spiral is considered as the actual hoop stress in the GFRP spiral divided by the tensile stress of the bent GFRP bars [Eq. (6)], hence the hoop stress was calculated by multiplying the GFRP spiral's strains at the failure load by the elastic modulus of the GFRP spiral itself. In Fig. 13, it can be seen that when the lateral stress index is higher than the concrete stress index, the spirals will fail before the concrete core. When the spirals fracture, the concrete column undergo crushing as was observed in columns HG40 and HG65. On the other hand, the concrete stress index in column HG90 was higher than the spiral stress index, resulting in the concrete core failing before bar rupture and without fracturing of spirals. The i/o ratio in HG90 can be taken as an optimum i/o ratio, as it results in a ductile failure behaviour of the hollow columns wherein the inner core fails first, followed by the longitudinal bars and without failure of the lateral spirals. This failure prediction may need some calibration to consider the size effect due to the changes in the aggregates size to the column diameter ratio or the volumetric ratio of the lateral reinforcement. Cui and Sheikh [65] however highlighted that columns with different sizes in general exhibits almost similar strength enhancement, ductility, and confinement efficiency with

**Fig. 13.** Stress index vs. i/o ratio.

the large scale samples only showing slower failure degradation compared to the rapid strength drop in the small scale columns.

5. Conclusion

This study investigated the axial behavior of hollow concrete columns reinforced with glass-fiber-reinforced-polymer (GFRP) bars and spirals with different inner-to-outer (i/o) diameter ratios. In addition, the applicability of existing design equations for solid concrete columns was assessed for hollow concrete columns reinforced with GFRP bars. Based on the results of this study, the following conclusions can be drawn:

- The hollow columns failed at a lower load than the solid column due to the reduced effective area. Nevertheless, the hollow columns yielded higher concrete compressive strength at peak load than the solid column. The concrete compressive strength of the hollow columns was up to 94% of the average compressive strength of the concrete cylinders.
- The concrete core can be more effectively confined in hollow columns than in solid columns. Up to 74% higher deformation capacity and 21% higher strength confinement efficiency were exhibited by the hollow columns compared to the solid column.
- Increasing the inner-to-outer diameter ratio (i/o) in the hollow columns changed the failure behavior from brittle to pseudo-ductile. After spalling of concrete cover, the failure in the hollow columns with i/o ratio of 0.16 and 0.26 was initiated by the longitudinal and spiral GFRP reinforcement, while the failure of columns with i/o ratio of 0.36 was initiated by crushing of the hollow concrete core.

- The hollow columns with high *i/o* ratio values showed better deformation capacity than those with low *i/o* ratio. This is due to the increased contribution of the GFRP bars to overall column stiffness and strength after spalling of the concrete cover.
- The hollow concrete columns reinforced with GFRP bars and spirals exhibited 11% higher axial capacity than the steel-reinforced hollow column. The GFRP-reinforced hollow columns showed 22% and 54% higher ductility and confinement efficiency, respectively, than the steel-reinforced hollow column.
- The design load capacity of the hollow concrete columns was predicted accurately by considering an axial strain in the GFRP bars of 0.0025 and the gross area of the concrete, while the second peak load was predicted by considering the confined strength of the concrete core and the contribution of GFRP bars at a strain of 0.011.
- A stress index was proposed to determine the final failure mode of hollow concrete columns reinforced with GFRP bars. It was found that the columns failed as the result of spiral failure when the lateral stress index is higher than the concrete stress index, while crushing of the concrete core occurs first when the concrete stress index is higher than the spiral stress index.

Conflict of interest

None.

Acknowledgments

The authors are grateful to Inconmat V-ROD Australia for providing the GFRP bars and spirals. The assistance of the postgraduate students and technical staff at the Centre of Future Materials (CFM) is also acknowledged. The first author is grateful for the PhD scholarship provided by Tafila Technical University (TTU), Jordan.

References

- [1] Y. Kusumawardaningsih, M.N. Hadi, Comparative behaviour of hollow columns confined with FRP composites, *Compos. Struct.* 93 (2010) 198–205.
- [2] M. Hadi, T. Le, Behaviour of hollow core square reinforced concrete columns wrapped with CFRP with different fibre orientations, *Constr. Build. Mater.* 50 (2014) 62–73.
- [3] J. Mander, M. Priestley, R. Park, Behaviour of ductile hollow reinforced concrete columns, *Bull. New Zealand Nat. Soc. Earthquake Eng.* 16 (1983) 273–290.
- [4] F. Zahn, R. Park, M. Priestley, Flexural strength and ductility of circular hollow reinforced concrete columns without confinement on inside face, *Struct. J.* 87 (1990) 156–166.
- [5] K. Osada, T. Yamaguchi, S. Ikeda, Seismic performance and the strengthening of hollow circular RC piers having reinforced cut-off planes and variable wall thickness, *Concr. Res. Technol.* 101 (1999) 13–24.
- [6] J.-I. Hoshikuma, M. Priestley, Flexural behavior of circular hollow columns with a single layer of reinforcement under seismic loading, *SSRP* 13 (2000).
- [7] A. Pinto, J. Molina, G. Tsionis, Cyclic tests on large-scale models of existing bridge piers with rectangular hollow cross-section, *Earthquake Eng. Struct. Dyn.* 32 (2003) 1995–2012.
- [8] Y. Mo, I. Nien, Seismic performance of hollow high-strength concrete bridge columns, *J. Bridge Eng.* 7 (2002) 338–349.
- [9] A. Pavese, D. Bolognini, S. Peloso, FRP seismic retrofit of RC square hollow section bridge piers, *J. Earthquake Eng.* 8 (2004) 225–250.
- [10] J.-H. Lee, J.-H. Choi, D.-K. Hwang, I.-J. Kwahk, Seismic performance of circular hollow RC bridge columns, *KSCE J. Civ. Eng.* 19 (2015) 1456–1467.
- [11] F.Q. Junior, B. Horowitz, Shear strength of hollow circular sections Resistência ao cisalhamento de seções circulares vazadas, 2016.
- [12] V. Yazici, Strengthening hollow reinforced concrete columns with fibre reinforced polymers, 2012.
- [13] J. Li, J. Gong, L. Wang, Seismic behavior of corrosion-damaged reinforced concrete columns strengthened using combined carbon fiber-reinforced polymer and steel jacket, *Constr. Build. Mater.* 23 (2009) 2653–2663.
- [14] C.P. Pantelides, M.E. Gibbons, L.D. Reaveley, Axial load behavior of concrete columns confined with GFRP spirals, *J. Compos. Constr.* 17 (2013) 305–313.
- [15] R. Modarelli, F. Micelli, O. Manni, FRP-confinement of hollow concrete cylinders and prisms, in: *Proceedings of the 7th International Symposium on FRP reinforcement for reinforced concrete structures*, Kansas City, Missouri: Citeseer, 2005. p. 6–9.
- [16] G. Lignola, A. Prota, G. Manfredi, E. Cosenza, Analysis of the confinement of RC hollow columns wrapped with FRP, *Mater. Charact.* 3 (2007) 300.
- [17] V. Yazici, M.N. Hadi, Axial load-bending moment diagrams of carbon FRP wrapped hollow core reinforced concrete columns, *J. Compos. Constr.* 13 (2009) 262–268.
- [18] T. Falsafi, S. Hadigheh, R. Morshed, R. Shaiganfar, Experimental Study on Behaviour of Prismatic and Cylindrical Hollow Concrete Columns Reinforced with FRP Materials, 2010.
- [19] G.P. Lignola, F. Nardone, A. Prota, A. De Luca, A. Nanni, Analysis of RC hollow columns strengthened with GFRP, *J. Compos. Constr.* 15 (2011) 545–556.
- [20] X.-L. Zhao, L. Zhang, State-of-the-art review on FRP strengthened steel structures, *Eng. Struct.* 29 (2007) 1808–1823.
- [21] M. Elchalakani, Rehabilitation of corroded steel CHS under combined bending and bearing using CFRP, *J. Constr. Steel Res.* 125 (2016) 26–42.
- [22] G. Nkurunziza, A. Debaiky, P. Cousin, B. Benmokrane, Durability of GFRP bars: a critical review of the literature, *Prog. Struct. Mat. Eng.* 7 (2005) 194–209.
- [23] A. Manalo, B. Benmokrane, K.-T. Park, D. Lutze, Recent developments on FRP bars as internal reinforcement in concrete structures, *Concr. Aus.* 40 (2014) 46–56.
- [24] A. Ashour, Flexural and shear capacities of concrete beams reinforced with GFRP bars, *Constr. Build. Mater.* 20 (2006) 1005–1015.
- [25] B. Abdul-Salam, A.S. Farghaly, B. Benmokrane, Mechanisms of shear resistance of one-way concrete slabs reinforced with FRP bars, *Constr. Build. Mater.* 127 (2016) 959–970.
- [26] A. Hassanein, N. Mohamed, A.S. Farghaly, STR-830: Enhancing the deformation capacity of concrete shear walls reinforced with GFRP bars, 2016.
- [27] M.Z. Afifi, H.M. Mohamed, B. Benmokrane, Axial capacity of circular concrete columns reinforced with GFRP bars and spirals, *J. Compos. Constr.* 18 (2013) 04013017.
- [28] H. Tobbi, A.S. Farghaly, B. Benmokrane, Concrete columns reinforced longitudinally and transversally with glass fiber-reinforced polymer bars, *ACI Struct. J.* 109 (2012) 551.
- [29] S. Alsayed, Y. Al-Salloum, T. Almusallam, M. Amjad, Concrete columns reinforced by glass fiber reinforced polymer rods, *Special Publ.* 188 (1999) 103–112.
- [30] H. Tobbi, A.S. Farghaly, B. Benmokrane, Behavior of concentrically loaded fiber-reinforced polymer reinforced concrete columns with varying reinforcement types and ratios, *ACI Struct. J.* 111 (2014) 375.
- [31] G. Maranan, A. Manalo, B. Benmokrane, W. Karunasena, P. Mendis, Behavior of concentrically loaded geopolymer-concrete circular columns reinforced longitudinally and transversely with GFRP bars, *Eng. Struct.* 117 (2016) 422–436.
- [32] H.J. Zadeh, A. Nanni, Design of RC columns using glass FRP reinforcement, *J. Compos. Constr.* 17 (2012) 294–304.
- [33] M.N. Hadi, H. Karim, M.N. Sheikh, Experimental investigations on circular concrete columns reinforced with GFRP bars and helices under different loading conditions, *J. Compos. Constr.* 20 (2016) 04016009.
- [34] A. Hadhood, H.M. Mohamed, B. Benmokrane, Experimental study of circular high-strength concrete columns reinforced with gfrp bars and spirals under concentric and eccentric loading, *J. Compos. Constr.* 04016078 (2016).
- [35] A. De Luca, F. Matta, A. Nanni, Behavior of full-scale glass fiber-reinforced polymer reinforced concrete columns under axial load, *ACI Struct. J.* 107 (2010) 589.
- [36] H. Karim, M.N. Sheikh, M.N. Hadi, Axial load-axial deformation behaviour of circular concrete columns reinforced with GFRP bars and helices, *Constr. Build. Mater.* 112 (2016) 1147–1157.
- [37] M.A. Ali, E. El-Salakawy, Seismic performance of GFRP-reinforced concrete rectangular columns, *J. Compos. Constr.* 20 (2015) 04015074.
- [38] A. Tavassoli, Behaviour of Circular Concrete Columns Internally Reinforced with Steel and GFRP under Combined Axial Load and Bending 2015.
- [39] A. Tavassoli, S.A. Sheikh, Seismic Resistance of Circular Columns Reinforced with Steel and GFRP, *J. Compos. Constr.* 04017002 (2017).
- [40] N. Mohamed, A.S. Farghaly, B. Benmokrane, K.W. Neale, Experimental investigation of concrete shear walls reinforced with glass fiber-reinforced bars under lateral cyclic loading, *J. Compos. Constr.* 18 (2013) A4014001.
- [41] CSA, Specification for fibre-reinforced polymers, Canadian Standards Association, CAN/CSA-S806-10, Rexdale, ON, Canada, 2010.
- [42] B. Benmokrane, A. Manalo, J.-C. Bouhet, K. Mohamed, M. Robert, Effects of diameter on the durability of glass fiber-reinforced polymer bars conditioned in alkaline solution, *J. Compos. Constr.* 21 (2017) 04017040.
- [43] ASTM, Standard test method for tensile properties of fiber reinforced polymer matrix composite bars, ASTM D7205/D7205M-06, West Conshohocken, PA, 2011b.
- [44] ASTM/C143, Standard Test Method for Slump of Hydraulic Cement Concrete, ASTM International, West Conshohocken, PA, 2005.
- [45] ASTM/C31, Standard Practice for Making and Curing Concrete Test Specimens in the Field, ASTM International, West Conshohocken, PA, 2015.
- [46] ASTM/C39, Standard Test Method for Compressive Strength of Cylindrical Concrete Specimens, ASTM International, West Conshohocken, PA, 2015.
- [47] ASTM/C1231, Standard Practice for Use of Unbonded Caps in Determination of Compressive Strength of Hardened Cylindrical Concrete Specimens, ASTM International, West Conshohocken, PA, 2015.
- [48] AS3600, Reinforced Concrete Design: in accordance with AS 3600-2009, Sydney, N.S.W: Cement & Concrete Aggregates Australia: Standards Australia, 2011.

- [49] A.Z. Fam, S.H. Rizkalla, Confinement model for axially loaded concrete confined by circular fiber-reinforced polymer tubes, *Struct. J.* 98 (2001) 451–461.
- [50] F. Micelli, R. Modarelli, Experimental and analytical study on properties affecting the behaviour of FRP-confined concrete, *Compos. B Eng.* 45 (2013) 1420–1431.
- [51] A. Cascardi, F. Micelli, M.A. Aiello, Unified model for hollow columns externally confined by FRP, *Eng. Struct.* 111 (2016) 119–130.
- [52] M.A. Maleque, M.S. Salit, *Materials Selection and Design*, Springer, 2013.
- [53] G.P. Lignola, A. Prota, G. Manfredi, E. Cosenza, Deformability of reinforced concrete hollow columns confined with CFRP, *ACI Struct. J.* 104 (2007) 629.
- [54] D. Deitz, I. Harik, H. Gesund, Physical properties of glass fiber reinforced polymer rebars in compression, *J. Compos. Constr.* 7 (2003) 363–366.
- [55] M. Saatcioglu, S.R. Razvi, Strength and ductility of confined concrete, *J. Struct. Eng.* 118 (1992) 1590–1607.
- [56] H.M. Mohamed, M.Z. Afifi, B. Benmokrane, Performance evaluation of concrete columns reinforced longitudinally with FRP bars and confined with FRP hoops and spirals under axial load, *J. Bridge Eng.* 19 (2014) 04014020.
- [57] G.P. Lignola, A. Prota, G. Manfredi, E. Cosenza, Unified theory for confinement of RC solid and hollow circular columns, *Compos. B Eng.* 39 (2008) 1151–1160.
- [58] CSA, Design and construction of building structures with fibre-reinforced polymers: Canadian Standards Association, CAN/CSA-S806-12, Rexdale, ON, Canada, 2012.
- [59] ACI, Guide for the Design and Construction of Concrete Reinforced with FRP Bars, American Concrete Institute, Farmington Hills, MI, 2015.
- [60] A.K. Samani, M.M. Attard, A stress-strain model for uniaxial and confined concrete under compression, *Eng. Struct.* 41 (2012) 335–349.
- [61] ACI, Building Code Requirements for Structural Concrete (ACI 318-08) and Commentary, ACI Committee 318, American Concrete Institute, Farmington Hills, MI, 2008, p. 473.
- [62] H. Karim, M.N. Sheikh, M.N. Hadi, Confinement of circular concrete columns: a review, *Parameters* 304 (2014) 4.
- [63] J.B. Mander, M.J. Priestley, R. Park, Theoretical stress-strain model for confined concrete, *J. Struct. Eng.* 114 (1988) 1804–1826.
- [64] B. Fillmore, P. Sadeghian, Contribution of longitudinal GFRP bars in concrete cylinders under axial compression, *Can. J. Civ. Eng.* (2018).
- [65] C. Cui, S. Sheikh, Experimental study of normal-and high-strength concrete confined with fiber-reinforced polymers, *J. Compos. Constr.* 14 (2010).

Chapter 4

Axial performance of hollow concrete columns reinforced with GFRP composite bars with different reinforcement ratios

The state-of-the-art review in Chapter 2 identified the reinforcement ratio (ρ) as one of the most critical design parameters for HCCs. Similarly, the findings from the experimental work in Chapter 3 showed that increasing the (i/o) ratio increased indirectly the reinforcement ratio (ρ) and improved the overall behavior of GFRP-reinforced HCCs. This chapter investigated the effect of varying the GFRP reinforcement ratio by changing the diameter and number of the longitudinal bars on the performance of the HCCs. To fulfil this objective, six large scale HCCs 250 mm in diameter and 1 m in height were prepared and tested. In this study, all HCCs had an (i/o) ratio of 0.36 based on the optimum (i/o) ratio in Chapter 3. Moreover, all HCCs were laterally reinforced by GFRP spirals 9.5 mm in diameter and spaced at 100 mm on their centres. Longitudinal ρ was varied between 1% and 4%, which was achieved by using different number (4, 6, and 8 bars – 15.9 mm diameter) and diameter (6 pcs of 12.7 mm, 15.9 mm, and 19.1 mm) of GFRP bars.

The test results showed that increasing the ρ , either by increasing the bar diameter or the bar number, increased the axial design load and the confined strength due to the increase in the reinforcement stiffness, where the stiffness of GFRP bars was unchanged until failure. Testing two HCCs with the same ρ but with different bar number and diameter was more effective in increasing the confined concrete core area by covering more unconfined concrete surfaces compared to the increase in bar diameter. However, the increase in bar diameter showed better displacement capacity than the increase in bar number caused by increased moment of inertia of the GFRP bar with a larger diameter. The developed new analytical model to predict the compressive behavior of HCCs considered the axial crushing strain at failure of GFRP bars in concrete. The crushing strain of GFRP bars in concrete is affected by the level of confinement provided by the lateral reinforcements and compressive strength of concrete. Therefore, the effect of these design parameters was investigated and the results are presented in Chapter 5.



Axial performance of hollow concrete columns reinforced with GFRP composite bars with different reinforcement ratios

Omar S. AlAjarmeh^a, Allan C. Manalo^{b,*}, Brahim Benmokrane^c, Warna Karunasena^b, Priyan Mendis^d

^a University of Southern Queensland, Centre for Future Materials (CFM), School of Civil Engineering and Surveying, Toowoomba 4350, Australia

^b University of Southern Queensland, School of Civil Engineering and Surveying, Centre for Future Materials (CFM), Toowoomba, QLD 4350, Australia

^c University of Sherbrooke, Department of Civil Engineering, Sherbrooke, Quebec, Canada

^d The University of Melbourne, Department of Infrastructure Engineering, Victoria 3010, Australia

ARTICLE INFO

Keywords:

Hollow columns
GFRP composite bars
Reinforcement ratio
Bar diameter
Number of bars
Crushing strain

ABSTRACT

A hollow concrete column (HCC) is a structurally efficient construction system and uses less material. Conventionally, HCCs are reinforced with steel bars, which are prone to corrosion. This study explored the use of glass-fiber-reinforced-polymer (GFRP) composite bars as reinforcement for HCCs and evaluated the effect of the reinforcement ratio on HCC structural behavior. A total of six HCCs reinforced longitudinally with GFRP bars with different reinforcement ratios (1.78%, 1.86%, 2.67%, 2.79%, 3.72, and 4.00%) were prepared and their behavior was investigated. The different reinforcement ratios were achieved by changing the bar diameter (12.7 mm, 15.9 mm, and 19.1 mm) and number of bars (4, 6, 8, and 9 bars). The results show that increasing the diameter and number of bars enhanced the strength, ductility and confinement efficiency of HCC. For columns with equal reinforcement ratios, using more and smaller-diameter GFRP bars yielded 12% higher confinement efficiency than in the columns with fewer and larger-diameter bars. The crushing strain of the GFRP bars embedded the HCC was 52.1% of the ultimate tensile strain. Lastly, the axial-load capacity of the GFRP-reinforced HCC can be reliably predicted by considering the contribution of the concrete and up to 3000 $\mu\epsilon$ in the longitudinal reinforcement.

1. Introduction

Hollow concrete columns (HCC) reinforced with steel bars are used in numerous civil-engineering applications such as bridge piers, power poles, and ground piles due to their superior structural performance and more economic design than solid columns with the same cross-sectional area [1]. The structural behavior and failure mechanism of HCCs depends strongly on the amount of longitudinal reinforcement or the reinforcement ratio [2,3]. Typically, the reinforcement ratio can be varied by either changing the bar diameter or increasing the number of longitudinal reinforcement bars. Lee et al. [3] indicated that increasing the reinforcement ratio from 1.17% to 2.00% in HCC by increasing the longitudinal reinforcement from 14 to 24 pieces of 19.1 mm diameter steel bars increased the cyclic load capacity by resisting 48% higher lateral load at the same lateral displacement. At the same time, however, the column ductility decreased by 20% and resulted in wide and severe crushing of the inner concrete wall. Hoshikuma and Priestley [2]

found that increasing the reinforcement ratio from 1.45% to 3.18% increased the flexural strength by 50% but the moment–curvature ductility decreased 47%. They increased the reinforcement ratio by increasing the bar diameter from 12.7 mm to 19.1 mm. In fact, the increase in reinforcement ratio decreases the ductility due to the yielding and buckling of the steel bars, followed by concrete crushing, as the concrete core had no inner radial confinement. The brittle failure behavior of the HCC with a higher reinforcement ratio can be considered as a result of limited axial strain in the longitudinal steel bars and no radial confinement at the inner concrete wall when the transverse steel yielded. This resulted in crushing of the concrete core and produced a drop in strength after the peak axial load had been reached [4,5].

While steel-reinforced HCCs have exhibited higher structural performance than solid concrete columns in terms of stiffness- and strength-to-weight ratios, steel corrosion is now becoming a global issue for both types of structure, as it leads to shortened service lives and/or premature failure [6]. Fiber-reinforced-polymer (FRP) bars are

* Corresponding author.

E-mail addresses: omar.alajarmeh@usq.edu.au (O.S. AlAjarmeh), allan.manalo@usq.edu.au (A.C. Manalo), Brahim.Benmokrane@USherbrooke.ca (B. Benmokrane), karu.karunasena@usq.edu.au (W. Karunasena), pamendis@unimelb.edu.au (P. Mendis).

<https://doi.org/10.1016/j.compstruct.2019.01.096>

Received 3 August 2018; Received in revised form 27 November 2018; Accepted 28 January 2019

Available online 29 January 2019

0263-8223/© 2019 Elsevier Ltd. All rights reserved.

becoming an effective alternative to steel as internal reinforcement in concrete structures exposed to severe environmental conditions to prevent steel corrosion problems [7]. Also, the GFRP bars are reported to be more compatible for concrete than steel due to have close modulus of elasticity [8,9]. Glass-FRP (GFRP) reinforcement is the preferred type due to its relatively lower cost than carbon- and basalt-fiber-based bars [10]. While some researchers have indicated that the GFRP bars are highly affected by alkaline solutions, Tannous and Saadatmanesh [11] reported that vinylester-based GFRP bars adds high protection to fibers and provides high resistance against chemical attacks. Moreover, Benmokrane et al. [12,13] found that the vinylester-based GFRP bars can retain almost all its original strength and stiffness properties even after long-term exposure to alkaline solution. Several studies [6,14–17] have demonstrated the effective use of GFRP bars as internal reinforcement in solid concrete columns. They have shown that GFRP-reinforced concrete columns have a more stable load–deformation response than steel-reinforced columns due to the higher confinement efficiency provided by transverse GFRP reinforcement. Similarly, adding longitudinal GFRP bars to a plain concrete columns reinforced by lateral GFRP spirals enhances their strength and ductility [17]. Afifi et al. [15] highlighted that increasing the reinforcement ratio from 1.13% to 3.38% by tripling the reinforcement from 4 to 12 GFRP bars 15.9 mm in diameter changed the column failure behavior from brittle to ductile and increased the ductility and confinement efficiency by 117% and 30%, respectively. Moreover, Tobbi et al. [14] concluded that increasing the GFRP-bar diameter from 12.7 mm to 19.1 mm increased the load capacity, mitigated the strength drop due to concrete cover spalling after the peak load, and increased confinement by 20%. These results highlight that the reinforcement ratio also affects the behavior of GFRP-reinforced solid concrete columns, while its effect on hollow concrete columns has yet to be determined.

This study aimed at investigating the axial compressive behavior of hollow concrete columns with different ratios of longitudinal GFRP reinforcement. Large-scale hollow concrete columns reinforced with GFRP bars of different diameters and quantities were prepared and tested under concentric loading to evaluate the load–displacement response, ductility, and failure mechanisms. Analytical equations to describe the compressive behavior and load contribution of the GFRP bars and to estimate the maximum load capacity of hollow concrete columns were developed. The results of this study provide a better understanding of the behavior of this new structural system and generated additional test data that will aid in developing design standards for concrete compressive members reinforced with GFRP bars.

2. Experimental program

2.1. Materials

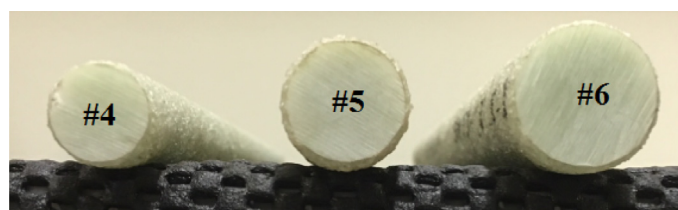
Sand-coated and high-modulus (Grade III) #4, #5, and #6 GFRP bars [18] with nominal diameters of 12.7, 15.9, and 19.1 mm, respectively, shown in Fig. 1(a), were used as longitudinal reinforcement in

the circular hollow concrete columns. The transverse reinforcement was Grade III #3 GFRP spirals with a nominal diameter of 9.5 mm [Fig. 1(b)]. The glass-fiber content by weight of the GFRP bars was around 82.1% [19]. The GFRP reinforcement was manufactured by pultrusion with the glass fibers impregnated with vinyl-ester resin. Table 1 provides the average mechanical properties of the GFRP bars as reported by Benmokrane et al. [19].

The hollow concrete columns were made with ready-mix concrete. The coarse aggregate had a maximum size of 10 mm and the mix had a slump of 105 mm. During concrete casting, six 100 mm diameter and 200 mm high concrete cylinders were prepared and tested on the day of column testing according to the procedures described in ASTM/C39 [20]. The average concrete compressive strength at 28 days was 25.0 MPa, with a standard deviation of 2.4 MPa.

2.2. Specimen details

Six GFRP-reinforced concrete columns 250 mm in diameter and 1 m in height were cast and tested. These dimensions were considered based on the capacity of the loading equipment. All columns were reinforced longitudinally with GFRP bars of different diameters (12.7, 15.9, or 19.1 mm) and amounts (4, 6, or 8 pieces of 15.9 mm diameter bars) but with the same configuration of lateral GFRP spirals. The reinforcement ratio varied in a range of 1.00%–4.00%, as recommended in AS3600 for steel-reinforced concrete columns [21]. The GFRP spirals were vertically spaced at 100 mm on centers (1.57% volumetric ratio) along 500 mm at mid-height and at 50 mm along 250 mm at the top and bottom of the columns to avoid premature failure due to stress concentration. The gross area of the hollow columns was 42704 mm² and the inner-to-outer diameter ratio was constant at 0.36, which was achieved by placing a 90 mm diameter PVC pipe with a wall thickness of 1 mm at the center of the specimens during concrete casting. This inner-to-outer diameter ratio was found to provide a ductile behavior resulting from the progressive failure of the concrete cover, followed by crushing of the concrete core and longitudinal bars with no spiral failure [22]. This inner-to-outer diameter ratio was also implemented by previous researchers [22–26], who demonstrated that this size of hollowness will result in biaxial stress which is the characteristics of hollow concrete columns and will change significantly the behavior of column compared to a solid one. This study focused mainly on the effect of reinforcement ratio as an important design parameter that affect the behavior of hollow concrete columns. Fig. 2 shows the cross section of the tested columns, and Table 2 provides the reinforcement details. Fig. 3 shows the assembled reinforcement cages. The specimens were designated with the letter, G indicating GFRP bars, followed by the amount of longitudinal reinforcement and bar diameter. For example, specimen G-8#5 is a hollow concrete column reinforced with eight pieces of #5 GFRP bars.



(a) Longitudinal GFRP bars



(b) GFRP spirals

Fig. 1. GFRP reinforcement.

Table 1
Mechanical properties of the reinforcement materials [19].

Properties	Test Method	Number of Samples Tested	Values			
			No. 6	No. 5	No. 4	No. 3
Nominal bar diameter	CSA S806, Annex A [15]	9	19.1	15.9	12.7	9.5
Nominal bar area	CSA S806, Annex A [15]	9	286.5	198.5	126.6	70.8
Ultimate tensile strength, f_u (MPa)	ASTM D7205/D7205M-06 [16]	6	1270.0 (31.4)	1237.4 (33.3)	1281.5 (35.3)	1315 (31.1)
Modulus of Elasticity, E_{GFRP} (GPa)	ASTM D7205/D7205M-06 [16]	6	60.5 (0.5)	60.5 (1.3)	61.3 (0.4)	62.5 (0.4)
Ultimate strain, ϵ_u (%)	ASTM D7205/D7205M-06 [16]	6	2.1 (0.1)	2.1 (0.1)	2.1 (0.1)	2.3 (0.1)

2.3. Test setup and instrumentation

The columns were tested under monotonic concentric loading with a 2000 kN hydraulic cylinder. Prior to testing, two strain gauges were mounted each on the longitudinal reinforcement, spiral reinforcement, and outer surface of the concrete to measure the strain at column mid-height. Fig. 4(a) shows the location of the electrical-resistance strain gauges attached to the reinforcement and concrete surface. Steel clamps 50 mm in width and 10 mm in thickness were used at the top and bottom of the columns with 3 mm thick neoprene rubber pads, as shown in Fig. 4(b), to prevent premature cracking and ensure that failure occurred in the test region (column mid-height). In addition, 3 mm thick neoprene rubber pads were placed on the top and bottom of the columns for uniform load distribution. The applied load was measured with a 2000 kN load cell, and the axial deformation was recorded with a string pot. Throughout testing, the loads, strains, and axial deformations were recorded with a System 5000 data logger. The failure propagation was also carefully observed and video-recorded during the entire loading regime.

3. Test results and discussion

3.1. Failure mode

The failure modes of the hollow concrete columns varied due to the different longitudinal GFRP-bar details. In the case of all the specimens, the failure progression was initiated by hairline cracks that spread and propagated along the column height as the applied load increased. Spalling of the concrete cover was then observed, followed by rupturing of the longitudinal bars and the inner confined hollow concrete core. The level of damage of the inner concrete core varied, however, with the reinforcement ratio. None of the transverse GFRP spirals evidenced damage in any of hollow columns. Table 3 summarizes the failure propagation in the tested hollow concrete columns.

3.2. Load-deformation behavior

Fig. 5 shows the axial load and deformation relationship of the six hollow concrete columns tested. Based on the test results, different concentric-load behavior was captured due to different longitudinal GFRP-bar details. Column G-6#4 initially had a linear ascending slope was up to an axial load of 1020.3 kN and axial deformation of 8.57 mm. After that, a slight nonlinear ascending part appeared due to cracks propagation, ending with the first peak axial load of 1035.3 kN at 8.83 mm. Afterwards, a sudden load drop to 922.2 kN with deformation

Table 2

Details of column specimens.

Specimen Name	Number of Bars	Bar Diameter (mm)	Total Reinforcement Area (mm ²)	Reinforcement Ratio, ρ (%)
G-6#4	6	12.7	759	1.78
G-6#5	6	15.9	1191	2.79
G-6#6	6	19.1	1710	4.00
G-4#5	4	15.9	794	1.86
G-8#5	8	15.9	1588	3.72
G-9#4	9	12.7	1139	2.67



Fig. 3. Assembled GFRP reinforcement cages.

of 10.35 mm was observed, owing to the concrete cover spalling. The load then again increased to 985.1 kN at 12.77 mm deformation due to lateral confinement by GFRP spirals and continuous load carrying of the longitudinal bars. The columns then failed due to bar rupture, as shown in Table 3. Columns G-6#5 and G-6#6 showed the same behavior as column G-6#4 in the linear-elastic range, but with a different degree of nonlinearity before the first peak load. This can be explained by the wider distribution of cracks along the outer concrete surface, as shown in Table 3. The drop in axial-load capacity after the first peak was also different, due to the different reinforcement area. After the load dropped, an ascending load–deformation response was noticed in columns G-6#4, G-6#5, and G-6#6, due to lateral confinement activation of the GFRP spirals and the continuous load contribution of the GFRP bars.

Column G-8#5 showed load–deformation behavior similar to that of column G-6#6, but with the first and second peak axial loads higher by 11% and 13%, respectively. Column G-4#5 evidenced distinctly different behavior than the other columns. The linear-elastic part stopped

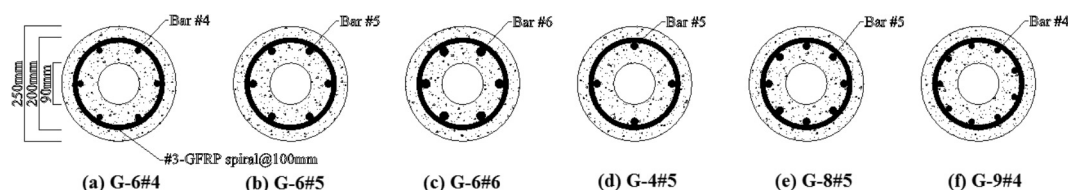


Fig. 2. Column cross sections.

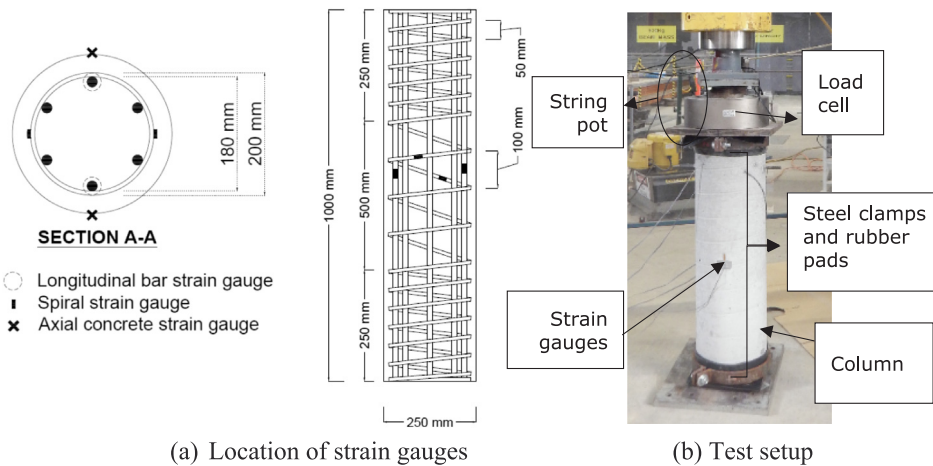








Fig. 4. Test setup and instrumentation of the hollow concrete columns.

Table 3
Description of the failure propagation in GFRP-reinforced hollow concrete columns.

Column	Description of Failure	Column	Description of Failure
 G-6#4	<ol style="list-style-type: none">1. Hairline cracks developed.2. Cracks propagated along column height.3. Concrete cover spalled at mid-height.4. One longitudinal GFRP bar ruptured.5. Concrete core slightly damaged.	 G-4#5	<ol style="list-style-type: none">1. Hairline cracks developed.2. Cracks propagated along column height.3. Limited concrete cover spalling at the upper half of the height.4. Rupturing in all longitudinal GFRP bars.5. Gradual degradation for whole concrete core.
 G-6#5	<ol style="list-style-type: none">1. Hairline cracks developed.2. Cracks propagated along column height.3. Overall concrete-cover spalling.4. Rupturing in all longitudinal GFRP bars.5. Partially damaged concrete core.	 G-8#5	<ol style="list-style-type: none">1. Hairline cracks developed.2. Cracks propagated along column height.3. Overall concrete-cover spalling.4. Buckling and splitting in the GFRP fibers in all longitudinal bars.5. Massive and loud damage in the concrete core.
 G-6#6	<ol style="list-style-type: none">1. Hairline cracks developed at the top of the column.2. Cracks propagated along column height.3. Overall concrete-cover spalling.4. Rupturing and buckling in the GFRP bars.5. Massive and loud damage in the concrete core.	 G-9#4	<ol style="list-style-type: none">1. Hairline cracks developed.2. Cracks propagated along column height.3. Overall concrete-cover spalling.4. Rupturing in all longitudinal GFRP bars.5. Partially damaged concrete core.

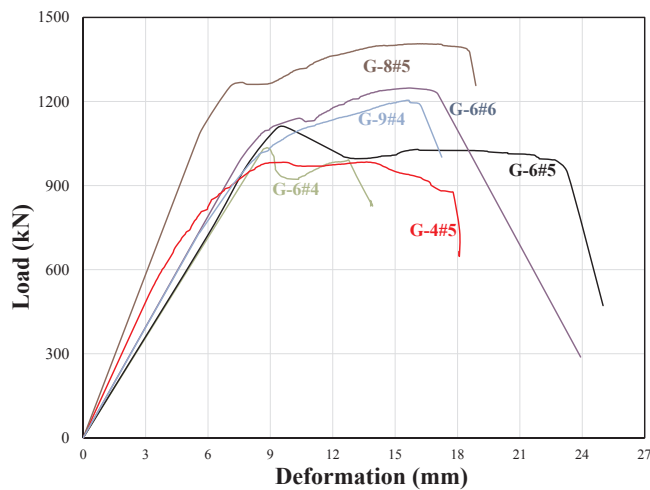


Fig. 5. Axial load–deformation behavior of the tested columns.

at 3.16 mm with an axial load of 510.5 kN, then continued with a wide nonlinear ascending part until the first peak load of 983.3 kN at 9.6 mm. After that, a continuous load degradation was noticed, due to gradual crushing of the concrete core, followed by rupturing of the longitudinal bars. Column G-9#4 had ascending linear-elastic load-deformation behavior until the axial capacity of 727.6 kN at 5.60 mm was reached. Then a nonlinear curve connected the elastic ascending behavior to another ascending part, ending at a maximum load peak of 1204.2 kN at 16.27 mm; the failure point was denoted by bar rupture (Table 3). The transition point between the two ascending parts occurred at an axial load of 1028 kN at 8.93 mm. Table 4 summarizes the loads at the first and second peaks, deformations, confined compressive strength, bars strains, and spiral strains.

3.3. Strain behavior of the GFRP bars and spirals

Fig. 6 shows the relationship between the load and strains in the longitudinal GFRP bars and spirals. In all of the columns, the axial compression strain recorded in the longitudinal bars was around $3000 \mu\epsilon$, which is about 14.7% of the ultimate tensile strain of the GFRP bars. On the other hand, the measured vertical strain in the concrete was around $1500 \mu\epsilon$, which corresponds to the strain at which hairline cracks started to develop. The vertical strain readings became unreliable once the hairline cracks developed. This, however, resulted in higher axial strains in the longitudinal GFRP bars. The measured strains in columns G-6#4, G-6#5, and G-6#6 were $2240 \mu\epsilon$, $2318 \mu\epsilon$, and $3634 \mu\epsilon$, respectively, while that in columns G-6#5 and G-8#5 were $2318 \mu\epsilon$ and $3649 \mu\epsilon$, respectively. Referring to these figures, the GFRP bars in the columns with high reinforcement ratios reached the concrete's crack-strain limit at the early stage, leading to early activation of the spiral reinforcement, as can be seen in Fig. 6; Table 4 provides the level of measured strains. Column G-4#5 recorded an exceptionally

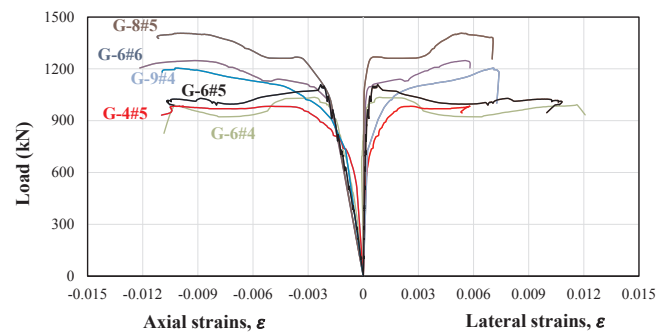


Fig. 6. Load and strain behavior in longitudinal and transverse GFRP reinforcement.

high axial strain of $3760 \mu\epsilon$ at peak due to early concrete cracking, which can be explained by early confinement by the GFRP spirals (Fig. 6). In the linear-elastic part, the GFRP spirals recorded less than 7% of the ultimate tensile strength before 85% of the peak axial load or before initiating the hairline cracks. The lateral confinement activation was related to crack appearance. Therefore, the columns with a wide nonlinear part or good confinement showed early activation of the GFRP spirals because of early spalling of the concrete cover. For example, column G-6#6 recorded a lateral strain of $2250 \mu\epsilon$ at peak load, while column G-6#5 recorded only $822 \mu\epsilon$. On the other hand, column G-8#5 recorded a strain of $1340 \mu\epsilon$ in the GFRP spirals. The same was observed in column G-9#4 with a strain of $1690 \mu\epsilon$, which is higher than column G-6#4 at $774 \mu\epsilon$. However, the situation was different in column G-4#5, which recorded a lateral strain of $2580 \mu\epsilon$, which was higher than that of columns G-8#5 and G-6#5.

After the peak axial load, the GFRP bars in the hollow concrete column kept resisting the axial loads, even after the concrete cover spalled. In fact, the column failure was addressed by the failure of the longitudinal bars. Accordingly, the #4 and #5 bars recorded average failure strains of $10,790 \mu\epsilon$ and $11,010 \mu\epsilon$, respectively, which represent 51.4% and 52.4%, respectively, of the ultimate tensile strain. These findings coincide with that reported by Maranan et al. [16]. In addition, the #6 bars recorded $12,160 \mu\epsilon$ at the failure point, representing 57.9% of the ultimate tensile strain. Interestingly, columns G-6#6 and G-8#5 recorded $6190 \mu\epsilon$ and $7060 \mu\epsilon$, respectively, less than the $10,816 \mu\epsilon$ in column G-6#5 at failure, while G-9#4 recorded $7390 \mu\epsilon$, compared to $12,770 \mu\epsilon$ in G-6#4 at failure. Increasing the reinforcement ratio by increasing the bar diameter or the number of bars reduced the lateral contribution of the GFRP spirals at the failure point. Column G-4#5 reached only $5770 \mu\epsilon$ at failure, since the concrete core degraded without effective confinement due to large bar spacing and the reasonable lateral spacing between spirals evidenced no ineffective confinement.

Table 4
Test results and sample details.

Sample	1st Peak Load (kN)	2nd Peak Load (kN)	Confined Strength f_{cc} (MPa)	C. E.	Δ_1 (mm)	Δ_2 (mm)	D. F.	Bar Strain at 1st Peak ($\mu\epsilon$)	Bar Strain at Failure ($\mu\epsilon$)	Spiral Strain at 1st Peak ($\mu\epsilon$)	Spiral Strain at Failure ($\mu\epsilon$)
G-6#4	1035.3	985.1	44.8	2.11	8.9	12.8	1.44	2240	10,845	774	12,770
G-6#5	1109.2	1024.4	46.6	2.19	9.2	23.3	2.53	2318	10,620	822	12,740
G-6#6	1140.0	1247.9	56.8	2.67	9.4	17.3	1.84	3634	10,850	3750	6190
G-4#5	983.3	875.5	39.8	2.11	6.0	17.8	2.97	3760	11,201	2580	5770
G-8#5	1267.9	1406.1	64.0	3.01	7.1	18.6	2.62	3649	11,210	1340	7060
G-9#4	1035.0*	1204.2	54.8	2.58	9.0*	16.0	1.78	2897	10,740	1690	7390

* Transition point between two ascending parts.

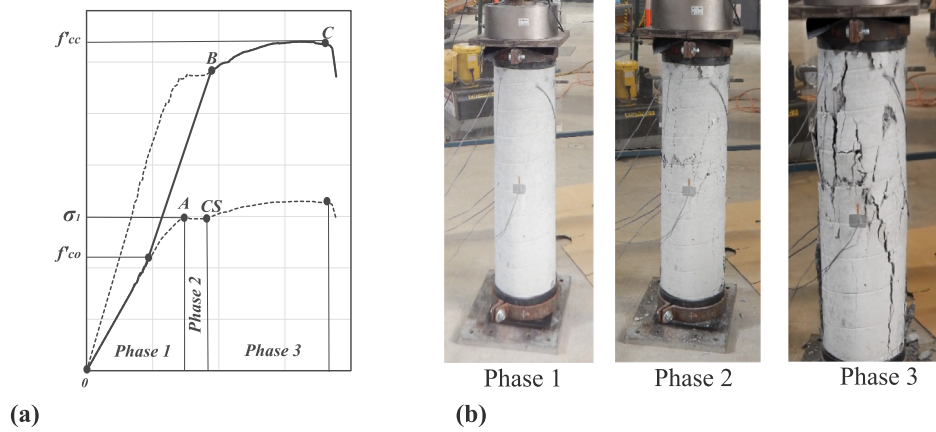


Fig. 7. (a) Typical stress–deformation behavior (b) Crack appearance at different load phases.

3.4. Axial strength and confinement efficiency

The typical stress–deformation behavior of the hollow concrete columns reinforced with GFRP bars and spirals (see Fig. 5) can be divided into three dominant phases based on the total cross sectional area of the concrete (see Fig. 7a).

Phase 1: Linear–elastic ascending behavior from the beginning of loading until the point of exhibiting nonlinear ascending behavior until reaching the first peak stress (σ_1) and the axial deformation (Δ_1). The column exhibited a linear elastic behavior as the entire concrete area in the section and all the longitudinal reinforcements are resisting the applied load and the deforming at the same time. The development of hairline cracks at the outer concrete cover was the main responsible for showing the nonlinear behavior until σ_1 . σ_1 is the maximum strength carried by the gross concrete area and longitudinal reinforcement before the total or partial spalling of the outer concrete cover, as shown in Fig. 7(a and b) (phase 1).

Phase 2: Significant drop in strength due to cracking of the concrete cover, leading to the concrete spalling point (CS). At this stage, the column's gross area gradually reduced as shown in Fig. 7(a and b) (phase 2), and the contribution of the concrete was reduced with the GFRP bars continuing to carry load and recording axial strain.

Phase 3: Partial or complete removal of the concrete cover, causing bulging in the lateral reinforcement and activating the confinement. At this point, the only active part of the concrete was the confined concrete core, as shown in Fig. 7(a and b) (phase 3).

After the maximum load was reached, the compressive strength of the tested columns was calculated considering only the area of the concrete core, since the concrete cover had already spalled. The effective circular area was taken between the centerlines of the transverse GFRP spirals. The dashed curves in Fig. 7a represent the stress path based on gross and effective section areas. The bold line represents the column's stress behavior. Correspondingly, stress in the elastic region (from 0 to A) was obtained by dividing the total applied load by the total concrete area (gross area), then dividing the total applied load by the confined concrete core area (A_{core}), which denoted by the distance between centerlines of the lateral spiral, in the region (from B to C) expressing the confined concrete area after subtracting the spalled

concrete cover. The transition area between A and B can be considered as a gradual cover degradation.

Confinement efficiency accounts for specimens sustaining axial loads after the first axial peak, even though the column cross-sectional area was reduced due to concrete-cover spalling. The confinement provided by the GFRP spirals or longitudinal bars [28] resulted in a confined concrete compressive strength (f'_{cc}), which was calculated by dividing the maximum applied load after cover spalling by the effective concrete area. The confinement efficiency was then calculated by dividing f'_{cc} by the unconfined concrete strength (f'_{co}). The unconfined concrete strength was set at approximately 85% f'_c or when the columns were still fully intact or free of cracks, where f'_c is the average compressive strength of concrete cylinders tested at 28 days. The factor of 85% was adopted representing the difference between full-scale reinforced-concrete columns and concrete cylinders in terms of the strength, size, and shape [14].

3.5. Ductility

Ductility is the ability to withstand plastic deformations [29], which was measured with a ductility factor (μ) using Eq. (1). Table 4 presents the axial deformations and ductility factor for all the tested columns. In Eq. (1), Δ_1 represents the axial strain corresponding to the maximum peak load, while Δ_u is the deformation at the point of reinforcement failure. This approach was implemented by Cui and Sheikh [30]. Fig. 8 shows how to determine the deformation limits for different load–deformation behaviors.

$$\mu = \frac{\Delta_u}{\Delta_1} \quad (1)$$

3.6. Influence of the bar diameter

The hollow concrete columns with smaller bar diameters exhibited longer linear–elastic behavior proportional to the peak axial capacity of 98%, 89%, and 86% for columns G-6#4, G-6#5, and G-6#6, respectively. This was followed an increase in the nonlinear ascending part as the bar diameter increased, as shown in Fig. 5. This behavior can be

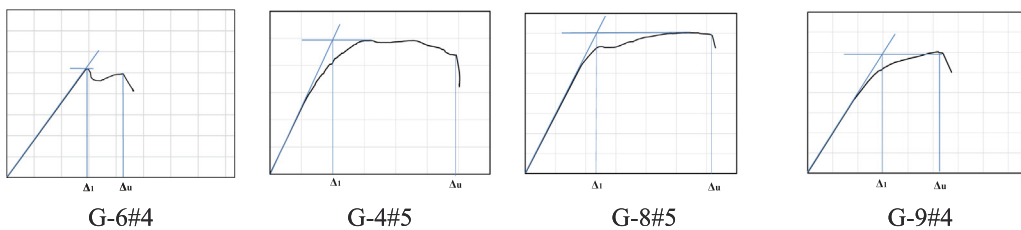


Fig. 8. Determination of Δ_1 and Δ_u for ductility calculations.

attributed to the reduction in the concrete area caused by the increase in the bar diameter. This resulted in high axial stress in the concrete and eventually high axial strains, leading to the concrete reaching $1500 \mu\epsilon$, which is the start of the nonlinear behavior, due to cracks initiating in the concrete cover [27]. Similar case was noticed by Itakura and Yagenji [31] and Bjerkeli et al. [32] where the increase in the reinforcement ratio resulted in short elastic-linear ascending behavior but with a wide nonlinear ascending behavior and a high strength at the peak due to the high modulus of steel bars. The bar diameter did not significantly affect the axial stiffness of the hollow columns. The axial stiffness ($E_{GFRP}A_{GFRP}$) of the bars in columns G-6#4, G-6#5, and G-6#6 was 46.5×10^6 N, 71.5×10^6 N, and 103.5×10^6 N, respectively, assuming the tensile elastic modulus to be similar to the compressive elastic modulus of the GFRP bars. The axial stiffness contribution of the longitudinal GFRP bars with respect to the overall axial stiffness of the column did not, however, reach 10% with values of 4.5%, 6.8%, and 9.7% for columns G-6#4, G-6#5, and G-6#6, respectively. This is due to the low elastic modulus of the GFRP bars [14]. Using larger bar diameters increased the column load capacity due to the increase in the reinforcement ratio from 1.78% to 2.79% to 4.00% with six 12.7 mm, six 15.9 mm, and six 19.7 mm bars, respectively. For example, column G-6#6 exhibited 2.8% and 9.2% higher strength than G-6#5 and G-4#6, respectively, at the first peak axial load. This increase was nevertheless lower than expected with bar diameters due to nonlinear ascending part. Interestingly, the load contribution of the GFRP bars at first peak increased from 9% to 11% to 32% as the bar diameter was increased from 12.7 mm to 15.9 mm to 19.1 mm, respectively. This finding is consistent with Tobbi et al. [14], who found that the load contribution of GFRP bars increased by around 200% by using bars 19.1 mm in diameter instead 12.7 mm. Actually, this finding can be explained by the fact that the nonlinear ascending part occurred earlier with a larger bar diameter, resulting in early activation of the lateral confinement by the GFRP spirals. This led to more axial strains in the larger-diameter bars. Accordingly, the load contribution of GFRP bars can be calculated by multiplying the average axial strain of the GFRP bars at the first peak axial load by their modulus of elasticity and cross-sectional area, and then dividing by the peak axial-load capacity. After the first peak, the larger bar diameters recorded lower drops in load percentage after the concrete cover spalled equivalent to 10.9%, 10.2%, and 1% of the axial load in columns G-6#4, G-6#5, and G-6#6, respectively. This observation can be related to the higher axial stiffness of the larger (6#6) and (6#5) bar diameters compared to the smaller (6#4) one by 122% and 54%, respectively, attributable to higher load contribution. On the other hand, the concrete cover spalled along the column's height with the larger bar diameters in column G6#6 and G6#5, producing higher axial stress than in column G-6#4, which experienced only limited spalling at mid-height.

Unlike the behavior before the peak load, the increase in diameter of the longitudinal reinforcement bars significantly affected stiffness and load capacity at the post-loading stage. The columns with larger bar diameters evidenced higher ascending load–deformation behavior than the columns with smaller bar diameters due to the significant increase in the effective axial bar stiffness with respect to the column's confined concrete core area (A_{core}) after concrete-cover spalling. In addition, the secant elastic modulus of the concrete (E_{sec}) after peak, which is normally less than the half of the Young's modulus of the concrete ($E_{GFRP}A_{GFRP}/(E_{GFRP}A_{GFRP} + E_{sec}A_{core})$) also played a role. At the end of the ascending part, column G-6#6 recorded a second peak load 22% and 27% higher than that of columns G-6#5 and G-6#4, respectively. This could be attributed to the increase in the effective reinforcement ratio after concrete-cover spalling, specifically 3.04%, 4.76%, and 6.83% for G-6#4, G-6#5, and G-6#6, respectively. In fact, this higher effective reinforcement ratio not only increased the second peak load, it also increased the lateral confined area by covering more unconfined concrete area between spirals.

The larger bar diameter also improved the ductility of hollow

concrete columns. This can be attributed to a mechanical aspect: increasing the area of the GFRP bars enhanced the overall axial-deformation capacity of the column, as observed with column G-6#5, which showed 76% higher ductility than G-6#4. On the other hand, using #6 bars in column G-6#6 decreased the thickness of the inner concrete wall, making it slender. This rendered the inner concrete shell highly vulnerable to cracking before achieving high axial-deformation values. This also explains the more massive and explosive damage of the concrete core in column G-6#6 compared with the smooth degradation and partial damage in columns G-6#4 and G-6#5. These findings are inconsistent with Hoshikoma and Priestley [2] about achieving low ductile behavior by using large diameter bars due to the limited axial compressive strain of steel bars. As a result, all the enhancements in terms of peak axial load, strength decay after concrete-cover spalling, confined strength, and ductility in this study obtained by using larger-diameter GFRP bars is consistent with what Tobbi et al. [14] reported for solid concrete columns.

3.7. Influence of the number of bars

Fig. 5 shows that the axial load and deformation behavior of the columns decreased the linear ascending part and increased the nonlinear part before the peak axial load as the number of bars increased. Again, using a high number of GFRP bars reduced the concrete area, making it easier to achieve $1500 \mu\epsilon$ earlier. This led to the start of nonlinear behavior compared to the specimens with smaller numbers of GFRP bars. Column G-4#5, however, had an early onset of the nonlinear load and deformation behavior due to the formation of the hairline cracks on the outer concrete surface. This nonlinear behavior was controlled by the unconfined concrete, which exhibited nonlinearity once the stress exceeded $0.5f_{co}$ [33], where f_{co} is the concrete stress limit before showing cracks on the outer surface of the sample. This might be attributable to inadequate distribution of the GFRP bars. Increasing the bar number increases the peak axial-load capacity by increasing the reinforcement ratio. Therefore, G-8#5 ($\rho = 3.72\%$) had 14.3% and 28.9% higher peak strength than G-6#5 ($\rho = 2.79\%$) and G-4#5 ($\rho = 1.86\%$). The increase in the axial-load capacity at the first peak was due to increasing the number of longitudinal bars. Moreover, the load contribution of the GFRP bars increased as did the number of bars: 27.4% and 13.8% in G-8#5 and G-6#5, but 18.2% in G-4#5, which might be caused by a high concentration of axial stress on the bars after the wide nonlinear part due to the outer cover cracking. There an inverse relationship between the number of longitudinal GFRP bars and the axial load, which could be attributed to the concrete cover spalling after the peak load. For instance, column G-8#5 experienced a load drop of 0.5% compared to 10.2% in column G-6#5 after the first peak due to the early contribution to confinement and the increased area of reinforcement (GFRP bars), which has higher axial stiffness than concrete. While this finding is consistent with Afifi et al. [15], a slight load drop was observed in G-4#5, which might be related to the limited and partial spalling of the concrete cover. G-9#4 ($\rho = 2.69\%$) did not show a drop in the axial-load capacity compared to the 11% axial-load drop in G-6#4 ($\rho = 1.76\%$) due to G-9#4's better reinforcement distribution and early confining stress, compensating for the load drop due to the loss in concrete-cover contribution.

In the post-loading stage, the columns with more GFRP reinforcement showed higher axial stiffness than those with fewer bars. This can be due to the higher effective ratio of axial stiffness of the reinforcement to the effective concrete area (A_{core}) compared to the uncracked column ($E_{GFRP}A_{GFRP}/(E_{GFRP}A_{GFRP} + E_{sec}A_{core})$) and the higher confined concrete core due to the decreased bar spacing. This accounts for the ascending load–deformation behavior of the specimens, except for column G-4#5, which exhibited continuous load degradation. As explained, this can be attributed to the wide unconfined area between the bars, which made the column more vulnerable to cracking and crushing than the columns with more longitudinal GFRP bars. Accordingly, column G-8#5 showed

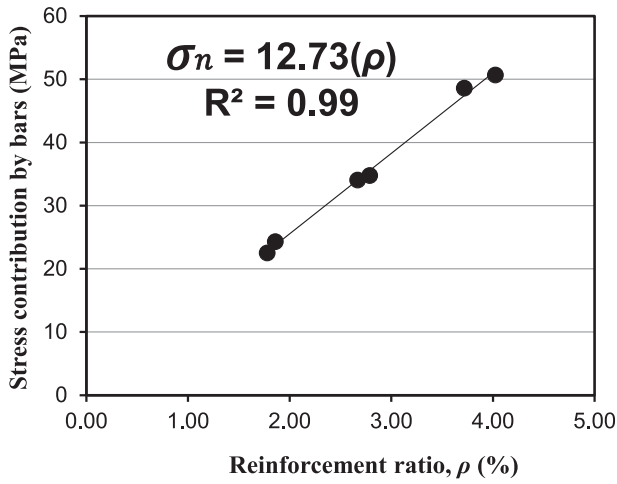


Fig. 9. Reinforcement ratio vs. stress contribution at failure point.

a failure load higher by 37% and 61% than columns G-6#5 and G-4#5, with 6 and 4 bars, respectively. The situation was similar for column G-9#4 and column G-6#4, with the former achieving a 22% higher load capacity at failure than the latter. Moreover, columns G-8#5 and G-9#4 showed 3.6% and 24% higher ductility than columns G-6#5 and G-6#4, respectively. This behavior can be explained by greater confinement of the concrete core as the result of increasing the number of bars and the increased flexural stiffness of the bars. The latter, in turn, increased column axial-deformation capacity. These findings emphasize the positive effects that increasing the reinforcement ratio have on enhancing the structural properties of hollow concrete columns. This contrasts with the findings of Lee et al. [3], who examined hollow concrete columns reinforced with steel bars. They stated that increasing the number of steel bars decreased the ductility and increased the damaged area of the inner concrete core due to the axial compressive strain of the steel bars, which was nearly the same as that of the concrete strain at peak load. On the other hand, Afifi et al. [15] reported that increasing the number of bars in solid concrete columns reinforced with GFRP bars enhanced the load–deformation ratio by increasing column ductility and confinement efficiency by 117% and 30%, respectively. Karim et al. [17] had similar findings in their experimental study in which column ductility and confinement efficiency increased by 39% and 19%, respectively.

3.8. Behavior of columns with similar reinforcement ratios

The behavior of hollow concrete columns with almost similar reinforcement ratios (2.69% and 2.78%) but different bar diameters and different numbers of bars was evaluated by comparing the behavior of columns G-9#4 and G-6#5. Both columns had almost equal axial stiffness until 80% of the first peak load [Fig. 5]. The column with more but smaller bars (G-9#4) had a wider nonlinear ascending behavior than column G-6#5 due to early concrete cover splitting from the concrete core owing to the small contact area between them. The column didn't experience any axial-load drop when the concrete cover spalled because of the lateral confinement of the concrete core provided by lateral spirals and longitudinal bars. In contrast, column G-6#5 revealed a noticeable load drop due to having less lateral confinement (wider unconfined concrete area) than column G-9#4. Column G-9#4 had stiffer load–deformation behavior after the concrete cover spalled compared to G-6#5, even though both columns had the same axial stiffness ratio of 10.4%. Column G-9#4 had better confinement, however. Column G-9#4 (more bars and smaller bar diameter) also produced higher confined concrete strength in the post-loading stage when the concrete cover is gone by 18% than in G-6#5. The influence of the well-distributed reinforcement on lateral confinement can be seen by

considering the measured strains in the lateral GFRP spirals in Fig. 6, accordingly, the tensile strains in the spirals in column G-9#4 were 58% lower than that in column G-6#5 at failure. This further highlights the contribution of the longitudinal reinforcement in lateral confinement. These findings are consistent with Tobbi et al. [34]. On the other hand, column G-9#4 recorded 30% lower ductility than column G-6#5. It is interesting to note that six #5 bars had twice the moment of inertia than six #4 bars, resulting in a more flexural stiffness capacity. Consequently, column G-6#5 had higher energy absorption, which could lead to withstanding more axial deformations before bar fracture. The test results for column G-9#4 show behavior consistent with steel-reinforced hollow columns wrapped with CFRP sheets [1,35]. These findings also reveal a similarity to those for the solid concrete columns reinforced with GFRP bars tested by Tobbi et al. [34]. They indicated that using 12 #5 GFRP bars compared to 8 #6 GFRP bars with the same reinforcement ratio increased the confinement efficiency.

4. Analytical evaluation of column behavior

4.1. Crushing strain and axial stress of the GFRP bars

The compression behavior of the GFRP reinforcement, which are nonhomogeneous and anisotropic, is complex due to the different failure modes such as global buckling or micromechanical failure caused by fiber micro-buckling or fibers splitting from the resin [36]. Accordingly, many studies have tried to help establish a standard test for the compression behavior of GFRP bars (see [36,37]). They concluded that the elastic modulus of GFRP bars in compression is similar to the tensile elastic modulus, but the compressive-strength capacity is only 50%–67% of the tensile strength. The compression behavior of GFRP bars embedded in concrete was quite different than the behavior of the bars alone. Tobbi et al. [14] found that the general compression behavior of GFRP bars in concrete is linear elastic. Therefore, axial stress in the bars can be found using linear-elastic theory. Similarly, the failure strain in compression of bars embedded in concrete was closely related to the tensile elastic modulus of the bars, concrete compressive strength, and lateral reinforcement spacing. This study focused on estimating the crushing strain of the high-modulus GFRP bars (60–66 GPa) as all columns were fabricated using the same concrete compressive strength and lateral-reinforcement spacing.

Fig. 9 shows the relationship of the reinforcement ratio to the stress contribution of the GFRP bars at failure. The latter is calculated by multiplying the average strain in the GFRP bars at failure by the elastic modulus of GFRP bars and their total area, then dividing the result by the effective concrete-core area confined by the transverse reinforcement. Based on this relationship, the stress contribution of the GFRP bars was found to be directly proportional to the reinforcement ratio using a linear regression with an R^2 of 0.99. Accordingly, Eq. (2) can be used to calculate the stress contribution of the GFRP bars, while Eq. (3) was used to find the exact stress in the GFRP bars at the failure. Using the linear-elastic theory, the crushing strain can be obtained from Eq. (4).

$$\sigma_n = 12.73 \times \rho \quad (2)$$

$$\sigma_t = \sigma_n \times \frac{A_{core}}{A_{GFRP}} \quad (3)$$

$$\epsilon_{cr} = \frac{\sigma_t}{E_{GFRP}} \quad (4)$$

where σ_n and σ_t are the contribution and exact stress of the GFRP bars, respectively; ρ is the reinforcement ratio; A_{core} and A_{GFRP} are the confined concrete core area and area of the GFRP bars, respectively; and E_{GFRP} and $\mu\epsilon_{cr}$ are the elastic modulus and the crushing strain of the GFRP bars, respectively.

The analytical results [Eq. (4)] of the crushing strain showed good agreement with the experimental results. The reliability of the

Table 5

Comparison between experimental and analytical crushing strain of GFRP bars.

Samples	Gross area (A_g) (mm ²)	A_{core} (mm ²)	ρ (%)	E_{GFRP} (GPa)	Experimental Crushing Strain, $\mu\epsilon_{cr}$	Analytical Crushing Strain, $\mu\epsilon_{cr,m}$	$(\mu\epsilon_{cr,m}/\mu\epsilon_{cr})^*100\%$
G-6#4	42,704	21,991	1.78	61.3	10,845	10,691	98.6
G-6#5	42,704	21,991	2.79	60.0	10,620	10,923	102.9
G-6#6	42,704	21,991	4.00	60.5	10,850	10,833	99.8
G-4#5	42,704	21,991	1.86	60.0	11,201	10,923	97.5
G-8#5	42,704	21,991	3.72	60.0	11,210	10,923	97.4
G-9#4	42,704	21,991	2.69	61.3	10,740	10,691	99.5
GGC-8-S100 [16]	49,063	28,353	2.43	62.5	11,808	11,785	99.8
GGC-8-H100 [16]	49,063	28,353	2.43	62.5	10,752	11,785	109.6
CG6-G60 [17]	32,990	20,106	2.30	66.0	11,819	11,708	99.1

analytical model was also checked against the experimental results reported in [16,17] (see Table 5). The predicted failure strain for the sample (GGC-8-H100) was, however, noticeably higher than the experimental one because the lateral hoops in this sample failed before bar rupture, as indicated by the authors [16].

4.2. Axial-load capacity

A number of researchers [14,15,34,38] have proposed theoretical equations to calculate the load capacity of GFRP-reinforced concrete columns. In all of these equations, the capacity of the columns was calculated by considering the net area of the concrete and the contribution of the longitudinal reinforcement. They differ, however, in the stress and/or strain in the longitudinal GFRP bars. These equations are shown below [15,34,14,38].

$$P_n = 0.85 \times f'_c \times (A_g - A_{GFRP}) + 0.35 \times f_{u,GFRP} \times A_{GFRP} \quad (7)$$

$$P_n = 0.85 \times f'_c \times (A_g - A_{GFRP}) + 0.002 \times E_{GFRP} \times A_{GFRP} \quad (8)$$

$$P_n = 0.85 \times f'_c \times (A_g - A_{GFRP}) + 0.003 \times E_{GFRP} \times A_{GFRP} \quad (9)$$

Tobbi et al. [34] and Afifi et al. [15] highlighted that the load contributions of GFRP bars can be taken as 35% of the ultimate tensile capacity of the GFRP bars, due to the difficulty in determining the compressive strength of GFRP bars [Eq. (7)]. On the other hand, Tobbi et al. [14] suggested Eq. (8) based on the linear-elastic theory of GFRP bars, since they assumed that the average axial strain of the GFRP bars at peak load is equal to 0.002. Finally, Hadi et al. [38] assumed that the axial strain of GFRP bars is compatible with the ultimate axial strain of concrete at 0.003, as mentioned in ACI-318 [39]. Table 6 shows a comparison of the predicted and experimental results. It reveals that the equation proposed by Hadi et al. [38] can reliably predict the axial-load capacity of hollow concrete columns reinforced with GFRP bars and spirals. This good correlation is due to the similar level of axial strains measured in the longitudinal reinforcement, which, on average, is equal to 0.003078. These results also highlight that the capacity of hollow concrete columns reinforced with GFRP bars and spirals can be calculated by considering both the concrete contribution and the longitudinal reinforcement.

Table 6

Comparison between analytical-to-experimental results.

Samples	Tobbi et al. [34] and Afifi et al. [15] P_{exp}/P_n	Tobbi et al. [14] P_{exp}/P_n	Hadi et al. [38] P_{exp}/P_n
G-6#4	1.19	0.95	1.00
G-6#5	1.17	0.86	0.92
G-6#6	1.43	0.95	1.04
G-4#5	1.26	1.00	1.05
G-8#5	1.23	0.84	0.91
G-9#4	1.32	0.97	1.04
Average	123.6%	92.7%	99.7%

4.3. Influence of number of bars and bar diameter on strength confinement

The number of bars and bar diameter had a noticeable impact on the load and strength capacity in the post-loading stage when the lateral confinement by the GFRP spirals was actually activated. The presence of a highly confining material (GFRP spirals) spaced at a reasonable distance between pitches enhanced the post-loading stage by keeping the concrete core as far as possible from failure and bracing the longitudinal bars. This resulted in high resistance to axial loads due to the high axial-strain capacity of GFRP bars [28]. In contrast of using the conventional confined strength thoughts in concrete columns, the second axial-load capacity of the GFRP-reinforced hollow concrete columns depends on the strength resisted by the remained part of concrete and the longitudinal GFRP bars. Therefore, predicting the second axial-load capacity requires that the contribution of both the concrete and the GFRP bars at the second peak load be calculated. Fortunately, the contribution of the GFRP bars can be predicted by multiplying the crushing strain, which was introduced in this study, by the elastic modulus of the GFRP bars. The contribution of concrete strength in such cases remains undefined since the concrete core is subjected to biaxial stress. The existing analytical models accounting for the confinement stresses in hollow concrete columns [40–42] are not valid in this study, because these models are based on wrapping the overall outer surface. Moreover, some involve steel bars as longitudinal reinforcement. In particular, the contribution of the GFRP bars and concrete stresses at the maximum confined strength (the second peak) are necessary to develop a comprehensive explanation of the continuous contribution of the GFRP bars until failure, unlike steel bars, which stop gaining strength at 0.0025 strains. This approach for finding the maximum confined strength is not mentioned in past models due to the difficulties in specifying the compression contribution of the GFRP bars. Simply, the stress contribution at failure (maximum confined strength) of the GFRP bars can be obtained with Eq. (2); the concrete contribution, on the other hand, is based on the effective lateral confinement of the GFRP spirals.

As shown in Fig. 10.a, the lateral-confinement (f_l) equation [Eq. (11)] is based on the mechanical-confinement concept [5] but considers the void in hollow columns. The GFRP spirals only partially confine the concrete core: there is unconfined concrete between the bars and spirals. Therefore, this study considered the effect of lateral damage in the unconfined concrete parts. In calculating the partial lateral confinement, the confinement effectiveness factor (k_e) [43] (see Fig. 10.b) was considered. The vertical spacing between spirals remained constant for the tested columns, but the k_e value varied, since it is also affected by the effective reinforcement ratio (ρ_e), which is the reinforcement area with respect to the A_{core} [Eq. (13)]. In addition, this study suggested another confinement effectiveness factor (opening factor, k_o) related to the lateral-opening distance between bars [Eq. (14)], which was found to be more effective with partial lateral confinement in some cases [Fig. 10.c].

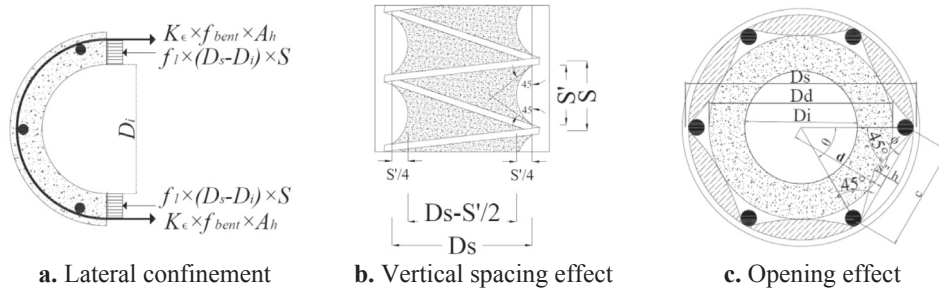


Fig. 10. Lateral confinement mechanism and confinement efficiency factors.

$$f_l = \frac{2A_h K_\epsilon f_{bent}}{S(D_s - D_i)}$$

$$f_{bent} = \left(0.05 \frac{r}{d_b} + 0.3\right) f_u \leq f_u$$

$$k_e = \frac{A_{ce}}{A_{cc}} = \frac{\frac{\pi}{4} \left(\left(D_s - \frac{s}{4} \right)^2 - D_i^2 \right)}{\frac{\pi}{4} (D_s^2 - D_i^2) (1 - \rho_e)}$$

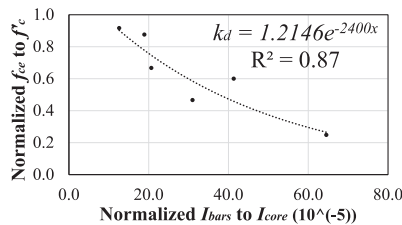
$$k_o = \frac{A_d}{A_{cc}} = \frac{\pi \left(\left(\frac{D_s}{2} - \left(\frac{h + \frac{s}{2}}{2} \right) \right)^2 - \frac{D_i^2}{4} \right)}{\frac{\pi}{4} (D_s^2 - D_i^2) (1 - \rho_e)}$$

$$= \frac{\pi \left(\left(\frac{D_s}{2} - \left(\frac{D_s - d}{2} + \frac{c \tan(\phi)}{2} \right) \right)^2 - \frac{D_i^2}{4} \right)}{\frac{\pi}{4} (D_s^2 - D_i^2) (1 - \rho_e)}$$

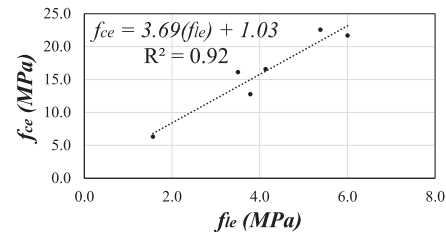
$$k_o = \frac{\pi \left(\frac{D_s}{2} - \frac{\left(\frac{D_s}{2} - \left(\frac{D_s}{2} \cos\left(\frac{\theta}{2}\right) \right) + \frac{\left(\frac{D_s}{2} \sin\left(\frac{\theta}{2}\right) \right) \tan\left(45 - \frac{\theta}{2}\right) \right)}{2} \right)^2 - \frac{D_i^2}{4}}{\frac{\pi}{4} (D_s^2 - D_i^2) (1 - \rho_e)}$$

$$k_o = \frac{\pi \frac{D_s^2}{4} \left(1 - \frac{\left(\left(1 - \cos\left(\frac{\theta}{2}\right) \right) + \frac{\left(\sin\left(\frac{\theta}{2}\right) \right) \tan\left(45 - \frac{\theta}{2}\right) \right)}{2} \right)^2 - \frac{D_i^2}{4}}{\frac{\pi}{4} (D_s^2 - D_i^2) (1 - \rho_e)}$$

$$k_o = \frac{\pi \frac{D_s^2}{4} \left(\frac{1}{2} + \frac{\cos\left(\frac{\theta}{2}\right)}{2} - \left(\frac{\sin\left(\frac{\theta}{2}\right) \tan\left(45 - \frac{\theta}{2}\right)}{4} \right) \right)^2 - \frac{D_i^2}{4}}{\frac{\pi}{4} (D_s^2 - D_i^2) (1 - \rho_e)}$$



(a) k_d factor



(b) Effective lateral confinement

Fig. 11. Determination of the bar-diameter factor and effective confined concrete core.

$$k_{of} = \left(\frac{1}{2} + \frac{\cos\left(\frac{\theta}{2}\right)}{2} - \left(\frac{\sin\left(\frac{\theta}{2}\right) \tan\left(45 - \frac{\theta}{2}\right)}{4} \right) \right)^2$$

$$(12)$$

$$k_o = \frac{A_d}{A_{cc}} = \frac{D_s^2 k_{of} - D_i^2}{(D_s^2 - D_i^2) (1 - \rho_e)} \quad (14)$$

In the above equations, A_h is the GFRP-spiral cross-sectional area; K_ϵ is the proportion of ultimate strain in GFRP spirals before failure to their ultimate tensile strength, taken as the average of the spiral strains before failure (0.533); f_{bent} is the tensile strength of the bent GFRP bars [Eq. (12)], as recommended in ACI-440.1R [44]; r is the inner radius of the spiral; d_b is the GFRP spiral diameter; S is the vertical on-center spacing of spirals; D_s is the diameter of spirals on centers; D_i is the diameter of the inner void; A_{ce} is the area of the concrete core, excluding the crushed concrete part due to unconfined concrete between the spirals; A_{cc} is the concrete-core area, excluding the effective reinforcement ratio of the GFRP bars; A_d is the concrete-core area, excluding the crushed concrete part due to the opening effect; s is the clear vertical spacing between spirals; and θ is the angle between two bars.

On the other hand, the effect of bar diameter on the concrete contribution was noticeable: the greater the bar diameter, the higher the degradation of the concrete-core strength at the second peak. This was due to the highly significant increase in the effective axial stiffness of the GFRP bar's area due to concrete-cover loss and the reduction in the elastic modulus of the concrete at peak strength, even though the elastic modulus of the GFRP bars remained the same. Therefore, the bar-diameter factor (k_d) has been suggested as a function of the strength degradation in the concrete core at the second peak and the normalized inertia moment of the bars to the inertia moment of the concrete core [Fig. 11.a] [Eq. (15)]. As a result, the confined concrete-core strength can be given as a function of the effective lateral confinement and the experimental concrete-core strength (f_{ce}) taken from the test results [Fig. 11.b] [Eq. (17)]. The effective lateral confinement (f_{le}) [Eq. (16)], however, is equal to the product of the lateral confinement [Eq. (11)] and opening factor (k_d) and the maximum of k_e and k_o , because the greater one will control partial damage. While these results are valid for such columns, further study is needed to initiate a unified analytical model for GFRP-reinforced hollow concrete columns with partial

Table 7
Comparison between experimental and analytical results.

Sample	k_e	k_o	k_d	f_l (MPa)	f_{ce} (MPa)	P_{nt2} (kN)	f'_{cct} (MPa)	P_{nt2}/P_{nt} f'_{cct}/f'_{cc}
G-6#4	0.737	0.781	0.897	5.38	20.9	940	42.8	0.95
G-6#5	0.752	0.797	0.577	3.79	15.1	1094	49.8	1.07
G-6#6	0.771	0.818	0.258	1.57	7.0	1263	57.5	1.01
G-4#5	0.738	0.674	0.740	3.34	13.5	806	36.7	0.92
G-8#5	0.767	0.870	0.451	4.13	16.3	1374	62.5	0.98
G-9#4	0.750	0.871	0.771	6.00	23.1	1228	55.9	1.02

confinement. Lastly, the predicted second peak load (P_{nt2}) is given as the summation of the axial contribution of the GFRP bars by multiplying the result of Eq. (2) with the total area of reinforcement in the section and the product of multiplying the result of Eq. (15) with the A_{cc} [Eq. (18)]. Moreover, the maximum confined concrete strength (f'_{cct}) is given as the result of dividing the predicted second peak load by A_{core} [Eq. (19)]. Table 7 shows the summary of the second peak load and maximum confined strength as well as the good agreement between the analytical and experimental results for the tested columns.

$$k_d = 1.215 \times e^{-2400 \times \frac{I_{bars}}{I_{core}}} \quad (15)$$

$$f_{le} = \text{Max}(k_e, k_o) \times k_d \times f_l \quad (16)$$

$$f_{ce} = 3.69f_{le} + 1.03 \quad (17)$$

$$P_{nt2} = f_{ce}A_{cc} + \varepsilon_{cr}E_{GFRP}A_{GFRP} \quad (18)$$

$$f'_{cct} = \frac{P_{nt2}}{A_{core}} = \frac{P_{nt2}}{\frac{\pi}{4}(D_s^2 - D_i^2)} \quad (19)$$

5. Conclusion

This study investigated the influence of reinforcement ratios on the concentric axial compression behavior of hollow concrete columns by changing the number and diameter of longitudinal GFRP bars. An analytical model for crushing stress and strain behavior of GFRP bars embedded in concrete was proposed. The applicability of the existing design equations for GFRP-reinforced solid concrete columns were assessed to determine appropriateness for hollow concrete columns. Based on the results of this study, the following conclusions can be drawn:

1. The reinforcement ratio significantly affected the axial load–deformation behavior of the hollow concrete columns reinforced with GFRP bars and spirals. Increasing the reinforcement ratio enhanced the axial-load capacity, confined strength, and ductility of the hollow concrete columns.
2. Using larger bar diameters enhanced the axial-load capacity and mitigated the load drop after the peak when the concrete cover spalled. Using 6 pieces of bars 19.7 mm in diameter increased the failure load by 27% compared to a hollow column reinforced with 6 pieces of bar 12.7 mm in diameter. It also enhanced the ductility by withstanding high axial deformation without spiral failure up to 65% from the recorded deformation at the first peak load.
3. Using more longitudinal GFRP bars in hollow concrete columns increased their load capacity, confinement efficiency, and ductility due to increased axial stiffness of the columns and lateral confinement of the concrete core. The capacity, confinement efficiency, and ductility of the hollow concrete columns increased by 6%, 27%, and 4%, respectively, when the longitudinal reinforcement increased from 4 to 8 pieces of 15.9 mm diameter GFRP bars.
4. At the same reinforcement ratio, using more and smaller-diameter GFRP bars exhibited failure modes and axial-load capacity similar to

that of fewer and larger-diameter bars. The former, however, exhibited 12% higher confinement efficiency due to better reinforcement distribution. The column with fewer and larger-diameter bars also showed 20% higher ductility than those with more and smaller-diameter bars due to the higher flexural capacity of the larger-diameter GFRP bars.

5. The crushing strain of the GFRP bars embedded in the hollow concrete columns was, on average, equal to 52.1% of the ultimate tensile strain for all the reinforcement ratios considered in this study.
6. The axial-load capacity of the GFRP-reinforced hollow concrete columns can be reliably predicted by considering the contribution of the concrete and longitudinal reinforcement. The axial strain of the GFRP bars at the peak load was equal to the ultimate concrete strain of 3000 $\mu\epsilon$.

Acknowledgments

The authors are grateful to Inconmat V-ROD Australia for providing the GFRP bars and spirals. The assistance of the postgraduate students and technical staff at the Centre of Future Materials (CFM) is also acknowledged. The first author is grateful for the PhD scholarship provided by Tafila Technical University (TTU), Jordan.

Appendix A. Supplementary data

Supplementary data to this article can be found online at <https://doi.org/10.1016/j.compstruct.2019.01.096>.

References

- [1] Kusumawardaningsih Y, Hadi MN. Comparative behavior of hollow columns confined with FRP composites. *Compos Struct* 2010;93:198–205.
- [2] Hoshikuma J-I, Priestley M. Flexural behavior of circular hollow columns with a single layer of reinforcement under seismic loading. *SSRP* 2000;13.
- [3] Lee J-H, Choi J-H, Hwang D-K, Kwahk I-J. Seismic performance of circular hollow RC bridge columns. *KSCSE J Civ Eng* 2015;19:1456–67.
- [4] Won DH, Han TH, Kim S, Jang IS, Kang YJ. Optimum confining effect in steel composite hollow RC column with inner tube under compressive load. *Mag Concr Res* 2014;66:433–46.
- [5] Han T, Lim N, Han S, Park J, Kang Y. Nonlinear concrete model for an internally confined hollow reinforced concrete column. *Mag Concr Res* 2008;60:429–40.
- [6] Pantelides CP, Gibbons ME, Reaveley LD. Axial load behavior of concrete columns confined with GFRP spirals. *J Compos Constr* 2013;17:305–13.
- [7] Manalo A, Benmokrane B, Park K-T, Lutze D. Recent developments on FRP bars as internal reinforcement in concrete structures. *Concr Austr* 2014;40:46–56.
- [8] Manalo A, Benmokrane B, Park K-T, Lutze D. Recent developments on FRP bars as internal reinforcement in concrete structures. *Concr Austr* 2014;40(2):46–56.
- [9] Maranan G, Manalo A, Benmokrane B, Karunasena W, Mendis P, Nguyen T. Shear behaviour of geopolymer-concrete beams transversely reinforced with continuous rectangular GFRP composite spirals. *Compos Struct* 2018;187:454–65.
- [10] Manalo A, Aravinthan T, Fam A, Benmokrane B. State-of-the-art review on FRP sandwich systems for lightweight civil infrastructure. *J Compos Constr* 2016;21(1):04016068.
- [11] Tannous FE, Saadatmanesh H. Durability of AR glass fiber reinforced plastic bars. *J Compos Constr* 1999;3(1):12–9.
- [12] Benmokrane B, Manalo A, Bouhet J-C, Mohamed K, Robert M. Effects of diameter on the durability of glass fiber-reinforced polymer bars conditioned in alkaline solution. *J Compos Constr* 2017;21(5):04017040.
- [13] Benmokrane B, Ali AH, Mohamed HM, ElSafy A, Manalo A. Laboratory assessment and durability performance of vinyl-ester, polyester, and epoxy glass-FRP bars for concrete structures. *Composites Part B* 2017;114:163–74.
- [14] Tobbi H, Farghaly AS, Benmokrane B. Behavior of concentrically loaded fiber-reinforced polymer reinforced concrete columns with varying reinforcement types and ratios. *ACI Struct J* 2014;111:375.
- [15] Afifi MZ, Mohamed HM, Benmokrane B. Axial capacity of circular concrete columns reinforced with GFRP bars and spirals. *ASCE J Compos Constr* 2013;18:04013017.
- [16] Maranan G, Manalo A, Benmokrane B, Karunasena W, Mendis P. Behavior of concentrically loaded geopolymer-concrete circular columns reinforced longitudinally and transversely with GFRP bars. *Eng Struct* 2016;117:422–36.
- [17] Karim H, Sheikh MN, Hadi MN. Axial load-axial deformation behavior of circular concrete columns reinforced with GFRP bars and helices. *Constr Build Mater* 2016;112:1147–57.
- [18] CSA. Design and construction of building structures with fibre-reinforced polymers. Rexdale, ON, Canada: Canadian Standards Association, CAN/CSA-S806-12; 2012.
- [19] Benmokrane B, Manalo A, Bouhet J-C, Mohamed K, Robert M. Effects of diameter

- on the durability of glass fiber-reinforced polymer bars conditioned in alkaline solution. *ASCE J Compos Constr* 2017;21:04017040.
- [20] ASTM/C39. Standard Test Method for Compressive Strength of Cylindrical Concrete Specimens. West Conshohocken, PA: ASTM International; 2015.
- [21] AS3600. Reinforced concrete design: in accordance with AS 3600-2009. Sydney, N.S.W: Cement & Concrete Aggregates Australia: Standards Australia; 2011.
- [22] AlAjarmeh OS, Manalo AC, Benmokrane B, Karunasena W, Mendis P, Nguyen KTQ. Compressive behavior of axially loaded circular hollow concrete columns reinforced with GFRP bars and spirals. *Constr Build Mater* 2019;194:12–23.
- [23] Fam AZ, Rizkalla SH. Confinement model for axially loaded concrete confined by circular fiber-reinforced polymer tubes. *Struct J* 2001;98(4):451–61.
- [24] Micelli F, Modarelli R. Experimental and analytical study on properties affecting the behaviour of FRP-confined concrete. *Composites Part B* 2013;45(1):1420–31.
- [25] Kusumawardaningsih Y, Hadi MN. Comparative behaviour of hollow columns confined with FRP composites. *Compos Struct* 2010;93(1):198–205.
- [26] Yazici V. Strengthening hollow reinforced concrete columns with fibre reinforced polymers; 2012.
- [27] Saatcioglu M, Razvi SR. Strength and ductility of confined concrete. *ASCE J Struct Eng* 1992;118:1590–607.
- [28] Karim H, Noel-Gough B, Sheikh MN, Hadi MN. Strength and ductility behavior of circular concrete columns reinforced with. GFRP Bars Helices 2015.
- [29] Gangarao H, Taly N, Vijay P. Reinforced concrete design with. FRP Compos 2007.
- [30] Cui C, Sheikh S. Experimental study of normal-and high-strength concrete confined with fiber-reinforced polymers. *ASCE J Compos Constr* 2010;14:553–61.
- [31] Itakura Y, Yagenji A. Compressive test on high-strength R/C columns and their analysis based on energy concept. *Notes* 1992;8(C8P9D):C8P9D.
- [32] Bjerkeli L, Tomaszewicz A, Jensen J. Deformation properties and ductility of high-strength concrete. *Spec Publ* 1990;121:215–38.
- [33] Jaejer L, Mufti A, Tadros G. The concept of the overall performance factor in rectangular-section reinforced concrete beams. In: *Proceedings of the 3rd International Symposium on Non-Metallic (FRP) Reinforcement for Concrete Structures*; 1997. p. 551–8.
- [34] Tobbi H, Farghaly AS, Benmokrane B. Concrete columns reinforced longitudinally and transversally with glass fiber-reinforced polymer bars. *ACI Struct J* 2012;109:551.
- [35] Hadi MN, Wang W, Sheikh MN. Axial compressive behavior of GFRP tube reinforced concrete columns. *Constr Build Mater J* 2015;81:198–207.
- [36] Deitz D, Harik I, Gesund H. Physical properties of glass fiber reinforced polymer rebars in compression. *ASCE J Compos Constr* 2003;7:363–6.
- [37] Fillmore B, Sadeghian P. Contribution of longitudinal GFRP bars in concrete cylinders under axial compression. *Can J Civ Eng* 2018;45(6):458–68.
- [38] Hadi MN, Karim H, Sheikh MN. Experimental investigations on circular concrete columns reinforced with GFRP bars and helices under different loading conditions. *ASCE J Compos Constr* 2016;20:04016009.
- [39] ACI-318. (American Concrete Institute), Building code requirements for structural concrete. Farmington Hills, MI: ACI 318-14M; 2014.
- [40] Lignola GP, Prota A, Manfredi G, Cosenza E. Unified theory for confinement of RC solid and hollow circular columns. *Composites Part B* 2008;39:1151–60.
- [41] Becque J, Patnaik AK, Rizkalla SH. Analytical models for concrete confined with FRP tubes. *ASCE J Compos Constr* 2003;7:31–8.
- [42] Cascardi A, Micelli F, Aiello MA. Unified model for hollow columns externally confined by FRP. *Eng Struct* 2016;111:119–30.
- [43] Mander J, Priestley M, Park R. Behavior of ductile hollow reinforced concrete columns. *Bull N Z Natl Soc Earthquake Eng* 1983;16:273–90.
- [44] ACI. Guide for the design and construction of concrete reinforced with FRP bars. Farmington Hills, MI: American Concrete Institute; 2015.

Chapter 5

Effect of spiral spacing and concrete strength on behavior of GFRP-reinforced hollow concrete columns

It was found in Chapter 4 that the lateral confinement provided by the longitudinal GFRP bars could be correlated to the crushing strain of GFRP bars in concrete, which was affected by the lateral reinforcements and compressive strength of concrete. In this chapter, the effect of lateral confinement by increasing the volumetric ratio (ρ_v) and the concrete compressive strength (f'_c) was investigated. Seven large scale HCCs, 250 mm in diameter and 1 m in height, were prepared and tested under a concentric compression load. All HCCs had similar longitudinal reinforcing details to six GFRP bars 15.9 mm in diameter and (i/o) ratio of 0.36. To investigate the effect of ρ_v , columns with three different spacing between the lateral spirals (50 mm, 100 mm, and 150 mm) were tested in addition to one control sample without any lateral spirals while f'_c was varied within the normal strength level of concrete (21.2 MPa, 26.8 MPa, 36.8 MPa, and 44.0 MPa) to determine the effect of concrete compressive strength.

The test results showed that reducing the spacing between lateral spirals made the failure more progressive and increased the displacement capacity and ductility of GFRP-reinforced HCCs. On the other hand, higher f'_c increased the load capacity of the HCCs but could result in a more brittle behaviour, lower displacement capacity and ductility compared to lower f'_c . In contrast, the volumetric strain behavior was significantly affected by f'_c , where the test results showed that the HCC with the highest f'_c showed a volume reduction with high absorbed energy compared to the lateral expansion of the HCCs with lower concrete strength. Overall, GFRP reinforcements were able to maintain the strength reduction cause by the brittle failure behavior of the high f'_c . An analytical expression considering the effect of confinement provided by the lateral spirals and the concrete compressive strength was developed.

From the results of Chapters 3 to 5, it was found that the (i/o) ratio, ρ , ρ_v , and f'_c affect the overall behavior of GFRP-reinforced HCCs. The effects of these design parameters were considered in the development of a new design-oriented model to accurately and reliably describe the behavior of the GFRP-reinforced HCCs. The development of this model is presented in Chapter 6.

Effect of Spiral Spacing and Concrete Strength on Behavior of GFRP-Reinforced Hollow Concrete Columns

Omar S. AlAjarmeh¹; Allan C. Manalo²; Brahim Benmokrane³;
Warna Karunasena⁴; and Priyan Mendis⁵

Abstract: Hollow concrete columns (HCCs) are one of the preferred construction systems for bridge piers, piles, and poles because they require less material and have a high strength-to-weight ratio. While spiral spacing and concrete compressive strength are two critical design parameters that control HCC behavior, the deterioration of steel reinforcement is becoming an issue for HCCs. This study explored the use of glass fiber-reinforced polymer (GFRP) bars as longitudinal and lateral reinforcement for hollow concrete columns and investigated the effect of various spiral spacing and different concrete compressive strengths (f'_c). Seven HCCs with inner and outer diameters of 90 and 250 mm, respectively, and reinforced with six longitudinal GFRP bars, were prepared and tested. The spiral spacing was no spirals, 50, 100, and 150 mm; the f'_c varied from 21 to 44 MPa. Test results show that reducing the spiral spacing resulted in increased HCC uniaxial compression capacity, ductility, and confined strength due to the high lateral confining efficiency. Increasing f'_c , on the other hand, increased the axial-load capacity but reduced the ductility and confinement efficiency due to the brittle behavior of high compressive-strength concrete. The analytical models considering the axial load contribution of the GFRP bars and the confined concrete core accurately predicted the behavior of the HCCs after the spalling of the concrete cover or at the post-loading behavior. DOI: 10.1061/(ASCE)CC.1943-5614.0000987. © 2019 American Society of Civil Engineers.

Author keywords: Hollow column; Glass fiber-reinforced polymer (GFRP) bar; Spiral spacing; Concrete compressive strength.

Introduction

Hollow concrete columns (HCCs) are one of the preferred construction systems in civil infrastructures—including bridge piers, ground piles, and utility poles—to minimize the overall weight and reduce costs, given the small amount of concrete in the columns themselves and their underlying foundations. HCCs are also considered a practical solution to increase the strength-to-mass ratio of structures compared to solid concrete columns (Lignola et al. 2007; Kusumawardaningsih and Hadi 2010; Hadi and Le 2014; Lee et al. 2015). Designing an HCC with sufficient strength and reliable structural performance, however, requires careful consideration of some critical parameters, including lateral-reinforcement details and concrete compressive strength (Zahn et al. 1990; Mo et al. 2003;

Lignola et al. 2007; Lee et al. 2015; Liang et al. 2015). Lignola et al. (2011) stated that providing widely spaced lateral reinforcement (greater than 400 mm) in HCCs leads to brittle failure, premature longitudinal-bar buckling, and decreased ductility. On the other hand, Lee et al. (2015) indicated that reducing the lateral-reinforcement spacing from 80 to 40 mm increased ductility by 20% and minimized damage in the inner concrete core. In addition, Mo et al. (2003) found that increasing the concrete compressive strength from 30 to 50 MPa yielded stiffer compression resistance in HCCs, but with up to a 50% reduction in displacement capacity due to faster crack propagation and easier concrete splitting. Based on these studies, it can be concluded that the displacement capacity of steel-reinforced HCCs is significantly affected by lateral-reinforcement details, while their mode of failure is associated with concrete compressive strength.

In aggressive environments, the steel reinforcement in concrete columns is highly vulnerable to corrosion, leading to the development of a rusted shell around the reinforcement and its expansion of about 6–10 times its original volume (Verma et al. 2014). This process initiates hairline cracks in the concrete that progress into wide cracks, which significantly reduce the ultimate axial capacity and lead to the brittle failure behavior of concrete columns owing to the damage to the lateral reinforcement (Pantelides et al. 2013). Steel corrosion costs the Australian economy more than \$13 billion per year (Cassidy et al. 2015), while Canada and the US spend from \$50 to 100 billion on repairing deteriorated concrete structures (Tannous 1997). This issue has motivated many researchers around the world to investigate the use of high-strength and noncorroding reinforcement in building new concrete structures.

Fiber-reinforced polymer (FRP) reinforcing bars are now becoming an effective alternative in concrete structures because of their noncorroding properties. FRP bars have also proven to be promising as longitudinal reinforcement in concrete columns due to their having a higher strength and strain capacity than steel

¹Ph.D. Candidate, Centre for Future Materials, School of Civil Engineering and Surveying, Univ. of Southern Queensland, Toowoomba, QLD 4350, Australia. Email: omar.alajarmeh@usq.edu.au

²Associate Professor of Structural Engineering, School of Civil Engineering and Surveying, Centre for Future Materials, Univ. of Southern Queensland, Toowoomba, QLD 4350, Australia (corresponding author). Email: allan.manalo@usq.edu.au; manalo@usq.edu.au

³Professor of Civil Engineering, Dept. of Civil Engineering, Univ. of Sherbrooke, 2500, boul. de l'Université, Sherbrooke, QC, Canada J1K 2R1. Email: Brahim.Benmokrane@USherbrooke.ca

⁴Professor of Structural Engineering, School of Civil Engineering and Surveying, Centre for Future Materials, Univ. of Southern Queensland, Toowoomba, QLD 4350, Australia. ORCID: <https://orcid.org/0000-0003-3636-3068>. Email: karu.karunasena@usq.edu.au

⁵Professor, Dept. of Infrastructure Engineering, Univ. of Melbourne, Parkville, VIC 3010, Australia. Email: pamendis@unimelb.edu.au

Note. This manuscript was submitted on October 3, 2018; approved on May 22, 2019; published online on October 29, 2019. Discussion period open until March 29, 2020; separate discussions must be submitted for individual papers. This paper is part of the *Journal of Composites for Construction*, © ASCE, ISSN 1090-0268.

(Manalo et al. 2014). In particular, glass FRP (GFRP) bars are considered to be the most cost-effective, noncorroding composite reinforcing material (Benmokrane et al. 1995). GFRP-reinforced solid concrete columns have been successfully tested and have exhibited enhanced postloading response (i.e., the response after spalling of the concrete cover), owing to the increased displacement capacity of the columns and adequate confined strength due to the high tensile strength of the lateral GFRP reinforcement (Pantelides et al. 2013; Hadi et al. 2016). Despite GFRP bars having lower elastic moduli than steel, Pantelides et al. (2013) noted an improvement of 3% and 5% in the confined strength and ductility, respectively, of solid concrete columns due to the ineffectiveness of the steel reinforcement in providing confinement after yielding. Moreover, Hadi et al. (2016) highlighted the benefit of using GFRP reinforcement instead of steel in solid concrete columns. Their comparison of the behavior of solid concrete columns reinforced with six pieces of 14.6-mm-diameter longitudinal GFRP bars and other concrete columns with six pieces of 12.0-mm-diameter steel bars showed that the GFRP-reinforced columns had 4% higher ductility than the steel-reinforced columns. In addition, the ductility of the GFRP-reinforced columns was further enhanced by up to 33% when the spacing between spirals was reduced from 60 to 30 mm. Similar to the case of steel-reinforced HCCs, these studies showed that both spiral spacing and concrete compressive strength are important design parameters that affect the behavior of solid columns reinforced with GFRP bars and spirals. It is therefore essential to determine the effects of these design parameters on the behavior of HCCs reinforced with GFRP bars. The significance of this work, on the other hand, lies in its extending previous attempts by AlAjarmeh et al. (2019a, b) in investigating the effect of different inner-to-outer (*i/o*) diameter ratios and reinforcement ratios (ρ), respectively, of HCCs with GFRP reinforcement. The test results show that creating a hollow within the concrete columns changed their failure mode from brittle to a more ductile and progressive mode. In addition, increases of 22% and 74% in the confined strength and ductility factor were observed. Moreover, they concluded that the increase in the *i/o* ratio led to a gradual failure and more stability in the loading history. In contrast, increasing ρ increased the strength and significantly contributed to lateral confinement.

This study aimed at investigating the effectiveness of GFRP bars and spirals as internal reinforcement in HCCs. It focused on evaluating the effect of lateral spiral spacing and concrete compressive strength on the failure mode, load-displacement behavior, ductility, and confined strength of hollow concrete columns. Understanding the behavior of this new construction system will help narrow the current knowledge gap related to using GFRP bars as internal reinforcement in concrete compressive members, and will provide additional data for establishing design guidelines and

specifications for the use of GFRP reinforcement in hollow concrete columns.

Experimental Program

Materials

Reinforcement

Grade III #5 GFRP bars with a 15.9-mm nominal diameter (CSA 2012), as shown in Fig. 1(a), were used to reinforce the HCCs longitudinally. The transverse reinforcement was Grade III #3 GFRP spirals with a 9.5-mm nominal bar diameter and an inside diameter of 180 mm, as shown in Fig. 1(b). This type of transverse reinforcement was adopted because it provides higher lateral confinement to the concrete core compared to conventional circular hoops (Maranan et al. 2016). The GFRP bars and spirals were manufactured by protruding glass fibers impregnated with vinyl-ester resin, and then coating the outer surface with sand. Table 1 provides the physical and mechanical properties of the GFRP bars determined following the CSA-S806 (CSA 2012) and ASTM D7205/D7205M-06 (ASTM 2016), as reported previously by Benmokrane et al. (2017) for the same reinforcements, which were manufactured from the same production lot, denoting that the standard deviation values are included between brackets. As recommended by the CSA S806 code (CSA 2012), the tensile strength and modulus of elasticity of the GFRP bars were calculated using the nominal bar area. It should be noted that the mechanical properties in Table 1 are for straight bars and the ultimate tensile strength of spirals was calculated based on the CSA S806 code (CSA 2012).

Concrete

Four different levels of normal-strength concrete were cast in the column samples. One mix was a ready-mixed concrete with a maximum coarse aggregate size of 10 mm, a slump of 103 mm, an average compressive strength (f'_c) of 26.8 MPa, and a standard deviation (SD) of 3.54 MPa. In addition, two batches of concrete were mixed in the laboratory with a maximum aggregate size of 10 mm and slumps of 91 and 106 mm for the samples with f'_c of 36.8 MPa (SD of 1.56) and 44.0 MPa (SD of 2.31), respectively. The other concrete mix was postmixed concrete (i.e., ready-packed dry mix) with a maximum aggregate size of 3 mm and a slump of 110 mm, which gave an average f'_c of 21.2 MPa (SD of 3.12). The compressive strengths of these concrete batches were measured by preparing six concrete cylinders 100 mm in diameter and 200 mm in height for each concrete mix based on ASTM C31 specifications (ASTM 2015a) and tested on the day of column testing according to the procedures described in the ASTM C39 specifications (ASTM 2015b).



Fig. 1. GFRP reinforcement: (a) longitudinal GFRP bars; and (b) GFRP spirals.

Table 1. Properties for the GFRP reinforcement

Property	Test method	Sample	No. 16	No. 10
Physical				
Nominal bar diameter (mm)	CSA-S806, Annex A (CSA 2012)	9	15.9	9.5
Nominal bar area ^a (mm ²)			198.5	70.8
Actual bar's cross-sectional area by immersion test (mm ²)			224.4 (1.2) ^b	83.8 (1.9) ^b
Mechanical				
Ultimate tensile strength, f_u (MPa)	ASTM D7205/D7205M-06 (ASTM 2016)	6	1,237 (33.3) ^b	1315 (31.1) ^b
Modulus of elasticity, E_{FRP} (GPa)			60.0 (1.3) ^b	62.5 (0.4) ^b
Ultimate strain, ε_u (%)			2.1 (0.1) ^b	2.3 (0.1) ^b

Source: Data from Benmokrane et al. (2017).

^aThe adopted area for calculating mechanical properties.

^bStandard deviation.

Specimen Details

Seven concrete columns fully reinforced with GFRP bars with overall dimensions of 250 mm in diameter and 1 m in height were cast and tested. The cross section was determined based on the maximum capacity testing machine. On the other hand, the height-to-diameter ratio of the samples was 4, which ensured the avoidance of global buckling for the column samples as reported by Maranan et al. (2016). All columns were longitudinally reinforced with six GFRP bars in accordance with the reinforcement details and ratio recommended in the AS3600 code (AS 2011) for steel reinforcement, owing to the lack of codes and standards regarding the use of GFRP bars in compression. Consequently, the reinforcement ratio of 2.79% was similar for all test columns, calculated by dividing the total area of the longitudinal GFRP bars (A_{FRP}) (1,191 mm²) by the gross cross-sectional area of the columns (A_g) (42,704 mm²). Concrete columns were divided into two groups to investigate the effect of spiral spacing and concrete compressive strength:

- Group A: Three columns were reinforced laterally with GFRP spirals with spacings of 50, 100, and 150 mm at the middle portion of the samples (500 mm). Another column without lateral reinforcement at the testing region (500 mm) was prepared to evaluate the effect of the lateral reinforcement. These lengths were chosen to ensure crushing failure in the bars with lengths of 50, 100, and 150 mm, and bar buckling failure in the last sample. This finding was reported by Maranan et al. (2016), who found that bar buckling failure occurred in bars with a length of more than 200 mm. While the CSA S806 code (CSA 2012) recommends a clear spacing between spirals of less than 85 mm for the tested columns, the biaxial stress distribution in HCCs compared to the triaxial stress distribution in solid concrete columns (AlAjarmeh et al. 2019a) requires that the most effective spiral spacing for HCCs be determined.
- Group B: Four columns were cast with different concrete strengths (21.2, 26.8, 36.8, and 44.0 MPa) and tested. These levels of compressive strength were considered normal-strength concrete, as indicated in the ACI 318 code (ACI 2008). The reinforcement details for all columns were kept the same by a reinforcement ratio of 2.79% and 100-mm spacing between lateral spirals to determine the effect of varying concrete compressive strengths. Moreover, the adopted reinforcement details resulted in stable load-carrying behavior and a gradual failure of the concrete core after the spalling of the concrete cover (AlAjarmeh et al. 2019a). Choosing different levels of normal-strength concrete led to significant change in the compressive behavior for HCCs, as reported by Mo et al. (2003).

The top and bottom 250 mm of the height of all the columns were laterally reinforced with GFRP spirals at a closed spacing of 50 mm to prevent stress-concentration failure at the column ends.

The hollow section was created by inserting a 1-mm-thick PVC pipe with an external diameter of 90 mm at the center of the samples during casting. This resulted in an HCC with a constant inner-to-outer diameter ratio of 0.36, which was found to provide ductile behavior due to the progressive failure of the concrete cover, followed by crushing of the concrete core and longitudinal bars with no spiral failure (AlAjarmeh et al. 2019a, b). It is worth mentioning that Kusumawardaningsih and Hadi (2010) and Hadi and Le (2014) used a similar inner-to-outer diameter ratio for steel-reinforced HCCs to precisely capture the behavior of hollowness by using this ratio.

Fig. 2 shows the typical cross section of the columns tested, while Table 2 provides the different volumetric ratios, spacing, and f'_c . The volumetric ratios were calculated by dividing the volume of one spiral by the concrete-core volume within one spiral pitch. Columns were designated as either A or B to represent the specimen group, followed by the spiral spacing, and then the concrete compressive strength f'_c . For example, column A-100-26.8 is a GFRP-reinforced hollow column from Group A with 100-mm spacing between lateral spirals and with a f'_c of 26.8 MPa. Column B-100-26.8, on the other hand, is a GFRP-reinforced hollow column from Group B with 100-mm spacing between lateral spirals and with a f'_c of 26.8 MPa.

Test Setup and Instrumentation

A total of six electrical-resistance strain gauges were attached to each column to measure the strain during testing. Two 3-mm long strain gauges were glued onto longitudinal GFRP bars at mid-height, and two were glued onto spirals at midheight. The last two gauges were 20 mm in length and glued onto the outer surface of the concrete at the column midheight to measure the axial strain. Fig. 3(a) shows the location of the strain gauges. Steel clamps measuring 50 mm in width and 10 mm in thickness were used at the top and bottom of the columns; in addition, 3-mm-thick neoprene cushions were used to prevent premature cracking and to ensure that failure occurred in the test region (i.e., column midheight). Furthermore, 3-mm-thick neoprene cushions were placed on the top and bottom of the columns for uniform load distribution. Moreover, wire mesh was used to cover the specimen for safety purposes and to prevent projectile debris upon column failure. Afterwards, the columns were tested under monotonic concentric loading with a 2,000-kN hydraulic cylinder. The applied load was measured with a 2,000-kN load cell, and the axial displacement was recorded with a string pot, as shown in Fig. 3(b). Throughout testing, the load, strain, and axial displacement were recorded with the System 5000 (Vishay Intertechnology, Malvern, Pennsylvania) data logger. Failure propagation was also carefully observed and video recorded during the entire loading regime.

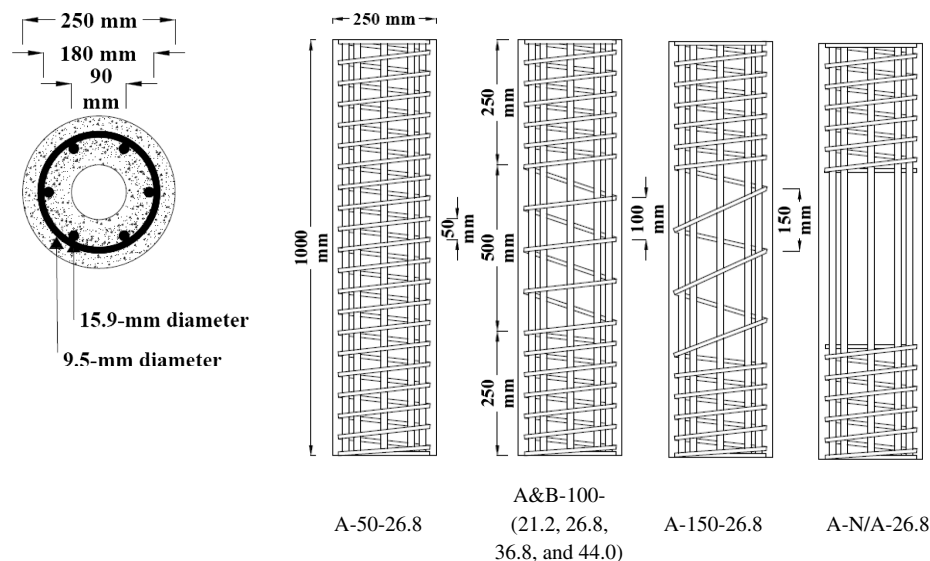


Fig. 2. Typical cross section of columns and lateral spiral details.

Table 2. Concrete-column matrices and details

Specimens	Volumetric ratio (%)	Spiral spacing (mm)	Concrete compressive strength (MPa)
A-N/A-26.8	0.00	N/A	26.8
A-150-26.8	1.28	150	26.8
A-100-26.8	1.93	100	26.8
B-100-26.8			
A-50-26.8	3.84	50	26.8
B-100-21.2	1.93	100	21.2
B-100-36.8	1.93	100	36.8
B-100-44.0	1.93	100	44.0

Behavior of Columns with Various Spiral Spacing

Failure Mode

Group A columns were tested under concentric compression load until failure. Lignola et al. (2007) indicated that the general failure for HCCs reinforced with steel bars is controlled by bar buckling and concrete crushing with highly spaced lateral reinforcement. The HCCs tested in our study experienced different modes of failure due to the GFRP bars having higher strength than the steel bars. Typically, the failure in all columns started as vertically spreading hairline cracks appearing on the outer concrete surface at advance loading levels. Once they appeared, the cracks propagated and widened, leading to different spalling features of the outer concrete cover, rupturing longitudinal GFRP bars, and damaging the concrete core, all of which are described in detail below:

- A-N/A-26.8: This column experienced explosive spalling and failing of both the concrete cover and core, causing large concrete pieces to fall from the specimen at midheight. Consequently, global buckling in the longitudinal GFRP bars without fracturing was observed, as shown in Fig. 4(a).
- A-150-26.8: Limited concrete-cover spalling localized at midheight occurred in this column. Lateral expansion of the perimeter at midheight was noted after concrete-cover spalling, leading to final failure, as highlighted by the rupturing of the longitudinal GFRP bars and massive damage to the concrete

core, as shown in Fig. 4(b). No damage to the lateral spiral was observed.

- A-100-26.8: Concrete-cover spalling in this column was gradual and continued until the entire column was affected. Lateral spirals held the concrete core and longitudinal bars. Final failure was due to ruptures in the longitudinal GFRP bars and crushing of the concrete core at midheight without damage to the lateral spirals, as shown in Fig. 4(c).
- A-50-26.8: Gradual overall concrete-cover spalling was observed, followed by lateral expansion in the concrete core, which was confined by the GFRP spirals. Sequential rupturing of the longitudinal GFRP bars in different locations throughout the column's height and concrete crushing of the concrete at the bottom also occurred and were caused by stress concentration, as shown in Fig. 4(d).

The different failure mechanisms after the spalling of the concrete cover were due to lateral-reinforcement spacing. The above results indicate that the HCCs with narrower spiral spacing evidenced more progressive failure and less damage to the concrete core than the columns with wider spacing. Lee et al. (2015) observed similar behavior with steel-reinforced hollow columns. This finding can be correlated to the unbraced length of the longitudinal GFRP bars, which tried to buckle with the application of the compressive load. In particular, the failure of the column without lateral reinforcement (A-N/A-26.8) was consistent with that of the GFRP-reinforced solid concrete columns tested by Maranan et al. (2016). In this case, the concrete cover and core experienced brittle and explosive failure due to the long unbraced length of the longitudinal GFRP bars. Narrow spiral spacing, however, stabilized the longitudinal GFRP bars and resulted in the column's progressive failure. For all spiral-reinforced columns, using GFRP reinforcement delayed final failure due to its higher axial displacement capacity compared to the steel-reinforced HCCs (Lignola et al. 2007; Kusumawardaningsih and Hadi 2010).

Load-Displacement Behavior

Spiral spacing affects the load displacement, confined strength, and ductility behavior of HCCs reinforced with GFRP bars, as shown in Fig. 5 and Table 3. As can be seen from Fig. 5, all the columns had

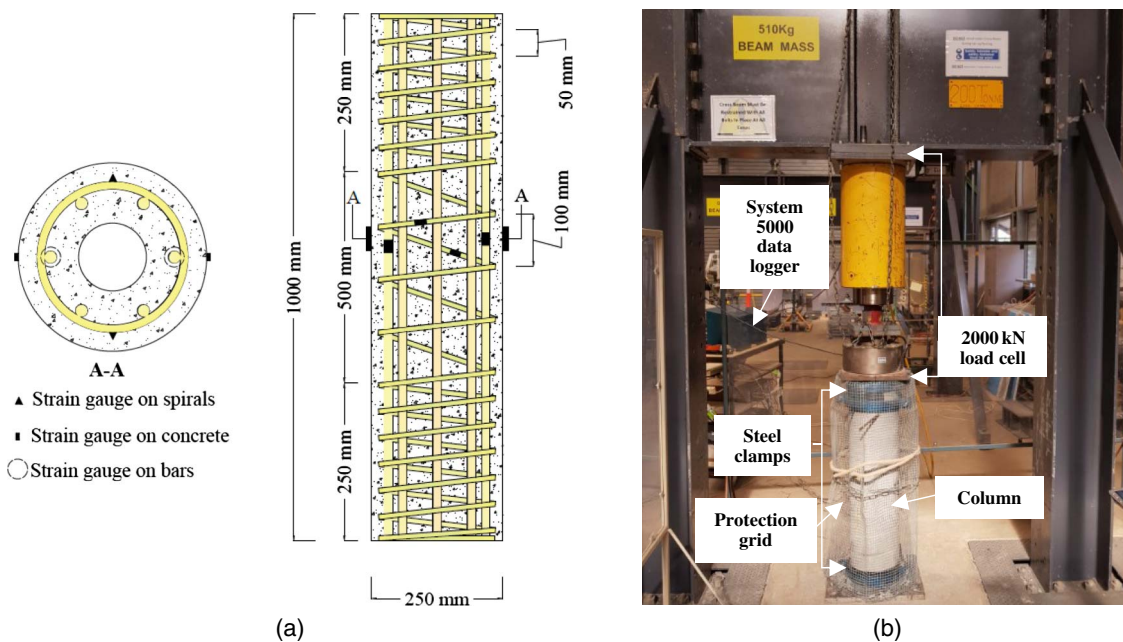


Fig. 3. Test setup and instrumentation for the hollow concrete columns: (a) location of strain gauges; and (b) test setup.

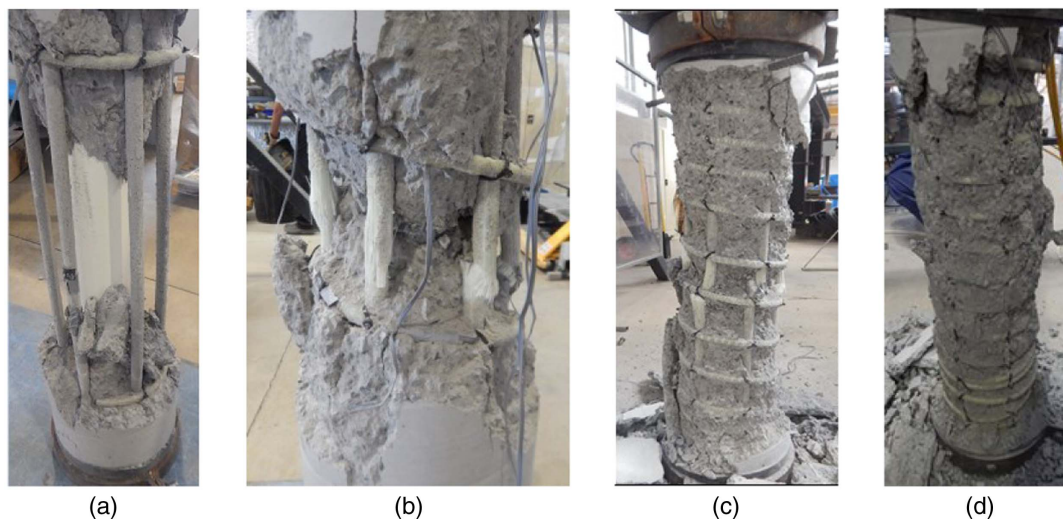


Fig. 4. Final failure of the columns in Group A: (a) A-N/A-26.8; (b) A-150-26.8; (c) A-100-26.8; and (d) A-50-26.8.

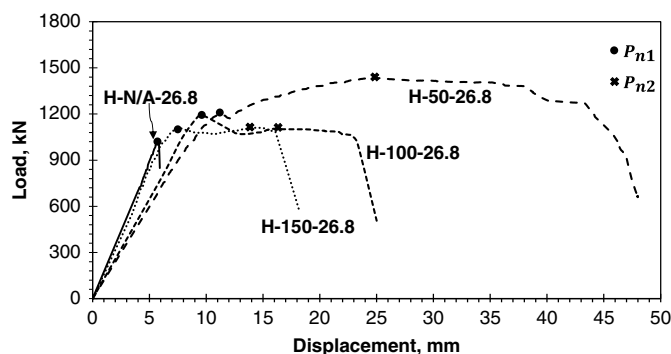


Fig. 5. Load-displacement behavior of Group A columns.

almost linear-elastic behavior up to the spalling of the concrete cover but with lower stiffness as the spiral spacing narrowed. Table 3 also provides the slope of the linear-elastic portion of the load-deflection curve, where the displacement is the axial displacement of the sample with respect to the original height of its top part. The lower axial stiffness for columns with narrower spiral spacing is due to the weaker plane between the outer concrete cover and the concrete core, creating a slender outer concrete shell. The columns with closer spiral spacing, however, had more stability than those columns with wider spiral spacing after concrete-cover spalling (postloading behavior), owing to the better lateral confinement provided by the lateral reinforcement. Hadi et al. (2016, 2017) and Maranan et al. (2016) made similar observations. The spiral spacing also affected the first axial peak load of the hollow columns.

Table 3. Test results of Group A columns

Sample	Stiffness (kN/mm)	P_{n1} (kN)	Yield displacement, Δ_y (mm)	P_{n2} (kN)	Ultimate displacement, Δ_u (mm)	P_f (kN)	$D.F.$	f'_{cc} (MPa)	$C.E.$	$\varepsilon_{c,P_{n1}}$ ($\mu\varepsilon$)	$\varepsilon_{b,P_{n1}}$ ($\mu\varepsilon$)	$\varepsilon_{b,P_{n2}}$ ($\mu\varepsilon$)	$\varepsilon_{s,P_{n1}}$ ($\mu\varepsilon$)	$\varepsilon_{s,P_{n2}}$ ($\mu\varepsilon$)
A-N/A-26.8	177	1,022	7.3	—	—	—	—	—	—	1,450	1,640	—	—	—
A-150-26.8	163	1,108	8.3	1,110	16.1	1,083	1.94	50.5	2.20	1,950	3,900	10,070	2,430	4,470
A-100-26.8	132	1,189	9.3	1,102	23.3	1,015	2.53	50.1	2.19	2,160	2,310	8,950	1,100	8,850
A-50-26.8	120	1,197	11.4	1,434	43.9	1,002	3.85	65.2	3.07	2,520	3,880	12,850	2,510	6,310

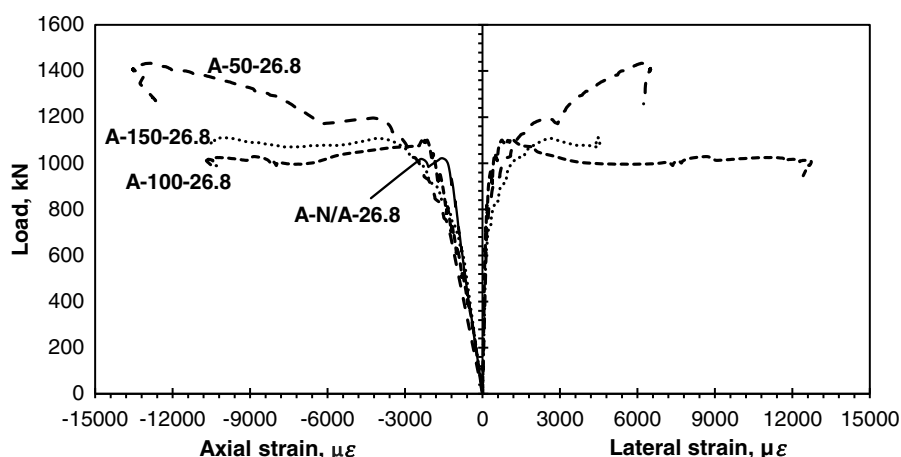
This first peak load (P_{n1}), denoted by the solid black circle in Fig. 5, represents the load carried by both the unconfined concrete and longitudinal GFRP bars. The HCCs with closer spiral spacing exhibited a higher load than the columns with wider spiral spacing. Column A-50-26.8 had the highest load capacity, specifically 1%, 8%, and 17% higher than columns A-100-26.8, A-150-26.8, and A-N/A-26.8, respectively. This increase in the axial load capacity—even with the same cross-sectional area and longitudinal reinforcement ratio—emphasizes the positive contribution of the lateral confinement in preventing crack propagation in the concrete. This led to a good distribution of the tensile stress in the concrete cover, resulting in spalling along the column height, as shown in Fig. 4.

While the spalling of the concrete cover after the uniaxial peak resulted in a drop of axial load, its level can be correlated to the spiral spacing. For the column without lateral reinforcement (A-N/A-26.8), the load dropped significantly, and the column was unable to carry more load. Providing spirals activated the lateral confinement at the load-displacement part after P_{n1} , so that columns A-50-26.8, A-100-26.8, and A-150-26.8 retained most of the applied load with only a 1%, 10%, and 7% reduction in P_{n1} , respectively. Karim et al. (2016) made similar observations. After that point, the lateral expansion of the cracking concrete was restricted by the lateral spirals, allowing the column to continue resisting the applied load at the postloading stage, at which point the concrete cover no longer makes a load contribution. This load-carrying resistance was controlled by the column volumetric ratio (Table 2), which prevented the concrete core from crushing and the unbraced length of the longitudinal bars from buckling and crushing. Because of the good confinement of the concrete core and longitudinal bars, column A-50-26.8 exhibited a second peak load (P_{n2}) and had a confined strength 29% higher than columns A-100-26.8 and A-150-26.8. The cross (x) in Fig. 5 can trace P_{n2} . Table 3 shows that columns A-100-26.8 and A-150-26.8 had similar maximum confined strength values (f'_{cc}), even with different spiral spacing. To calculate f'_{cc} , P_{n2} was divided by the

concrete-core area (A_{core}) with a diameter denoted by the distance between the spiral centers. The axial strain of the GFRP bars was, however, 13% higher in column A-150-26.8 than in column A-100-26.8, suggesting that neither a spacing of 100 mm nor 150 mm was able to increase the confined strength of the concrete core. Moreover, the column with 50-mm spiral spacing made the concrete core fail more progressively than columns A-100-26.8 and A-150-26.8. This was due to the efficiency of the closer spirals in delaying the crack progression in the concrete core and in reducing the unbraced length of the longitudinal GFRP bars. This also accounts for the higher ductility of the columns with smaller spiral spacing. For instance, column A-50-26.8 had 30% and 50% higher ductility than columns A-100-26.8 and A-150-26.8, respectively. The ductility of the HCCs was calculated as the ratio between ultimate displacement (Δ_u , which represents the displacement at the failure point) to the yield displacement (Δ_y , which represents the displacement at the level of the uniaxial load with respect to the extended linear-elastic line), as suggested by Cui and Sheikh (2010). In the HCCs in this study, the lateral spiral reinforcement provided nonuniform confining stress along the column height, resulting in crack development in the concrete core at the unconfined region, i.e., between spirals, decreasing column capacity after P_{n2} [Fig. 5]. Consequently, a narrower spiral spacing in the tested region yielded a longer descending part and the area under the load-displacement curve was larger than with the columns with wider spiral spacing, indicating that the column had a higher toughness. Finally, columns A-50-26.8 and A-100-26.8 recorded failure loads that were 7% and 2% higher than A-150-26.8, since the closer spiral spacing protected the concrete core from sudden failure and gave the GFRP bars a chance to withstand greater axial loads.

Load-Strain Behavior

Fig. 6 shows the load versus axial strain (negative sign) in the longitudinal GFRP bars and lateral strain (positive sign) in the spirals

**Fig. 6.** Axial and lateral strain versus applied load for Group A columns.

for the Group A columns. These strain readings were taken as the average of the strain readings at longitudinal bars and spirals where the difference between the maximum and minimum strains did not exceed 5% of the average value. After the axial linear-elastic load-strain response, the columns started to show a nonlinear ascending part due to hairline cracks appearing in the concrete cover. Interestingly, the hairline cracks started to appear at a strain of around $1,500 \mu\epsilon$, measured by the strain gauges attached to the concrete. This value is similar to the concrete cracking limit reported by Saatcioglu and Razvi (1992). This observation was further verified in column A-N/A-26.8, which failed after reaching this axial strain ($\epsilon_{c,P_{n1}}$) (Table 3). In fact, the narrower the spiral spacing, the higher the ultimate recorded axial concrete strain was due to the delay in crack propagation and greater concrete-cover stability. For instance, a strain ($\epsilon_{c,P_{n1}}$) of $1,450 \mu\epsilon$, $1,950 \mu\epsilon$, $2,160 \mu\epsilon$, and $2,520 \mu\epsilon$ was recorded in columns A-N/A-26.8, A-150-26.8, A-100-26.8, and A-50-26.8, respectively. In the longitudinal bars, the axial compressive-strain values at the first peak load ($\epsilon_{b,P_{n1}}$) were $1,640 \mu\epsilon$, $3,900 \mu\epsilon$, $2,310 \mu\epsilon$, and $3,880 \mu\epsilon$ in columns A-N/A-26.8, A-150-26.8, A-100-26.8, and A-50-26.8, respectively. These strain values are between 7% and 17% of the ultimate tensile strain of the GFRP bars, suggesting that they contributed significantly to the uniaxial compression capacity of the columns. Consequently, their contribution should not be ignored, as indicated in the current design codes (CSA 2012; ACI 2015). It is also noteworthy to mention that the GFRP spirals recorded significant lateral strain only after the column's first peak load, indicating that the lateral reinforcement was activated and provided confinement only after the concrete cover spalled.

After the cover spalled (postloading stage), the longitudinal GFRP bars continued carrying a load, and the strain of the lateral spirals increased dramatically due to dilation of the concrete core. It is important to note in Fig. 6 that the strains in the longitudinal GFRP bars and spirals in columns A-100-26.8 and A-150-26.8 plateaued in the postloading stage, unlike column A-50-26.8, where it continued to increase. This behavior indicates that the spiral spacings of 100 and 150 mm were adequate to prevent the bars from buckling but not to prevent or delay the initiation of cracks in the concrete core (Fig. 4). From this result, it can be deduced that effective confinement is related more to the concrete core rather than to the longitudinal bars, because GFRP bars have linear-elastic behavior up to failure. This finding also explains the observed final failure in all hollow columns tested, in which the longitudinal GFRP bars ruptured at a strain of $10,540 \mu\epsilon$, $10,690 \mu\epsilon$, and

$13,530 \mu\epsilon$ in columns A-150-26.8, A-100-26.8, and A-50-26.8, respectively, as shown in Fig. 6. These strain levels ranged from 50.2% to 64.5% of the ultimate tensile strain of the GFRP bars. It is interesting to note that using a spiral spacing of 50 mm resulted in a crushing strain of the GFRP bars 27% higher than when using the 100- and 150-mm spacing. The average of these values matches the proposed average of $12,200 \mu\epsilon \pm 1,200 \mu\epsilon$ as the maximum compressive strain for GFRP bars suggested by Fillmore and Sadeghian (2018).

Fig. 6 shows that increasing the spiral spacing increased the efficiency of concrete-core confinement and the longitudinal GFRP bars until failure. For instance, column A-150-26.8 recorded the lowest lateral strain of $4,542 \mu\epsilon$ at failure, because the widely spaced lateral spirals were unable to limit and delay crushing of the concrete core. On the other hand, column A-100-26.8 recorded $12,740 \mu\epsilon$ at failure, resulting in a higher displacement capacity (as can be seen in Fig. 5), while column A-50-26.8 recorded $6,500 \mu\epsilon$. Although column A-100-26.8 had a higher lateral strain than column A-50-26.8, the latter had higher lateral confinement proportional to the vertical spacing between spirals. Finally, columns with closer spiral spacing showed higher engagement in terms of hoop stress in confining the concrete core proportional to the vertical spacing between spirals. Consequently, this study recommends the 50-mm spacing as lateral reinforcement for HCCs, or the equivalent volumetric ratio, to get significantly enhanced strength and ductility. The hoop stress was calculated by multiplying the spiral strain at the failure by its modulus of elasticity.

Volumetric Strain Behavior

Fig. 7(a) shows the normalized first peak load for Group A columns. The normalized first peak load was calculated by dividing P_{n1} by the multiplication of the gross cross-sectional area of the column and characterized concrete compressive strength ($f'_c \times A_g$). The figure shows that the normalized first peak load (P_{n1}) increased as the spacing between spirals narrowed. This is an interesting result because both the concrete strength and number of bars were the same for all columns. This finding indicates that the lateral confinement provided by the GFRP spirals contributed to the uniaxial compression capacity of the HCCs by preventing lateral plastic concrete dilation after the appearance of cracks and thereby enhancing the concrete's compressive strength. This phenomenon can be explained by the volumetric strain (ϵ_v) or the dilation rate of the concrete, which is defined in Eq. (1) for solid concrete columns (Mirmiran and Shahawy 1997)

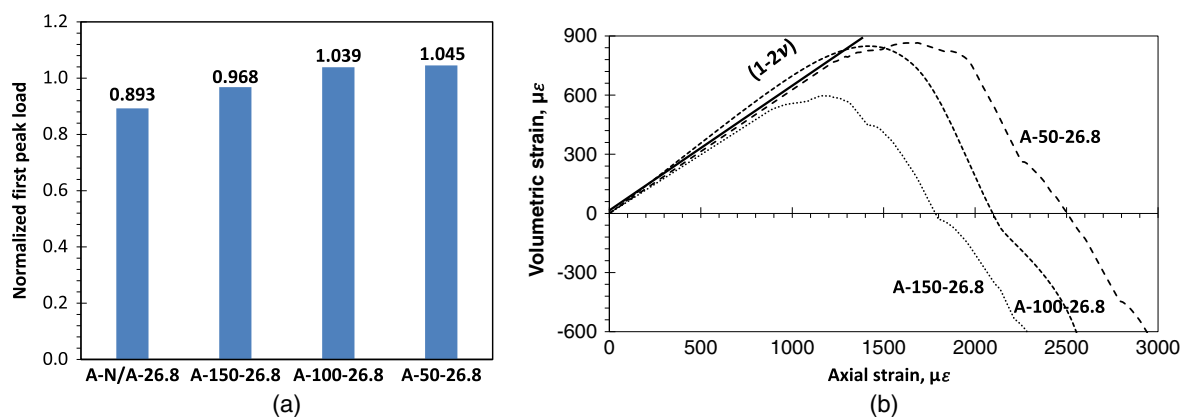


Fig. 7. Strength enhancement and volumetric strain behavior of Group A columns: (a) first peak-load enhancement; and (b) volumetric strain behavior versus axial strain behavior.

$$\varepsilon_v = \varepsilon_c + 2\varepsilon_r \quad (1)$$

where ε_c = axial strain measured in the longitudinal GFRP bars; and ε_r = lateral strains measured in the GFRP spirals. This formula expresses the change of volume with respect to a unit volume in solid concrete columns loaded under a triaxial stress state. In perfectly elastic conditions for solid columns, the conventional slope of the ascending line between the volumetric strain and axial strain is given as $(1 - 2\nu)$ (Mohamed et al. 2014), where ν is the Poisson's ratio of the concrete (equal to 0.2), as shown in Fig. 7(b). In this figure, positive ε_v represents volume reduction, whereas negative ε_v represents expansion. The curve's deviation from the slope line represents crack initiation until the spalling of the concrete cover at ε_v . A similar slope for HCCs was obtained by modifying Eq. (1) by multiplying ε_r by 3 instead of 2 to attain a slope of $(1 - 2\nu)$. This means that the lateral dilation of the concrete in HCCs is lower than in solid columns. This is because of the non-uniform distribution of biaxial stresses in HCCs, which causes a portion of the concrete dilation to be inward, as indicated by Cascardi et al. (2016), who also referred to the higher stability in the concrete core due to the use of hollow sections, which allows a higher axial-to-lateral strain ratio, as reported by Lignola et al. (2008). Moreover, based on the slope equation, the Poisson's ratio for the tested columns was 0.18, which is within the typical range for normal-strength concrete (0.15–0.22) (Mohamed et al. 2014). According to Fig. 7(b), the spiral spacing significantly affected concrete stability by delaying the elastic dilation of the concrete, as shown by the higher volumetric strain at the higher axial compressive strain.

Behavior of Columns with Different Concrete Strength

Failure Mode

Group B columns, which had different concrete compressive strengths (f'_c), exhibited different failure modes in terms of spalling and the degree of damage to the concrete core. All, however, failed because of the rupturing of the longitudinal GFRP bars with the GFRP spirals remaining intact. Therefore, after the hairline cracks

appeared on the outer concrete cover, column failure progressed as described below:

- B-100-21.2: Cracks extended at the bottom half of the column, leading to the spalling of the concrete cover. The cracks then propagated to the middle portion and the concrete core. This resulted in the crushing of the entire concrete core at midheight, as shown in Fig. 8(a).
- B-100-26.8: Concrete-cover spalling in this column was gradual and continued until it affected the entire height, as shown in Fig. 8(b).
- B-100-36.8: Vertical cracks along the column height appeared, followed by overall spalling of the concrete cover. Partial degradation was observed in the concrete core at different locations, which resulted in the rupture of GFRP bars at these locations [Fig. 8(c)].
- B-100-44.0: Cracks extending and propagating at the midbottom half of the column height were observed, followed by large concrete pieces splitting off at the outer concrete cover. Slow degradation in the concrete core resulted in the rupture of two longitudinal GFRP bars and the loss of the concrete core, as shown in Fig. 8(d).

From the above observations, it can be concluded that increasing the f'_c changed the failure of HCCs reinforced with GFRP bars from ductile to brittle. This was clearly evidenced by column B-100-44.0, which failed abruptly after the whole concrete core degraded, with limited failure in the longitudinal bars. Consistent with Mo et al. (2003), column B-100-44.0 showed faster spalling of the concrete cover as flakes, compared to the other columns, which exhibited gradual concrete spalling. More longitudinal GFRP bars ruptured in the columns with a lower f'_c , which can be attributed to the GFRP bars having a greater stiffness than the concrete, and therefore the reinforcement carried more of the load after the concrete cover spalled. The localized concrete spalling in column B-100-21.2 can be attributed to the smaller aggregate size (3 mm), which resulted in more microcracks between the concrete paste and the fine aggregate particles, which was also reported by Cui and Sheikh (2010).

Load-Displacement Behavior

The variation in f'_c (21.2–44.0 MPa) significantly affected the load-displacement behavior, confinement efficiency, and ductility of the

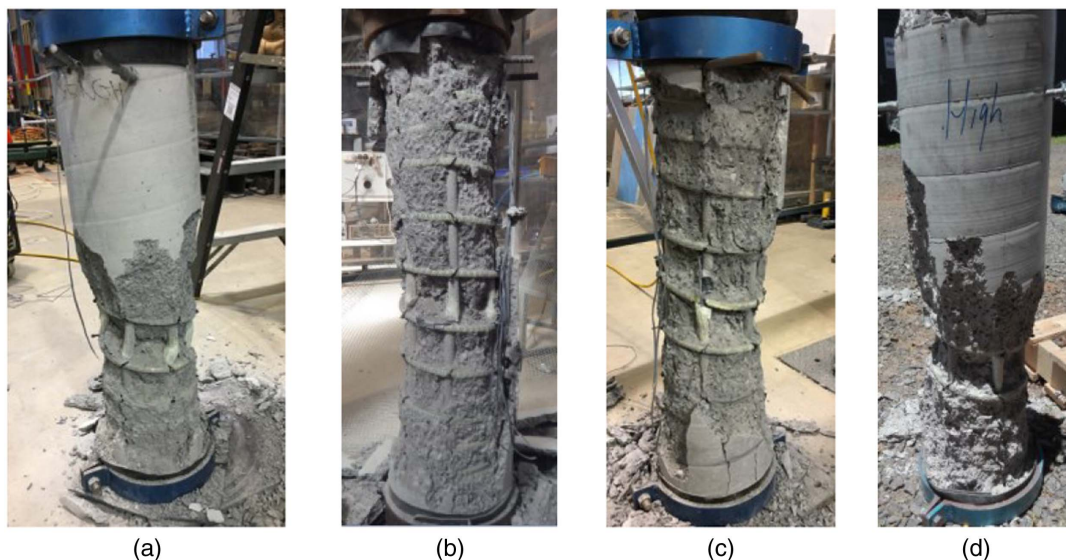


Fig. 8. Final failure of Group B columns: (a) B-100-21.2; (b) B-100-26.8; (c) B-100-36.8; and (d) B-100-44.0.

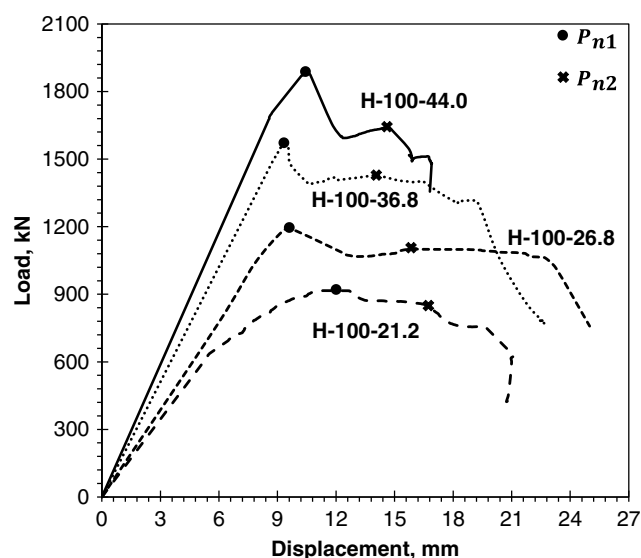


Fig. 9. Load-displacement behavior of Group B columns.

tested HCCs. Fig. 9 and Table 4 show that the use of higher concrete compressive strength resulted in stiffer load-displacement behavior because of the increase in the concrete's elastic modulus from 21.6 GPa ($f'_c = 21.2$ MPa) to 31.2 GPa ($f'_c = 44$ MPa). Predictably, increasing the f'_c increased the axial-load capacity at the first load peak (P_{n1}) of columns B-100-26.8, B-100-36.8, and B-100-44.0, respectively, by 31.1%, 73.1%, and 107.3% compared to column B-100-21.2. The insignificant deviation between these percentages with respect to the percentage increase of the concrete compressive strength can be attributed to the concrete being a non-homogeneous material that is affected by placing, compacting, and curing (Neville 1995). The increase in f'_c , however, decreased the contribution of the longitudinal GFRP bars due to the increased concrete stiffness, which was getting closer to the GFRP-bar stiffness. The contribution of the longitudinal GFRP bars to the P_{n1} of columns B-100-21.2, B-100-26.8, B-100-36.8, and B-100-44.0 was 22.1%, 11.7%, 8.2%, and 6.9%, respectively. The axial load contribution of the GFRP bars was calculated by multiplying bar axial strain by bar elastic modulus and total bar area divided by P_{n1} . Cracks that widened and extended along the outer concrete cover resulted in a load reduction after P_{n1} , in which the magnitude of the drop in load capacity can be correlated to the f'_c . The load drop was 15.2%, 11.5%, 10.2%, and 4.1% for columns B-100-44.0, B-100-36.8, B-100-26.8, and B-100-21.2, respectively, which emphasizes the significant contribution of the concrete cover, especially for the columns with higher f'_c . This finding is consistent with Mo et al. (2003), who observed a higher load drop in columns with higher f'_c . Addressing such an issue would involve using lower concrete-cover area to gross area or increasing the lateral reinforcement to mitigate the load drop after P_{n1} , as noticed in the Group A columns.

After the load drop (after P_{n1}), the Group B columns exhibited different postloading behavior until the second axial peak load (P_{n2}). Note that P_{n2} is the contribution of the confined concrete core in addition to the longitudinal GFRP bars. Therefore, column H-100-44.0 showed higher load-displacement capacity and recorded P_{n2} 49.2% and 15.4% higher than columns B-100-26.8 and B-100-36.8, respectively. This was due to the former's higher f'_c . Fig. 9 shows a slightly higher stiffness after the maximum load with increasing f'_c , which is due to the strength enhancement in the post-loading stage, as reported by Martinez et al. (1984). This increase was not enough, however, to increase the confinement efficiency with respect to the unconfined concrete strength (f'_{co}) of the columns. In fact, column B-100-44.0 showed 8.7% and 3.4% lower confinement efficiency than columns B-100-26.8 and B-100-36.8, respectively. This behavior can be explained by the significant load drop after the first axial peak load for the columns with high concrete compressive strength and emphasized the CSA S806 code (CSA 2012) recommendation of using a high volumetric ratio for high f'_c .

In order to further evaluate the effect of the compressive strength of concrete for hollow columns reinforced with GFRP bars, the confinement efficiency ($C.E.$) was calculated from the ratio of confined strength (f'_{cc}) to the unconfined strength (f'_{co}) when the outer concrete surface was free of cracks ($0.85f'_c$). The confined concrete-core strength was calculated by dividing P_{n2} by the concrete-core area (A_{core}). The A_{core} was calculated based on the diameter measured from the lateral spiral centers, as was also implemented by Tobbi et al. (2014). After P_{n2} , the load-displacement behavior continued to deteriorate until the longitudinal GFRP bars and concrete core recorded the final failure load (P_f) (Table 4). This strength degradation was caused by cracks developing in the concrete core, while the longitudinal GFRP bars were still intact and carrying the applied load. In the case of column B-100-21.2, the decrease in the slope of the load-displacement curve was due to the concrete core crushing, as initiated by the small aggregate size (3 mm) used and highlighted by the failure mode, leading to a wide load-displacement curve but without enhanced peak loads. Cui and Sheikh (2010) made similar findings, concluding that using smaller aggregate size can decrease the concrete compressive strength but increase ductility. In contrast, the CSA S806 code (CSA 2012) states that more lateral spirals are needed with a small aggregate size to compensate for the loss in strength capacity. This is impractical in designing HCCs with GFRP reinforcement. On the other hand, the columns with higher f'_c evidenced lower displacement capacity at failure, despite having the same reinforcement details. To illustrate, column B-100-44.0 had a ductility factor 14.1%, 31.2%, and 33.3% lower than columns B-100-36.8, B-100-26.8, and B-100-21.2, respectively (Table 4). This finding is related to the increased brittleness of concrete with higher f'_c (Cui and Sheikh 2010; Hadhood et al. 2016; Hadi et al. 2017). As a result, the tested GFRP-reinforced HCCs with higher f'_c exhibited lower structural performance than those with lower f'_c but with the same construction details.

Table 4. Test results of Group B columns

Sample	Stiffness (kN/mm)	P_{n1} (kN)	Δ_y (mm)	P_{n2} (kN)	Δ_u (mm)	P_f (kN)	$D.F.$	f'_{cc} (MPa)	$C.E.$	$\epsilon_{c,P_{n1}}$ ($\mu\epsilon$)	$\epsilon_{b,P_{n1}}$ ($\mu\epsilon$)	$\epsilon_{b,P_{n2}}$ ($\mu\epsilon$)	$\epsilon_{s,P_{n1}}$ ($\mu\epsilon$)	$\epsilon_{s,P_{n2}}$ (μ)
B-100-21.2	121	907	8.0	849	21.1	642	2.64	38.6	2.14	—	3,300	7,550	1,200	3,050
B-100-26.8	132	1,189	9.3	1,102	23.3	1,073	2.53	50.1	2.19	2,160	2,310	8,950	1,100	8,850
B-100-36.8	169	1,570	9.5	1,424	19.5	1,309	2.05	64.7	2.07	2,010	2,150	9,500	820	11,850
B-100-44.0	196	1,880	9.6	1,644	16.9	1,481	1.76	74.8	2.00	1,600	2,180	9,140	360	2,670

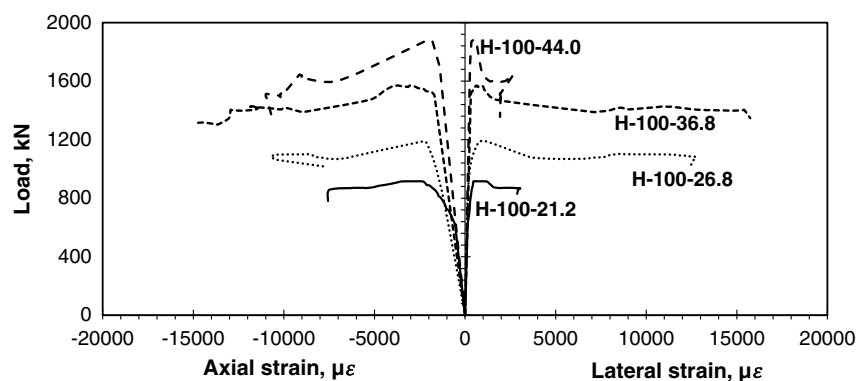


Fig. 10. Axial and lateral strain versus applied load for Group B columns.

Load-Strain Behavior

Fig. 10 shows the load and axial strain (negative sign) in the longitudinal GFRP bars and lateral strain (positive sign) in the spirals for the Group B columns. As shown, the axial strain measured in the longitudinal bars ascended linearly until P_{n1} . The maximum measured axial longitudinal bar strain at P_{n1} ($\epsilon_{b,P_{n1}}$) was 3,300 $\mu\epsilon$, 2,310 $\mu\epsilon$, 2,150 $\mu\epsilon$, and 2,180 $\mu\epsilon$ in columns B-100-21.2, B-100-26.8, B-100-36.8, and B-100-44.0, respectively. This represents 10%–16% of the ultimate tensile strain of the GFRP bars. Table 4 gives the ultimate recorded concrete strain ($\epsilon_{c,P_{n1}}$) in columns B-100-26.8 and B-100-36.8 as 3,160 $\mu\epsilon$ and 2,010 $\mu\epsilon$, respectively, which is close to the recorded axial strain in the GFRP bars, while column H-100-44.0 recorded a strain of only 1,600 $\mu\epsilon$, owing to early crack formation in the outer concrete cover. Moreover, the increase of f'_c reduced the spiral engagement at P_{n1} (Table 4), because Poisson's ratio decreases as f'_c increases, as also suggested by Simmons (1955). Generally, the strain readings ($\epsilon_{s,P_{n1}}$) were less than 5% of the ultimate tensile strain of the GFRP spirals at P_{n1} .

After the concrete-cover spalling, GFRP bars and spirals experienced an increase in strain values, suggesting the outward deformation of the column and activation of reinforcement confining pressure on the concrete core. At failure, the maximum axial compressive strain measured in the longitudinal bars was 8,050 $\mu\epsilon$, 10,690 $\mu\epsilon$, 14,700 $\mu\epsilon$, and 1,0940 $\mu\epsilon$ (38.4%, 50.9%, 70%, and 52.1% of tensile strain) in columns B-100-21.2, B-100-26.8, B-100-36.8, and B-100-44.0, respectively, as can be seen in Fig. 10. Fig. 10 also shows that the lateral strain in the spirals plateaued after P_{n1} in columns B-100-21.2, B-100-26.8, and B-100-36.8 until reaching 3,050 $\mu\epsilon$, 12,740 $\mu\epsilon$, and 15,880 $\mu\epsilon$. Although the spirals in column B-100-44.0 showed a strength enhancement, it was stopped early at 2,740 $\mu\epsilon$ because of bar rupture. Moreover, the low spiral strain recorded by column B-100-21.2 is related to the specimen's failure mode, since the unconfined concrete part was gradually smashed without effective engagement from the lateral GFRP spirals.

Volumetric Strain Behavior

The tested HCCs exhibited an increase in volumetric strain with increasing f'_c (Fig. 11). Similar to the Group A columns, a lateral strain factor of 3 gives a slope of $(1-2\nu)$. In general, a negative volumetric strain was observed due to the concrete-cover spalling. An ascending slope was then observed due to the lateral expansion of the GFRP spirals, with the slope descending again when the concrete core failed. Interestingly, column B-100-44.0 showed no negative volumetric strain, which indicates high shortening axial strain

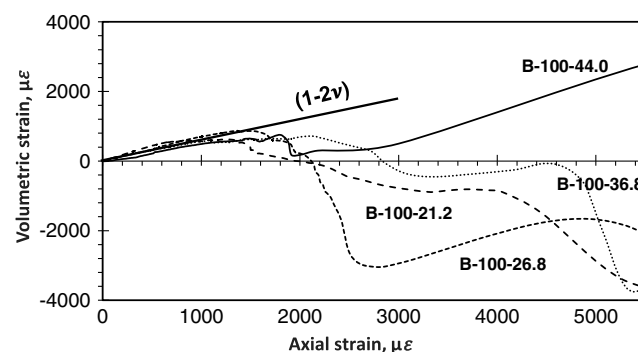


Fig. 11. Volumetric strain versus axial strain for Group B columns.

with insignificant lateral expansion. This resulted in a volume reduction phenomenon due to the high energy stored in the concrete, and the longitudinal bars ended with massive failure in those components due to the lack in lateral reinforcement. In this case, more spirals are recommended to reinforce HCCs with high f'_c , as indicated by the CSA S806 code (CSA 2012). This finding is supported by the low lateral strain in Fig. 10 caused by the low lateral expansion of the high compressive-strength concrete, which is due to the Poisson's ratio effect, as suggested by Simmons (1955).

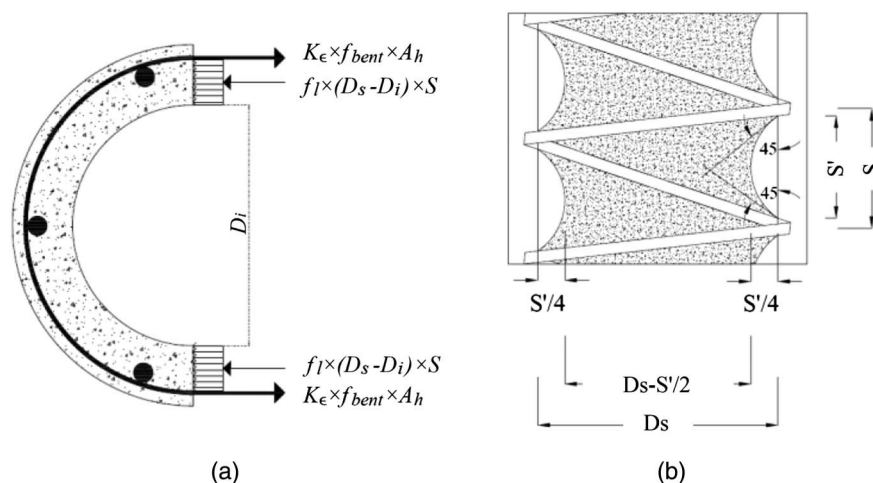
Theoretical Prediction

Design-Load Capacity

The first peak (P_{n1}) in the load-displacement curve (Figs. 4 and 9) was considered the maximum design capacity of the specimens. This peak represents the contribution of the gross concrete and the longitudinal GFRP bars in compression. It should be noted that current design standards ignore the contribution of GFRP bars (CSA 2012; ACI 2015) in compression members. The concrete contribution was calculated by multiplying f'_c and the cross-sectional area of the concrete (A_c), excluding the bar area. A reduction factor (α_2) of 0.85 for f'_c less than 50 MPa was applied, as suggested by the ACI 318 (ACI 2008) and AS3600 codes (AS 2011), representing the difference between full-scale reinforced-concrete columns and concrete cylinders in terms of strength, size, and shape. On the other hand, the load contribution of the GFRP bars was calculated as the product of the axial strain in the longitudinal GFRP bars (ϵ_{FRP}) at P_{n1} , the elastic modulus of the GFRP bars (E_{FRP}), and the nominal cross-sectional area (A_{FRP}).

Table 5. Comparison between experimental and theoretical axial-load capacity values

Column	Experimental load capacity (kN)	Theoretical load (CSA 2012; ACI 2015) (kN) (Error %)	Theoretical load in proposed model (kN) (Error %)
A-N/A-26.8	1,022	973 (5%)	1,160 (−12%)
A-150-26.8	1,108	973 (12%)	1,160 (−5%)
A-100-26.8	1,189	973 (18%)	1,160 (2%)
B-100-26.8			
A-50-26.8	1,197	973 (19%)	1,160 (3%)
B-100-21.2	907	770 (15%)	962 (−6%)
B-100-36.8	1,570	1,336 (15%)	1,513 (3%)
B-100-44.0	1,880	1,597 (15%)	1,767 (6%)
Average error	—	14%	2%

**Fig. 12.** Lateral confinement mechanism and confinement effectiveness factor: (a) lateral confinement; and (b) confinement effectiveness factor.

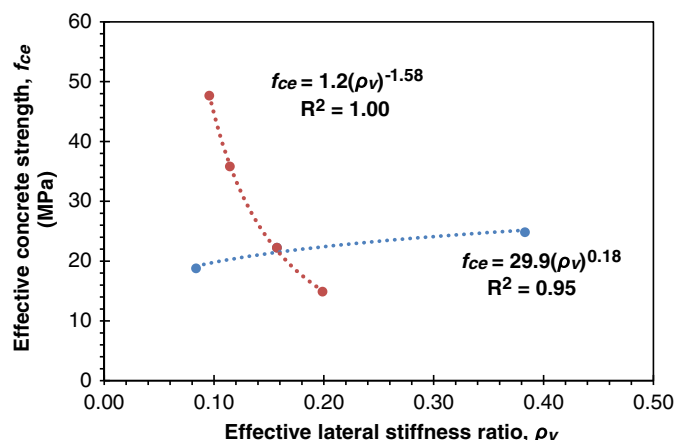
It should be mentioned that the axial load contribution of the GFRP bars at P_{n1} varied from 6.9% to 25.2%, with the higher f'_c values leading to a significant reduction in this percentage. The experimental results show that the maximum recorded axial strain of longitudinal bars at P_{n1} was 0.003, and therefore this value was used in predicting the design-load capacity (P_n), as shown in Eq. (2) and Table 5. Interestingly, this strain value is consistent with the ultimate concrete strain in compression recommended by ACI 318-14M (ACI 2014). This strain value is also similar to the findings of Park and Paulay (1975) and Sheikh and Uzumeri (1980), who observed concrete-cover spalling at a strain between 0.003 and 0.004. For comparison, the load capacity of the HCCs, neglecting the contribution of the GFRP bars, was also calculated and compared with the experimental results (Table 5)

$$P_n = \alpha_2 \times f'_c \times A_c + 0.003 \times E_{FRP} \times A_{FRP} \quad (2)$$

where P_n is the design-load capacity, α_2 is a reduction factor for concrete (0.85), A_c is the cross-sectional area of the concrete, f'_c is the concrete compressive strength, E_{FRP} is the modulus of elasticity of the GFRP bars, and A_{FRP} is the total cross-sectional area of the GFRP bars.

Second Peak Load and Failure Point

Reinforcing the HCCs laterally with GFRP spirals resulted in the columns exhibiting postloading behavior as a result of lateral confinement. The spirals laterally restricted the expansion of the concrete core and limited the buckling of the longitudinal GFRP bars,

**Fig. 13.** Influence of lateral-stiffness ratio (ρ_v) on the effective concrete strength (f_{ce}).

allowing the columns to keep resisting applied loads until reaching P_{n2} and showing the maximum confined strength. The contribution of the GFRP spirals [Fig. 12(a)] was determined by evaluating the relationship between the confining stress (f_l) [Eqs. (4) and (5) (CSA 2012)], as a function of the lateral confinement stiffness ratio (ρ_v) [Eq. (3)], and the effective concrete-core strength (f_{ce}) [Eqs. (7) and (8) and Fig. 13]. A confinement effectiveness factor (K_e) [Fig. 12(b)] was applied to account for the discontinuity in the lateral confining stress in the concrete core at the unconfined

Table 6. Comparison between the theoretical and experimental second peak load

Column	k_e	f_l (MPa)	ρ_v	f_{ce} (MPa)	P_{n2t} (kN)	P_{n2t}/P_{n2}
A-150-26.8	0.60	3.7	0.084	19.4	1,082	0.97
A-100-26.8	0.75	5.6	0.157	21.4	1,124	1.01
B-100-26.8						
A-50-26.8	0.92	11.2	0.383	25.2	1,203	0.85
B-100-21.2	0.75	5.6	0.199	15.4	999	1.18
B-100-36.8	0.75	5.6	0.115	36.6	1,440	1.01
B-100-44.0	0.75	5.6	0.096	48.7	1,691	1.03

sections between spirals [Eq. (6)]. Eq. (4) was adopted from Karim et al. (2016), who evaluated the lateral confinement of the solid GFRP-reinforced columns, and Eq. (6) from Mander et al. (1988) to reduce the lateral-stress effectiveness caused by the discontinuous lateral confinement. Both equations take into account the inner void. The ratio of the average recorded spiral strain ($\varepsilon_{s,P_{n2}}$) to the ultimate tensile strain of spirals (K_e) in Eq. (4) equals 0.39. The influence of the lateral-stiffness ratio (ρ_v) on the effective concrete strength (f_{ce}) was obtained and plotted in Fig. 13. The decreasing trend line represents the effect of spiral spacing [Eq. (7)], while the increasing trend line represents the effect of increasing concrete compressive strength [Eq. (8)]. These trends are valid for the test results of this study. The contribution of the GFRP bars at the second peak load ($\varepsilon_{s,P_{n2}}$) was measured experimentally corresponding to an average axial strain equal to 0.0095 (Tables 3 and 4). This strain value was therefore taken as the maximum strain of the confined concrete core. This axial strain value evidently is close to 0.010 and 0.008, as suggested by Zahn et al. (1990) and Hoshikuma and Priestley (2000), respectively, for the maximum observed axial strain of the confined concrete in steel-reinforced HCCs. The theoretical second peak load (P_{n2t}) can then be calculated by adding the contribution of the confined concrete core and the GFRP bars at an axial strain (ε_{FRP2}) of 0.0095 [Eq. (9)]. It was observed that the GFRP bars contributed in a range of 40%–69% from P_{n2} and were negatively affected by increasing f'_c values. The axial load contribution of the GFRP bars at P_{n2} was calculated by multiplying $\varepsilon_{s,P_{n2}}$ by A_{FRP} and E_{FRP} and then dividing the result by the corresponding P_{n2} .

Table 6 shows the comparison between the theoretical and experimental results, which are in good agreement. Nevertheless, the P_{n2t} of column H-50-26.8 corresponds to 85% of the P_{n2} due to the lower predicted axial strain of the GFRP bars compared to the experimental one. Consequently, a more comprehensive study is required to investigate the compressive behavior of GFRP bars with different unbraced lengths. On the other hand, the P_{n2t} of column H-100-21.2 corresponds to 118% of the P_{n2} due to the use of different size aggregates, which reduced the sample's overall strength

$$\rho_v = \frac{k_e f_l}{f'_c} \quad (3)$$

$$f_l = \frac{2A_h K_e f_{bent}}{S(D_s - D_i)} \quad (4)$$

$$f_{bent} = \left(0.05 \frac{r}{d_b} + 0.3\right) f_u \leq f_u \quad (5)$$

$$k_e = \frac{A_{ce}}{A_{cc}} = \frac{\frac{\pi}{4}((D_s - \frac{S'}{4})^2 - D_i^2)}{\frac{\pi}{4}(D_s^2 - D_j^2)(1 - \rho_e)} \quad (6)$$

$$f_{ce} = 4.4 \ln(\rho_v) + 31.3 \quad (7)$$

$$f_{ce} = 0.57 \rho_v^{-1.6} \quad (8)$$

$$P_{n2t} = f_{ce} A_{cc} + \varepsilon_{FRP2} A_{FRP} E_{FRP} \quad (9)$$

where D_s and D_i = concrete core diameter and the void diameter, respectively; S and S' = center-to-center distance and the clear spacing between spirals, respectively; A_{ce} = concrete-core area with the damage effect; and A_{cc} = concrete-core area excluding the longitudinal bars area.

Conclusions

This study investigated the effect of using various lateral spiral spacing and the effect of concrete compressive strength on the behavior of concentrically loaded HCCs reinforced with GFRP bars. Moreover, the applicability of the existing equations for determining the design-load capacity of GFRP-reinforced concrete members in compression was validated, and a model was proposed to describe the postloading behavior of the columns. Based on the results of this study, the following conclusions can be drawn:

- The GFRP-reinforced HCCs with closer lateral spiral spacing exhibited higher axial load capacity than those with broader spacing due to the early activation of confinement. Decreasing the spacing from 150 to 50 mm increased the capacity by 8%. Moreover, narrowing the spiral spacing led to more progressive failure of the concrete core and longitudinal bars.
- Reducing the spiral spacing from 150 and 100 mm to 50 mm increased the ductility and confined strength of the columns by 98% and 69%, respectively. This outcome was due to the increased axial strain capacity of the longitudinal bars with reduced unbraced length and a lesser extent of the unconfined concrete core between spirals.
- Using concrete with higher compressive strength increased the axial load capacity and stiffness of the columns by up to 107% and 70%, respectively, due to the concrete's higher elastic modulus. Column failure, however, changed from ductile to brittle.
- The concrete columns with higher compressive strength had lower confinement efficiency and ductility compared to the columns with lower compressive strength. Increasing the concrete compressive strength from 21.6 to 44.0 MPa decreased the confinement efficiency and ductility by 7% and 50%, respectively, due to the higher brittleness of the concrete with higher compressive strength.
- The design-load capacity of the GFRP-reinforced HCCs can be reliably predicted by considering the contribution of the concrete gross section and the longitudinal GFRP bars at 0.003 axial strain. Herein, the contribution of the longitudinal GFRP bars to load capacity ranged from 10% to 20%.
- The second peak-load capacity of HCCs reinforced with GFRP bars can be described well by considering the contribution of the longitudinal GFRP bars at an ultimate axial strain of 0.0095 and the effective area of the confined concrete core.

Data Availability Statement

All data, models, and code generated or used during the study appear in the published article.

Acknowledgments

The authors are grateful to Pultrall Canada and Inconmat V-ROD Australia for providing the GFRP bars and spirals. The assistance

of the postgraduate students and technical staff at the Centre of Future Materials (CFM) is also acknowledged. The first author is also grateful for the doctoral scholarship provided by Tafila Technical University (TTU) in Jordan.

Notation

The following symbols are used in this paper:

- A_c = concrete area in the section (without the area of the GFRP bars) ($A_g - A_{FRP}$) (mm^2);
- A_{cc} = concrete-core area (without the area of the GFRP bars) ($A_{core} - A_{FRP}$) (mm^2);
- A_{ce} = area of the concrete core, excluding the crushed concrete part due to unconfined concrete between the spirals (mm^2);
- A_{core} = effective core area denoted by the distance between spiral centers (mm^2);
- A_{FRP} = total area of the GFRP bars (mm^2);
- A_g = total cross-sectional area (mm^2);
- A_h = GFRP-spiral cross-sectional area (mm^2);
- D_i = diameter of the inner void (mm);
- D_s = diameter of spirals on-centers (mm);
- D.F. = ductility factor;
- d_b = bar diameter of the lateral reinforcement (mm);
- E_{FRP} = elastic modulus of the GFRP bars (MPa);
- f_{bent} = tensile strength of the bent GFRP bars ACI (2015) (MPa) [Eq. (5)];
- f'_c = concrete compressive strength at the day of testing the HCCs (MPa);
- f'_{cc} = confined strength of the concrete core after concrete-cover spalling (MPa);
- f_{ce} = effective concrete strength (MPa) [Eqs. (7) and (8)];
- f_{co} = unconfined concrete strength ($0.85f'_c$) (MPa);
- f_l = lateral confining stress (MPa) [Eq. (4)];
- f_u = ultimate tensile strength of the GFRP reinforcements (MPa);
- K_ϵ = the proportion of ultimate strain in the GFRP spirals before failure to their ultimate tensile strength (0.39 as an average);
- k_e = reduction factor regarding the vertical unconfined area between spirals [Eq. (6)];
- P_f = failure load (kN);
- P_n = theoretical design-load capacity (kN);
- P_{n1} = first axial peak load (kN);
- P_{n2} = experimental second axial peak load (kN);
- P_{nt2} = theoretical second axial peak load (kN);
- r = inner radius of the spiral (mm);
- S = vertical spacing of spirals on-centers (mm);
- S' = clear vertical spacing between spirals (mm);
- α_2 = effect of the concrete compressive strength factor (0.85);
- Δ_u = ultimate displacement (mm);
- Δ_y = yield displacement (mm);
- $\epsilon_{b,P_{n1}}$ = axial strain of the GFRP bars at P_{n1} ;
- $\epsilon_{b,P_{n2}}$ = axial strain of the GFRP bars at P_{n2} ;
- $\epsilon_{c,P_{n1}}$ = maximum recorded concrete strain at P_{n1} ;
- ϵ_{co} = unconfined concrete strain;
- ϵ_{FRP2} = maximum strain of the GFRP bars at P_{n2} ;
- $\epsilon_{s,P_{n1}}$ = axial strain of the GFRP spirals at P_{n1} ;
- $\epsilon_{s,P_{n2}}$ = axial strain of the GFRP spirals at P_{n2} ;
- ϵ_u = ultimate tensile strain;

ρ = reinforcement ratio with respect to the total cross-sectional area (A_g);

ρ_e = effective reinforcement ratio with respect to the effective core area; and

ρ_v = lateral-stiffness ratio [Eq. (3)].

References

- ACI (American Concrete Institute). 2008. *Building code requirements for structural concrete*. ACI 318. Farmington Hills, MI: ACI.
- ACI (American Concrete Institute). 2014. *Building code requirements for structural concrete*. ACI 318-14M. Farmington Hills, MI: ACI.
- ACI (American Concrete Institute). 2015. *Guide for the Design and construction of concrete reinforced with FRP bars*. ACI 440.1R. Farmington Hills, MI: ACI.
- AlAjarmeh, O. S., A. C. Manalo, B. Benmokrane, W. Karunasena, P. Mendis, and K. Nguyen. 2019a. "Compressive behavior of axially loaded circular hollow concrete columns reinforced with GFRP bars and spirals." *Constr. Build. Mater.* 194 (Jan): 12–23. <https://doi.org/10.1016/j.conbuildmat.2018.11.016>.
- AlAjarmeh, O. S., A. C. Manalo, B. Benmokrane, W. Karunasena, and P. Mendis. 2019b. "Axial performance of hollow concrete columns reinforced with GFRP composite bars with different reinforcement ratios." *Compos. Struct.* 213 (Apr): 153–164. <https://doi.org/10.1016/j.compstruct.2019.01.096>.
- AS (Standards Australia). 2011. *Reinforced concrete design: In accordance with AS 3600-2009*. Sydney, Australia: AS.
- ASTM. 2015a. *Standard practice for making and curing concrete test specimens in the field*. ASTM C31. West Conshohocken, PA: ASTM.
- ASTM. 2015b. *Standard test method for compressive strength of cylindrical concrete specimens*. ASTM C39 West Conshohocken, PA: ASTM.
- ASTM. 2016. *Standard test method for tensile properties of fiber reinforced polymer matrix composite bars*. ASTM D7205/D7205M-06. West Conshohocken, PA: ASTM.
- Benmokrane, B., O. Chaallal, and R. Masmoudi. 1995. "Glass fibre reinforced plastic (GFRP) rebars for concrete structures." *Constr. Build. Mater.* 9 (6): 353–364. [https://doi.org/10.1016/0950-0618\(95\)00048-8](https://doi.org/10.1016/0950-0618(95)00048-8).
- Benmokrane, B., A. Manalo, J.-C. Bouhet, K. Mohamed, and M. Robert. 2017. "Effects of diameter on the durability of glass fiber-reinforced polymer bars conditioned in alkaline solution." *J. Compos. Constr.* 21 (5): 04017040. [https://doi.org/10.1061/\(ASCE\)CC.1943-5614.0000814](https://doi.org/10.1061/(ASCE)CC.1943-5614.0000814).
- Cascardi, A., F. Micelli, and M. A. Aiello. 2016. "Unified model for hollow columns externally confined by FRP." *Eng. Struct.* 111 (Mar): 119–130. <https://doi.org/10.1016/j.engstruct.2015.12.032>.
- Cassidy, M., J. Waldie, and S. Palanisamy. 2015. "A method to estimate the cost of corrosion for Australian defence force aircraft." In *Proc., 16th Australian Int. Aerospace Congress*. Melbourne, Australia: Barton, ACT, Australia: Engineers Australia.
- CSA (Canadian Standards Association). 2012. *Design and construction of building structures with fibre-reinforced polymers*. CAN/CSA-S806. Rexdale, Canada: CSA.
- Cui, C., and S. A. Sheikh. 2010. "Experimental study of normal-and high-strength concrete confined with fiber-reinforced polymers." *J. Compos. Constr.* 14 (5): 553–561. [https://doi.org/10.1061/\(ASCE\)CC.1943-5614.0000116](https://doi.org/10.1061/(ASCE)CC.1943-5614.0000116).
- Fillmore, B., and P. Sadeghian. 2018. "Contribution of longitudinal GFRP bars in concrete cylinders under axial compression." *Can. J. Civ. Eng.* 45 (6): 458–468. <https://doi.org/10.1139/cjee-2017-0481>.
- Hadhood, A., H. M. Mohamed, and B. Benmokrane. 2016. "Experimental study of circular high-strength concrete columns reinforced with GFRP bars and spirals under concentric and eccentric loading." *J. Compos. Constr.* 21 (2): 04016078. [https://doi.org/10.1061/\(ASCE\)CC.1943-5614.0000734](https://doi.org/10.1061/(ASCE)CC.1943-5614.0000734).
- Hadi, M., and T. Le. 2014. "Behaviour of hollow core square reinforced concrete columns wrapped with CFRP with different fibre orientations." *Constr. Build. Mater.* 50 (Jan): 62–73. <https://doi.org/10.1016/j.conbuildmat.2013.08.080>.

- Hadi, M. N. S., H. A. Hasan, and M. N. Sheikh. 2017. "Experimental investigation of circular high-strength concrete columns reinforced with glass fiber-reinforced polymer bars and helices under different loading conditions." *J. Compos. Constr.* 21 (4): 04017005. [https://doi.org/10.1061/\(ASCE\)CC.1943-5614.0000784](https://doi.org/10.1061/(ASCE)CC.1943-5614.0000784).
- Hadi, M. N. S., H. Karim, and M. N. Sheikh. 2016. "Experimental investigations on circular concrete columns reinforced with GFRP bars and helices under different loading conditions." *J. Compos. Constr.* 20 (4): 04016009. [https://doi.org/10.1061/\(ASCE\)CC.1943-5614.0000670](https://doi.org/10.1061/(ASCE)CC.1943-5614.0000670).
- Hoshikuma, J.-I., and M. Priestley. 2000. *Flexural behavior of circular hollow columns with a single layer of reinforcement under seismic loading*, SSRP, 13. Oakland, CA: Univ. of California.
- Karim, H., M. N. Sheikh, and M. N. Hadi. 2016. "Axial load-axial deformation behaviour of circular concrete columns reinforced with GFRP bars and helices." *Constr. Build. Mater.* 112 (Jun): 1147–1157. <https://doi.org/10.1016/j.conbuildmat.2016.02.219>.
- Kusumawardaningsih, Y., and M. N. Hadi. 2010. "Comparative behaviour of hollow columns confined with FRP composites." *Compos. Struct.* 93 (1): 198–205. <https://doi.org/10.1016/j.compstruct.2010.05.020>.
- Lee, J.-H., J.-H. Choi, D.-K. Hwang, and I.-J. Kwahk. 2015. "Seismic performance of circular hollow RC bridge columns." *KSCE J. Civ. Eng.* 19 (5): 1456–1467. <https://doi.org/10.1007/s12205-014-1173-z>.
- Liang, X., R. Beck, and S. Sritharan. 2015. *Understanding the confined concrete behavior on the response of hollow bridge columns*. Ames, IA: Iowa State Univ.
- Lignola, G. P., F. Nardone, A. Prota, A. De Luca, and A. Nanni. 2011. "Analysis of RC hollow columns strengthened with GFRP." *J. Compos. Constr.* 15 (4): 545–556. [https://doi.org/10.1061/\(ASCE\)CC.1943-5614.0000192](https://doi.org/10.1061/(ASCE)CC.1943-5614.0000192).
- Lignola, G. P., A. Prota, G. Manfredi, and E. Cosenza. 2007. "Experimental performance of RC hollow columns confined with CFRP." *J. Compos. Constr.* 11 (1): 42–49. [https://doi.org/10.1061/\(ASCE\)1090-0268\(2007\)11:1\(42\)](https://doi.org/10.1061/(ASCE)1090-0268(2007)11:1(42)).
- Lignola, G. P., A. Prota, G. Manfredi, and E. Cosenza. 2008. "Unified theory for confinement of RC solid and hollow circular columns." *Composites Part B* 39 (7): 1151–1160. <https://doi.org/10.1016/j.compositesb.2008.03.007>.
- Manalo, A., B. Benmokrane, K.-T. Park, and D. Lutze. 2014. "Recent developments on FRP bars as internal reinforcement in concrete structures." *Concr. Aust.* 40 (2): 46–56.
- Mander, J. B., M. J. N. Priestley, and R. Park. 1988. "Theoretical stress-strain model for confined concrete." *J. Struct. Eng.* 114 (8): 1804–1826. [https://doi.org/10.1061/\(ASCE\)0733-9445\(1988\)114:8\(1804\)](https://doi.org/10.1061/(ASCE)0733-9445(1988)114:8(1804)).
- Maranan, G., A. Manalo, B. Benmokrane, W. Karunasena, and P. Mendis. 2016. "Behavior of concentrically loaded geopolymer-concrete circular columns reinforced longitudinally and transversely with GFRP bars." *Eng. Struct.* 117 (Jun): 422–436. <https://doi.org/10.1016/j.engstruct.2016.03.036>.
- Martinez, S., A. H. Nilson, and S. Floyd. 1984. *Spirally-reinforced high-strength concrete columns*. NASA STI/Recon Technical Rep. No: 84. Naples, FL: American Concrete Institute.
- Mirmiran, A., and M. Shahawy. 1997. "Behavior of concrete columns confined by fiber composites." *J. Struct. Eng.* 123 (5): 583–590. [https://doi.org/10.1061/\(ASCE\)0733-9445\(1997\)123:5\(583\)](https://doi.org/10.1061/(ASCE)0733-9445(1997)123:5(583)).
- Mo, Y., D. Wong, and K. Maekawa. 2003. "Seismic performance of hollow bridge columns." *Struct. J.* 100 (3): 337–348.
- Mohamed, H. M., M. Z. Afifi, and B. Benmokrane. 2014. "Performance evaluation of concrete columns reinforced longitudinally with FRP bars and confined with FRP hoops and spirals under axial load." *J. Bridge Eng.* 19 (7): 04014020. [https://doi.org/10.1061/\(ASCE\)BE.1943-5592.0000590](https://doi.org/10.1061/(ASCE)BE.1943-5592.0000590).
- Neville, A. M. 1995. *Properties of concrete*. London: Longman.
- Pantelides, C. P., M. E. Gibbons, and L. D. Reaveley. 2013. "Axial load behavior of concrete columns confined with GFRP spirals." *J. Compos. Constr.* 17 (3): 305–313. [https://doi.org/10.1061/\(ASCE\)CC.1943-5614.0000357](https://doi.org/10.1061/(ASCE)CC.1943-5614.0000357).
- Park, R., and T. Paulay. 1975. *Reinforced concrete structures*. Hoboken, NJ: Wiley.
- Saatcioglu, M., and S. R. Razvi. 1992. "Strength and ductility of confined concrete." *J. Struct. Eng.* 118 (6): 1590–1607. [https://doi.org/10.1061/\(ASCE\)0733-9445\(1992\)118:6\(1590\)](https://doi.org/10.1061/(ASCE)0733-9445(1992)118:6(1590)).
- Sheikh, S. A., and S. M. Uzumeri. 1980. "Strength and ductility of tied concrete columns." *J. Struct. Div.* 106 (ST5): 1079.
- Simmons, J. 1955. "Poisson's ratio of concrete: A comparison of dynamic and static measurements." *Mag. Concr. Res.* 7 (20): 61–68. <https://doi.org/10.1680/mac.1955.7.20.61>.
- Tannous, F. E. 1997. "Durability of non-metallic reinforcing bars and prestressing tendons." Ph.D. thesis, Dept. of Civil Engineering and Engineering Mechanics, Univ. of Arizona.
- Tobbi, H., A. S. Farghaly, and B. Benmokrane. 2014. "Behavior of concentrically loaded fiber-reinforced polymer reinforced concrete columns with varying reinforcement types and ratios." *ACI Struct. J.* 111 (2): 375.
- Verma, S. K., S. S. Bhadauria, and S. Akhtar. 2014. "Monitoring corrosion of steel bars in reinforced concrete structures." *Sci. World J.* 2014: 1–9. <https://doi.org/10.1155/2014/957904>.
- Zahn, F., R. Park, and M. Priestley. 1990. "Flexural strength and ductility of circular hollow reinforced concrete columns without confinement on inside face." *Struct. J.* 87 (2): 156–166.

Chapter 6

A new design-oriented model for GFRP reinforced hollow concrete columns

The experimental results presented in Chapters 3 to 5 showed that the (*i/o*) ratio, ρ , ρ_v , and f'_c affect the overall behavior of GFRP-reinforced HCCs. It was found that the existing equations for steel-reinforced HCCs and GFRP-reinforced SCCs are not applicable to GFRP-reinforced HCCs. Therefore, a new design-oriented model considering the investigated design parameters in the previous chapters was developed to accurately and reliably describe the behavior of the GFRP-reinforced HCCs. The experimental results of the fourteen large-scale GFRP-reinforced HCCs with different influential design parameters were systematically analysed. The new design-oriented model was based on the plasticity theory of concrete and considering the critical design parameters to accurately describe the compressive load–strain behavior of GFRP-reinforced HCCs under monotonic and concentric loading. In the development of the design-oriented model for GFRP-reinforced HCCs, the Hognestad model was adopted to represent the concrete behavior from the unloading case until the peak and then the Wu or Muguruma model was adopted until failure, but with a modified value for the inflection strain. In both cases, the linear elastic behavior up to failure of the GFRP bars was considered. Moreover, the load–strain behavior of GFRP-reinforced HCCs was based on the total cross-sectional area of the column throughout its loading.

The proposed design-oriented model can accurately predict the concentric compressive behavior of the hollow concrete columns reinforced with GFRP bars and spirals. This model is preferable for design and analysis engineers because of the ease in identifying critical stress and strain points as well as quantifying material contribution (concrete and GFRP bars) separately. From these results, it was concluded that GFRP bars can be effective longitudinal and lateral reinforcements to HCCs. Moreover, the behavior of this new construction system can be reliably predicted considering the effect of the influential design parameters. The significant outcomes of this research are highlighted in the next chapter. In addition, recommendations for future research were suggested to reveal the many benefits of this new construction system.

MS No. S-2019-069.R1

A New Design-Oriented Model of Glass Fiber-Reinforced Polymer-Reinforced Hollow Concrete Columns

by O. S. AlAjarmeh, A. C. Manalo, B. Benmokrane, W. Karunasena, W. Ferdous, and P. Mendis

Hollow concrete columns (HCCs) reinforced with glass fiber-reinforced polymer (GFRP) bars and spirals are considered an effective design solution for bridge piers, electric poles, and ground piles because they use less material and maximize the strength-to-weight ratio. HCC behavior is affected by critical design parameters such as inner-to-outer diameter ratio, reinforcement and volumetric ratios, and concrete compressive strength. This paper proposes a new design-oriented model based on the plasticity theory of concrete and considering the critical design parameters to accurately describe the compressive load-strain behavior of GFRP-reinforced HCCs under monotonic and concentric loading. The validity of the proposed model was evaluated against experimental test results for 14 full-scale hollow concrete columns reinforced with GFRP bars and spirals. The results demonstrated that the proposed design-oriented model was accurate and yielded a very good agreement with the axial compressive load behavior of GFRP-reinforced hollow concrete columns.

Keywords: concrete modelling; confinement; design-oriented; glass fiber-reinforced polymer (GFRP) bars; glass fiber-reinforced polymer (GFRP) spirals.

INTRODUCTION

Hollow concrete columns (HCCs) are economical and practical for the construction of bridge piers, ground piles, and electric poles because they use fewer materials and significantly reduce weight, leading to a structure with a high strength-to-weight ratio and minimal cost.¹⁻⁴ The design and behavior of steel-reinforced HCCs are affected by several parameters such as inner-to-outer diameter ratio (i/o),²⁻⁵ longitudinal-reinforcement ratio (ρ),^{4,6} volumetric ratio (ρ_v),^{1,3,4,7} and concrete compressive strength (f'_c).⁸ Zahn et al.⁵ observed that increasing the i/o from 0.53 to 0.73 in steel-reinforced HCCs results in a brittle failure of the concrete core and approximately 50% reduction in deformation capacity. Lee et al.⁴ reported that increasing the reinforcement ratio from 1.17 to 2.00% in HCCs increased the cyclic load capacity and allowed the specimens to withstand 48% higher lateral loads at the same level of lateral displacement. At the same time, the column ductility decreased by 20% due to the wide and severe crushing of the inner concrete wall. They also observed that reducing the lateral-reinforcement spacing from 80 to 40 mm (3.1 to 1.6 in.) increased ductility by 20% and minimized damage in the inner concrete core. On the other hand, Mo et al.⁸ found that high-strength concrete (f'_c of 50 MPa [7.3 ksi]) instead of normal-strength concrete (30 MPa [4.4 ksi]) provided stiffer compression resistance in HCC, but with up to a 50% reduction in ductility due to faster crack propagation and easier

concrete splitting. These studies showed that these important parameters mainly affect the capacity and deformation of such columns. Relaxing the design of these parameters leads this structure to be more vulnerable to steel corrosion problem due to their high exposed surface area owing to the void existence, which may lead to a dysfunctional structural element. Li et al.⁹ and Pantelides et al.¹⁰ found that steel corrosion reduced the axial-load capacity of the concrete columns they tested and negated lateral confinement by damaging the lateral steel reinforcement.

Recently, glass fiber-reinforced polymer (GFRP) bars have been utilized as alternative internal reinforcements in concrete structures to prevent corrosion problems when using steel bars in locations exposed to severe environmental conditions.¹¹

Some authors, on the other hand, have reported that GFRP bars are more compatible with concrete than steel due to their similar moduli of elasticity.^{11,12} Several studies have been conducted to understand the behavior of this construction system and to evaluate the effects of different design parameters. Afifi et al.¹³ highlighted that increasing the reinforcement ratio from 1.13 to 3.38% by tripling the bar number from four to 12 (15.9 mm [0.63 in.] GFRP bars) changed the column failure behavior from brittle to ductile and increased the ductility and confinement efficiency by 117% and 30%, respectively. Moreover, Hadi et al.¹⁴ observed a 33% enhancement in ductility with GFRP-reinforced columns when the spacing between spirals was reduced from 60 to 30 mm (2.4 to 1.2 in.). These studies motivated investigation of the behavior of HCCs incorporating GFRP reinforcement, as pioneered by AlAjarmeh et al.^{15,16} This study was the first to explore the potential of GFRP bars and spirals as reinforcing materials for hollow concrete columns to develop high structural efficiency and a corrosion-resistant construction system. The results of their investigation revealed that increasing the i/o in HCCs reinforced with GFRP bars and spirals changed the failure behavior from brittle to a progressive failure.¹⁵ Moreover, the enhancement of the confined strength and deformation capacity of the HCCs was proportional to the increase in i/o . They found, on the other hand, that the increase in ρ increases the axial load capacity and, furthermore, longitudinal reinforcements proved the major contribution in lateral confinement.¹⁶ In addition, a compre-

ACI Structural Journal, V. 117, No. 2, March 2020.

MS No. S-2019-069.R1, doi: 10.14359/51720204, received February 26, 2019, and reviewed under Institute publication policies. Copyright © 2020, American Concrete Institute. All rights reserved, including the making of copies unless permission is obtained from the copyright proprietors. Pertinent discussion including author's closure, if any, will be published ten months from this journal's date if the discussion is received within four months of the paper's print publication.

hensive experimental program has been conducted by testing large-scale GFRP-reinforced concrete (RC) columns to investigate the effects of other critical design parameters such as ρ_v and f'_c on the compressive behavior of HCCs, and this work is now under review.

Many researchers have developed analytical models to accurately describe the behavior of new structural systems under compression loads. These models were also developed to minimize the number of experiments to determine the effects of the critical design parameters.¹⁷ With respect to the existing analytical models for concrete columns, the lateral-confinement level (either full or partial) is considered the first step in determining the confined strength and the overall stress-strain behavior. The main limitation of the existing models lies with the difficulty in quantifying the amount and level of lateral confinement correlating to the corresponding confined strength. This is especially true when the lateral confinement is in the form of non-uniform stress, such as provided by lateral reinforcement.^{18,19} The existing analytical models separate the contribution of design parameters such as the confinement status (active or passive),²⁰ full or partial confinement,¹⁸ amount of lateral confinement,^{21,22} longitudinal reinforcement,^{17,21} section geometry,²³ and concrete compressive strength.²⁴ Currently, GFRP-reinforced solid concrete columns are modeled using the available experimental data or with the existing analytical models for steel-reinforced solid concrete columns that have been modified.^{17,18,21} These models are limited to predicting behavior up to the maximum load,^{2,7} with some models related to fully wrapped hollow unreinforced concrete sections.²⁵⁻²⁸

RESEARCH SIGNIFICANCE

There are no analytical models for hollow reinforced concrete columns with partial lateral confinement, especially incorporating GFRP reinforcement, or that describe their post-peak behavior. In this study, the modeling procedures for GFRP-reinforced solid concrete columns were modified and examined along the lines of Mander's confinement model,²³ which is based on the concrete-plasticity theory to predict the confined strength of GFRP-reinforced HCCs. A new analytical model is proposed, which considers the constituent materials' contribution to accurately describe the overall compressive behavior of GFRP-reinforced HCCs, including the strength capacity and the expected failure mode under advanced loading stages, leading to a precise and safe design. The design recommendations herein may support the work of the technical committees engaged in the development of standards and design provisions for GFRP-RC columns.

SUMMARY OF EXPERIMENTAL PROGRAM AND RESULTS

A total of 14 circular hollow concrete columns reinforced with GFRP bars and spirals with specimen dimensions of 250 mm (9.8 in.) in diameter by 1 m (39.4 in.) in height were prepared and tested under concentric compression loading until failure. The columns have different configurations, shown in Fig. 1, to investigate four influential design parameters: inner-to-outer diameter ratio (i/o), longitudinal-re-

inforcement ratio (ρ), volumetric ratio (ρ_v), and concrete compressive strength (f'_c). The height-to-diameter ratio was similar to that considered by Maranan et al.²⁹ and Karim et al.,³⁰ which confirmed eliminating global buckling in the columns with the specified ratio. The use of short column specimens was considered to clearly investigate the effects of the design parameters on pure axial compressive behavior and without the effects of buckling. These columns were all reinforced with high-modulus sand-coated GFRP bars (Grade III)³¹ with physical and mechanical properties determined in accordance with CSA S806³¹ and ACI 440.1R-15³² and as reported by Benmokrane et al.³³ as the reinforcement was taken from the same production lot. The mechanical properties of the reinforcements were determined based on the nominal area of the reinforcement, as recommended by CSA S806.³¹ An overview of specimen properties and the material characteristics can be found in Fig. 1 and Table 1, respectively. All the columns had concrete with 10 mm aggregate size except for column H90-6#5-100-21, which had 3 mm aggregate size, as the low-strength concrete used to manufacture this sample was a premix concrete. All columns were tested under monotonic compressive load using a 2000 kN hydraulic cylinder with a loading rate of 1.5 mm/min. A total of six strain gauges were mounted on each column to measure the strain in the longitudinal reinforcement (two gauges 3 mm in length), spiral reinforcement (two gauges 3 mm in length), and outer surface of the concrete (two gauges 20 mm in length). Steel clamps with a 50 mm in width and 10 mm in thickness were attached to the top and bottom of the columns to avoid the stress concentration and the premature failure. The applied load was measured with a 2000 kN load cell and the axial deformation was recorded using a string pot. All data were recorded with a data logger. Figure 2 shows the test setup and instrumentation for the hollow concrete columns. Detailed information and experimental results can be found in AlAjarmeh et al.^{15,16}

Table 2 shows the test results for the 14 concrete columns under concentric compression loading until failure, which was used to evaluate the effect of the aforementioned parameters (i/o , ρ , ρ_v , and f'_c). This table includes the gross section area (A_g), total core area (A_{core}), peak loads (P_1 and P_2), stress at the peak point (f_{ci}), concrete stress alone at the peak point (f_i), number of longitudinal bars (#bar), bar diameter (d_b), and spacing between spirals (S). The first peak load (P_1) is the maximum load resistance by the entire cross-sectional area when the concrete cover started to spall, while the second peak load (P_2) is the maximum load resistance provided by the concrete core. The parameter f_{ci} was calculated by dividing P_1 by A_g , while f_i was calculated by subtracting the contribution of the GFRP bars from P_1 at the peak point and then dividing the magnitude by A_g . The contribution of the GFRP bars was calculated by multiplying the total area of the bars, their elastic modulus, and the strain at the peak point (ϵ_i). The parameter ρ was calculated from the nominal area of the longitudinal reinforcement by dividing by A_g , while ρ_v was calculated from the volume of one spiral round divided by the concrete-core volume within one spiral pitch, because the diameter of the inner concrete core was measured from the center of the spirals and the height was

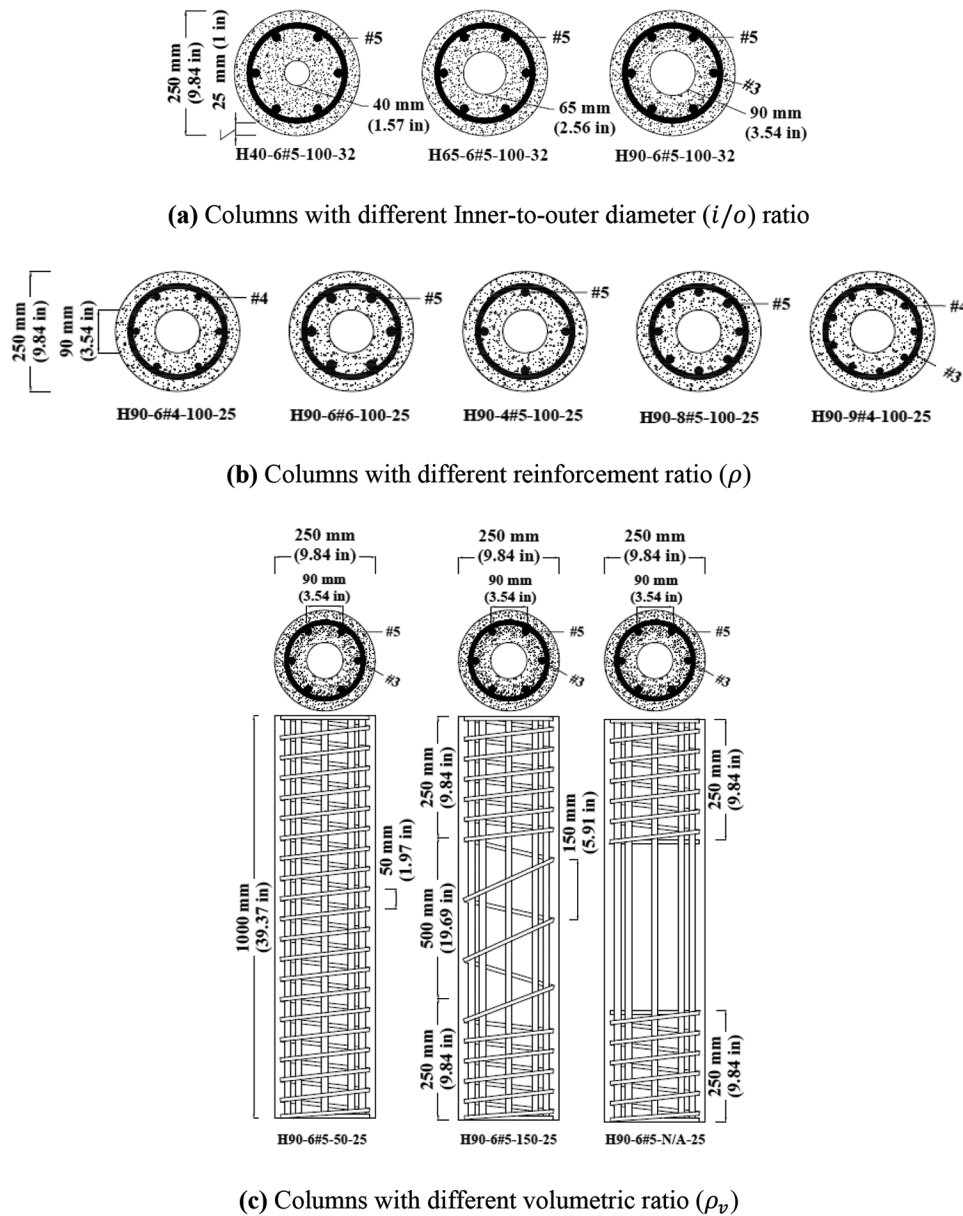


Fig. 1—Details of tested GFRP-reinforced hollow concrete columns.

Table 1—Physical and mechanical properties of GFRP reinforcement materials³³

Properties		Test method	Tested samples	Values			
				No. 6	No. 5	No. 4	No. 3
Physical	Nominal bar diameter, mm (in.)	CSA S806 ³¹	9	19.1 (0.79)	15.9 (0.63)	12.7 (0.50)	9.5 (0.37)
	Nominal bar area, mm ² (in. ²)	CSA S806 ³¹	9	286.5 (0.44)	198.5 (0.31)	126.6 (0.20)	70.8 (0.11)
	Cross-sectional area, mm ² (in. ²)	CSA S806 ³¹	9	317.3 (0.49)	224.4 (0.35)	145.0 (0.22)	83.8 (0.13)
Mechanical	Tensile strength f_u , MPa (ksi)	ASTM D7205 ³²	6	1270 (184.2) [31.4 (4.5)]*	1237 (179.4) [33.3 (4.8)]*	1281 (185.8) [35.3 (5.1)]*	1315 (190.7) [31.1 (4.5)]*
	Elastic modulus E_{GFRP} , GPa (ksi)	ASTM D7205 ³²	6	60.5 (877.5) [0.5 (73)]*	60.5 (877.5) [1.3 (189)]*	61.3 (889.1) [0.4 (58)]*	62.5 (906.5) [0.4 (58)]*
	Ultimate tensile strain ϵ_u , %	ASTM D7205 ³²	6	2.1 (0.1)*	2.1 (0.1)*	2.1 (0.1)*	2.3 (0.1)*

*Standard division

the spiral pitch. The identification of all the samples starts with the hollow section diameter followed by the number and diameter of the longitudinal reinforcement. Then comes

the spacing between lateral reinforcement, followed by the concrete compressive strength. All of these properties are separated by a hyphen.

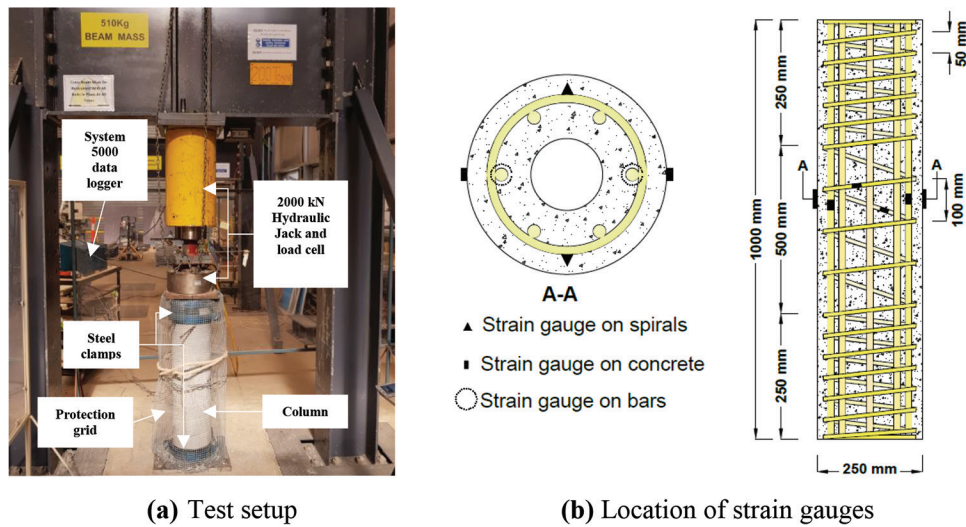


Fig. 2—Test setup and instrumentation for GFRP-reinforced hollow concrete columns.

Table 2—Specimen details, test matrix, and experimental test results

Column	A_g , mm ² (in. ²)	A_{core} , mm ² (in. ²)	P_1 , kN (kip)	P_2 , kN (kip)	f_{ci} , MPa (psi)	ϵ_i , με	f_b , MPa (psi)	f'_c , MPa (psi)	No. of bars	d_b , mm (in.)	S , mm (in.)	i/o	ρ , %	ρ_v , %
H40-6#5-100-32	47,807 (74.1)	27,083 (42.0)	1408 (317)	1295 (291)	29.4 (4264)	2780	25.2 (3655)	31.8 (4612)	6	15.9 (0.63)	100 (3.94)	0.16	2.49	1.56
H65-6#5-100-32	45,746 (70.9)	25,022 (38.8)	1559 (350)	1458 (328)	34.1 (4946)	2550	29.9 (4337)	31.8 (4612)	6	15.9 (0.63)	100 (3.94)	0.26	2.60	1.69
H90-6#5-100-32	42,704 (66.2)	21,980 (34.1)	1411 (317)	1226 (276)	33.0 (4786)	2320	28.8 (4177)	31.8 (4612)	6	15.9 (0.63)	100 (3.94)	0.36	2.79	1.92
H90-6#4-100-25	42,704 (66.2)	21,980 (34.1)	1035 (233)	985 (221)	24.2 (3510)	2850	21.9 (3176)	25.0 (3626)	6	12.7 (0.50)	100 (3.94)	0.36	1.78	1.92
H90-6#6-100-25	42,704 (66.2)	21,980 (34.1)	1140 (256)	1248 (281)	26.7 (3873)	2100	19.6 (2843)	25.0 (3626)	6	19.1 (0.75)	100 (3.94)	0.36	4.00	1.92
H90-4#5-100-25	42,704 (66.2)	21,980 (34.1)	983 (221)	876 (197)	23.0 (3336)	3200	19.0 (2756)	25.0 (3626)	4	15.9 (0.63)	100 (3.94)	0.36	1.86	1.92
H90-8#5-100-25	42,704 (66.2)	21,980 (34.1)	1268 (285)	1406 (316)	29.7 (4308)	2219	22.8 (3307)	25.0 (3626)	8	15.9 (0.63)	100 (3.94)	0.36	3.72	1.92
H90-9#4-100-25	42,704 (66.2)	21,980 (34.1)	1035 (233)	1204 (271)	24.2 (3510)	2500	19.8 (2872)	25.0 (3626)	9	12.7 (0.50)	100 (3.94)	0.36	2.67	1.92
H90-6#5-N/A-25	42,704 (66.2)	21,980 (34.1)	1022 (230)	—	23.9 (3466)	1658	22.3 (3234)	25.0 (3626)	6	15.9 (0.63)	—	0.36	2.79	0.00
H90-6#5-150-25	42,704 (66.2)	21,980 (34.1)	1108 (249)	1110 (250)	25.9 (3756)	2350	20.5 (2973)	25.0 (3626)	6	15.9 (0.63)	150 (5.91)	0.36	2.79	1.28
H90-6#5-50-25	42,704 (66.2)	21,980 (34.1)	1197 (269)	1434 (322)	28.0 (4061)	3800	21.9 (3176)	25.0 (3626)	6	15.9 (0.63)	50 (1.97)	0.36	2.79	3.84
H90-6#5-100-21	42,704 (66.2)	21,980 (34.1)	907 (204)	849 (191)	21.2 (3075)	2350	18.0 (2611)	21.2 (3075)	6	15.9 (0.63)	100 (3.94)	0.36	2.79	2.14
H90-6#5-100-37	42,704 (66.2)	21,980 (34.1)	1570 (353)	1424 (320)	36.9 (5352)	2203	33.8 (4902)	36.8 (5337)	6	15.9 (0.63)	100 (3.94)	0.36	2.79	2.14
H90-6#5-100-44	42,704 (66.2)	21,980 (34.1)	1880 (423)	1644 (370)	43.8 (6353)	2181	41.6 (6034)	44.0 (6382)	6	15.9 (0.63)	100 (3.94)	0.36	2.79	2.14

EXISTING DESIGN MODELS FOR GFRP-REINFORCED CONCRETE COLUMNS

A number of empirical and analytical design-oriented models have been developed to express the stress-strain behavior of confined concrete solid columns.^{34,35} Abd El Fattah³⁴ highlighted that most of these models involve the

use of steel as a lateral confining material with some models developed for fiber-reinforced polymer (FRP)-confining systems. In addition, Ozbakkaloglu et al.³⁵ reviewed 88 models of fully wrapped or encased columns using FRP as a confining material. In contrast, very few studies have been done on partially confined columns using FRP materials^{18,19}

or GFRP reinforcement in solid concrete columns.^{17,21,36} Abd El Fattah³⁴ suggested that describing the behavior of GFRP-reinforced solid concrete columns as a form of partially confined columns with a non-uniform lateral stress can be investigated by modifying the confinement models for lateral steel reinforcement.

Existing design models: background

Based on using steel reinforcement as confining materials, Abd El Fattah³⁴ identified three general approaches for modeling confined concrete: the empirical approach based on experimental test results,^{37,38} the physical engineering approach based on the confining stress provided by the lateral reinforcement,^{23,39} and a combination of the first two approaches but assuming that no lateral steel yields and using compatibility conditions.^{40,41} According to their review, 50, 10, and 40% of the proposed models were based on the first, second, and third approaches, respectively. On the other hand, Lokuge et al.²⁴ classified the stress-strain models into three main categories as Sargin-based,⁴² Kent and Park-based,⁴³ and Popovics-based⁴⁴ to represent the stress-strain curves of concrete columns. These models were constructed with respect to some selected parameters in the stress-strain curves, then calibrated with the experimental test results. Recently, GFRP-reinforced solid concrete columns have been modeled based on the above approaches and categories. For example, Afifi et al.¹⁷ deployed empirical and physical engineering approaches separately by using the modified Mander model²³ as a confinement model, then they used Muguruma⁴⁵ model for stress-strain behavior, which is considered as a mixture of Popovics-based⁴⁴ and Kent and Park-based⁴³ models. On the other hand, Hales et al.²¹ and Sankholkar⁴⁶ used the physical-engineering approach with the modified Mander model²³ for confinement due to the lack of experimental data on GFRP-reinforced concrete columns and then applied the Popovics-based model⁴⁴ for stress-strain behavior. It can be concluded that the Mander model²³ for confinement is commonly used because it has been verified with large-scale columns.²⁴ Therefore, the next section describes the development of the prediction model for GFRP-reinforced HCCs according to the modified Mander model.²³

Modified Mander model for confinement

The confinement model proposed by Mander et al.²³ was derived from the Willam-Warnke five-parameter failure criterion⁴⁷ based on the plasticity theory of concrete. The Mander model²³ formula was modified to reflect the accurate behavior of columns reinforced with GFRP bars. This modification refers to the confinement criteria provided by GFRP reinforcement, which differs from steel given the diversity in material behavior.^{17,21} Tobbi et al.³⁶ reported that the Mander model overestimated the confined strength of GFRP-reinforced concrete columns by 30%. Therefore, the modification was adopted by changing the constants b_0 , b_1 , and b_2 in the plasticity equation—Eq. (1) to (4)—which are responsible for showing the relation between mean normal and mean shear stresses, as follows

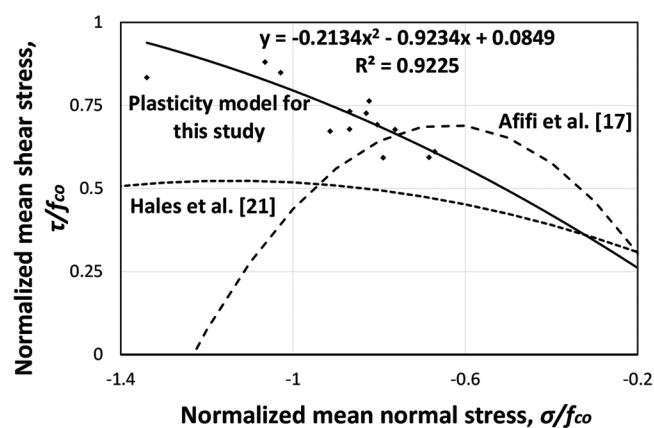


Fig. 3—Plasticity model of experimental results of this study compared with other plasticity models.

$$\frac{\tau_{octa}}{f_{co}} = b_0 + b_1 \frac{\sigma_{octa}}{f_{co}} + b_2 \left(\frac{\sigma_{octa}}{f_{co}} \right)^2 \quad (1)$$

$$\tau_{octa} = \frac{1}{3} \left[(\sigma_x - \sigma_y)^2 + (\sigma_y - \sigma_z)^2 + (\sigma_z - \sigma_x)^2 \right]^{0.5} \quad (2)$$

$$\sigma_{octa} = \frac{\sigma_x + \sigma_y + \sigma_z}{3} \quad (3)$$

$$f'_{cc} = f_{co} \left(\frac{3(\sqrt{2} + b_1)}{2b_2} + \sqrt{\left(\frac{3(\sqrt{2} + b_1)}{2b_2} \right)^2 - \frac{9b_0}{b_2} - \frac{9\sqrt{2}}{b_2} \frac{f'_l}{f_{co}} - 2 \frac{f'_l}{f_{co}}} \right) \quad (4)$$

where $\sigma_x = f'_{cc}$; $\sigma_y = \sigma_z = f'_l$; f'_{cc} is the confined strength of the column; and f'_l is the effective lateral confinement suggested by Mander ($f'_l = k_e \times f_l$, where k_e is Eq. (16) and f_l is Eq. (14)). For the experimental results, f'_{cc} was calculated from the second peak axial load (P_2) after the yield point or after concrete-cover spalling divided by the total core area (A_{core}) (as shown in Table 2), which is the area denoted by the diameter between spiral centers. Using the parabolic regression of the experimental mean shear stress (τ_{octa}) versus mean normal stress (σ_{octa}) curve provided the constant values of $b_2 = -0.2134$, $b_1 = -0.9234$, and $b_0 = 0.0849$, as shown in Fig. 3. Accordingly, these constants in Eq. (4) yield a new expression for the confinement-strength equation for GFRP-reinforced HCCs, as shown in Eq. (5). In this equation, the predicted confined strength values ($f'_{cc,n1}$) calculated from the new confinement-strength model (Eq. (5)), in addition to the $f'_{cc,n2}$ and $f'_{cc,n3}$ values, were derived from the confined strength models proposed by Afifi et al.¹⁷ and Hales et al.²¹ This approach, however, resulted in a large discrepancy between the predicted values and the experimental results, as tabulated in Table 3.

$$f'_{cc,n1} = f_{co} \left(-3.45 + \sqrt{15.48 + 59.61 \frac{f'_l}{f_{co}} - 2 \frac{f'_l}{f_{co}}} \right) \quad (5)$$

Table 3—Comparison between experimental and theoretical values for f_{cc}'

Column	Experimental results	Eq. (5)		Afifi et al. ¹⁷		Hales et al. ²¹	
	f_{cc}' , MPa (psi)	$f_{cc,n1}'$, MPa (psi)	Variation, %	$f_{cc,n2}'$, MPa (psi)	Variation, %	$f_{cc,n3}'$, MPa (psi)	Variation, %
H40-6#5-100-32	47.8 (6933)	31.3 (4540)	34.5	43.4 (6295)	9.2	36.1 (5236)	24.5
H65-6#5-100-32	58.3 (8456)	34.0 (4931)	41.7	44.1 (6396)	24.4	37.4 (5424)	35.8
H90-6#5-100-32	59.6 (8644)	37.4 (5424)	37.2	44.8 (6498)	24.8	39.2 (5685)	34.2
H90-6#4-100-25	44.8 (6498)	33.1 (4801)	26.1	35.8 (5192)	20.1	32.7 (4743)	27.0
H90-6#6-100-25	56.8 (8238)	34.0 (4931)	40.1	35.8 (5192)	37.0	33.2 (4815)	41.5
H90-4#5-100-25	39.8 (5773)	33.2 (4815)	16.6	35.8 (5192)	10.1	32.8 (4757)	17.6
H90-8#5-100-25	64.0 (9282)	33.9 (4917)	47.0	35.8 (5192)	44.1	33.1 (4801)	48.3
H90-9#4-100-25	54.8 (7948)	33.5 (4859)	38.9	35.8 (5192)	34.7	32.9 (4772)	40.0
H90-6#5-150-25	50.5 (7324)	24.9 (3611)	50.7	36.2 (5250)	28.3	29.6 (4293)	41.4
H90-6#5-50-25	65.2 (9456)	56.0 (8122)	14.1	37.9 (5497)	41.9	45.7 (6628)	29.9
H90-6#5-100-21	38.6 (5598)	31.1 (4511)	19.4	30.6 (4438)	20.7	29.3 (4250)	24.1
H90-6#5-100-37	64.7 (9384)	40.1 (5816)	38.0	51.2 (7426)	20.9	43.7 (6338)	32.5
H90-6#5-100-44	74.8 (10,849)	43.7 (6338)	41.6	60.2 (8731)	19.5	50.1 (7266)	33.0

Comparison with experimental results

Referring to Table 3, the large discrepancy between the experimental and theoretical confined strengths for the GFRP-reinforced HCCs can be explained as follows. First, the analytical models were developed from limited experimental test results for GFRP-reinforced solid concrete columns with partial confinement.^{17,21,30} Secondly, the compressive behavior of HCCs differs from that of solid concrete columns due to the biaxial stress distribution within the confined concrete wall of the hollow sections.^{28,48} Accordingly, the final failure of the GFRP-reinforced HCCs was failure of longitudinal GFRP bars and concrete with no failure in the lateral GFRP spirals. In contrast, the failure mode of GFRP-reinforced solid columns are normally due to the failure in lateral reinforcement followed by a total collapse of the sample.^{13,29,49} Thirdly, the effect of steel longitudinal bars on the behavior of HCCs has not been investigated before, which can merely be attributed to the unchanged strength contribution after yielding. However, the behavior is entirely different with GFRP bars due to their linear elastic response until failure.^{14,29,49} Karim et al.³⁰ suggested considering effect of GFRP bars separately from the concrete due to the apparent strength enhancement resulting from adding GFRP bars, particularly those with a high modulus of elasticity. This finding is evidenced by the typical behavior of steel-reinforced concrete columns that showed only one peak strength at the yield point, followed by a descending or softening stress-strain response until failure.³⁴ Fourthly, the difficulty of identifying the confined-strength point and the corresponding strain value for reinforced-concrete columns due to the irregular post-peak softening responses from the concrete cover spalling. Different perspectives are available to specify this peak, especially with different ascending and descending post-loading behaviors. For example, Afifi et al.¹⁷ took the point to be just after the peak strength with respect to the concrete core area, while Karim et al.³⁰ took the second peak load in the post-loading stage for the same condition. A new view of

capturing the entire stress-strain behavior of GFRP-reinforced HCCs by considering the constitutive behavior of the concrete and GFRP bars is presented next.

DEVELOPMENT OF A NEW DESIGN-ORIENTED MODEL FOR GFRP-REINFORCED HCCS

Theory and assumptions

A new model is proposed to accurately describe the compressive behavior of GFRP-reinforced HCCs considering the behavior of the GFRP bars and the partially confined concrete. The first assumption in this model is the linear-elastic theory of the GFRP bars^{49,50} to predict the stress contribution of the longitudinal reinforcement until failure. Stress contribution of GFRP bars (f_{GFRP}) was calculated using the normalized area of the bars with respect to the total area of the column (Eq. (6))

$$\overline{f_{GFRP}} = f_{GFRP} \frac{A_{GFRP}}{A_g} = (\epsilon_{GFRP} E_{GFRP}) \frac{A_{GFRP}}{A_g} = (\epsilon_{GFRP} E_{GFRP}) \rho_{GFRP} \quad (6)$$

The second important assumption is the perfect bond between the concrete and GFRP reinforcement, as is evident from the experimental results: no splitting between the bars and concrete was observed, and the failure occurred in the concrete and bars at the same time. This assumption takes on that, at any point in the plane, the axial strain in concrete and GFRP bars is the same,³⁰ which made it possible to subtract the stress contribution of GFRP bars from the total behavior of the column and to establish the stress-strain behavior of the concrete alone, as shown in Fig. 4. After subtracting the contribution of GFRP bars, the concrete of all the columns showed softening after reaching the peak concrete strength (f_i) and up until final failure. However, f_i expresses the concrete stress with respect to the total area of the section including the reinforcement area. Therefore, f_i needs normalizing to be $\overline{f_i}$ for accurately measuring the concrete stress as

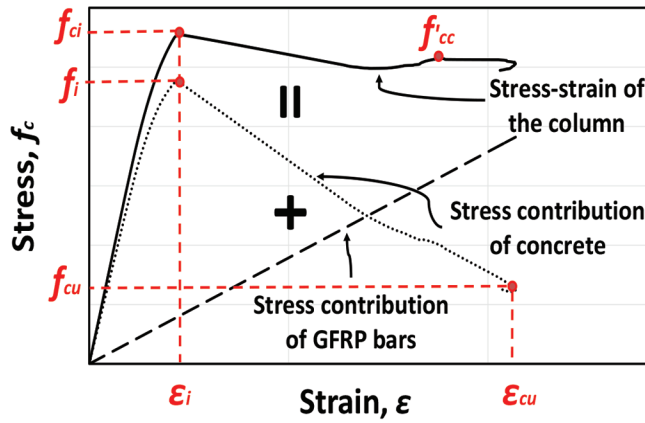


Fig. 4—Stress-strain contribution of column's components.

shown in Eq. (7). On the other hand, the overall behavior ended with rupturing in the longitudinal bars and crushing in concrete core, with no failure of the lateral reinforcement. Therefore, the last strain point of the column is related to the maximum compressive strain capacity of the GFRP bars. Figure 4 depicts the concrete as having a semi-parabolic ascending behavior followed by an almost linear descending behavior. This indicates that the Kent and Park-based model⁴³ best represents the concrete stress-strain curves.

$$\bar{f}_i = f_i \times \frac{A_g}{A_{gc}} = f_i \times \frac{A_g}{A_g \times (1-\rho)} = \frac{f_i}{(1-\rho)} \quad (7)$$

Model development

The compressive behavior of the GFRP-reinforced hollow concrete columns, as shown in Fig. 4, can be defined with two main points: the point of the peak strength of the concrete (f_i) and the corresponding inflection strain (ϵ_i), and the point of the concrete strength at failure (f_{cu}) and its corresponding maximum strain (ϵ_{cu}). The description of these critical points and their identification in developing the prediction model are discussed in the following subsections.

Peak strength of concrete (f_i)—The most noticeable observation for all the columns was the peak stress of concrete (f_i) after subtracting the stress contribution of the longitudinal GFRP bars. According to f_i values tabulated in Table 2, the normalized values of f_i (\bar{f}_i) are close to that of the unconfined concrete strength ($f_{co} = 0.85f'_c$), where f_{co} represents the concrete stress limit before any cracks on the column outer surface. Showing this finding, the average of \bar{f}_i with respect to f_{co} was plotted against the effective lateral-confinement stiffness (f''/f_{co} , which will be discussed later), as given in Fig. 5. It can be concluded that the different levels of lateral confinement considered in this study did not significantly affect the strength enhancement of f_{co} . Therefore, it was assumed that the concrete peak strength for the tested columns is equals to f_{co} . This finding is consistent with Roy and Sozen,⁵¹ Kent and Park,⁴³ Lam and Teng,²² and Wu et al.,⁵² as a result of the passive confinement for the partially confined columns as opposed to the fully confined systems. The lateral confinement, however, had a noticeable effect on the inflection-strain point (ϵ_i) of \bar{f}_i compared to the strain (ϵ_{co}) related to f_{co} . This is also consistent with the findings of the

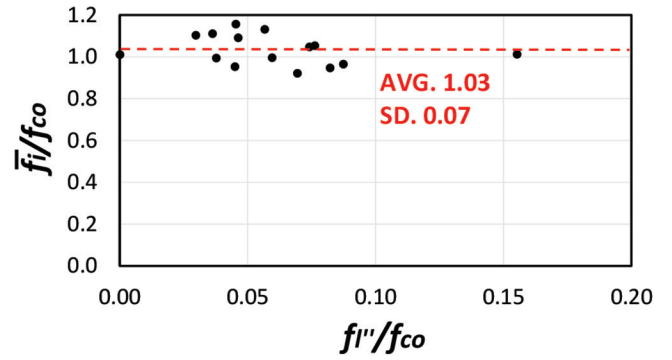


Fig. 5—Effect of effective lateral confinement stiffness on normalized \bar{f}_i over f_{co} .

researchers cited previously. The strain ϵ_{co} can be calculated with Tasdemir et al.'s equation [$\epsilon_{co} = (-0.067f_{co}^2 + 29.9f_{co} + 1053)10^{-6}$],⁵³ which deals with different levels of concrete compressive strength.

Inflection strain (ϵ_i)—The inflection strain (ϵ_i) is taken as the level of concrete strain when spalling of the concrete cover occurs in reinforced concrete, which is different from the typical crushing strain of plain concrete (ϵ_{co}). Therefore, all the variables (i/o , ρ , ρ_v , f'_c) in the HCC's design matrix were considered to determine their effect on shifting ϵ_{co} to ϵ_i . Figure 6 shows that the strain enhancement of ϵ_{co} resulting from changing these parameters created four main factors (α_1 , α_2 , α_3 , and α_4), which can be identified by the strain enhancement factor $(\epsilon_i - \epsilon_{co})/\epsilon_{co}$, as given in Eq. (8) to (11). These various factors were derived from the relationship of the concrete inflection strain and unconfined strain to that of the column design parameters. Equation (12) is used to predict ϵ_i by considering the individual effects of the reinforcement ratio (α_1), concrete compressive strength (α_2), volumetric ratio (α_3), and the inner-to-outer diameter ratio (α_4) to the strain of the unconfined concrete ϵ_{co} . Figure 7 shows that Eq. (12) can accurately predict the values of $(\epsilon_i/\epsilon_{co})$ to within $\pm 15\%$. Figure 6(b) references the compressive-strength levels based on the lowest concrete compressive strength of 21.2 MPa

$$\alpha_1 = 1.73 \times \rho^{1.36} \quad (8)$$

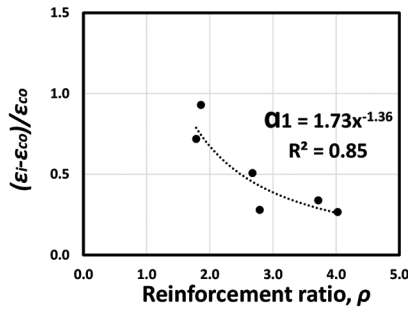
$$\alpha_2 = -0.42 \times \left(\frac{f'_c}{21.2} \right) + 0.91 \quad (9)$$

$$\alpha_3 = 0.1 \times (\rho_v)^2 + 0.15 \times (\rho_v) + 0.01 \quad (10)$$

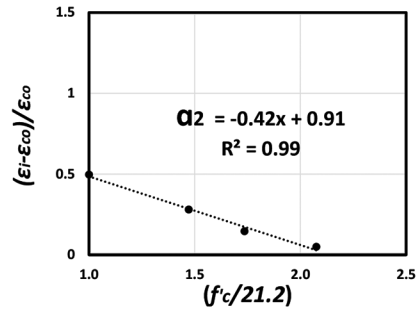
$$\alpha_4 = -1.27 \times (i/o) + 0.74 \quad (11)$$

$$\epsilon_i = \epsilon_{co} + 3(\alpha_1 \alpha_2 \alpha_3 \alpha_4)(\epsilon_{co})^4 \times 10^{15} \quad (12)$$

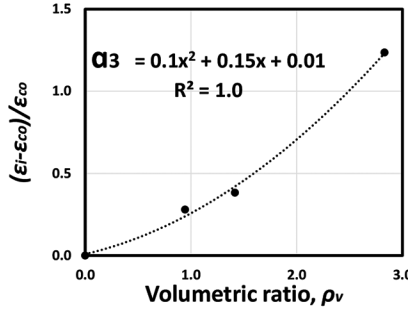
Ultimate strain (ϵ_{cu})—The final failure of the HCCs occurred simultaneously in the longitudinal bars and concrete core. The crushing strain of the GFRP bars was therefore used as the basis for identifying the ultimate strain ϵ_{cu} . Some studies have determined the compressive strength of high-elastic-modulus GFRP bars ($E_{GFRP} = 60$ to 66 GPa [870 to 957 ksi]) to be approximately 50 to 67% of their ulti-



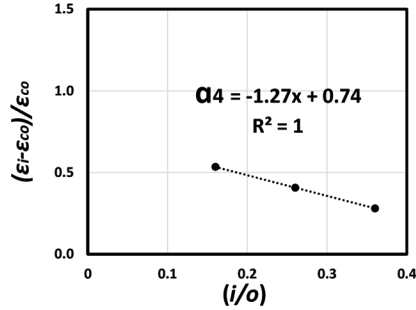
(a) Effect of reinforcement ratio, ρ



(b) Effect of concrete compressive strength, f'_c



(c) Effect of volumetric ratio, ρ_v



(d) Effect of inner-to-outer diameter (i/o) ratio

Fig. 6—Four main factors affecting inflection strain ε_i .

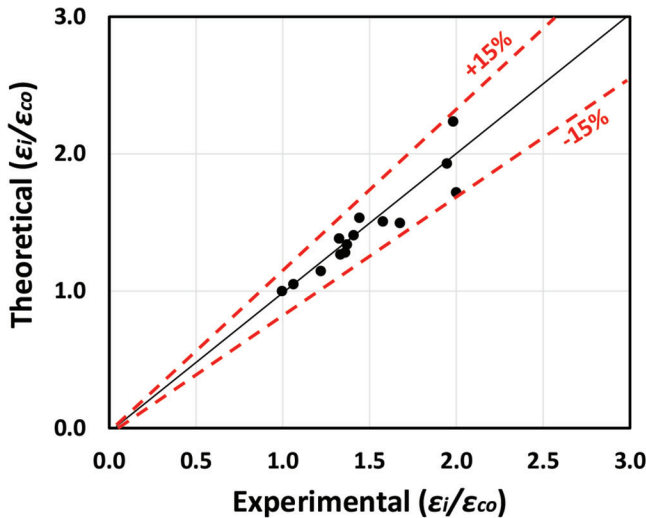


Fig. 7—Comparison between experimental and theoretical normalized inflection strain point $\varepsilon_i/\varepsilon_{co}$.

mate tensile strength.^{29,49,50,54} These studies also indicated that the GFRP bars behave differently depending on whether they were embedded in concrete or tested alone. Therefore, in another study conducted by the authors,¹⁶ the GFRP-bar crushing strain (ε_{cr}) was modeled using a very representative empirical equation based on ρ and the ratio of the total core area to bar area A_{core}/A_{GFRP} , as presented in Eq. (13). As a result, the ultimate-strain point (ε_{cu}) was found to be equal to the GFRP-bar crushing strain (ε_{cr}).

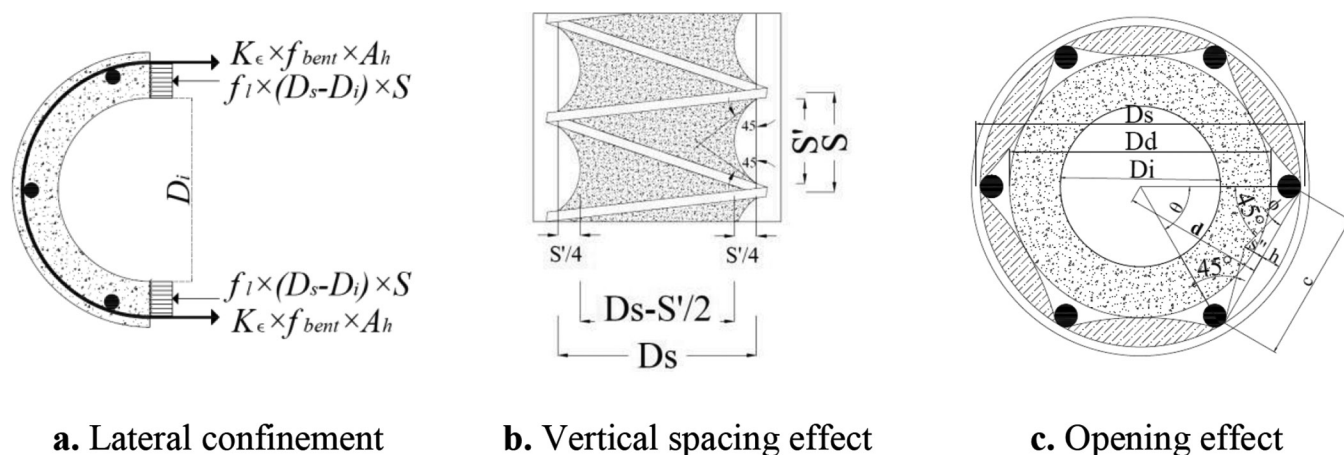
$$\varepsilon_{cu} = \varepsilon_{cr} = \frac{12.73 \times \rho \times \frac{A_{core}}{A_{GFRP}}}{E_{GFRP}} \quad (13)$$

It is important to mention that the ε_{cr} values reported in Table 4 for columns H90-6#5-100-21 and H90-6#5-50-25 were overestimated and underestimated, respectively. This was due to the first column failing prematurely owing to the use of a small aggregate size that may have initiated many microcracks in the concrete core, which reduced the strength and led to easier concrete crushing. On the other hand, the latter specimen recorded a strain 22% greater than the theoretical value due to the 50 mm (1.97 in.) spacing between bars. A comprehensive testing program needs to be conducted to determine the crushing strain of GFRP bars with small slenderness ratios.

Strength at ultimate strain (f_{cu})—Table 2 shows a discrepancy in f_{cu} values due to differences in effective lateral-confinement stiffness (f_l''/f_{co}), which can account for the descending slope between f_{co} and f_{cu} . The effective lateral confining stress (f_l'') (Eq. (20)) was calculated initially by determining the confining stress provided by the lateral reinforcement (Eq. (14)^{15,16} and (15)³²) (Fig. 8(a)). Reduction factors related to the partial lateral confinement (k_e) were considered: the spacing between longitudinal bars (k_o) and the flexural moment of inertia of the bars with respect to the section's total moment of inertia (k_d). k_e is a common factor first suggested by Sheikh and Uzumeri³⁹ to represent the effect of using discrete lateral reinforcement (Eq. (16)) (Fig. 8(b)). In contrast, k_o is a factor suggested by the authors¹⁶ to refer to the opening between longitudinal bars according to the same criteria of k_e . This factor accounts for the considerable contribution of lateral confinement measured in the longitudinal bars,⁵⁵ which prevented the lateral expansion of the concrete core (Eq. (17) and (18)) (Fig. 8(c)). k_d is a factor related to the contribution of the load carried by GFRP bars at the last point in a stress-strain curve.¹⁶ In fact, the presence of GFRP longitudinal bars has

Table 4—Comparison between experimental values and theoretical results using proposed model

Column	f_{cis} MPa (psi)			$\mu\epsilon_i$			$\mu\epsilon_{co}$	f_{cus} MPa (psi)			$\mu\epsilon_{cu}$		
	Exp.	Theo.	(% Dif.)	Exp.	Theo.	(% Dif.)		Exp.	Theo.	(% Dif.)	Exp.	Theo.	(% Dif.)
H40-6#5-100-32	29.4 (4264)	30.9 (4482)	−5	2780	2611	6	1811	12.8 (1856)	12.0 (1740)	6	10,972	12,019	−9
H65-6#5-100-32	34.1 (4946)	31.0 (4496)	9	2550	2549	0	1811	13.9 (2016)	12.9 (1871)	7	11,109	11,605	−4
H90-6#5-100-32	33.0 (4786)	31.6 (4583)	4	2320	2462	−6	1811	14.1 (2045)	13.9 (2016)	1	10,620	10,920	−3
H90-6#4-100-25	24.2 (3510)	24.8 (3597)	−2	2850	3313	−15	1658	12.8 (1865)	12.2 (1769)	5	10,845	10,689	1
H90-6#6-100-25	26.7 (3873)	26.6 (3858)	0	2100	2207	−5	1658	11.2 (1624)	11.4 (1653)	−2	10,850	10,849	0
H90-4#5-100-25	23.0 (3336)	24.8 (3597)	−8	3200	3224	−1	1658	11.9 (1726)	11.9 (1726)	0	11,201	10,920	3
H90-8#5-100-25	29.7 (4308)	26.8 (3887)	10	2219	2269	−2	1658	10.8 (1566)	12.3 (1784)	−9	11,210	10,920	3
H90-9#4-100-25	24.2 (3510)	25.4 (3684)	−5	2500	2613	−5	1658	12.4 (1798)	12.6 (1827)	−1	10,740	10,689	0
H90-6#5-N/A-25	23.9 (3466)	24.1 (3495)	−1	1658	1649	1	1658	—	—	—	4287	—	—
H90-6#5-150-25	25.9 (3756)	25.0 (3626)	3	2350	2250	4	1658	9.6 (1392)	11.1 (1610)	−9	10,592	10,920	−3
H90-6#5-50-25	28.0 (4061)	28.4 (4119)	−1	3800	3366	11	1658	15.5 (2248)	16.0 (2320)	−3	13,284	10,920	22
H90-6#5-100-21	21.2 (3075)	22.4 (3249)	−6	2350	2628	−12	1570	4.9 (711)	10.8 (1566)	−120	8301	10,920	−24
H90-6#5-100-37	36.9 (5352)	35.2 (5105)	5	2203	2343	−6	1923	16.4 (2379)	15.3 (2219)	6	12,756	10,920	15
H90-6#5-100-44	43.8 (6353)	41.1 (5961)	6	2181	2204	−1	2078	18.3 (2654)	16.7 (2422)	9	10,714	10,920	−2


Fig. 8—Lateral confinement mechanism and confinement efficiency factors.

a significant effect on the compressive behavior of concrete columns. For example, Karim et al.³⁰ noticed that using ρ of 2.4% for GFRP longitudinal bars increased the axial load capacity by 50%. Moreover, Hadi et al.¹⁴ estimated that the load contribution of GFRP bars in circular concrete columns was one-half that of steel bars due to the former's linear elastic behavior. Therefore, the increased axial load capacity of concrete columns reinforced with GFRP bars, especially

in the post-loading stage after the yield point, means that the bars can affect lateral confinement. This is because the post-loading behavior depends on the strength of the constituent materials, the lateral resistance of the lateral reinforcement, and the resistance provided by the longitudinal bars. The presence of longitudinal bars with stiffness and dilation ratios different from that of the concrete mitigates the full confining engagement by the lateral reinforcement. There-

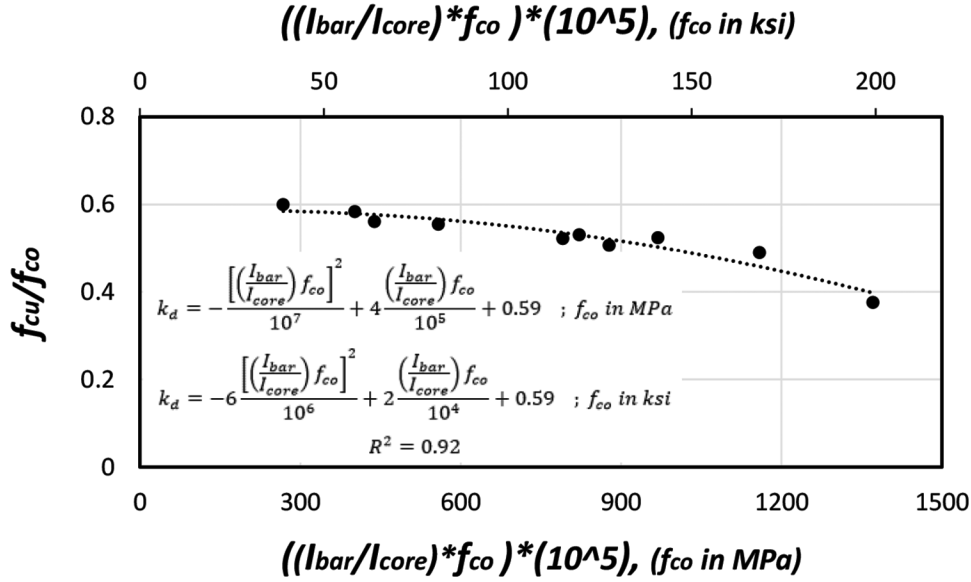


Fig. 9—Effect of longitudinal reinforcement (k_d) in post-loading stage.

fore, k_d as a reduction factor for the lateral confinement extracted from the GFRP spirals has been proposed. To evaluate this effect, columns with the same volumetric ratio (ρ_v)—including those with different f'_c —were evaluated by plotting the effect of the normalized moment of inertia of the bars (I_{bar}) to that of the concrete core section (I_{core}) versus the normalized f_{cu} with respect to f_{co} , as shown in Fig. 9 and Eq. (19a) and (19b), respectively. Considering the influential factors (k_e , k_o , and k_d) for partial lateral confinement, the effective lateral confining stress can be calculated with Eq. (20). In Eq. (20), the maximum between k_e and k_o needs to be considered because the higher value will prevent the degradation of the confined concrete core, thus allowing the concrete core to reach maximum confined resistance. The resulting lateral confinement is then reduced by a k_d factor as the linear elastic longitudinal GFRP bars are still acting with the concrete to resist the axial load until failure.

$$f_l = \frac{2A_h K_\epsilon f_{bent}}{S(D_s - D_i)} \quad (14)$$

$$f_{bent} = \left(0.05 \frac{r}{d_s} + 0.3\right) f_u \leq f_u \quad (15)$$

$$k_e = \frac{A_{ce}}{A_{cc}} = \frac{\frac{\pi}{4} \left(\left(D_s - \frac{s'}{4} \right)^2 - D_i^2 \right)}{\frac{\pi}{4} (D_s^2 - D_i^2) (1 - \rho_e)} \quad (16)$$

$$k_o = \frac{A_d}{A_{cc}} = \frac{x D_s^2 - D_i^2}{(D_s^2 - D_i^2) (1 - \rho_e)} \quad (17)$$

$$x = \left(\frac{1}{2} + \frac{\cos\left(\frac{\theta}{2}\right)}{2} - \left(\frac{\sin\left(\frac{\theta}{2}\right) \tan\left(45 - \frac{\theta}{2}\right)}{4} \right) \right)^2 \quad (18)$$

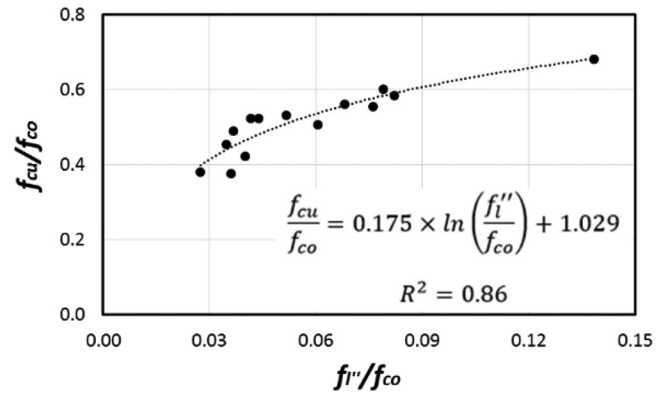


Fig. 10—Normalized concrete strength versus lateral confinement stiffness.

$$k_d = -\left[\left(\frac{I_{bars}}{I_{core}} \right) f_{co} \right]^2 / 10^7 + 4 \left(\frac{I_{bars}}{I_{core}} \right) f_{co} / 10^5 + 0.59; f_{co} \text{ in MPa} \quad (19a)$$

$$k_d = -6 \left[\left(\frac{I_{bars}}{I_{core}} \right) f_{co} \right]^2 / 10^6 + 2 \left(\frac{I_{bars}}{I_{core}} \right) f_{co} / 10^4 + 0.59; f_{co} \text{ in ksi} \quad (19b)$$

$$f_l'' = \text{Max}(k_e, k_o) \times k_d \times f_l \quad (20)$$

The effect of the effective lateral confinement stiffness (f_l''/f_{co}) on the confined strength of concrete at the last point can be seen in Eq. (21) and Fig. 10. Consequently, Table 4 shows a comparison between the experimental and analytical results for the main two points in x and y axes that resulted in a good agreement.

$$\frac{f_{cu}}{f_{co}} = 0.175 \times \ln\left(\frac{f_l''}{f_{co}}\right) + 1.029 \quad (21)$$

Table 5—Confined strength values (f_{cc}) and load contribution of concrete

f_{ci} , MPa (psi)	$\mu\epsilon_i$	f_{co} , MPa (psi)	f_{cc} , MPa (psi)	f_{cc}/f_{co}	$f_{co} \times A_{gc}$, kN (kip)	$f_{cc} \times A_{cc}$, kN (kip)
29.4 (4264)	2780	26.5 (3844)	42.9 (6222)	1.62	1236 (278)	1110 (250)
34.1 (4946)	2550	26.5 (3844)	52.4 (7600)	1.97	1182 (266)	1248 (281)
33.0 (4786)	2320	26.5 (3844)	52.8 (7658)	1.99	1101 (248)	1099 (247)
24.2 (3510)	2850	21.3 (3089)	39.9 (5787)	1.88	891 (200)	847 (190)
26.7 (3873)	2100	21.3 (3089)	36.2 (5250)	1.70	871 (196)	733 (165)
23.0 (3336)	3200	21.3 (3089)	37.0 (5366)	1.74	891 (200)	785 (176)
29.7 (4308)	2219	21.3 (3089)	43.0 (6237)	2.03	874 (196)	878 (197)
24.2 (3510)	2500	21.3 (3089)	36.5 (5294)	1.72	883 (199)	760 (171)
23.9 (3466)	1658	22.8 (3307)	—	—	—	—
25.9 (3756)	2350	22.8 (3307)	39.4 (5714)	1.73	946 (213)	820 (184)
28.0 (4061)	3800	22.8 (3307)	40.9 (5932)	1.79	946 (213)	850 (191)
21.2 (3075)	2350	18.0 (2611)	30.6 (4438)	1.70	748 (168)	635 (143)
36.9 (5352)	2203	31.3 (4511)	60.2 (8731)	1.92	1299 (292)	1252 (281)
43.8 (6353)	2181	37.4 (5424)	73.2 (10,617)	1.96	1553 (349)	1523 (342)

Effect of concrete-cover spalling

Reaching the concrete f_{co} causes a spalling in the concrete cover. At this point, high stress is concentrated at the core by the lateral confinement provided by the GFRP spirals. The effect of concrete cover spalling or the confined stress in the core in the behavior of HCC can be accounted by considering the stresses (unconfined and confined) with respect to their corresponding area, as suggested by Pantelides et al.¹⁰ and Hales et al.²¹ and by complying Eq. (22). Hereby, confined stress (f_{cc}) can be calculated by Eq. (23). The strain of 0.003 is recommended by ACI 318,⁵⁶ although, if ϵ_i is greater, it shall be used instead of 0.003. The value of f_{cc} at this level of strain is considered to be maximum for confined concrete strength due to the increase in GFRP-bar contribution and the softening behavior of the concrete. Applying Eq. (22) for all tested columns resulted in the second part of the equation to be more dominant as shown in the tabulated results in Table 5. This means that the total area of concrete is more realistic to be taken into account instead of the core concrete area

$$f_{cc} \times A_{cc} \geq f_{co} \times A_{gc} \quad (22)$$

$$f_{cc} = \left(f_{ci} - \frac{\epsilon_{cc} E_{GFRP} A_{GFRP}}{A_g} \right) \left(\frac{A_{gc}}{A_{cc}} \right) \quad (23)$$

where ϵ_{cc} is the greater of 0.003 or ϵ_i .

Development of stress-strain (f_c versus ϵ_c) relationship

Modeling the stress-strain relationship (f_c versus ϵ_c) is important in analyzing and designing concrete columns as well as in assessing their strength and deformability. First, the analysis requires that the f_c versus ϵ_c behavior of each material in the column and their combined effects be identified. Then mathematical formulae must be generalized and developed to describe the entire f_c versus ϵ_c relationship. In

this study, the model was simplified to express the compressive behavior of the nonhomogeneous columns with GFRP reinforcement. The relationship accounted for the main influential factors (f_{ci} , ϵ_i , ϵ_{cu} , and f_{cu}) which are a function of number and diameter of longitudinal reinforcement, ratio of inner-to-outer diameter, spacing between transverse reinforcement, and concrete compressive strength, respectively. As seen in Fig. 4, the experimental f_c versus ϵ_c of concrete included two segments—that is, the ascending (0 to ϵ_i) and descending (ϵ_i to ϵ_{cu}) segments of concrete behavior. In addition, an ascending linear elastic line representing the behavior of GFRP bars started from the beginning up until failure. The summation of these concrete and GFRP responses is the total compressive behavior of the GFRP-reinforced hollow concrete columns.

Ascending segment of concrete behavior—There are many empirical models that can describe the ascending confined and unconfined concrete behavior.^{22,57,58} Hognestad's ascending parabolic equation⁵⁹ is one of the most widely used models, as in the model based on Kent and Park.⁴³ This parabola is commonly used to describe the ascending part of the stress-strain curve of unconfined concrete based on BS 8110⁶⁰ and Eurocode 8.⁶¹ It has also been adopted for FRP-confined concrete.^{52,62} Therefore, referring to the procedures mentioned earlier (Fig. 4) and observations (Fig. 5), Hognestad's equation was adopted to develop the model in this study (Eq. (24a)) but adopting ϵ_{ci} (calculated using Eq. (12)) as a strain value at the peak strength of the column instead of a fixed value of $\epsilon_{co} = 0.002$, as suggested by Hognestad,⁵⁹ and the stress contribution of the GFRP bars to concrete was considered based on linear elastic theory as the additional term (f_{GFRP}) in Eq. (24a)

$$f_c = f_{co} \left[\left(\frac{2\epsilon_c}{\epsilon_i} \right) - \left(\frac{\epsilon_c}{\epsilon_i} \right)^2 \right] + \overline{f_{GFRP}} \quad \text{if } 0 \leq \epsilon_c \leq \epsilon_i \quad (24a)$$

Descending segment of concrete behavior—Simplifying the stress-strain behavior of each component by subtracting the

stress contribution of the GFRP bars from the total stress-strain behavior of the column clearly highlighted the softening behavior of the concrete after f_{co} (Fig. 4). All the columns exhibited an almost descending linear line with a negative slope from f_{co} until f_{cu} . This behavior is reflected by a descending linear line (Eq. (24b)) between the points (ϵ_i, f_{co}) and (ϵ_{cu}, f_{cu}) in the idealized stress-strain curve in Fig. 6, where the values of ϵ_i and f_{cu} are identified in Eq. (14) and (21). The softening behavior commonly occurs with steel-reinforced,³⁴ GFRP-reinforced,¹⁷ and FRP-confined⁶³ concrete columns with low lateral confinement. This reducing of the linear post-peak response was implemented by Wu et al.⁵² and Muguruma⁴⁵ for rectangular plain-concrete columns with full concrete confinement. The continuous stress contribution of the GFRP bars (f_{GFRP}) was added until bar failure strain ($\epsilon_{cu} = \epsilon_{cr}$).

$$f_c = \left[f_{co} + \left(\frac{(f_{cu} - f_{co})(\epsilon_c - \epsilon_i)}{(\epsilon_{cu} - \epsilon_i)} \right) \right] + \overline{f_{GFRP}} \quad \text{if } \epsilon_i < \epsilon_c \leq \epsilon_{cu} \quad (24b)$$

VALIDITY OF PROPOSED DESIGN-ORIENTED MODEL

The good agreement between theoretical and experimental (load-strain) test results shown in Fig. 11 validates that the proposed model can reliably represent the axial compressive-load behavior of the tested GFRP-reinforced hollow concrete columns. The theoretical load-strain behavior in this figure was calculated by multiplying the stress value (f_c) from Eq. (24a) and (24b) by the total cross-sectional area of the hollow column (A_g). The small variation between the predicted and experimental results for column H90-6#5-100-21 (Fig. 11(l), which shows a descending line from the theoretical prediction) was due to the effect of aggregate size (maximum aggregate size was 3 mm instead of 10 mm for others) as was also discussed by Cui and Sheikh.⁶⁴ This behavior was not considered in this study; additional work should investigate the aggregate-size effect on the post-loading behavior. Moreover, it is important to mention that column H90-6#5-N/A-25 in Fig. 11(i) (without lateral confinement)—representing an unconfined concrete column—used the Hognestad model⁵⁹ without any modification.

CONCLUSIONS

This study proposed a new design-oriented model to accurately describe the behavior of circular hollow concrete columns reinforced with GFRP bars and spirals under concentric compressive loading. This model incorporates four influential design parameters: inner-to-outer diameter ratio (i/o), longitudinal-reinforcement ratio (ρ), lateral-reinforcement ratio (ρ_v), and concrete compressive strength (f'_c). Based on the results of the study, the following conclusions have been drawn:

1. The behavior of the hollow concrete columns was strongly affected by the inner-to-outer diameter ratio (i/o), longitudinal reinforcement ratio (ρ), volumetric ratio (ρ_v), and concrete compressive strength (f'_c). More ductile failure due to the increase in the biaxial-stress effect can be observed

by increasing the i/o , while increased f'_c increased column brittleness. On the other hand, increasing ρ and ρ_v increased both the strength and deformation capacity of the HCCs due to the increased stiffness and confinement.

2. The existing concrete plasticity model (originally developed for solid columns) proposed by Mander was not applicable for the GFRP-reinforced hollow concrete columns due to the inner void and the presence of linear-elastic longitudinal reinforcement, which contributed to the concrete's confined strength.

3. The overall behavior of the GFRP-reinforced HCCs was a combination of the axial-stress contribution of the GFRP bars and the softening behavior of concrete once the peak strength had been reached.

4. The maximum capacity of the GFRP-reinforced HCCs was defined by the unconfined concrete strength and the total column gross area. The corresponding strain value at peak strength depends significantly on the inner-to-outer diameter ratio, longitudinal reinforcement ratio, volumetric ratio, and concrete compressive strength.

5. The softening behavior of concrete up to the failure of the hollow concrete columns was caused by the partial confinement of concrete core provided by the lateral reinforcements and the contribution of the longitudinal bars. The ultimate strain at failure was governed by the crushing strain of the GFRP bars.

6. The behavior of the GFRP-reinforced HCCs can be reliably described by modeling the concrete's behavior until the peak using the Hognestad model and then Wu or Muguruma's concept of descending linear behavior to represent the softening of the reinforced concrete until failure. The constitutive variables (inflection point, confined strength, and ultimate strain) in these models were modified based on the experimental results from large-scale hollow concrete columns reinforced with GFRP bars. For analysis and design purposes, the load-strain behavior of GFRP-reinforced HCCs should be based on the total cross-sectional area of the column throughout its loading history.

7. The proposed design-oriented model can accurately predict the concentric compressive behavior of the hollow concrete columns reinforced with GFRP bars and spirals. This model is more preferable for design and analysis engineers due to ease in identifying critical stress and strain points as well as quantifying material contribution (concrete and GFRP bars) separately.

Additional research, however, is recommended to further calibrate the model to include other ranges of concrete compressive strength and other types of FRP bars. Moreover, the behavior of hollow concrete columns with larger cross-sectional areas and higher slenderness ratios should be investigated. This information will be useful to develop a unified design model for hollow concrete columns reinforced with FRP bars.

AUTHOR BIOS

Omar S. AlAjarmeh is a PhD Candidate at the School of Civil Engineering and Surveying in the University of Southern Queensland (USQ), Springfield Central, Australia. He received his BS from Tafila Technical University, Tafifah, Jordan, and his MEng from the University of Jordan, Amman, Jordan.

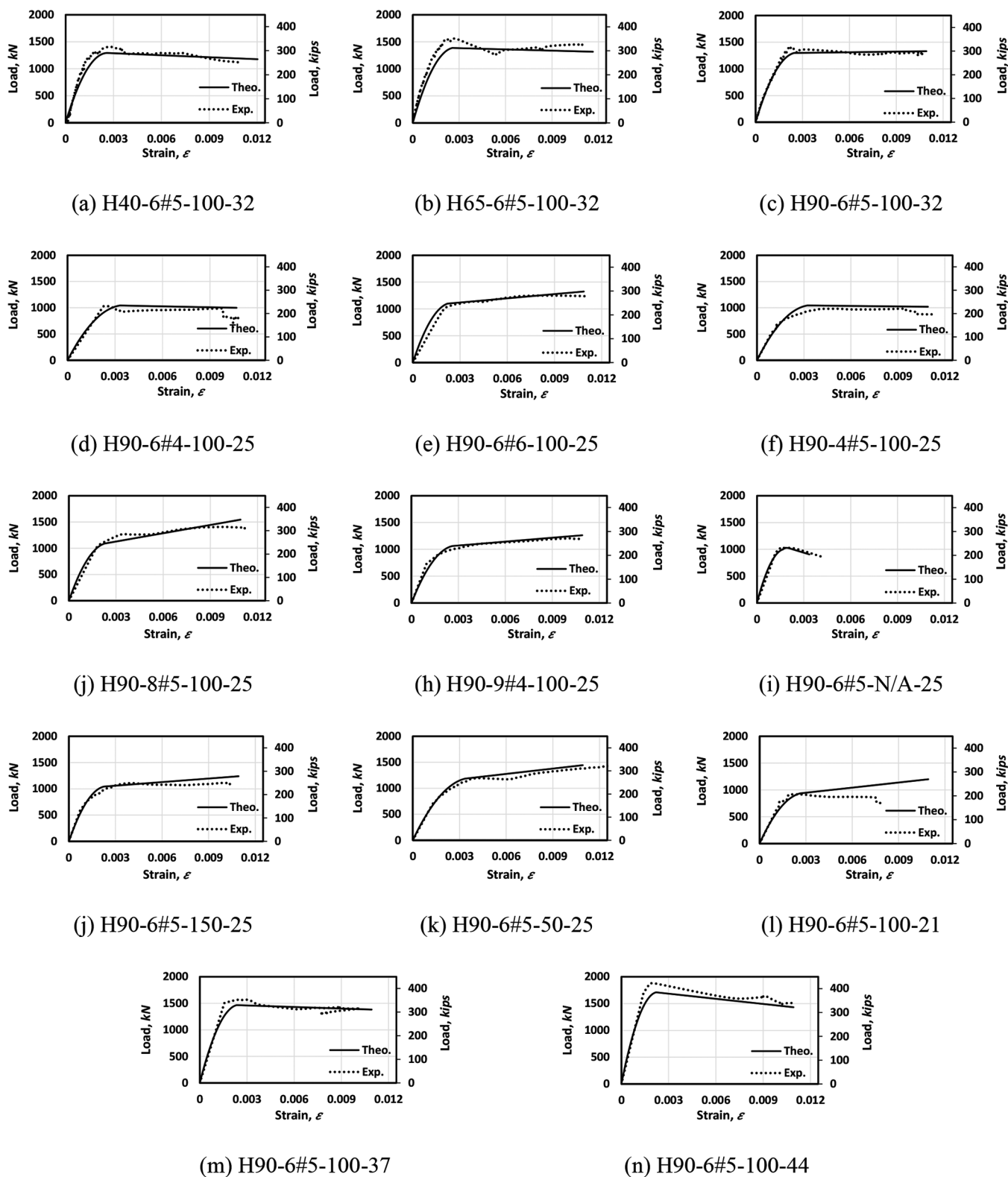


Fig. 11—Comparison between experimental and proposed stress-strain curves of GFRP-reinforced hollow concrete columns.

Allan C. Manalo is an Professor at the School of Civil Engineering and Surveying and the leader of the Civil Composites Research Group at USQ. His research interests include engineered composite materials and structures, polymer railway sleepers, and structural testing.

Brahim Benmokrane, FACI, is Professor of Civil Engineering and NSERC Research Chair in FRP Reinforcement for Concrete Infrastructure and Tier-1 Canada Research Chair in Advanced Composite Materials for Civil Structures in the Department of Civil Engineering at the University of Sher-

brooke, Sherbrooke, QC, Canada. He is a member of ACI Committee 440, Fiber-Reinforced Polymer Reinforcement.

Warna Karunasena is a Professor at the School of Civil Engineering and Surveying at USQ. His research interests include composite materials, and modeling and analysis of structures.

Wahid Ferdous is a Research Fellow at USQ. His research interests include engineered composite structures and polymer railway sleepers.

ACI member **Priyan Mendis** is a Professor in the Department of Infrastructure Engineering and the Leader of the Advanced Protective Technology of Engineering Structures Group at the University of Melbourne, Melbourne, Australia. His research interests include fire behavior of structures, high-strength concrete, and modeling and durability of infrastructure.

ACKNOWLEDGMENTS

The authors would like to thank Pultrall Canada and Inconmat V-ROD Australia for providing the GFRP bars and spirals. The assistance of the technical staff at the Centre of Future Materials in the University of Southern Queensland is gratefully acknowledged. The technical support from the Natural Science and Engineering Research Council of Canada (NSERC) Research Chair in Innovative FRP Reinforcement for Sustainable Concrete Infrastructures (University of Sherbrooke, Canada) is appreciated. The first author would like to thank Tafila Technical University (TTU) in Jordan for awarding him the PhD scholarship.

NOTATION

A_{core}	= effective core area denoted by distance between spiral centers, mm ² (in. ²)
A_{cc}	= concrete core area (without bars area), mm ² (in. ²)
A_{ce}	= area of concrete core excluding crushed concrete part due to unconfined concrete between spirals, mm ² (in. ²)
A_g	= total cross-section area, mm ² (in. ²)
A_d	= Concrete-core area excluding the crushed concrete part due to the opening effect, mm ² (in. ²)
A_{gc}	= concrete area in section (without bars area), mm ² (in. ²)
A_{GFRP}	= total area of GFRP bars, mm ² (in. ²)
A_h	= GFRP-spiral cross-sectional area, mm ² (in. ²)
b_0, b_1, b_2	= constants (Eq. (1))
d_b	= bar diameter, mm (in.)
D_i	= diameter of inner void, mm (in.)
D_s	= diameter of spirals on-centers, mm (in.)
d_s	= spiral diameter, mm (in.)
E_{GFRP}	= elastic modulus of GFRP bars, MPa (ksi)
f_{bent}	= tensile strength of bent GFRP bars, ACI 440.1R-15, ³² MPa (psi) (Eq. (9))
f_c	= stress in HCC, MPa (psi) (Eq. (18))
f'_c	= concrete compressive strength at day of testing HCCs, MPa (psi)
f_{cc}	= maximum confined strength of concrete, MPa (psi) (Eq. (16))
$f_{cc'}$	= concrete confined strength at second peak load (P_2), MPa (psi)
$f_{cc,n1'}$	= theoretical confined strength using modified Mander model using experimental results of HCCs, MPa (psi) (Eq. (5))
$f_{cc,n2'}$	= theoretical confined strength using modified Mander model introduced by Afifi et al., ¹⁷ MPa (psi)
$f_{cc,n3'}$	= theoretical confined strength using modified Mander model introduced by Hales et al., ²¹ MPa (psi)
f_{ci}	= axial stress of column at first axial peak load (P_1), MPa (psi)
f_{co}	= unconfined concrete strength ($0.85f'_c$), MPa (psi)
f_{cu}	= concrete strength at ultimate strain (ϵ_{cu}), MPa (psi) (Eq. (15))
f_{GFRP}	= stress contribution by GFRP bars, MPa (psi) (Eq. (1))
f_i	= concrete strength alone at first axial peak load (P_1), MPa (psi)
f_l	= lateral confining stress, MPa (psi) (Eq. (8))
f_l'	= effective lateral confining stress suggested by Mander, MPa (psi)
f_l''	= effective lateral confining stress considering proposed reduction factor in this study, MPa (psi) (Eq. (14))
I_{bar}	= moment of inertia of GFRP bars, mm ⁴ (in. ⁴)
I_{core}	= moment of inertia of concrete core, mm ⁴ (in. ⁴)
i/o	= inner-to-outer diameter ratio
k_d	= reduction factor regarding presence of GFRP bars in core area (Eq. (12))
k_e	= reduction factor regarding vertical unconfined area between spirals (Eq. (10))
k_o	= reduction factor regarding lateral spacing between GFRP bars (Eq. (11))
K_e	= proportion of ultimate strain in GFRP spirals before failure to their ultimate tensile strength (0.462 as an average)
P_1	= first axial peak load, kN (kip)
P_2	= second axial peak load, kN (kip)
r	= inner radius of spiral, mm (in.)
S	= vertical spacing of spirals on centers, mm (in.)
s'	= clear vertical spacing between spirals, mm (in.)
x	= reduction factor for D_s related to lateral spacing between bars
α_1	= effect of reinforcement ratio factor (Eq. (2))
α_2	= effect of concrete compressive strength factor (Eq. (3))

α_3	= effect of volumetric ratio factor (Eq. (4))
α_4	= effect of inner-to-outer diameter ratio factor (Eq. (5))
θ	= angle between two bars
ϵ_c	= concrete strain
ϵ_{cc}	= assumed concrete strain at f_{cc}
ϵ_{co}	= unconfined concrete strain
ϵ_{cr}	= crushing strain of the GFRP bars (Eq. (7))
ϵ_{cu}	= ultimate strain (equals to ϵ_{cu}) (Eq. (7))
ϵ_i	= inflection strain (strain at f_{ci} and f_i) (Eq. (6))
ρ	= reinforcement ratio with respect to total cross-section area (A_g)
ρ_e	= effective reinforcement ratio with respect to effective core area
ρ_v	= volumetric ratio of lateral reinforcements
σ_{octa}	= mean normal stress, MPa (psi)
σ_x, σ_y	= lateral stresses perpendicular to center line of sample (equal f_l), MPa (psi)
σ_z	= axial stress, MPa (psi)
τ_{octa}	= mean shear stress, MPa (psi)

REFERENCES

- Lignola, G. P.; Prota, A.; Manfredi, G.; and Cosenza, E., "Experimental Performance of RC Hollow Columns Confined with CFRP," *Journal of Composites for Construction*, ASCE, V. 11, No. 1, 2007, pp. 42-49. doi: 10.1061/(ASCE)1090-0268(2007)11:1(42)
- Kusumawardaningsih, Y., and Hadi, M. N., "Comparative Behaviour of Hollow Columns Confined with FRP Composites," *Composite Structures*, V. 93, No. 1, 2010, pp. 198-205. doi: 10.1016/j.compstruct.2010.05.020
- Hadi, M., and Le, T., "Behaviour of Hollow Core Square Reinforced Concrete Columns Wrapped with CFRP with Different Fibre Orientations," *Construction and Building Materials*, V. 50, 2014, pp. 62-73. doi: 10.1016/j.conbuildmat.2013.08.080
- Lee, J.-H.; Choi, J.-H.; Hwang, D.-K.; and Kwahk, I.-J., "Seismic Performance of Circular Hollow RC Bridge Columns," *KSCE Journal of Civil Engineering*, V. 19, No. 5, 2015, pp. 1456-1467. doi: 10.1007/s12205-014-1173-z
- Zahn, F.; Park, R.; and Priestley, M., "Flexural Strength and Ductility of Circular Hollow Reinforced Concrete Columns without Confinement on Inside Face," *ACI Structural Journal*, V. 87, No. 2, Mar.-Apr. 1990, pp. 156-166.
- Hoshikuma, J., and Priestley, M. J. N., "Flexural Behavior of Circular Hollow Columns with a Single Layer of Reinforcement under Seismic Loading," *Report No. SSRP-2000/13*, Department of Structural Engineering, University of California, San Diego, La Jolla, CA, 2000, pp. 13.
- Yazici, V., "Strengthening Hollow Reinforced Concrete Columns with Fibre Reinforced Polymers," PhD thesis, University of Wollongong, Wollongong, Australia, 2012.
- Mo, Y.; Wong, D.; and Maekawa, K., "Seismic Performance of Hollow Bridge Columns," *ACI Structural Journal*, V. 100, No. 3, May-June 2003, pp. 337-348.
- Li, J.; Gong, J.; and Wang, L., "Seismic Behavior of Corrosion-Damaged Reinforced Concrete Columns Strengthened Using Combined Carbon Fiber-Reinforced Polymer and Steel Jacket," *Construction and Building Materials*, V. 23, No. 7, 2009, pp. 2653-2663. doi: 10.1016/j.conbuildmat.2009.01.003
- Pantelides, C. P.; Gibbons, M. E.; and Reaveley, L. D., "Axial Load Behavior of Concrete Columns Confined with GFRP Spirals," *Journal of Composites for Construction*, ASCE, V. 17, No. 3, 2013, pp. 305-313. doi: 10.1061/(ASCE)CC.1943-5614.0000357
- Manalo, A.; Benmokrane, B.; Park, K.-T.; and Lutze, D., "Recent Developments on FRP Bars as Internal Reinforcement in Concrete Structures," *Concrete in Australia*, V. 40, No. 2, 2014, pp. 46-56.
- Maranan, G.; Manalo, A.; Benmokrane, B.; Karunasena, W.; Mendis, P.; and Nguyen, T., "Shear Behaviour of Geopolymer-Concrete Beams Transversely Reinforced with Continuous Rectangular GFRP Composite Spirals," *Composite Structures*, V. 187, 2018, pp. 454-465. doi: 10.1016/j.compstruct.2017.12.080
- Afifi, M. Z.; Mohamed, H. M.; and Benmokrane, B., "Axial Capacity of Circular Concrete Columns Reinforced with GFRP Bars and Spirals," *Journal of Composites for Construction*, ASCE, V. 18, No. 1, 2014, p. 04013017. doi: 10.1061/(ASCE)CC.1943-5614.0000438
- Hadi, M. N.; Karim, H.; and Sheikh, M. N., "Experimental Investigations on Circular Concrete Columns Reinforced with GFRP Bars and Helices under Different Loading Conditions," *Journal of Composites for Construction*, ASCE, V. 20, No. 4, 2016, p. 04016009. doi: 10.1061/(ASCE)CC.1943-5614.0000670
- AlAjarmeh, O. S.; Manalo, A.; Benmokrane, B.; Karunasena, W.; Mendis, P.; and Nguyen, K., "Compressive Behavior of Axially Loaded Circular Hollow Concrete Columns Reinforced with GFRP Bars and

- Spirals," *Construction and Building Materials*, V. 194, 2019, pp. 12-23. doi: 10.1016/j.conbuildmat.2018.11.016
16. AlAjarmeh, O. S.; Manalo, A. C.; Benmokrane, B.; Karunasena, W.; and Mendis, P., "Axial Performance of Hollow Concrete Columns Reinforced with GFRP Composite Bars with Different Reinforcement Ratios," *Composite Structures*, V. 213, No. 1, 2019, 12 pp.
17. Afifi, M. Z.; Mohamed, H. M.; and Benmokrane, B., "Theoretical Stress-Strain Model for Circular Concrete Columns Confined by GFRP Spirals and Hoops," *Engineering Structures*, V. 102, 2015, pp. 202-213. doi: 10.1016/j.engstruct.2015.08.020
18. Zeng, J.-J.; Guo, Y.-C.; Gao, W.-Y.; Chen, W.-P.; and Li, L.-J., "Stress-Strain Behavior of Circular Concrete Columns Partially Wrapped with FRP Strips," *Composite Structures*, V. 200, 2018.
19. Zeng, J.-J.; Guo, Y.-C.; Gao, W.-Y.; Li, J.-Z.; and Xie, J.-H., "Behavior of Partially and Fully FRP-Confined Circularized Square Columns under Axial Compression," *Construction and Building Materials*, V. 152, 2017, pp. 319-332. doi: 10.1016/j.conbuildmat.2017.06.152
20. Candappa, D.; Sanjayan, J.; and Setunge, S., "Complete Triaxial Stress-Strain Curves of High-Strength Concrete," *Journal of Materials in Civil Engineering*, ASCE, V. 13, No. 3, 2001, pp. 209-215. doi: 10.1061/(ASCE)0899-1561(2001)13:3(209)
21. Hales, T. A.; Pantelides, C. P.; Sankholkar, P.; and Reaveley, L. D., "Analysis-Oriented Stress-Strain Model for Concrete Confined with Fiber-Reinforced Polymer Spirals," *ACI Structural Journal*, V. 114, No. 5, Sept.-Oct. 2017, pp. 1263-1272. doi: 10.14359/51689788
22. Lam, L., and Teng, J., "Design-Oriented Stress-Strain Model for FRP-Confined Concrete," *Construction and Building Materials*, V. 17, No. 6-7, 2003, pp. 471-489. doi: 10.1016/S0950-0618(03)00045-X
23. Mander, J. B.; Priestley, M. J.; and Park, R., "Theoretical Stress-Strain Model for Confined Concrete," *Journal of Structural Engineering*, ASCE, V. 114, No. 8, 1988, pp. 1804-1826. doi: 10.1061/(ASCE)0733-9445(1988)114:8(1804)
24. Lokuge, W. P.; Sanjayan, J.; and Setunge, S., "Stress-Strain Model for Laterally Confined Concrete," *Journal of Materials in Civil Engineering*, ASCE, V. 17, No. 6, 2005, pp. 607-616. doi: 10.1061/(ASCE)0899-1561(2005)17:6(607)
25. Lignola, G. P.; Protá, A.; Manfredi, G.; and Cosenza, E., "Unified Theory for Confinement of RC Solid and Hollow Circular Columns," *Composites. Part B, Engineering*, V. 39, No. 7-8, 2008, pp. 1151-1160. doi: 10.1016/j.compositesb.2008.03.007
26. Cascardi, A.; Micelli, F.; and Aiello, M. A., "Unified Model for Hollow Columns Externally Confined by FRP," *Engineering Structures*, V. 111, 2016, pp. 119-130. doi: 10.1016/j.engstruct.2015.12.032
27. Fam, A. Z., and Rizkalla, S. H., "Confinement Model for Axially Loaded Concrete Confined by Circular Fiber-Reinforced Polymer Tubes," *ACI Structural Journal*, V. 98, No. 4, July-Aug. 2001, pp. 451-461.
28. Yazici, V., and Hadi, M. N., "Normalized Confinement Stiffness Approach for Modeling FRP-Confined Concrete," *Journal of Composites for Construction*, ASCE, V. 16, No. 5, 2012, pp. 520-528. doi: 10.1061/(ASCE)CC.1943-5614.0000283
29. Maranan, G.; Manalo, A.; Benmokrane, B.; Karunasena, W.; and Mendis, P., "Behavior of Concentrically Loaded Geopolymer-Concrete Circular Columns Reinforced Longitudinally and Transversely with GFRP Bars," *Engineering Structures*, V. 117, 2016, pp. 422-436. doi: 10.1016/j.engstruct.2016.03.036
30. Karim, H.; Sheikh, M. N.; and Hadi, M. N., "Axial load-Axial Deformation Behaviour of Circular Concrete Columns Reinforced with GFRP Bars and Helices," *Construction & Building Materials*, V. 112, 2016, pp. 1147-1157. doi: 10.1016/j.conbuildmat.2016.02.219
31. CAN/CSA-S806-12, "Design and Construction of Building Structures with Fibre-Reinforced Polymers," Canadian Standards Association, Rexdale, ON, Canada, 2012.
32. ACI Committee 440, "Guide for the Design and Construction of Concrete Reinforced with FRP Bars (ACI 440.1R-15)," American Concrete Institute, Farmington Hills, MI, 2015, 88 pp.
33. Benmokrane, B.; Manalo, A.; Bouhet, J.-C.; Mohamed, K.; and Robert, M., "Effects of Diameter on the Durability of Glass Fiber-Reinforced Polymer Bars Conditioned in Alkaline Solution," *Journal of Composites for Construction*, ASCE, V. 21, No. 5, 2017, p. 04017040 doi: 10.1061/(ASCE)CC.1943-5614.0000814
34. Abd El Fattah, A. M., "Behavior of Concrete Columns under Various Confinement Effects," PhD thesis, Kansas State University, Lawrence, KS, 2012.
35. Ozbakkaloglu, T.; Lim, J. C.; and Vincent, T., "FRP-Confined Concrete in Circular Sections: Review and Assessment of Stress-Strain Models," *Engineering Structures*, V. 49, 2013, pp. 1068-1088. doi: 10.1016/j.engstruct.2012.06.010
36. Tobbi, H.; Farghaly, A. S.; and Benmokrane, B., "Strength Model for Concrete Columns Reinforced with Fiber-Reinforced Polymer Bars and Ties," *ACI Structural Journal*, V. 111, No. 4, July-Aug. 2014, pp. 789-798. doi: 10.14359/51686630
37. Fafitis, A., and Shah, S., "Lateral Reinforcement for High-Strength Concrete Columns," High-Strength Concrete, SP-87, American Concrete Institute, Farmington Hills, MI, 1985, pp. 213-232.
38. Hoshikuma, J.; Kawashima, K.; Nagaya, K.; and Taylor, A., "Stress-Strain Model for Confined Reinforced Concrete in Bridge Piers," *Journal of Structural Engineering*, ASCE, V. 123, No. 5, 1997, pp. 624-633. doi: 10.1061/(ASCE)0733-9445(1997)123:5(624)
39. Sheikh, S. A., and Uzumeri, S. M., "Strength and Ductility of Tied Concrete Columns," *Journal of the Structural Division*, ASCE, V. 106, No. 15, 1980, pp. 1072-1102.
40. Cusson, D., and Paultre, P., "Stress-Strain Model for Confined High-Strength Concrete," *Journal of Structural Engineering*, ASCE, V. 121, No. 3, 1995, pp. 468-477. doi: 10.1061/(ASCE)0733-9445(1995)121:3(468)
41. Saatcioglu, M., and Razvi, S. R., "Strength and Ductility of Confined Concrete," *Journal of Structural Engineering*, ASCE, V. 118, No. 6, 1992, pp. 1590-1607. doi: 10.1061/(ASCE)0733-9445(1992)118:6(1590)
42. Sargin, M., "Stress-Strain Relationships for Concrete and Analysis of Structural Concrete Sections," Study No 4, Solid Mechanics Division, University of Waterloo, Waterloo, ON, Canada, 1971.
43. Kent, D. C., and Park, R., "Flexural Members with Confined Concrete," *Journal of the Structural Division*, ASCE, V. 97, No. 7, 1971, pp. 1969-1990.
44. Popovics, S., "A Numerical Approach to the Complete Stress-Strain Curve of Concrete," *Cement and Concrete Research*, V. 3, No. 5, 1973, pp. 583-599. doi: 10.1016/0008-8846(73)90096-3
45. Murguma, H., "A stress-Strain Model of Confined Concrete," *Annual Report on Cement Engineering*, V. 34, 1980, pp. 429-432.
46. Sankholkar, P. P., "Confinement Model for Concrete Columns Internally Reinforced with Glass Fiber Reinforced Polymer Spirals," master's thesis, University of Utah, Salt Lake City, UT, 2016.
47. Willam, K. J., "Constitutive Model for the Triaxial Behaviour of Concrete," *Proceedings, International Association for Bridge and Structural Engineering*, V. 19, 1975, pp. 1-30.
48. Yazici, V., and Hadi, M. N., "Axial Load-Bending Moment Diagrams of Carbon FRP Wrapped Hollow Core Reinforced Concrete Columns," *Journal of Composites for Construction*, ASCE, V. 13, No. 4, 2009, pp. 262-268. doi: 10.1061/(ASCE)CC.1943-5614.0000010
49. Tobbi, H.; Farghaly, A. S.; and Benmokrane, B., "Behavior of Concentrically Loaded Fiber-Reinforced Polymer Reinforced Concrete Columns with Varying Reinforcement Types and Ratios," *ACI Structural Journal*, V. 111, No. 2, Mar.-Apr. 2014, pp. 375-386.
50. Deitz, D.; Harik, I.; and Gesund, H., "Physical Properties of Glass Fiber Reinforced Polymer Rebars in Compression," *Journal of Composites for Construction*, ASCE, V. 7, No. 4, 2003, pp. 363-366. doi: 10.1061/(ASCE)1090-0268(2003)7:4(363)
51. Roy, H. E. H., and Sozen, M. A., "Ductility of Concrete," *Flexural Mechanics of Reinforced Concrete*, SP-12, American Concrete Institute, Farmington Hills, MI, 1965, pp. 213-235.
52. Wu, G.; Wu, Z.; and Lü, Z., "Design-Oriented Stress-Strain Model for Concrete Prisms Confined with FRP Composites," *Construction & Building Materials*, V. 21, No. 5, 2007, pp. 1107-1121. doi: 10.1016/j.conbuildmat.2005.12.014
53. Tasdemir, M.; Tasdemir, C.; Akyüz, S.; Jefferson, A.; Lydon, F.; and Barr, B., "Evaluation of Strains at Peak Stresses in Concrete: A Three-Phase Composite Model Approach," *Cement and Concrete Composites*, V. 20, No. 4, 1998, pp. 301-318. doi: 10.1016/S0958-9465(98)00012-2
54. Fillmore, B., and Sadeghian, P., "Contribution of Longitudinal Glass Fiber-Reinforced Polymer Bars in Concrete Cylinders under Axial Compression," *Canadian Journal of Civil Engineering*, V. 45, No. 6, 2018, pp. 458-468. doi: 10.1139/cjce-2017-0481
55. Karim, H.; Noel-Gough, B.; Sheikh, M. N.; and Hadi, M. N., "Strength and Ductility Behavior of Circular Concrete Columns Reinforced with GFRP Bars and Helices," The 12th International Symposium on Fiber Reinforced Polymers for Reinforced Concrete Structures (FRPRCS-12) & The 5th Asia-Pacific Conference on Fiber Reinforced Polymers in Structures (APFIS-2015) Joint Conference, Nanjing, China, 2015.
56. ACI Committee 318, "Building Code Requirements for Structural Concrete (ACI 318-08) and Commentary," American Concrete Institute, Farmington Hills, MI, 2008, 471 pp.
57. Yang, K.-H.; Mun, J.-H.; Cho, M.-S.; and Kang, T. H.-K., "Stress-Strain Model for Various Unconfined Concretes in Compression," *ACI Structural Journal*, V. 111, No. 4, July-Aug. 2014, pp. 819-826.
58. Li, B.; Park, R.; and Tanaka, H., "Stress-Strain Behavior of High-Strength Concrete Confined by Ultra-High- and Normal-Strength Transverse Reinforcements," *ACI Structural Journal*, V. 98, No. 3, May-June 2001, pp. 395-406.

59. Hognestad, E., "Study of Combined Bending and Axial Load in Reinforced Concrete Members," University of Illinois at Urbana Champaign, College of Engineering. Engineering Experiment Station, 1951.

60. BS 8110-1:1997, "Structural Use of Concrete, Part 1: Code of Practice for Design and Construction," British Standards Institution, London, UK, 1997.

61. Eurocode 8, "Design of Structures for Earthquake Resistance-Part 1: General Rules, Seismic Actions and Rules for Buildings," European Committee for Standardization, Brussels, Belgium, 2005.

62. Miyauchi, K.; Inoue, S.; Kuroda, T.; and Kobayashi, A., "Strengthening Effects of Concrete Column with Carbon Fiber Sheet," *Transactions of the Japan Concrete Institute*, V. 21, 2000, pp. 143-150.

63. Teng, J.; Jiang, T.; Lam, L.; and Luo, Y., "Refinement of a Design-Oriented Stress-Strain Model for FRP-Confined Concrete," *Journal of Composites for Construction*, ASCE, V. 13, No. 4, 2009, pp. 269-278. doi: 10.1061/(ASCE)CC.1943-5614.0000012

64. Cui, C., and Sheikh, S., "Experimental Study of Normal- and High-Strength Concrete Confined with Fiber-Reinforced Polymers," *Journal of Composites for Construction*, ASCE, V. 14, No. 5, 2010. doi: 10.1061/(ASCE)CC.1943-5614.0000116

Chapter 7

Conclusions

Hollow concrete columns (HCCs) reinforced with steel bars have been employed extensively for civil infrastructure because they use fewer materials and offer higher structural efficiency compared to solid concrete columns with the same concrete area. Many experimental studies have been conducted to investigate the behavior of HCCs under different loading conditions and found that the structural performance of HCCs is critically affected by many design parameters. If not designed properly, HCCs exhibit brittle failure behavior, due to longitudinal bars buckling or the concrete wall failing in shear. In addition, the corrosion of steel bars has become an issue in reinforced-concrete structures. Therefore, this study focused on developing HCCs reinforced with GFRP bars and spirals to achieve a durable infrastructure and investigating their structural performance. The major findings of this work are presented below:

State-of-the-art review on the behavior of HCCs

This study reviewed the behavior of hollow concrete columns and identified the critical design parameters and their structural performance under different loading conditions. The challenges in the existing design and opportunities in using GFRP reinforcement in this type of construction system were analyzed. The major findings of this study can be drawn as follows:

- There is a growing interest in the use of hollow concrete columns as shown by the great number of relevant studies in the last 10 years. There were at least 41 reported studies from 1993 to 2018 investigating the behavior of the HCCs under different loading conditions and with different design parameters.
- Steel-reinforced HCCs are mostly investigated under hysteretic and axial compression loading representing more than 87% of the total studies, as these are the loading conditions required in designing bridge piers.
- The ratio of the inner-to-outer diameter, reinforcement ratio, volumetric ratio, and concrete compressive strength have been identified as the most critical and well-investigated design parameters primarily affecting the structural performance of steel-reinforced hollow concrete columns.

- Steel-reinforced HCCs behaved differently than steel-reinforced SCCs due to the discontinuity in the radial stress inside the concrete core of the HCCs owing to the hollowness. However, the capacity of hollow concrete columns is comparable to or even higher than their solid counterparts when the appropriate levels of design parameters are used.
- Steel-reinforced HCCs typically failed in a brittle manner due to either crushing of inner concrete core or buckling/yielding of the longitudinal bars. Effective design of the steel-reinforced HCCs can be achieved by providing adequate inner-wall thickness or sufficient spacing between lateral reinforcement.
- Corrosion resistant glass fibre reinforced polymer (GFRP) bars can potentially overcome the brittle behavior of steel-reinforced hollow concrete columns due to their high strength and linear elastic behavior up to failure. Combining this with the nonlinear behavior of concrete in compression and their relatively close moduli of elasticity can result in HCCs with a higher deformation capacity and a more progressive failure behavior than steel-reinforced HCCs.

The findings from the state-of-the-art review indicate that HCCs will benefit from the high strength and strain capacities of GFRP bars. Understanding on how the critical design parameters affect the structural performance of GFRP-reinforced hollow concrete columns under concentric axial compression loads should be gained in order to safely and effectively design this new construction system.

Effect of (i/o) ratio on the behavior of GFRP-reinforced HCCs

In this study, the effect of removing the inner concrete core from the SCC was evaluated by comparative investigating the behavior between solid and hollow concrete columns. The effect of (*i/o*) ratio by increasing from inner-to-outer diameter ratio from 0.16 to 0.36 was also evaluated. Moreover, the behavior of HCCs when longitudinally reinforced with steel and GFRP bars was compared and analyzed. The following conclusions can be drawn out of this study:

- The GFRP-reinforced SCCs having the higher concrete area exhibited higher carrying load than the GFRP-reinforced HCCs. However, the latter showed 74% higher deformation capacity and 21% higher strength confinement

efficiency than the former one due to the lower lateral expansion of the cross-section.

- The increase in (i/o) ratio changed the failure behavior from brittle to ductile, where the final failure of the sample with an (i/o) ratio of 0.36 occurred by crushing only of the longitudinal bars and concrete core. On the other hand, HCCs with (i/o) ratios of 0.16 and 0.26 failed by the tensile rupture of the GFRP spirals.
- Reinforcing the HCC with GFRP bars resulted in 11%, 22% and 54% higher axial capacity, ductility, and confinement efficiency, respectively, compared to the steel-reinforced HCC. This was due to the high strength and the linear elastic behavior of the GFRP bars until failure.
- The design load capacity of the GFRP-reinforced HCCs was accurately predicted by considering an axial strain in the GFRP bars of 0.0025 and the gross area of the concrete, while the second peak load was predicted by considering the confined strength of the concrete core and the contribution of GFRP bars at an axial strain of 0.011. These findings emphasize the significant load-carrying contribution of the GFRP bars in HCCs due to their linear elastic behaviour.
- Stress index approach can be used to accurately predict the failure mode of the GFRP-reinforced HCCs. This approach is based on comparing the hoop stress index and the circumferential stress index. HCCs will fail by crushing of the concrete core and bars when the former is lesser than the latter stress. If the case is reversed, the failure will be rupture of the GFRP spirals.

Based on this study, the optimal (i/o) ratio was 0.36 as it resulted in the most stable behavior and the highest confined strength and ductility for GFRP-reinforced HCCs. Similarly, reinforcing with longitudinal GFRP bars significantly enhanced the overall behavior of HCCs. The effect of varying the amount of longitudinal GFRP bars was therefore investigated.

Effect of the reinforcement ratio (ρ) on the behavior of GFRP-reinforced HCCs

The effect of reinforcement ratio (ρ) on the behavior of the GFRP-reinforced HCCs either by changing the bar number or diameter was evaluated. Also, the compressive

behavior of the GFRP-reinforced HCCs was modelled considering the crushing strain of the GFRP bars. The major findings of this study are the following:

- Increasing ρ significantly enhanced the strength and ductility, and made the failure more progressive of the GFRP-reinforced HCCs. Increasing the bar diameter from 12.7 mm to 19.1 mm resulted in 27% and 65% higher confined strength and displacement capacity, respectively due to increase the axial and flexural stiffness of the longitudinal GFRP bars. Moreover, this increase in bar diameter mitigated the drop of the load carrying caused by the concrete cover spalling.
- The increase of ρ by increasing the number of 15.9 mm diameter GFRP bars from 4 to 8 pieces improved the overall behavior of the GFRP-reinforced HCCs. This increase led to a 6%, 27%, and 4% higher load capacity, confinement efficiency, and ductility, respectively, due to increased axial stiffness of the columns and the lateral confinement using more bars by covering more unconfined concrete core.
- Having the same reinforcement ratio but with more longitudinal bars and smaller diameter showed 12% increase in the confined strength due to the effectiveness of more bars in increasing the lateral confinement. However, using a larger bar diameter and a smaller number of bars exhibited 20% increase in displacement capacity of the HCCs due to the higher flexural capacity of the larger bars diameter.
- The crushing strain at failure of GFRP bars is almost 52% of the ultimate tensile strength while the concrete strain is at 3000 $\mu\epsilon$. Considering this level of strains and both the contribution of the concrete and GFRP bars can accurately predict the axial load capacity and the confined strength of the GFRP-reinforced HCCs.

The crushing strain of GFRP bars in concrete is affected by the level of confinement provided by the lateral reinforcements and compressive strength of concrete. The effect of these design parameters was investigated in detail.

Effect of volumetric ratio (ρ_v) on the behavior of GFRP-reinforced HCCs

The effect of varying the volumetric ratio from 0 to 3.84 % by changing the spacing between the 9.5 mm GFRP lateral spirals was examined on the behavior of concentrically loaded GFRP-reinforced HCCs. Based on the results of this study, the following conclusions can be drawn.

- The provision of the lateral spirals made the HCCs to exhibit post-loading stage after the concrete cover spalling. Providing closer spirals in GFRP-reinforced HCCs increased the axial load capacity by 8% compared to the HCC with wide spiral spacing due to early activation of the lateral confinement.
- The confinement effectiveness induced by the close spiral spacing resulted in more progressive failure and delaying the crushing of the longitudinal GFRP bars.
- Ductility and confined strength of the HCCs were highly affected by the decrease in the spacing between spirals, where using 50 mm instead of 150 mm resulted in 98% and 69% increase in ductility and confined strength, respectively. This finding caused by the increase in the brace length of the longitudinal bars leading to increase their axial contribution and their compressive strength capacity.
- The load contribution of the GFRP bars in the design load capacity for the laterally reinforced HCCs was from 13% to 17%. While the GFRP bars contribution in the unconfined HCC was only 7% of the design load capacity. Moreover, the load carrying contribution of the GFRP bars at the second peak was from 59% to 64%.

Effect of concrete compressive strength (f'_c) on the behavior of GFRP-reinforced HCCs

The effect of changing the concrete compressive strength (f'_c) from 21.2 MPa to 44.0 MPa on the behavior of concentrically loaded GFRP-reinforced HCCs was analyzed. Based on the results of this study, the following conclusions can be drawn.

- The axial load capacity and stiffness of HCCs increased up to 107% and 70%, respectively, due to the increase in the concrete modulus of elasticity as a

result of increasing f'_c . Nevertheless, the behavior tended to be more brittle due to the increase in brittleness attached to the increase in concrete strength.

- The contribution of the GFRP bars in the axial load design of the GFRP-reinforced HCCs decreases with increasing f'_c . This is due to the increase in the stiffness of the concrete part even the GFRP bars recorded almost an axial strain of $3000 \mu\epsilon$.
- High axial strength contribution of the GFRP bars were observed at the second peak, where they represented 40% to 64% of the total confined strength of the HCCs with average axial strain of 0.0095. Due to different stiffness of concrete, the GFRP bars showed less strength contribution with the high concrete strength, the opposite is also true.

From the results of the conducted experimental studies, the behavior of GFRP-reinforced HCCs under concentric axial load is affected by the inner-to-outer diameter ratio, reinforcement ratio, spacing of spirals and concrete compressive strength. The effects of these critical design parameters were considered in the development of an analytical model to describe the overall behavior of GFRP-reinforced HCCs.

Modelling the compressive behavior of the GFRP-reinforced HCCs

A new design-oriented model was proposed and validated to describing accurately the behavior of circular GFRP-reinforced HCCs under concentric compressive loads. This model considered the effect of the investigated critical design parameters including (i/o) ratio, reinforcement ratio (ρ), volumetric ratio (ρ_v), and concrete compressive strength (f'_c). The major findings from this approach are the following:

- The increase in (i/o) ratio, (ρ), and (ρ_v) increased the displacement capacity and confined strength of the HCCs reinforced with GFRP bars and spirals but decreases with the increase in (f'_c).
- Plasticity theory of concrete was not applicable to GFRP-reinforced HCCs due to the absence of the inner concrete core which disrupt the radial stresses and decrease the lateral expansion of the concrete as well as the high strength and linear-elastic behavior of GFRP bars which contributes to the concrete confined strength up to the final failure of the HCC.
- The behavior of the GFRP-reinforced HCCs can be accurately predicted by considering the combed effect of the linear elastic behavior of the GFRP bars

and the non-linear behavior of concrete in compression. The latter consisted of two different behavior including the ascending unconfined concrete behavior and the descending confined concrete behavior (concrete softening).

- The new oriented-design model was able to precisely describe the concentrically loaded behavior of the GFRP-reinforced HCCs. The novelty of this model being in the ease of identifying the critical stress and strain points, which is more preferable for design and analysis engineers.

Contribution of the study

The results obtained from this research discovered the many benefits of reinforcing the hollow concrete columns with GFRP bars and spirals. This research also generated many experimental data and design tools useful for design engineers to effectively and safely design this new construction system, and to expand their use in different civil engineering applications. The significant contribution of this study are the following:

- Addressing the knowledge gap on the effect of the critical design parameters on the structural behavior of HCCs and identifying the many benefits of reinforcing HCCs with GFRP bars and spirals;
- Understanding the structural performance of the GFRP-reinforced HCCs with different influential design parameters including inner-to-outer diameter ratio (i/o), longitudinal-reinforcement ratio (ρ), lateral-reinforcement ratio (ρ_v), and concrete compressive strength (f'_c);
- Developing simple analytical tools to accurately predict the failure behaviour, strength at peak, and the overall load-deformation behavior of GFRP-reinforced HCCs to support the work of the technical committees engaged in the development of standards and design provisions for GFRP-reinforced concrete columns.

New opportunities and future research

The effectiveness of the GFRP reinforcement in HCCs as presented in this thesis demonstrates the high potential to extensively investigate the behavior of this new construction system to provide a non-corrosion and structurally reliable civil engineering structure. Based on the outcome of this research, opportunities and new research areas can be explored to further understand on how the critical design

parameters affect the structural performance of GFRP-reinforced hollow concrete columns as follows:

- The optimal (i/o) ratio for GFRP-reinforced HCCs was found at (0.36) at it provides the most stable behavior among the investigated columns. This is the highest (i/o) ratio that can be tested in this study due to the limited capacity of the testing equipment. Further research considering higher (i/o) ratios and bigger outer diameter of the columns can be implemented to determine the most optimum i/o ratio that will provide a more cost effective section for GFRP-reinforced HCCs.
- The maximum number and diameter of the GFRP bars in this study were 8 pieces and 19.1 mm, respectively. These limitations are implemented to avoid the segregation and congestion in the reinforcements, and to ensure providing sufficient concrete wall thickness for the 250 mm diameter concrete columns. These reinforcing arrangements yielded GFRP-reinforced HCCs with sufficient concrete core area and increased axial stiffness. Investigation on the behavior of columns reinforced with more and bigger diameter bars should be explored for large sections on HCCs as this may replicate closer the behavior of actual infrastructure.
- The most effective spacing between the spirals for the GFRP-reinforced HCCs in this study was 50 mm as it provides significant ductility and confined strength. This is the lowest spacing that can be fabricated to avoid the segregation in between these spirals. The diameter of the spirals was limited to 9.5 mm due to the sections of the investigated columns. Research on increasing the diameter of the GFRP spirals to further increase the volumetric ratio should be conducted to provide HCCs with higher ductility and confined strength than the columns investigated in this study.
- The contribution of longitudinal GFRP bars increase with the increase in the concrete compressive strength due to their elastic modulus becoming closer to each other. Investigating the behavior of GFRP-reinforced HCCs using concrete with a compressive strength higher than 44 MPa can be implemented to significantly increase the axial behavior of GFRP-reinforced HCCs.

- The developed design-oriented model accurately describe the compressive behavior of the GFRP-reinforced HCCs. Further research and analysis can be conducted to extend the application of this model for GFRP-reinforced SCCs.
- The effect of the most critical design parameters for HCCs including (*i/o*) ratio, (ρ), (ρ_v), (f'_c) was evaluated in this study. There is an opportunity to investigate the effect of other design parameters such as slenderness and geometry to provide extensive understanding on the behavior of GFRP-reinforced HCCs.
- Moreover, this thesis focused on the mechanical properties only where the long-term durability and thermal behavior of the GFRP bars should be focused on in the future. In addition, the GFRP-reinforced HCC system should be examined against fire to investigate the fire behavior.

Appendix A: Mechanical and physical properties of the GFRP reinforcements

Table A.1. Mechanical and physical properties of the GFRP reinforcement

	Property	Test Method	Sample	No.19	No.16	No.13	No.10
Physical	Nominal bar diameter (mm)		9	19.1	15.9	12.7	9.5
	Nominal bar area [†] (mm ²)	CSA-S806 Annex A	9	286.5	198.5	126.6	70.8
	Actual bar's cross-sectional area by immersion test (mm ²)			317.3 (1.9)*	224.4 (1.2)*	145.0 (1.7)*	83.8 (1.9)*
Mechanical	Ultimate tensile strength, f_u (MPa)	ASTM D7205/D7205M- 06	6	1270.0 (31.4)*	1237 (33.3)*	1281.5 (35.3)*	1315 (31.1)*
	Modulus of elasticity, E_{FRP} (GPa)		6	60.5 (0.5)*	60.0 (1.3)*	61.3 (0.4)*	62.5 (0.4)*
	Ultimate strain, ε_u (%)		6	2.1 (0.1)*	2.1 (0.1)*	2.1 (0.1)*	2.3 (0.1)*

[†] The adopted area for calculating mechanical properties

* Standard deviation

Appendix B: Conference papers

1. CICE-09 (2018)-France

AXIAL PERFORMANCE CAPACITY OF HOLLOW CONCRETE COLUMNS REINFORCED WITH GFRP BARS

Omar AlAjarmeh¹, Allan Manalo¹, Warnar Karunasena¹, Brahim Benmokrane²

¹ Centre of Future Materials CFM, Faculty of Health, Engineering and Science, University of Southern
Toowoomba 4350, Queensland, Australia. (Corresponding author: allanmanalo@usq.edu.au)

² Department of Civil Engineering, University de Sherbrooke, Sherbrooke, Quebec J1K 2R1, Canada.

ABSTRACT:

Hollow concrete sections are widely used in bridge piers, electrical poles, and piles, owing to reduced material usage and high strength-to-weight ratio. However, environmental conditions can be the main reason that affect the performance of concrete elements reinforced with conventional steel by corrosion and rusting the internal reinforcements. In fact, repairing and rehabilitating structural deficient elements experiencing corrosion of steel reinforcements have cost many countries billions of dollars. To address this issue, the potential of hollow concrete sections reinforced with non-corrosive glass fibre reinforced polymer (GFRP) bars should be explored. In this study, four 250 mm diameter and 1000 mm high concrete columns longitudinally reinforced with 6 – 16 mm diameter GFRP bars and 10 mm diameter spirals spaced at 100 mm on centres were cast and tested under concentric compressive load. The effect of the inner-to-diameter ratio on the axial strength capacity and the overall behavior was investigated. This was achieved changing the inside hollow size from 40mm (HG40) and 65mm (HG65) to 100mm (HG100), in addition to a solid column (SG). Hollow concrete columns were tested concentrically until failure. The results showed that the stiffness was approximately same for all concrete columns, i.e. 180 kN/mm. However, the strength enhancement and confinement efficiency was more noticeable for columns with high than low inner-to-outer diameter ratio especially after the post-peak stage. Similarly, the ductility factor was ascending as the inner-to-outer diameter ratio is increasing. The average contribution of GFRP bars in carrying the load was 12.2% and with the compressive strength of the GFRP bars around 51% of the tensile strength capacity at the maximum load.

Keywords: Hollow columns; concrete; GFRP bars; spirals; inner-to-outer diameter ratio; compressive behavior.

2. ACCM-11 (2018)-Australia

ORAL CIVIL AND INFRASTRUCTURE APPLICATIONS HOLLOW CONCRETE COLUMNS REINFORCED WITH GFRP BARS

Omar S. AlAjarmeh¹, Allan Manalo^{1*}, Warna Karunasena¹ and Brahim Benmokrane²

¹ Centre of Future Materials CFM, Faculty of Health, Engineering and Science, University of Southern Toowoomba 4350, Queensland, Australia. (Corresponding author: allanmanalo@usq.edu.au)

² Department of Civil Engineering, University de Sherbrooke, Sherbrooke, Quebec J1K 2R1, Canada.

Keywords: Hollow columns, GFRP bars, Steel bars, Spirals, confined strength, ductility.

ABSTRACT

Steel-reinforced hollow concrete columns have many applications in civil engineering such as bridge piers, poles, and ground piles, owing to reduced material usage and high strength-to-weight ratio. However, such columns suffer from brittle failure mechanism when the reinforcing steel yields. In addition, the corrosion of steel bars is a major issue which affects the performance of the hollow concrete columns [1]. On the other side, strengthening and retrofitting of this deteriorating hollow concrete columns is costly and could not completely stop the corrosion process. Therefore, using non-corrosive reinforcements such as glass fibre reinforced polymer (GFRP) can eliminate the corrosion problem and have a potential to develop a more structurally efficient structure. Accordingly, this study explore the use of GFRP bars and spirals as internal reinforcement to hollow concrete columns. Therefore, test results of three 250mm and 65mm outer and inner –if available- diameter and 1000 mm high concrete columns (Solid and GFRP reinforced “SG”, Hollow and GFRP-reinforced “HG”, and Hollow and Steel-reinforced “HS”) longitudinally reinforced with 6–16 mm diameter GFRP and steel bars and laterally reinforced by 10mm diameter GFRP spirals spaced at 100mm on centers were analyzed and compared to each other. As a result, HG showed more confined strength and ductility than SG and HS by (20% and 22%) and (35% and 61%), respectively.

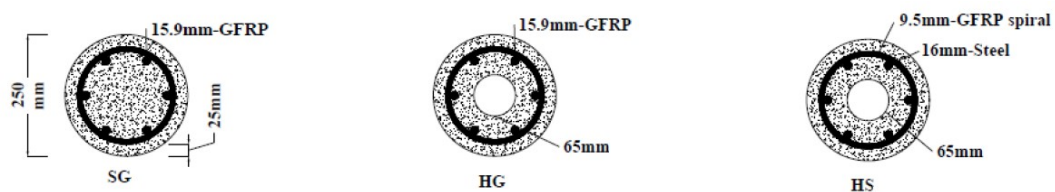


Fig 1. Hollow column cross-sections

REFERENCES

[1] Kusumawardaningsih Y, Hadi MN. Comparative behavior of hollow columns confined with FRP composites. *Composite Structures*. 2010; 93:198-205.

3. *Second Young Researchers Conference (2018)- Australia*

HOLLOW CONCRETE COLUMNS REINFORCED WITH GFRP BARS

Omar AlAjarmeh, Allan Manalo

Centre of Future Materials CFM, Faculty of Health, Engineering and Science, University of Southern Toowoomba 4350, Queensland, Australia. (Corresponding author: omar.alajarmeh@usq.edu.au)

ABSTRACT:

Hollow concrete sections are widely used in bridge piers, electrical poles, and piles, owing to reduced material usage and high strength-to-weight ratio. However, environmental conditions can be the main reason that affect the performance of concrete elements reinforced with conventional steel by corrosion and rusting the internal reinforcements. In fact, repairing and rehabilitating structural deficient elements experiencing corrosion of steel reinforcements have cost many countries billions of dollars. To address this issue, the potential of hollow concrete sections reinforced with non-corrosive glass fibre reinforced polymer (GFRP) bars should be explored. In this study, four 250 mm diameter and 1000 mm high concrete columns longitudinally reinforced with 6 – 16 mm diameter GFRP bars and 10 mm diameter spirals spaced at 100 mm on centres were cast and tested under concentric compressive load. The effect of the inner-to-diameter ratio on the axial strength capacity and the overall behavior was investigated. This was achieved changing the inside hollow size from 40mm (HG40) and 65mm (HG65) to 90mm (HG90), in addition to a solid column (SG). Hollow concrete columns were tested concentrically until failure. The results showed that the stiffness was approximately same for all concrete columns, i.e. 180 kN/mm. However, the strength enhancement and confinement efficiency was more noticeable for columns with high than low inner-to-outer diameter ratio especially after the post-peak stage. Similarly, the ductility factor was ascending as the inner-to-outer diameter ratio is increasing. The average contribution of GFRP bars in carrying the load was 12.2% and with the compressive strength of the GFRP bars around 51% of the tensile strength capacity at the maximum load.

4. *APFIS (2019) Australia*

COMPRESSIVE BEHAVIOR OF GFRP REINFORCED HOLLOW CONCRETE COLUMNS WITH DIFFERENT INNER VOID SIZES AND REINFORCEMENT RATIOS

Omar Alajarmeh¹, Allan Manalo¹, Brahim Benmokrane², Karu Karunasena¹, and Pryian Mendis³

¹University of Southern Queensland, Centre for Future Materials (CFM), School of Civil Engineering and Surveying, Toowoomba 4350, Australia

²University of Sherbrooke, Department of Civil Engineering, Sherbrooke, Quebec, Canada

³The University of Melbourne, Department of Infrastructure Engineering, Victoria 3010, Australia

Hollow reinforced concrete columns reduces self-weight and overall cost, and has a better stiffness-to-strength performance than solid columns. The current design of such members uses steel bars as an internal reinforcements which are, however, prone to corrosion leading to reduce serviceability and structural performance of the structure. There is a priority, therefore, to investigate the use of non-corroded reinforcements such as glass fibre reinforced polymer (GFRP) bars as longitudinal and transverse reinforcements in hollow concrete columns (HCCs). This study experimentally investigate the effect of inner void size denoted by the inner-to outer diameter (i/o) ratio (0, 0.16, 0.26, 0.36) and the reinforcement ratio (1.86%, 2.79%, and 3.72%) on the concentric compressive behavior of HCCs with outside diameter of 250 mm and height of 1.0 m. Test results showed a more stable loading behavior for the HCCs reinforced with the GFRP bars and spirals than steel bars resulted in obtaining high deformation capacity without any significant degradation in the strength before failure. On the other hand, increasing the i/o ratio enhanced the ductility, increased the confined strength of the concrete core, and led to a more progressive failure. The increase in reinforcement ratio significantly increased the compressive strength especially after the post-yield strength peak. These results showed the efficiency of GFRP bars as reinforcement to hollow concrete columns and provided a better understanding on the behavior of this new structural system.

Mr. Omar Alajarmeh, PhD Candidate, University of Southern Queensland-Centre of Future Materials-Australia, oajarmeh@yahoo.com, +61497394088